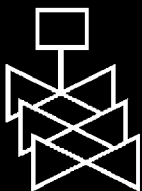
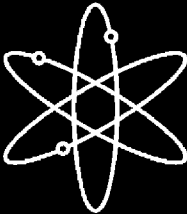


Development of a Pressure Drop Calculation Method for Debris-Covered Sump Screens in Support of Generic Safety Issue 191



**U.S. Nuclear Regulatory Commission
Office of Nuclear Regulatory Research
Washington, DC 20555-0001**



Development of a Pressure Drop Calculation Method for Debris-Covered Sump Screens in Support of Generic Safety Issue 191

Manuscript Completed: December 2006

Date Published: February 2007

Prepared by

W.J. Krotiuk, Principal Investigator

W.J. Krotiuk, NRC Project Manager

Prepared for

Division of Risk Assessment and Special Projects

Office of Nuclear Regulatory Research

U.S. Nuclear Regulatory Commission

Washington, DC 20555-0001



AVAILABILITY OF REFERENCE MATERIALS IN NRC PUBLICATIONS

NRC Reference Material

As of November 1999, you may electronically access NUREG-series publications and other NRC records at NRC's Public Electronic Reading Room at <http://www.nrc.gov/reading-rm.html>.

Publicly released records include, to name a few, NUREG-series publications; *Federal Register* notices; applicant, licensee, and vendor documents and correspondence; NRC correspondence and internal memoranda; bulletins and information notices; inspection and investigative reports; licensee event reports; and Commission papers and their attachments.

NRC publications in the NUREG series, NRC regulations, and Title 10, "Energy," in the *Code of Federal Regulations* may also be purchased from one of these two sources:

1. The Superintendent of Documents
U.S. Government Printing Office
Mail Stop SSOP
Washington, DC 20402-0001
Internet: <http://bookstore.gpo.gov>
Telephone: 202-512-1800
Fax: 202-512-2250
2. The National Technical Information Service
Springfield, VA 22161-0002
<http://www.ntis.gov>
1-800-553-6847 or, locally, 703-605-6000

A single copy of each NRC draft report for comment is available free, to the extent of supply, upon written request as follows:

Address: Office of the Chief Information Officer
Reproduction and Distribution
Services Section
U.S. Nuclear Regulatory Commission
Washington, DC 20555-0001

Email: DISTRIBUTION@nrc.gov
Facsimile: 301-415-2289

Some publications in the NUREG series that are posted at NRC's Web site address <http://www.nrc.gov/reading-rm/doc-collections/nuregs> are updated periodically and may differ from the last printed version. Although references to material found on a Web site bear the date the material was accessed, the material available on the date cited may subsequently be removed from the site.

Non-NRC Reference Material

Documents available from public and special technical libraries include all open literature items, such as books, journal articles, and transactions; *Federal Register* notices; Federal and State legislation; and congressional reports. Such documents as theses, dissertations, foreign reports and translations, and non-NRC conference proceedings may be purchased from their sponsoring organizations.

Copies of industry codes and standards used in a substantive manner in the NRC regulatory process are maintained at the following:

The NRC Technical Library
Two White Flint North
11545 Rockville Pike
Rockville, MD 20852-2738

These standards are available in the library for reference use by the public. Codes and standards are usually copyrighted and may be purchased from the originating organization or, if they are American National Standards, from the following:

American National Standards Institute
11 West 42nd Street
New York, NY 10036-8002
<http://www.ansi.org>
212-642-4900

Legally binding regulatory requirements are stated only in laws; NRC regulations; licenses, including technical specifications; or orders, not in NUREG-series publications. The views expressed in contractor-prepared publications in this series are not necessarily those of the NRC.

The NUREG series comprises (1) technical and administrative reports and books prepared by the staff (NUREG-XXXX) or agency contractors (NUREG/CR-XXXX), (2) proceedings of conferences (NUREG/CP-XXXX), (3) reports resulting from international agreements (NUREG/IA-XXXX), (4) brochures (NUREG/BR-XXXX), and (5) compilations of legal decisions and orders of the Commission and Atomic and Safety Licensing Boards and of Directors' decisions under Section 2.206 of NRC's regulations (NUREG-0750).

ABSTRACT

A set of equations has been derived to calculate the pressure drop for flow across a compressible porous medium debris bed composed of thermal insulation such as fiberglass fibers (Nukon) and calcium silicate (CalSil) particles. The equations account for the kinetic and viscous contributions to pressure drop. The compressibility of the porous medium debris bed is considered by initially assuming an irreversible, inelastic process followed by elastic behavior with constant compressibility. Semiempirical relations and constants required to solve the flow and compression relations are determined using available test data. An iterative procedure has been developed to estimate the pressure drop across a debris bed composed of one debris type (e.g., fibers) by applying the flow and compression relations to a one-volume, homogeneous debris bed model. The pressure drop across a debris bed composed of two debris types (e.g., fibers and particles) depends on the distribution of the two debris types in the bed. Procedures have been developed to estimate the lower bound pressure drop for a debris bed composed of two debris types by using the one-volume, homogeneous model, and the upper bound pressure drop by using a two-volume, nonhomogeneous calculational model that assumes that the particles concentrate or saturate a part of the fiber bed. Predictions using the developed approaches are compared to test data.

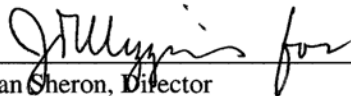
FOREWORD

In the event of a loss-of-coolant accident (LOCA) at a nuclear power plant, the impingement of a high-energy steam-water jet or exposure to the high containment temperature, pressure, and humidity environment can dislodge thermal insulation, coatings, and other material. Some of the dislodged debris can fall near the containment sump or can be transported in the containment water pool to the vicinity of the sump. After the start of recirculation, the debris can accumulate on the sump screen surface and possibly increase the pressure drop (i.e., head loss) across the sump screens. The increased head loss could challenge the ability to provide adequate long-term cooling water to the emergency core cooling system (ECCS) and the containment spray system pumps.

Since the nuclear industry recognized this phenomenon, U.S. and international researchers have performed testing to characterize the pressure drop across a debris-covered sump screen. Researchers have also sought to develop a calculational method to predict the pressure drop across a debris-covered sump screen. One study sponsored by the U.S. Nuclear Regulatory Commission (NRC), documented in NUREG/CR-6224, "Parametric Study of the Potential for BWR ECCS Strainer Blockage Due to LOCA-Generated Debris," issued October 1995, used available test data to develop a head loss correlation to evaluate suppression pool strainer performance in boiling-water reactors (BWRs). However, the tests and data used for the development of the NUREG/CR-6224 correlation focused on debris constituents that were not dominant contributors to debris beds at pressurized-water reactors (PWRs). A significant number of PWR plants use calcium silicate (CalSil) thermal insulation, often in combination with other insulation materials such as fiberglass (i.e., Nukon) or reflective metal insulation. Consequently, the NRC sponsored another study to provide test data for head losses resulting from the accumulation of CalSil-laden insulation debris on a PWR sump screen and to evaluate the suitability of the NUREG/CR-6224 correlation for application to PWR plants that can accumulate CalSil insulation in combination with other debris on a sump screen. The agency documented this study in NUREG/CR-6874, "GSI-191: Experimental Studies of Loss-of-Coolant-Accident-Generated Debris Accumulation and Head Loss with Emphasis on the Effects of Calcium Silicate Insulation," issued May 2005.

The NRC's Advisory Committee on Reactor Safeguards (ACRS), Thermal-Hydraulic Subcommittee, raised concerns regarding the application of the NUREG/CR-6224 methodology for calculating head loss through debris-covered PWR sump screens in an ACRS letter, "Safety Evaluation of the Industry Guidelines Related to Pressurized Water Reactor Sump Performance," dated October 18, 2004. As a result of these technical comments, the staff of the NRC Office of Nuclear Regulatory Research concluded that the head loss methodology should be redeveloped and correlated against test data. It also recognized that the available head loss test data did not include the effects of water temperature on a debris-laden sump screen, did not provide data for a broad enough range of CalSil and Nukon concentrations on a sump screen to address a large portion of expected PWR sump screen conditions, and did not address head loss resulting from the accumulation of coating debris on a sump screen. In addition, all previous testing involved the use of a woven metal screen to represent the sump screen. In contrast, many of the proposed PWR sump designs use perforated metal plates instead of woven metal screens and are designed for lower water approach velocities. To support the development of an improved head loss correlation and provide test data to address these concerns, the NRC sponsored additional testing, which is documented in NUREG/CR-6917, "Experimental Measurements of Pressure Drop Across Debris Beds on PWR Sump Screens in Support of Generic Safety Issue 191," issued January 2007.

The goal of the NRC's activities is to enhance the safety of nuclear power plants and not to perform research activities that will answer all the unknown behavior observed during testing. To this end, this document develops a conservative bounding methodology for calculating head loss through a sump screen, but still conforms to conventional theory for calculating pressure drop through a porous medium such as a debris-laden sump screen.



Brian Sheron, Director
Office of Nuclear Regulatory Research
U.S. Nuclear Regulatory Commission

CONTENTS

	<u>Page</u>
ABSTRACT	iii
FOREWORD	v
EXECUTIVE SUMMARY	xv
ABBREVIATIONS	xvii
NOTATION	xix
1. INTRODUCTION	1
2. HEAD LOSS ACROSS A DEBRIS-COVERED SUMP SCREEN	3
2.1 Approaches for Calculating Head Loss Across a Porous Medium	3
2.2 Viscous Component for Pressure Drop Through a Porous Medium	5
2.3 Pressure Drop Through a Woven Metal Screen	8
2.4 Kinetic Component for Pressure Drop Through a Porous Medium	10
2.5 Head Loss Across a Clean Unclogged Sump Screen	11
2.5.1 Screen Pressure Drop for LANL/UNM Tests	13
2.5.2 Pressure Drops for PNNL Tests with a Woven Metal Screen or Perforated Plate ...	14
2.6 Recommended Pressure Drop Equations	15
2.7 Temperature Upper Limit	18
3. COMPRESSIBILITY OF A DEBRIS BED ON A SUMP SCREEN	23
3.1 Pressure Forces Through a Porous Medium with Flowing Liquid	24
3.2 Compressibility of a Porous Medium During the First Compression	25
3.3 Compressibility of a Porous Medium After the First Compression	26
4. DETERMINATION OF DEBRIS BED AND MATERIAL PROPERTIES	27
4.1 Mass of Debris Bed Constituents During Testing	31
4.1.1 Constituent Debris Bed Masses for PNNL Tests	31
4.1.2 Constituent Debris Bed Masses for LANL/UNM Tests	36
4.2 Reference Debris Bed Thickness at Low-Velocity Formation	36
4.2.1 Low-Velocity Reference Debris Bed Thickness Using PNNL Test Data	37
4.2.2 Low-Velocity Reference Debris Bed Thickness Using LANL/UNM Series 6 Test Data	41
4.2.3 Low-Velocity Reference Debris Bed Thickness Using LANL/UNM and PNNL Test Data	42
4.3 Material Properties and Empirical Values for the Head Loss Equation	44
4.3.1 Determination of Material Properties	44
4.3.2 Determination of Multiplier and Exponent Values for Kinetic Term of the Head Loss Equation	45

4.4	Particulate Maximum Concentration Model for Nukon/CalSil Debris Beds	46
4.4.1	Nukon/CalSil Maximum Concentration Model Developed Using PNNL Test Data	46
4.5	Material-Specific Compression Parameter Determination	58
4.5.1	Determination of Material-Specific Parameter Using PNNL Test Data	58
4.5.2	Determination of Material-Specific Parameter Using LANL/UNM Series 6 Test Data	61
4.5.3	Recommended Material-Specific Parameter Value	61
5.	GUIDELINES FOR CALCULATING HEAD LOSS THROUGH A DEBRIS BED	63
5.1	Application Limits	63
5.1.1	Approach Velocity Limit	63
5.1.2	Temperature Limit	63
5.2	Pressure Drop and Compressibility Across a One-Volume Debris Bed	64
5.2.1	Debris Characteristic Values	64
5.2.2	Head Loss Application Procedure for a One-Volume Nukon/CalSil Debris Bed	64
5.2.3	Head Loss Application Procedure for a One-Volume Nukon Debris Bed	68
5.2.4	Head Loss Application Procedure for a One-Volume CalSil Debris Bed	68
5.3	Pressure Drop and Compressibility Across a Two-Volume Debris Bed	70
5.3.1	Description of a Two-Volume Nukon/CalSil Debris Bed Model	70
5.3.2	Head Loss Application Procedure for a Two-Volume Nukon/CalSil Debris Bed	72
5.3.3	Head Loss Application Procedure for a Two-Volume Oversaturated CalSil Debris Bed	77
6.	COMPARISONS OF HEAD LOSS PREDICTIONS WITH TEST DATA	81
6.1	PNNL Large Head Loss Test Facility	81
6.2	Comparisons of Head Loss Predictions with PNNL Test Data	83
6.2.1	Comparison of Head Loss Predictions to PNNL Series 1 Tests	84
6.2.2	Comparison of Head Loss Predictions to PNNL Series 2 Tests	103
6.2.3	Comparison of Head Loss Predictions to PNNL Coatings Tests	142
6.3	Comparisons of Head Loss Predictions to ANL Benchmark Test Data	144
6.3.1	Comparison of Head Loss Predictions to ANL Benchmark Tests	145
6.3.2	Comparison of Head Loss Data for the ANL and PNNL Benchmark Tests	150
6.4	Comparisons of Head Loss Predictions with LANL/UNM Test Data	156
7.	CONCLUSIONS	171
8.	REFERENCES AND BIBLIOGRAPHY	173
8.1	References	173
8.2	Bibliography	174

FIGURES

	<u>Page</u>
2.2-1 Multiplier for Viscous Term of Ergun Equation for Porous Medium Consisting of Cylindrical Fibers Perpendicular to Flow	7
2.2-2 Multiplier for Viscous Term of Ergun Equation for Porous Medium Composed of Spherical Particles	7
2.5-1 Wire Screen and Perforated Plate Used in PNNL Head Loss Testing	14
2.7-1 Downstream Void Fraction Versus Water Temperature at 14.5 psia (1.0×10^5 Pa)	19
2.7-2 Downstream Void Fraction Versus Water Temperature at 20 psia (1.38×10^5 Pa)	19
2.7-3 Downstream Void Fraction Versus Screen Pressure Drop at 14.5 psia (1.0×10^5 Pa)	20
2.7-4 Downstream Void Fraction Versus Screen Pressure Drop at 20 psia (1.38×10^5 Pa)	20
2.7-5 Maximum Allowable Sump Pool Water Temperature and Total Containment Pressure Versus Sump Screen Pressure Drop	21
3.0-1 Volume Reduction Mechanisms for Granular and Fibrous Materials	23
3.1-1 Pressure Distribution in a Porous Medium	24
4.0-1 Transition from Homogeneous to Local Saturation Condition for PNNL Nukon/CalSil Test 051117_NC_2776_L1	28
4.2-1 Initial Low-Velocity Debris Bed Thickness Using PNNL Series 1 Test Data	37
4.2-2 Comparison of Initial Low-Velocity Debris Bed Thickness Using PNNL Series 1 Test Data	39
4.2-3 Comparison of Initial Low-Velocity Debris Bed Thickness Using PNNL Series 2 Test Data	40
4.2-4 Initial Low-Velocity Debris Bed Thickness Using LANL Series 6 Test Data	41
4.2-5 Initial Low-Velocity Debris Bed Thickness Using PNNL, LANL and ANL Test Data	43
4.2-6 Initial Formation Debris Bed Thickness Test Data for a 0.03 m/s Approach Velocity	43
4.4-1 CalSil Particle End Volume Bed Density in a Nukon/CalSil Debris Bed	50
4.4-2 CalSil End Volume Porosity in a Nukon/CalSil Debris Bed	50
4.4-3 CalSil End Volume Bed Thickness in a Nukon/CalSil Debris Bed	51
4.4-4 Head Loss Comparisons for PNNL Test 051115_NC_4098_L1 to Determine Y	52
4.4-5 Head Loss Comparisons for PNNL Test 051117_NC_2776_L1 to Determine Y	52
4.4-6 Head Loss Comparisons for PNNL Test 051121_NC_1586_L1 to Determine Y	53
4.4-7 Head Loss Comparisons for PNNL Test 051123_NC_2181_L1 to Determine Y	53
4.4-8 Head Loss Comparisons for PNNL Test 051128_NC_2776_L2 to Determine Y	54
4.4-9 Head Loss Comparisons for PNNL Test 060331_NC_2024_LP1 to Determine Y	54
4.4-10 Head Loss Comparisons for PNNL Test 060817_NC_2024_LP1 to Determine Y	55
4.4-11 Head Loss Comparisons for PNNL Test 060509_NC_0505_LP1 to Determine Y	55
4.4-12 Head Loss Comparisons for PNNL Test 060426_NC_0708_LP1 to Determine Y	56
4.4-13 Head Loss Comparisons for PNNL Test 060807_NC_0708_LP1 to Determine Y	56
4.4-14 Head Loss Comparisons for PNNL Test 060809_NC_0708_LP1 to Determine Y	57
4.4-15 Head Loss Comparisons for PNNL Test 060517_NC_0808_LP1 to Determine Y	57
4.5-1 Debris Bed Plastic First Compression Parameter Using PNNL Test Data	59
4.5-2 Debris Bed Elastic Compression Parameter Using PNNL Test Data	59
4.5-3 Debris Bed Plastic First Compression Parameter Using PNNL and ANL Test Data	60
4.5-4 Debris Bed Elastic Compression Parameter Using PNNL and ANL Test Data	60
4.5-5 Bed Plastic First Compression Parameter Using LANL/UNM Series 6 Test Data	62
4.5-6 Debris Bed Elastic Compression Parameter Using LANL/UNM Series 6 Test Data	62
5.3-1 Debris Bed Compression	71
6.1-1 Schematic of PNNL Large Head Loss Test Facility	82
6.2-1 Comparison of Measured and Correlation Loss Coefficient Versus Approach Velocity	87

6.2-2	Comparison of Measured and Correlation Loss Coefficient Versus Reynolds Number.	87
6.2-3	Measured Pressure Drop Used for Irreversible Loss Coefficient Calculation	88
6.2-4	PNNL Test Data Showing Head Loss Dependence on Debris Distribution in Bed	89
6.2-5	Head Loss for PNNL Series 1 Nukon-Only Test 051108_NO_3067_L1	92
6.2-6	Bed Thickness for PNNL Series 1 Nukon-Only Test 051108_NO_3067_L1	92
6.2-7	Head Loss for PNNL Series 1 Nukon-Only Test 060125_NO_3067_L1	93
6.2-8	Bed Thickness for PNNL Series 1 Nukon-Only Test 060125_NO_3067_L1	93
6.2-9	Head Loss for PNNL Series 1 Nukon/CalSil Test 051110_NC_0595_L1	97
6.2-10	Bed Thickness for PNNL Series 1 Nukon/CalSil Test 051110_NC_0595_L1	97
6.2-11	Head Loss for PNNL Series 1 Nukon/CalSil Test 051115_NC_4098_L1	98
6.2-12	Bed Thickness for PNNL Series 1 Nukon/CalSil Test 051115_NC_4098_L1	98
6.2-13	Head Loss for PNNL Series 1 Nukon/CalSil Test 051117_NC_2776_L1	99
6.2-14	Bed Thickness for PNNL Series 1 Nukon/CalSil Test 051117_NC_2776_L1	99
6.2-15	Head Loss for PNNL Series 1 Nukon/CalSil Test 051128_NC_2776_L2	100
6.2-16	Bed Thickness for PNNL Series 1 Nukon/CalSil Test 051128_NC_2776_L2	100
6.2-17	Head Loss for PNNL Series 1 Nukon/CalSil Test 051121_NC_1586_L1	101
6.2-18	Bed Thickness for PNNL Series 1 Nukon/CalSil Test 051121_NC_1586_L1	101
6.2-19	Head Loss for PNNL Series 1 Nukon/CalSil Test 051123_NC_2181_L1	102
6.2-20	Bed Thickness for PNNL Series 1 Nukon/CalSil Test 051123_NC_2181_L1	102
6.2-21	Measured and Correlation Loss Coefficients Versus Approach Velocity	105
6.2-22	Measured and Correlation Loss Coefficients Versus Reynolds Number.	105
6.2-23	Measured Pressure Drop Used for Irreversible Loss Coefficient Calculation	106
6.2-24	Head Loss for PNNL Series 2 Nukon-Only Test 060425_NO_2703_LP1	108
6.2-25	Bed Thickness for PNNL Series 2 Nukon-Only Test 060425_NO_2703_LP1	108
6.2-26	Head Loss for PNNL Series 2 Nukon-Only Test 060425_NO_2703_LP2	109
6.2-27	Bed Thickness for PNNL Series 2 Nukon-Only Test 060425_NO_2703_LP2	109
6.2-28	Head Loss for PNNL Series 2 Nukon-Only Test 060425_NO_2703_LP3	110
6.2-29	Bed Thickness for PNNL Series 2 Nukon-Only Test 060425_NO_2703_LP3	110
6.2-30	Head Loss for PNNL Series 2 Benchmark Nukon-Only Test 060321_NO_0405_LP1	111
6.2-31	Bed Thickness for Series 2 Benchmark Nukon-Only Test 060321_NO_0405_LP1	111
6.2-32	Head Loss for PNNL Series 2 Benchmark Nukon-Only Test 060313_NO_1349_LP1	112
6.2-33	Bed Thickness for PNNL Series 2 Benchmark Nukon-Only Test 060313_NO_1349_LP1	112
6.2-34	Head Loss for PNNL Series 2 Nukon-Only Test 060731_NO_2073_LP1	113
6.2-35	Bed Thickness for PNNL Series 2 Nukon-Only Test 060731_NO_2073_LP1	113
6.2-36	Head Loss for PNNL Series 2 Nukon-Only Test 060731_NO_2073_LP2	114
6.2-37	Bed Thickness for PNNL Series 2 Nukon-Only Test 060731_NO_2073_LP2	114
6.2-38	Head Loss for PNNL Series 2 Nukon-Only Test 060802_NO_2073_LP1	115
6.2-39	Bed Thickness for PNNL Series 2 Nukon-Only Test 060802_NO_2073_LP1	115
6.2-40	Head Loss for PNNL Series 2 Nukon-Only Test 060802_NO_2073_LP2	116
6.2-41	Bed Thickness for PNNL Series 2 Nukon-Only Test 060802_NO_2073_LP2	116
6.2-42	Head Loss for PNNL Series 2 Benchmark Nukon/CalSil Test 060323_NC_1619_LP1	119
6.2-43	Bed Thickness for Series 2 Benchmark Nukon/CalSil Test 060323_NC_1619_LP1	119
6.2-44	Head Loss for PNNL Series 2 Benchmark Nukon/CalSil Test 060323_NC_1619_LP1	120
6.2-45	Head Loss for PNNL Series 2 Nukon/CalSil Test 060331_NC_2024_LP1	121
6.2-46	Bed Thickness for PNNL Series 2 Nukon/CalSil Test 060331_NC_2024_LP1	121
6.2-47	Head Loss for PNNL Series 2 Nukon/CalSil Test 060331_NC_2024_LP1	122
6.2-48	Head Loss for PNNL Series 2 Nukon/CalSil Test 060817_NC_2024_LP1	123
6.2-49	Bed Thickness for PNNL Series 2 Nukon/CalSil Test 060817_NC_2024_LP1	123
6.2-50	Head Loss for PNNL Series 2 Nukon/CalSil Test 060817_NC_2024_LP1	124

6.2-51	Head Loss for PNNL Series 2 Nukon/CalSil Test 060509_NC_0505_LP1	125
6.2-52	Bed Thickness for PNNL Series 2 Nukon/CalSil Test 060509_NC_0505_LP1	125
6.2-53	Head Loss for PNNL Series 2 Nukon/CalSil Test 060509_NC_0505_LP1	126
6.2-54	Head Loss for PNNL Series 2 Nukon/CalSil Test 060426_NC_0708_LP1	127
6.2-55	Bed Thickness for PNNL Series 2 Nukon/CalSil Test 060426_NC_0708_LP1	127
6.2-56	Head Loss for PNNL Series 2 Nukon/CalSil Test 060426_NC_0708_LP1	128
6.2-57	Head Loss for PNNL Series 2 Nukon/CalSil Test 060807_NC_0708_LP1	129
6.2-58	Bed Thickness for PNNL Series 2 Nukon/CalSil Test 060807_NC_0708_LP1	129
6.2-59	Head Loss for PNNL Series 2 Nukon/CalSil Test 060807_NC_0708_LP1	130
6.2-60	Head Loss for PNNL Series 2 Nukon/CalSil Test 060809_NC_0708_LP1	131
6.2-61	Bed Thickness for PNNL Series 2 Nukon/CalSil Test 060809_NC_0708_LP1	131
6.2-62	Head Loss for PNNL Series 2 Nukon/CalSil Test 060809_NC_0708_LP1	132
6.2-63	Head Loss for PNNL Series 2 Nukon/CalSil Test 060517_NC_0808_LP1	133
6.2-64	Bed Thickness for PNNL Series 2 Nukon/CalSil Test 060517_NC_0808_LP1	133
6.2-65	Head Loss for PNNL Series 2 Nukon/CalSil Test 060517_NC_0808_LP1	134
6.2-66	Temperature Sensitivity for PNNL Nukon Test 060425_NO_2703_LP1, LP2, LP3	138
6.2-67	Temperature Sensitivity for PNNL Nukon/CalSil Test 060426_NC_0708_LP1, LP2	138
6.2-68	Temperature Sensitivity for First Velocity Cycle of PNNL Nukon-Only Tests	139
6.2-69	Temperature Sensitivity for First Velocity Cycle of PNNL Nukon/CalSil_0708 Tests	139
6.2-70	Temperature Sensitivity for First Velocity Cycle of PNNL Nukon/CalSil_2024 Tests	140
6.2-71	Data and One-Volume Predictions for First Velocity Cycle of Nukon-Only Tests	140
6.2-72	Data and Two-Vol. Predictions for First Velocity Cycle of Nukon/CalSil_0708 Tests	141
6.2-73	Data and Two-Vol. Predictions for First Velocity Cycle of Nukon/CalSil_2024 Tests	141
6.2-74	Head Loss for Alkyd Coatings Test 060501_PQC_2609_LP1, LP2	143
6.3-1	Head Loss for ANL BM-1 Benchmark Nukon Test BM-1-A2-N4.6	146
6.3-2	Bed Thickness for ANL BM-1 Benchmark Nukon Test BM-1-A2-N4.6	146
6.3-3	Head Loss for ANL BM-1 Benchmark Nukon Test BM-1-A2-N4.4 repeat2	147
6.3-4	Bed Thickness for ANL BM-1 Benchmark Nukon Test BM-1-A2-N4.4 repeat2	147
6.3-5	Head Loss for ANL BM-2 Benchmark Nukon Test BM-2-A2-N15.5	148
6.3-6	Bed Thickness for ANL BM-2 Benchmark Nukon Test BM-2-A2-N15.5	148
6.3-7	Head Loss for ANL BM-2 Benchmark Nukon Test BM-2-A2-N15.5 repeat	149
6.3-8	Bed Thickness for ANL BM-2 Benchmark Nukon Test BM-2-A2-N15.5 repeat	149
6.3-9	Head Loss Data for ANL and PNNL BM-1 Benchmark Nukon Tests	153
6.3-10	Bed Thickness Data for ANL and PNNL BM-1 Benchmark Nukon Tests	153
6.3-11	Head Loss Data for ANL and PNNL BM-2 Benchmark Nukon Tests	154
6.3-12	Bed Thickness Data for ANL and PNNL BM-2 Benchmark Nukon Tests	154
6.3-13	Head Loss Data for ANL and PNNL BM-3 Benchmark Nukon/CalSil Tests	155
6.3-14	Bed Thickness Data for ANL and PNNL BM-3 Benchmark Nukon/CalSil Tests	155
6.4-1	Head Loss for LANL/UNM Nukon-Only Test 1a	158
6.4-2	Bed Thickness for LANL/UNM Nukon-Only Test 1a	158
6.4-3	Head Loss for LANL/UNM Nukon-Only Test 1a Using 80 Percent Added Mass	159
6.4-4	Head Loss for LANL/UNM Nukon/CalSil Test 6b	161
6.4-5	Bed Thickness for LANL/UNM Nukon/CalSil Test 6b	161
6.4-6	Head Loss for LANL/UNM Nukon/CalSil Test 6e	163
6.4-7	Bed Thickness for LANL/UNM Nukon/CalSil Test 6e	163
6.4-8	Head Loss for LANL/UNM Nukon/CalSil Test 6e2	164
6.4-9	Bed Thickness for LANL/UNM Nukon/CalSil Test 6e2	164
6.4-10	Head Loss for LANL/UNM Nukon/CalSil Test 6f	166
6.4-11	Bed Thickness for LANL/UNM Nukon/CalSil Test 6f	166

6.4-12	Head Loss for LANL/UNM Nukon/CalSil Test 6h	168
6.4-13	Bed Thickness for LANL/UNM Nukon/CalSil Test 6h	168
6.4-14	Head Loss for LANL/UNM Nukon/CalSil Test 6i	170
6.4-15	Bed Thickness for LANL/UNM Nukon/CalSil Test 6i	170

TABLES

		<u>Page</u>
2.5-1	Screen Multiplier (k') for $50 < Re_{\text{screen}} < 1000$	12
2.5-2	Thick Plate Multiplier (τ)	12
2.5-3	Low Reynolds Number Multiplier (ϵ_{oRe})	13
2.5-4	Dimensions of Wire Screen and Perforated Plate Used in PNNL Head Loss Testing	14
2.7-1	Acceptable Range of Sump Pool Water Temperature	21
4.0-1	Conditions for a Fiber/Particle (e.g., Nukon/CalSil) Debris Bed	30
4.1-1	Debris Mass Summary for PNNL Tests	33
4.1-2	Debris Bed Masses Used for the PNNL Test Calculations	35
4.1-3	Debris Bed Mass Comparison for Similar PNNL and LANL/UNM Tests	36
4.3-1	Debris Properties for Head Loss Calculations	44
4.4-1	CalSil End Volume Concentration Conditions Determined from PNNL Test Data	49
5.2-1	Recommended Bounding Debris Properties for Head Loss Calculations	64
6.2-1	PNNL Series 1 and LANL/UNM Head Loss Tests Using a Metal Screen	85
6.2-2	PNNL Series 2 Including Benchmark Head Loss Tests Using a Perforated Plate	104
6.2-3	Debris Bed Temperature Sensitivity	135
6.2-4	Coatings Systems Used for PNNL Head Loss Testing	142
6.2-5	PNNL Coatings Head Loss Tests Using a Perforated Plate	142
6.3-1	ANL Benchmark Head Loss Tests Using a Perforated Plate	144
6.3-2	Debris Mass Summary for ANL Tests	145
6.3-3	Calculated Mass Fractions in Debris Bed for ANL Tests	145
6.3-4	PNNL Series 2 Benchmark Head Loss Tests Using a Perforated Plate	150
6.3-5	Debris Bed Comparisons of the PNNL and ANL Benchmark Tests	150
6.4-1	Debris Bed Mass Comparisons for Similar PNNL and LANL/UNM Tests	156

EXECUTIVE SUMMARY

In 1996, the U.S. Nuclear Regulatory Commission (NRC) established Generic Safety Issue (GSI) 191, “Potential Impact of Debris Blockage on Emergency Recirculation During Design-Basis Accidents at PWRs” (Ref. 1), to identify, prioritize, and resolve concerns regarding debris blockage of the sump screens in the emergency core cooling system (ECCS) and containment spray system (CSS) of a pressurized-water reactor (PWR). Specifically, GSI-191 deals with the possibility that in the event of a loss-of-coolant accident (LOCA) within the containment of a PWR, thermal insulation and other materials (e.g., coatings and concrete) in the vicinity of the pipe break may be damaged and dislodged as debris. A fraction of that debris may subsequently be transported to the containment recirculation sump(s), where it may accumulate on the sump screen(s). Over time, the accumulated debris could potentially form a bed that progressively blocks the screen(s) and exceeds the net positive suction head (NPSH) safety margin of the ECCS and/or CSS pump(s).

Following several strainer clogging events at boiling-water-reactors (BWRs), the NRC Office of Nuclear Regulatory Research (RES) contracted with Science and Engineering Associates to perform a parametric evaluation of the susceptibility of a reference plant to a loss of NPSH margin attributable to debris blockage of suppression pool strainers. This evaluation formed the basis for NUREG/CR-6224, “Parametric Study of the Potential for BWR ECCS Strainer Blockage Due to LOCA-Generated Debris,” which the NRC published in October 1995 (Ref. 2). The agency published additional information regarding the testing and analysis activities performed in support of GSI-191 in NUREG/CR-6874, “GSI-191: Experimental Studies of Loss-of-Coolant-Accident-Generated Debris Accumulation and Head Loss with Emphasis on the Effects of Calcium Silicate Insulation,” issued May 2005 (Ref. 3).

The NRC’s Advisory Committee on Reactor Safeguards, Thermal-Hydraulic Subcommittee, raised concerns regarding the application of the NUREG/CR-6224 methodology for calculating head loss through debris-covered sump screens (Ref. 4). In September 2004, the RES staff received two additional documents authored by Dr. G. Wallis, “NUREG/CR-6224 Head Loss Correlation” (Ref. 5) and “Flow Through a Compressible Mat: Analysis of the Data Presented in Series 6 Test Reported by LANL in LA-UR-04-1227” (Ref. 6), which technically reviewed and critiqued the head loss calculational method recommended in NUREG/CR-6224. The RES staff independently assessed these two documents (Ref. 7). As a result of the technical comments contained in the two documents, the RES staff concluded that the head loss methodology should be redeveloped and correlated against test data. Consequently, as a result of this review of the NUREG/CR-6224 head loss methodology, the RES staff has revised the head loss calculational method to obtain better agreement with existing and new test data and to conform more closely with conventional theory.

The goal of the NRC’s activities is to enhance the safety of nuclear power plants and not to perform research activities that will answer all the unknown behavior observed during testing. To this end, it is appropriate to develop a conservative bounding methodology for calculating head loss through a sump screen. Consequently, the staff has adjusted the head loss calculational methods described in this report to provide conservative predictions that bound test data and have an improved theoretical basis.

The equations and procedures developed to calculate the head loss and compressibility for flow across a porous medium debris bed have been applied to debris beds composed of fiberglass thermal insulation fibers (Nukon) and calcium silicate (CalSil) insulation particles. The equations account for the kinetic and viscous contributions to pressure drop. The compressibility of the porous medium debris bed is considered by initially assuming an irreversible, inelastic process followed by elastic behavior with

constant compressibility. Semiempirical relations and constants required to solve the flow and compression relations have been determined using data obtained from testing performed at the Pacific Northwest National Laboratory (PNNL), Los Alamos National Laboratory/University of New Mexico (LANL/UNM), and Argonne National Laboratory (ANL).

The iterative procedure developed to solve the flow and compression relations using a one-volume, homogeneous debris bed model has been successful in providing upper bound pressure drop estimates for PNNL, LANL/UNM, and ANL tests for flow across a debris bed composed of one debris type (e.g., Nukon fibers). The pressure drop across a debris bed composed of two debris types (e.g., fibers and particles) depends on the distribution of the two debris types in the bed. Consequently, two approaches have been used to estimate the upper and lower bound pressure drops across a debris bed composed of two debris types. The lower bound pressure drop solves the flow and compression relations using a one-volume model of the debris bed with a homogeneous distribution of the two debris types. The upper bound pressure drop is calculated by using a two-volume, nonhomogeneous model that assumes that the particles concentrate or saturate a part of the fiber bed.

The head loss calculations for a Nukon-only debris bed using the one-volume model predict comparable or slightly higher values than the PNNL, LANL/UNM, and ANL test data. The one-volume head loss predictions for a homogeneous Nukon/CalSil debris bed provide a reasonable lower pressure drop limit when compared to available test data. The two-volume head loss predictions for the nonhomogeneous Nukon/CalSil debris bed provide an upper limit for pressure drop test data for most test comparisons; however, for some test cases, the two-volume approach underpredicts the measured pressure drop. These underpredictions are related to the empirical equation developed to calculate the thickness of the concentrated CalSil particle layer within a Nukon fiber debris bed. Although this empirical equation provides adequate concentration thickness values for large CalSil thicknesses, at lower CalSil thicknesses, small differences in determining concentration thickness can result in large changes in the calculated pressure drop. Consequently, the methodology to calculate the concentrated particle thickness in a fiber bed needs to be improved for smaller CalSil concentration thicknesses.

In summary, the methodology described in this report provides a verified approach to calculate head losses across a sump screen covered with Nukon, a Nukon/CalSil mixture, and CalSil. The one-volume calculational method can provide good or conservative estimates of pressure drop across a debris bed composed of one debris type. For debris beds composed of particles and fibers, the two-volume calculational method can predict conservative pressure drops for larger CalSil concentration thicknesses and can provide an adequate estimate of pressure drop, in the correct order of magnitude, for debris beds with lower CalSil concentration thicknesses. The methodology described in this report is based on new test data that provide high-quality measurements of head loss, debris bed thickness, and the constituent masses of the debris bed for a range of approach velocities and water temperatures.

In addition, it can generally be concluded that the pressure drop across a debris bed depends on water temperature as well as on the flows and temperatures to which the debris bed has been exposed. The developed calculational method generally predicts higher pressure drops at lower liquid temperatures, which follows classical theory expectations.

ABBREVIATIONS

ACRS	Advisory Committee on Reactor Safeguards (NRC)
ANL	Argonne National Laboratory
BWR	boiling-water reactor
°C	degree Celsius
cc	cubic centimeter
CalSil	calcium silicate
CSS	containment spray system
ECCS	emergency core cooling system
°F	degree Fahrenheit
ft	foot
ft/s	foot per second
g	gram
GSI	generic safety issue
in	inch
kg	kilogram
LANL	Los Alamos National Laboratory
lbm	pound mass
LOCA	loss-of-coolant accident
m	meter
m/s	meter per second
NPSH	net positive suction head
NRC	U.S. Nuclear Regulatory Commission
Pa	Pascal

psi	pounds per square inch
psia	pounds per square inch absolute
PNNL	Pacific Northwest National Laboratory
PWR	pressurized-water reactor
RES	Office of Nuclear Regulatory Research (NRC)
UNM	University of New Mexico

NOTATION

A	total cross-sectional surface area of debris bed, screen or perforated plate
A_{plate}	flow area through perforated plate
A_{screen}	flow area through screen
a	empirical multiplier
b	multiplier for the kinetic term of porous medium pressure drop equation (equals 1.95 for a cylindrical fibrous bed, 3.89 for a spherical particle bed)
b_c	material-specific parameter ($b_c = 1$) for porous medium compression
c	exponent for the kinetic term of porous medium pressure drop equation (equals 0.071 for a cylindrical fibrous bed, 0.13 for a spherical particle bed)
c_m	solid material concentration density for porous medium compression
d_h	hydraulic diameter of flow area through a screen or perforated plate
$\text{dens}_{\text{CalSil}}$	CalSil debris bed density (mass per debris bed volume)
$\text{dens}_{\text{CalSilmax}}$	maximum saturated CalSil debris bed density (mass per debris bed volume)
$\text{dens}_{\text{debris}}$	total debris bed mass over total debris bed area
$\text{dens}_{\text{fiber}}$	fiber debris bed density (mass per debris bed volume)
$\text{dens}_{\text{Nukon}}$	Nukon debris bed density (mass per debris bed volume)
$\text{dens}_{\text{particle}}$	particle debris bed density (mass per debris bed volume)
$\text{dens}_{\text{particlesatmax}}$	maximum saturated particle debris bed density (mass per debris bed volume)
D_p	mean particle diameter for a packed bed
f	flow area of screen or perforated plate divided by the total screen or plate area
f_k	porous medium friction factor
k'	multiplier for low Reynolds numbers from Reference 22 (Table 2.5-1)
k_k	Kozeny constant
K	permeability
$K(X)$	dimensionless permeability function
K_{plate}	irreversible loss coefficient for clean unclogged perforated plate
K_{screen}	irreversible loss coefficient for clean unclogged screen
L	thickness of porous medium
$L_{\text{debrisbed}}$	debris bed thickness
L_{screen}	screen thickness
L_{sheet}	sheet thickness
$L'_{\text{debrisbed}}$	debris bed thickness (m) at an approach velocity of about 0.0305 m/s (0.1 ft/s)
ΔL	thickness for a debris bed composed of a single debris type
$\Delta L'_{\text{entr}}$	thickness of control volume at debris bed entrance at a reference bed formation approach velocity
$\Delta L'_{\text{exit}}$	thickness of particle saturated control volume at debris bed exit at a reference bed formation approach velocity
$\Delta L_{\text{debrisbed}}$	debris bed thickness
$\Delta L_{\text{debrisbedsubscript}}$	control volume bed thickness
$\Delta L'_{\text{debrisbedsubscript}}$	control volume bed thickness at reference bed formation approach velocity
$\Delta L_{\text{initial}}$	debris bed thickness at a reference bed formation approach velocity
ΔL_{min}	thickness of debris bed saturated with CalSil particles
ΔL_{pmax}	debris bed thickness at highest approach velocity
ΔL_{total}	total bed thickness
m_{CalSil}	CalSil mass in the debris bed
$m_{\text{CalSilentr}}$	CalSil particle mass in entrance volume

$m_{\text{CalSilentr}}^{\text{tot}}$	total CalSil mass in entrance volume
$m_{\text{CalSilexit}}$	CalSil mass in exit control volume
$m_{\text{CalSilfiber}}$	CalSil fiber mass in debris bed
$m_{\text{CalSiltotal}}$	total fiber and particle CalSil mass
m_{Nukon}	Nukon mass in the debris bed
$m_{\text{Nukonentr}}$	fiber mass in entrance control volume
$m_{\text{Nukonexit}}$	Nukon mass in exit control volume
m_{solid}	mass of solid material in the debris bed
$m_{\text{fract}}^{\text{fiber}}$	fiber mass fraction in total CalSil mass
M	material-specific empirical constant for porous medium compression
N	material-specific parameter for porous medium compression
P_h	hydraulic pressure of the fluid flow
P_i	inlet pressure upstream of the porous medium
P_m	mechanical stress exerted on the porous medium
P_m'	mechanical stress for the first compression of the porous medium at bed formation
P_{max}	highest compressive stress to which the porous material has been exposed
P_o	outlet pressure downstream of the porous medium
P_{screen}	perimeter of flow area through a metal screen
P_{tot}	total applied pressure on a porous medium
Δp	pressure drop
$\Delta p'_{\text{debrisbed}}$	debris pressure drop at a reference bed formation approach velocity
$\Delta p'_{\text{debrisbedsubscript}}$	control volume pressure drop at a reference bed formation approach velocity
Δp_{contr}	irreversible contraction pressure drop at debris bed entrance
$\Delta p_{\text{debrisbed}}$	debris bed pressure drop
$\Delta p_{\text{debrisbedsubscript}}$	debris bed control volume pressure drop
$\Delta p_{\text{expexit}}$	irreversible expansion pressure drop for the part of the debris bed exit with flow
$\Delta p_{\text{irreversibleloss}}$	irreversible pressure drop
Δp_{plate}	pressure drop (head loss) across a clean unclogged perforated plate
Δp_{pmax}	pressure drop at highest approach velocity
$\Delta p_{\text{pmaxsubscript}}$	control volume pressure drop at highest approach velocity
Δp_{screen}	pressure drop (head loss) across a clean unclogged screen
Δp_{total}	total pressure drop across the debris bed and screen or perforated plate
ΔP_h	pressure drop across porous medium
ΔP_{ha}	pressure drop across porous medium at $y = a$
Re_{plate}	Reynolds number using plate flow area A_{plate} and hydraulic diameter
Re_{screen}	Reynolds number using screen flow area A_{screen} and hydraulic diameter
S_{CalSil}	CalSil specific surface area in debris bed
S_{CalSilf}	specific surface area of fiber material of CalSil in debris bed
S_{Nukon}	Nukon specific surface area in debris bed
S_v	specific surface area
t	thickness
V	approach velocity through cross-sectional area of porous medium
Vol_{CalSil}	volume of CalSil in porous medium
$Vol_{\text{CalSilsubscript}}$	CalSil volume in debris bed control volume
Vol_{Nukon}	volume of Nukon in porous medium
$Vol_{\text{Nukonsubscript}}$	Nukon volume in debris bed control volume
Vol_{solid}	volume of solid material in porous medium
$Vol_{\text{solidsubscript}}$	Nukon and CalSil volume in debris bed control volume
Vol_{tot}	total volume of porous medium

Vol_{total}	total debris bed volume
$Vol_{totalsubscript}$	total debris bed volume of control volume
Vol_{void}	void volume of porous medium
$Vol_{voidsubscript}$	void volume in debris bed control volume
X	void ratio
X'	void ratio at P_m' for the first compression at bed formation
X'_{debris}	void ratio at a reference bed formation approach velocity
$X'_{debrissubscript}$	control volume void ratio at a reference bed formation approach velocity
$X(P_{max})$	void ratio at P_{max}
X_{CalSil}	CalSil void ratio in debris bed (equals $Vol_{void} / Vol_{CalSil}$)
$X_{CalSilsubscript}$	effective void ratio of CalSil in debris bed control volume
X_{debris}	void ratio
$X_{debrissubscript}$	control volume void ratio
X_{Nukon}	Nukon void ratio in debris bed (equals Vol_{void} / Vol_{Nukon})
$X_{Nukonsubscript}$	effective void ratio of Nukon in debris bed control volume
X_{pmax}	void ratio at Δp_{pmax}
$X_{pmaxsubscript}$	control volume void ratio at Δp_{pmax}
Y	ratio of particle density in the particle concentrated volume and the fiber bed density

Greek

α	constant multiplier for the viscous term of porous medium pressure drop equation
β	constant multiplier for the kinetic term of porous medium pressure drop equation
β_t	compressibility of the total volume
β_v	compressibility of the void volume
ε	porosity
ε'_{debris}	debris bed porosity at a reference bed formation approach velocity
ε_{CalSil}	porosity of CalSil in debris bed
$\varepsilon_{CalSil_{sat}}$	CalSil particle saturation porosity in end Nukon/CalSil volume
$\varepsilon_{CalSil_{subscript}}$	effective porosity of CalSil in debris bed control volume
ε_{debris}	debris bed porosity (equals Vol_{void} / Vol_{tot})
$\varepsilon_{debrisentr}$	porosity at debris bed entrance
$\varepsilon_{debrisexit}$	porosity at debris bed exit
$\varepsilon_{debrissubscript}$	control volume porosity
ε_{Nukon}	porosity of Nukon in debris bed
$\varepsilon_{Nukon_{subscript}}$	effective porosity of Nukon in debris bed control volume
ε_{oRe}	parameter for calculating pressure drop across a perforated plate or screen
ζ_{ϕ}	parameter for calculating pressure drop across a perforated plate or screen
ζ_{1qu}	parameter for calculating pressure drop across a perforated plate or screen
λ	wall friction factor from Reference 22 (Moody friction factor)
μ	fluid absolute viscosity
μ_{water}	water absolute viscosity
ρ	fluid density
ρ_{CalSil}	CalSil material density
$\rho_{CalSilf}$	density of fiber material in CalSil
ρ_{Nukon}	Nukon material density
ρ_{solid}	density of solid material in the debris bed
ρ_{water}	water density

τ multiplier from Diagram 8-3 of Reference 22 (Table 2.5-2)

Subscripts

entr entrance control volume
exit exit control volume

1. INTRODUCTION

In 1996, the U.S. Nuclear Regulatory Commission (NRC) established Generic Safety Issue (GSI) 191, “Potential Impact of Debris Blockage on Emergency Recirculation During Design-Basis Accidents at PWRs” (Ref. 1), to identify, prioritize, and resolve concerns regarding debris blockage of the sump screens in the emergency core cooling system (ECCS) and containment spray system (CSS) of a pressurized-water reactor (PWR). Specifically, GSI-191 deals with the possibility that debris could accumulate on—and potentially block—the sump screen during or following a loss-of-coolant accident (LOCA) or other high-energy line break and thereby impede or prevent reactor cooling during recirculation. The concern is that in the event of a LOCA within the containment of a PWR, thermal insulation and other materials (e.g., coatings and concrete) in the vicinity of the pipe break may be damaged and dislodged as debris. A fraction of that debris may subsequently be transported to the containment recirculation sump(s), where it may accumulate on the sump screen(s). Over time, the accumulated debris could potentially form a bed that progressively blocks the screen(s) and exceeds the net positive suction head (NPSH) safety margin of the of the ECCS and/or CSS pump(s). In particular for sump screens, excessive head loss across the debris bed may prevent water from entering the sump and thereby impede or prevent the flow of water to cool the reactor core.

In support of the NRC’s resolution of boiling-water reactor (BWR) suppression pool strainer blockage issues, the NRC Office of Nuclear Regulatory Research (RES) contracted with Science and Engineering Associates to perform a parametric evaluation of the susceptibility of a reference plant to a loss of NPSH margin attributable to debris blockage of suppression pool strainers. To represent the debris that might be present following a LOCA, the study used fibrous thermal insulation shreds and fibers. The study concluded that debris blockage could lead to a rapid loss of NPSH margin for most postulated breaks. This evaluation formed the basis for NUREG/CR-6224, “Parametric Study of the Potential for BWR ECCS Strainer Blockage Due to LOCA-Generated Debris,” which the NRC published in October 1995 (Ref. 2). The NRC also contracted with Los Alamos National Laboratory (LANL) to perform additional head loss testing using different insulation types to further support the calculation method proposed in NUREG/CR-6224. The NRC published additional information regarding the testing and analysis activities performed in support of GSI-191 in NUREG/CR-6874, “GSI-191: Experimental Studies of Loss-of-Coolant-Accident-Generated Debris Accumulation and Head Loss with Emphasis on the Effects of Calcium Silicate Insulation,” issued May 2005 (Ref. 3).

The NRC’s Advisory Committee on Reactor Safeguards (ACRS), Thermal-Hydraulic Subcommittee, raised concerns regarding the application range of the NUREG/CR-6224 methodology for calculating head loss through debris-covered sump screens (Ref. 4). In September 2004, the RES staff received two additional documents by Dr. G. Wallis, “NUREG/CR-6224 Head Loss Correlation” (Ref. 5) and “Flow Through a Compressible Mat: Analysis of the Data Presented in Series 6 Test Reported by LANL in LA-UR-04-1227” (Ref. 6), which technically reviewed and critiqued the head loss calculational method recommended in NUREG/CR-6224. These documents criticized the NUREG/CR-6224 head loss equation and the compression relation for the debris bed, indicating that the head loss calculation method should not be based on variances in the specific surface area of the debris and should not theoretically correct to vary debris specific surface area as a function of bed thickness (the “thin bed” effect). The documents further indicated that the NUREG/CR-6224 compression relation for the debris bed was inconsistent with the limited test data and that additional test data were needed.

The RES staff independently assessed the ACRS comments (Ref. 7). As a result of the technical comments contained in the two ACRS review documents, the RES staff concluded that the head loss methodology should be redeveloped and correlated against test data. Consequently, as a result of this

review of the NUREG/CR-6224 head loss methodology, the RES staff has revised the head loss calculational method to obtain better agreement with test data and to conform more closely with conventional theory. The RES staff also contracted for additional testing to provide high-quality data to reduce uncertainties in the head loss calculational method.

The goal of the NRC's activities is to enhance the safety of nuclear power plants and not to perform research activities that will answer all the unknown behavior observed during testing. To this end, it is appropriate to develop a conservative bounding methodology for calculating head loss through a sump screen. The following sections describe a head loss calculation method that provides predictions that more closely match test data and have a better theoretical basis.

Section 2 presents derivations and details the basis for a methodology for calculating a pressure drop across a debris-covered screen.

Section 3 discusses the debris bed compression model for a debris-covered sump screen.

Section 4 develops the values for the initial conditions and empirical parameters needed for the pressure drop calculational method described in Sections 2 and 3.

Section 5 provides the calculational procedures for predicting head loss across a sump screen covered with Nukon fiberglass insulation, calcium silicate (CalSil) insulation, and Nukon/CalSil mixture debris beds.

Section 6 compares the predictions obtained using the pressure drop calculational methods described in Section 5 with previously available and new test data.

Section 7 presents the report conclusions.

Section 8 lists the references cited in this report and provides the bibliography.

2. HEAD LOSS ACROSS A DEBRIS-COVERED SUMP SCREEN

As indicated in Reference 1, during periods of recirculation pump operation following a LOCA at a PWR, a debris-covered sump screen can produce a substantial increase in pressure drop when compared to a clean unclogged screen. The NRC had previously published a proposed method to calculate the pressure drop or head loss across a sump screen covered with a porous medium debris bed (Refs. 2 and 3). However, the ACRS questioned the appropriateness of this method in References 4, 5, and 6. The RES staff provided an initial assessment of these concerns in Reference 7.

This section develops an improved method to calculate the steady-state pressure drop across a debris-covered sump screen by assuming that the debris consists of fibers and particles that can be treated as a porous medium. The correlations developed in this section assume that steady-state flow conditions exist through the porous medium.

2.1 Approaches for Calculating Head Loss Across a Porous Medium

For viscous (laminar) flow through a porous medium, pressure drop for one-phase flow can be calculated using the classical Darcy equation (Ref. 8). The Darcy equation can be written as:

$$\frac{\Delta p}{L} = \frac{\mu V}{K} \quad (2.1-1)$$

where

Δp	pressure drop
L	thickness of porous medium
μ	fluid absolute viscosity
V	approach velocity through cross-sectional area of porous medium
K	permeability

For flow at higher Reynolds numbers, the pressure drop equation must include a kinetic (turbulent) term. The equation used to determine the pressure drop across a packed bed composed of spherical particles is the Ergun equation presented in Reference 8. The Ergun equation, which was derived to model flow through a packed bed with a spherical particle diameter of D_p , possesses viscous and kinetic terms. The multipliers to the viscous and kinetic terms, 150 and 1.75, are semiempirical multipliers that were determined using experimental measurements.

$$\frac{\Delta p}{L} = \frac{\text{Viscous Term}}{D_p^2} + \frac{\text{Kinetic Term}}{D_p} \quad (2.1-2)$$

$$\frac{\Delta p}{L} = \frac{150 \mu V}{D_p^2 \varepsilon^3} + \frac{1.75 \rho V^2}{D_p \varepsilon^3}$$

where

ε	porosity
D_p	mean particle diameter for a packed bed
ρ	fluid density

The specific surface area, S_v , is defined as the ratio of the surface area of the solid portion of a porous medium divided by the solid volume of a porous medium. Geometric considerations can be used to relate the specific surface area to the mean particle or fiber diameter. Therefore, for a porous medium composed of spherical particles, S_v can be defined as:

$$S_v = 6 / D_p \quad \text{for a porous medium composed of spherical particles (Ref. 7)} \quad (2.1-3)$$

where

S_v specific surface area

Using equation (2.1-3) for a porous medium composed of spherical particles, the Ergun equation can be written as:

$$\frac{\Delta p}{L} = 4.167 \mu V S_v^2 \frac{(1-\epsilon)^2}{\epsilon^3} + 0.2917 \rho V^2 S_v \frac{(1-\epsilon)}{\epsilon^3} \quad (2.1-4)$$

The relationship between S_v and D_p for packed beds composed of cylindrical fibers oriented perpendicular to the flow direction can also be determined using geometrical considerations.

$$S_v = 4 / D_p \quad \text{for a porous medium composed of cylinders (Ref. 8)} \quad (2.1-5)$$

The Ergun equation for a porous medium composed of cylindrical fibers can be written as:

$$\frac{\Delta p}{L} = 9.375 \mu V S_v^2 \frac{(1-\epsilon)^2}{\epsilon^3} + 0.4375 \rho V^2 S_v \frac{(1-\epsilon)}{\epsilon^3} \quad (2.1-6)$$

The Ergun equation can be written in a more general form using the specific surface area of the porous medium.

$$\frac{\Delta p}{L} = \alpha \mu V S_v^2 \frac{(1-\epsilon)^2}{\epsilon^3} + \beta \rho V^2 S_v \frac{(1-\epsilon)}{\epsilon^3} \quad (2.1-7)$$

Viscous Term Kinetic Term

where

α constant multiplier for the viscous term

β constant multiplier for the kinetic term

The Darcy equation and the viscous component of the Ergun equation both solve the same flow condition. Therefore, the viscous term in the Ergun equation can be replaced with the Darcy equation.

$$\frac{\Delta p}{L} = \frac{\mu V}{K} + \beta \rho V^2 S_v \frac{(1-\epsilon)}{\epsilon^3} \quad (2.1-8)$$

The relations presented in this section assume that the value of the specific surface area, S_v , is constant for all porosities and Reynolds numbers. Reference 9 questions whether the values for the specific surface area vary with porosity and Reynolds number. References 10, 12, 13, 14, and 15 provide multipliers for S_v that vary with porosity and Reynolds number. The following sections will develop pressure drop correlations in the general form of the Ergun equation that use empirical multipliers to provide variations with porosity and Reynolds number.

2.2 Viscous Component for Pressure Drop Through a Porous Medium

References 10 and 11 relate the classical Darcy equation to the particle properties in the viscous term of the Ergun equation using the Kozeny-Carman equation, which provides a relationship between K , S_v , and ε for flow around particles in a porous medium packed bed.

$$K = \frac{\varepsilon^3}{k_k S_v^2 (1-\varepsilon)^2} \quad (2.2-1)$$

where

k_k Kozeny constant

Reference 10 lists the values for the Kozeny constant for different types of beds. For beds composed of sand and randomly packed powders, k_k has been determined to be approximately equal to 5.0. For flow through beds of glass spheres, the value of k_k ranges between 4.50 and 4.65.

Inserting equation (2.2-1) for K into the modified form of the Ergun equation (2.1-8) results in the following relationship.

$$\frac{\Delta p}{L} = k_k \mu V S_v^2 \frac{(1-\varepsilon)^2}{\varepsilon^3} + \beta \rho V^2 S_v \frac{(1-\varepsilon)}{\varepsilon^3} \quad (2.2-2)$$

By comparing equation (2.1-7) and equation (2.2-2), it can be concluded that k_k in equation (2.2-2) is equal to the α in equation (2.1-7). The values of the Kozeny constant, k_k , are also close in value to the constant multiplier, 4.167, in Ergun equation (2.1-4) for a packed bed composed of spherical particles.

Reference 10 provides permeability relationships for flow in a porous medium composed of cylindrical fibrous materials and for a packed bed composed of spherical particles. To provide these relationships, a dimensionless permeability function, $K(X)$, is related to the Kozeny constant, k_k , and the void ratio, X . These parameters are defined as follows.

$$K(X) = \frac{X^3}{k_k (1+X)^2} \quad (2.2-3)$$

$$X = \text{Vol}_{\text{void}} / \text{Vol}_{\text{solid}} = \varepsilon / (1 - \varepsilon) \quad (2.2-4)$$

where

$K(X)$ dimensionless permeability function

X void ratio

Vol_{void} void volume of porous medium

$\text{Vol}_{\text{solid}}$ volume of solid material in porous medium

Equation (2.2-3) can be solved for k_k using the definition for void ratio, X .

$$k_k = \frac{X^3}{K(X) (1+X)^2} \quad (2.2-5)$$

The void ratio is related to the porosity by the following equation.

$$\varepsilon = \frac{\text{Vol}_{\text{void}}}{\text{Vol}_{\text{tot}}} = \frac{X}{(1+X)} \quad (2.2-6)$$

where

Vol_{tot} total volume of porous medium

Reference 10 provides the following relationships, called the Happel free surface model (Refs. 12, 13, and 14), for calculating $K(X)$ for flow around cylindrical fibrous materials in the following orientations.

For flow perpendicular to fiber cylinders:

$$K(X) = -0.5 + 0.5 \ln(1+X) + \frac{1}{(2 + 2X + X^2)} \quad (2.2-7)$$

For flow parallel to fiber cylinders:

$$K(X) = \ln(1+X) - \frac{X(1+1.5X)}{(1+X)^2} \quad (2.2-8)$$

For a bed composed of spherical particles, Reference 10 provides the following relationship.

$$K(X) = 2 - \frac{3}{(1+X)^{1/3}} + \frac{5}{3(1+X)^{5/3} + 2} \quad (2.2-9)$$

Figure 2.2-1 plots the values of the empirical Kozeny constant (9.375) used in equations (2.1-6) and (2.2-2) and the values calculated using the Happel model ($X^3/(K(X)(1+X)^2)$) in equations (2.2-5) and (2.2-7) for a porous medium composed of cylindrical fibers perpendicular to the flow direction as a function of porosity. Figure 2.2-2 compares the Kozeny constant (4.167) for a porous medium composed of spherical particles from equations (2.1-4) and (2.2-2) with values calculated using the Happel model ($X^3/(K(X)(1+X)^2)$) in equations (2.2-5) and (2.2-9). These figures show that the values for the Kozeny constant and the comparative value calculated using the Happel model are similar in magnitude. This favorable comparison qualitatively indicates the acceptability of the Happel models. References 12 and 13 indicate that the Happel relations are not appropriate for porosities less than about 0.4 to 0.5. However, Figures 2.2-1 and 2.2-2 show that the values of the Kozeny constant (k_k) are relatively constant below these porosities. The three relations for $K(X)$ result in unrealistic values at the low and high ends. Consequently, the application of these equations should be limited to $X > 1.0 \times 10^{-4}$. References 12 and 13 also indicate that the Happel equations have not been compared to test data with porosities greater than about 0.994. Consequently, the application of these equations should be limited to $\varepsilon < 0.995$. Therefore, for a bed composed of spherical particles, equation (2.2-5) is limited to the following values.

$$\frac{X^3}{K(X)(1+X)^2} = 132.47 \quad \text{for } \varepsilon \geq 0.995 \quad (2.2-10)$$

$$\frac{X^3}{K(X)(1+X)^2} = 5.0 \quad \text{for } X \leq 1.0 \times 10^{-4} \quad (2.2-11)$$

Similar limits should be applied to the equations for the fibrous materials.

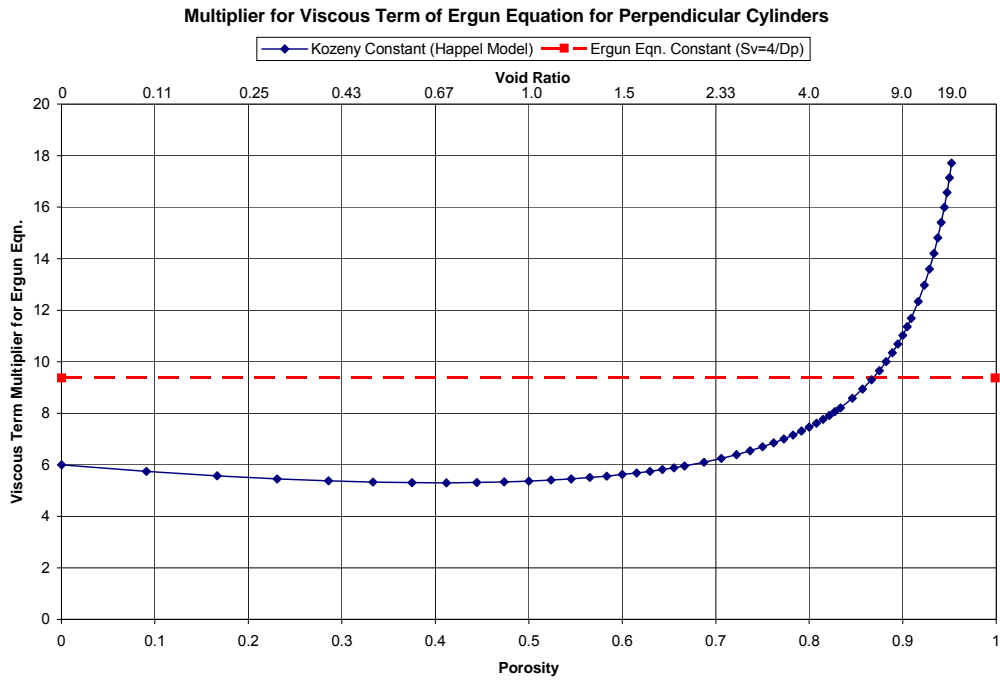


Figure 2.2-1 Multiplier for Viscous Term of Ergun Equation for Porous Medium Consisting of Cylindrical Fibers Perpendicular to Flow

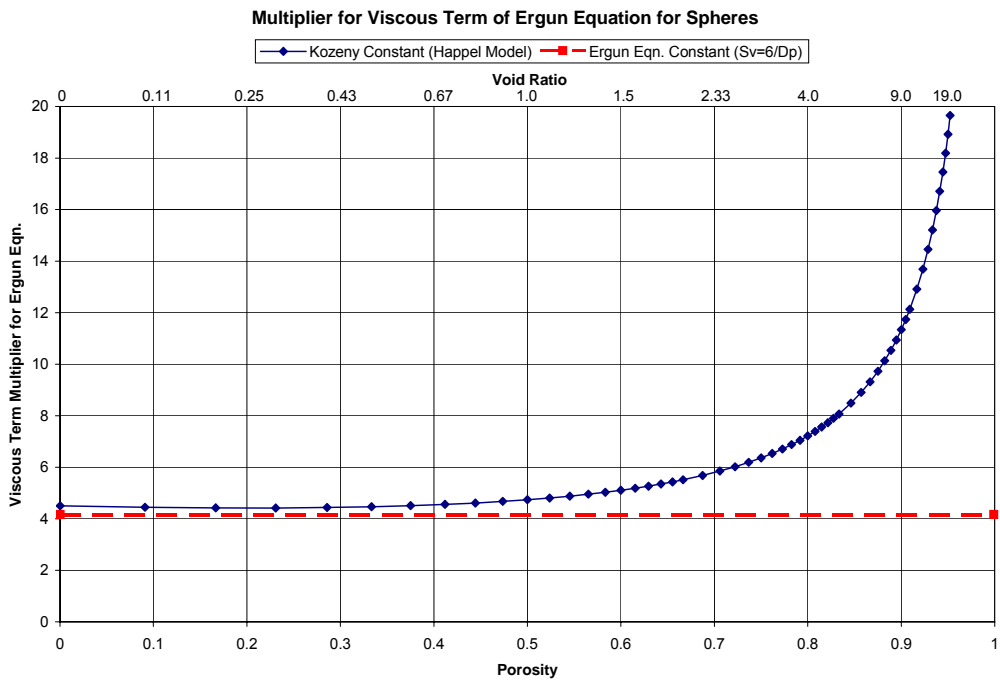


Figure 2.2-2 Multiplier for Viscous Term of Ergun Equation for Porous Medium Composed of Spherical Particles

Finally, equation (2.2-5) can be inserted into equation (2.2-2) to write the viscous term of the Ergun equation in the following form.

$$\frac{\Delta p}{L} = \mu V S_v^2 \frac{\text{Viscous Term}}{K(X) (1+X)^2} \frac{(1-\epsilon)^2}{\epsilon^3} + \beta \rho V^2 S_v \frac{\text{Kinetic Term}}{\epsilon^3} \quad (2.2-12)$$

Reference 10 indicates that the approach used to develop the viscous flow term for the pressure drop equation can be applied to a gel medium.

Equation (2.2-12) can be further simplified by using the definitions for void ratio (X) and porosity (ϵ). If one debris type comprises the debris bed, the void ratio as defined in equation (2.2-4) can be written as:

$$X = \frac{A L \rho_{\text{solid}}}{m_{\text{solid}}} - 1 \quad (2.2-13)$$

where

A debris bed cross-sectional surface area
 m_{solid} mass of solid material in the debris bed
 ρ_{solid} density of solid material in the debris bed

The porosity can also be simplified.

$$\epsilon = 1 - \frac{m_{\text{solid}}}{A L \rho_{\text{solid}}} \quad (2.2-14)$$

Using these two relations, equation (2.2-12) can be written as:

$$\frac{\Delta p}{L} = \frac{\mu V S_v^2}{K(X)} \frac{\text{Viscous Term}}{A L \rho_{\text{solid}}} + \beta \rho V^2 S_v \frac{\text{Kinetic Term}}{\epsilon^3} \quad (2.2-15)$$

In many cases, the viscous term dominates the pressure drop through a porous medium. If the pressure drop contribution of the kinetic term can be ignored, using equation (2.2-15), the pressure drop can be simplified to the following equation for a bed composed of a single debris type such as spherical particles.

$$\Delta p = \frac{\mu V S_v^2}{K(X)} \frac{m_{\text{solid}}}{A \rho_{\text{solid}}} \quad (2.2-16)$$

This form of the viscous equation is similar to the Darcy equation (2.1-1).

2.3 Pressure Drop Through a Woven Metal Screen

Reference 15 provides a version of the Ergun equation that can be used to calculate the pressure drop for flow through clean unclogged woven metal screens similar to those used in many older PWR sump screen designs. This approach applies the methods used to calculate pressure drop across a porous medium to flow across a woven metal screen. The equations to calculate flow through a plain square-type screen have been verified using a large number of data points. All the test data have been shown to fall with ± 30 percent of the results calculated using this method. Reference 15 also provides different empirical

multipliers to enable application of the analytical approach to screen designs with different weaves in addition to a plain square-type screen. Using the Ergun approach for flow through a granular porous material, Reference 15 starts with the following equations to calculate pressure drop across a plain square-type woven metal screen.

$$\frac{\Delta p}{L} = \frac{f_k \rho V^2 (1-\varepsilon)}{D_p \varepsilon^3} \quad (2.3-1)$$

$$f_k = a \frac{(1-\varepsilon)}{Re} + b \left[\frac{(1-\varepsilon)}{Re} \right]^c \quad (2.3-2)$$

$$D_p = 6 / S_v$$

where

- f_k porous medium friction factor
- D_p equivalent diameter for a packed bed with spherical particles = $6 / S_v$
- S_v screen-specific surface area
- a, b, c empirical multipliers

Equations (2.3-1) and (2.3-2) can be combined to produce an equation similar in form to the Ergun equation (2.1-2).

$$\frac{\Delta p}{L} = \frac{a \rho V^2}{Re D_p} \frac{(1-\varepsilon)^2}{\varepsilon^3} + b \left[\frac{(1-\varepsilon)}{Re} \right]^c \frac{\rho V^2}{D_p} \frac{(1-\varepsilon)}{\varepsilon^3} \quad (2.3-3)$$

Using the following modified Reynolds number definition, equation (2.3-3) can be written as:

$$Re = \frac{\rho V D_p}{\mu} = \frac{\rho V 6}{\mu S_v} \quad (2.3-4)$$

$$\frac{\Delta p}{L} = \frac{a \mu V}{D_p^2} \frac{(1-\varepsilon)^2}{\varepsilon^3} + b \left[\frac{(1-\varepsilon)}{Re} \right]^c \frac{\rho V^2}{D_p} \frac{(1-\varepsilon)}{\varepsilon^3} \quad (2.3-5)$$

Equation (2.3-5) would be equivalent to the Ergun equation (2.1-2) if:

$$a = 150, \quad b \left[\frac{(1-\varepsilon)}{Re} \right]^c = 1.75 \quad (b=1.75, c = 0)$$

For application to a plain square-type metal screen that is similar to the screen design found in many existing PWR sump screens, Reference 15 recommends that:

$$a = 250, b = 1.69, c = 0.071 \quad \text{for } 0.5 < \frac{Re}{(1-\varepsilon)} < 9.85 \times 10^4 \text{ and } 0.602 < \varepsilon < 0.919$$

Reference 15 recommends different values of a and b for different woven metal screen designs.

Equation (2.3-3) or (2.3-5) can be rewritten using the screen-specific surface area with $D_p = 6 / S_v$.

$$\frac{\Delta p}{L} = \frac{a \mu V S_v^2}{36} \frac{(1-\varepsilon)^2}{\varepsilon^3} + b \left[\frac{(1-\varepsilon) \mu S_v}{\rho V 6} \right]^c \frac{\rho V^2 S_v}{6} \frac{(1-\varepsilon)}{\varepsilon^3} \quad (2.3-6)$$

2.4 Kinetic Component for Pressure Drop Through a Porous Medium

Equation (2.2-12) provides a form of the pressure drop equation that should be used to calculate the pressure drop across a porous medium debris bed.

$$\frac{\Delta p}{L} = \mu V S_v^2 \frac{\text{Viscous Term}}{K(X) (1+X)^2} \frac{(1-\varepsilon)^2}{\varepsilon^3} + \beta \rho V^2 S_v \frac{\text{Kinetic Term}}{\varepsilon^3} \quad (2.2-12)$$

This equation provides a method for calculating the viscous term for pressure drop; however, a methodology must be developed to address the calculation of the kinetic term. Specifically, a value or relation for β must be determined. Consistent with the recommendation for $K(X)$, it appears necessary to specify a different relation for β for a bed composed of particles and one composed of cylindrical fibers.

As indicated in Section 2.3, Reference 15 developed a porous medium friction factor defined in equation (2.3-2).

$$f_k = a \frac{(1-\varepsilon)}{Re} + b \left[\frac{(1-\varepsilon)}{Re} \right]^c \quad (2.3-2)$$

where Re is defined by equation (2.3-4):

$$Re = \frac{\rho V D_p}{\mu} = \frac{\rho V 6}{\mu S_v} \quad (2.3-4)$$

The first term of equation (2.2-12) calculates the viscous portion of the pressure drop, and the second term provides the kinetic pressure drop relation. As indicated in Reference 15 and Section 2.3, it would appear appropriate to specify β in equation (2.2-10) using the following form.

$$\beta = b \left[\frac{(1-\varepsilon)}{Re} \right]^c$$

Consistent with the head loss equation for a porous medium, Reference 15 developed a general equation to calculate pressure drop across a woven metal screen of any weave. The developed values for parameters a , b , and c are:

$$a = 138, b = 1.95, c = 0.071 \quad \text{for } 0.5 < \frac{Re}{(1-\varepsilon)} < 9.85 \times 10^4 \text{ and } 0.564 < \varepsilon < 0.919$$

Reference 15 indicates that this relation has a greater deviation from data than the empirical variable recommended for specific screen weaves. However, it is recommended that these values for b and c serve as the starting values for calculating the kinetic term of the pressure drop across a bed composed of fibrous cylindrical materials.

Reference 16 provides empirical values for a , b , and c for a bed composed of spherical particles.

$$a = 150, b = 3.89, c = 0.13 \quad \text{for } 440 < Re < 7.92 \times 10^4 \text{ and } 0.38 < \varepsilon < 0.44$$

The values for b and c should be used as starting values for calculating the kinetic term of the pressure drop across a bed composed of spherical particles.

Therefore, the pressure drop equation across a porous medium takes the following form.

$$\frac{\Delta p}{L} = \underbrace{\mu V S_v^2 \frac{X^3}{K(X)(1+X)^2} \frac{(1-\varepsilon)^2}{\varepsilon^3}}_{\text{Viscous Term}} + \underbrace{b \left[\frac{(1-\varepsilon)}{Re} \right]^c \frac{\rho V^2}{D_p} \frac{(1-\varepsilon)}{\varepsilon^3}}_{\text{Kinetic Term}} \quad (2.4-1)$$

Using the definition of Reynolds number, this equation can be written in the following form.

$$\frac{\Delta p}{L} = \underbrace{\mu V S_v^2 \frac{X^3}{K(X)(1+X)^2} \frac{(1-\varepsilon)^2}{\varepsilon^3}}_{\text{Viscous Term}} + \underbrace{b \left[\frac{(1-\varepsilon) \mu S_v}{\rho V 6} \right]^c \frac{\rho V^2 S_v}{6} \frac{(1-\varepsilon)}{\varepsilon^3}}_{\text{Kinetic Term}} \quad (2.4-2)$$

2.5 Head Loss Across a Clean Unclogged Sump Screen

The pressure drop across a clean unclogged, thin ($L_{\text{screen}}/d_h < 0.015$), plain, square-type circular metal wire screen can be calculated using the irreversible pressure drop multiplier obtained from the *Handbook of Hydraulic Resistance* (Ref. 22). Using Diagram 8-6 of Reference 22, the irreversible pressure drop for the clean unclogged screen used in the head loss tests described in NUREG/CR-6874 (Ref. 3) can be calculated using the following equations.

$$\Delta p = K_{\text{screen}} \rho V^2 / 2 \quad (2.5-1)$$

$$K_{\text{screen}} = 1.3 (1 - f) + (1/f - 1)^2 \quad \text{for } Re_{\text{screen}} \geq 10^3 \quad (2.5-2)$$

$$K_{\text{screen}} = k' [1.3 (1 - f) + (1/f - 1)^2] \quad \text{for } 50 < Re_{\text{screen}} < 10^3 \quad (2.5-2a)$$

$$f = A_{\text{screen}} / A \quad (2.5-3)$$

where

- d_h hydraulic diameter of flow area through a screen (equals $4 A_{\text{screen}} / P_{\text{screen}}$)
- L_{screen} screen thickness
- Δp pressure drop (head loss) across a clean unclogged screen
- ρ fluid density
- V approach flow velocity upstream of screen
- K_{screen} irreversible loss coefficient for clean unclogged screen
- k' multiplier for low Reynolds numbers from Table 2.5-1 in Diagram 8-6 of Reference 22
- P_{screen} perimeter of flow area through a metal screen
- Re_{screen} Reynolds number using screen flow area A_{screen} and screen hydraulic diameter
- A_{screen} flow area through screen
- A total cross-sectional surface area of screen

Table 2.5-1 Screen Multiplier (k') for 50 < Re_{screen} < 1000

Re _{screen}	50	100	150	200	300	400	500	1000
k'	1.44	1.24	1.13	1.08	1.03	1.01	1.01	1.00

For a clean unclogged thin perforated sheet of metal, Diagram 8-1 of Reference 22 suggests the following equation to calculate the loss coefficient.

$$K_{\text{plate}} = [0.707 (1 - f)^{1/2} + 1 - f]^2 / f^2 \quad \text{for } L_{\text{sheet}} / d_h < 0.015 \text{ and } Re_{\text{plate}} > 10^5 \quad (2.5-4)$$

$$f = A_{\text{plate}} / A \quad (2.5-5)$$

where

- K_{plate} irreversible loss coefficient for clean unclogged perforated plate
- L_{sheet} sheet thickness
- d_h hydraulic diameter of flow area through the perforated sheet
- Re_{plate} Reynolds number using plate flow area A_{plate} and hydraulic diameter
- A_{plate} flow area through perforated plate

For a thick perforated sheet of metal, Diagram 8-3 of Reference 22 suggests the following equation to calculate the loss coefficient.

$$K_{\text{plate}} = \{ [0.5 + \tau (1 - f)^{1/2}] (1 - f) + (1 - f)^2 + \lambda L_{\text{sheet}} / d_h \} / f^2 \quad \text{for } L_{\text{sheet}} / d_h > 0.015 \text{ and } Re_{\text{plate}} > 10^5 \quad (2.5-6)$$

where

- τ multiplier from Table 2.5-2 in Diagram 8-3 of Reference 22
- λ wall friction factor from Reference 22 (Moody friction factor)

Table 2.5-2 Thick Plate Multiplier (τ)

L _{sheet} /d _h	0.0	0.2	0.4	0.6	0.8	1.0	1.2	1.6	2.0	2.4
τ	1.35	1.22	1.10	0.84	0.42	0.24	0.16	0.07	0.02	0.0

For a screen or perforated plate with laminar or transition flow through the plate open area, Reference 22 recommends the following relation. Diagram 8-5 in Reference 22 provides the values for the variables contained in the equation.

$$K_{\text{plate}} = \zeta_{\phi} / f^2 + \epsilon_{\text{oRe}} \zeta_{\text{1qu}} \quad \text{for } 30 < Re_{\text{plate}} < 10^4\text{-}10^5 \quad (2.5-7)$$

where

- ζ_φ = f (Re_{plate}, f) value from Diagram 8-5 of Reference 22
- ε_{oRe} = f (Re_{plate}) multiplier from Table 2.5-3 in Diagram 8-5 of Reference 22
- ζ_{1qu} = K_{plate} value from Equation (2.5-2), (2.5-4), or (2.5-6) depending on value of L_{sheet} / d_h

Table 2.5-3 Low Reynolds Number Multiplier (ϵ_{oRe})

Re_{plate}	25	40	60	10^2	2×10^2	4×10^2	10^3	2×10^3	4×10^3	10^4	2×10^4	10^5
ϵ_{oRe}	0.34	0.36	0.37	0.40	0.42	0.46	0.53	0.59	0.64	0.74	0.81	0.94

The previously described wire screen and perforated plate pressure drop equations can be related to the woven metal screen equation discussed in Section 2.3. Specifically, for a plain square-type woven metal screen, equation (2.3-6) can be related to equation (2.5-1).

$$\frac{\Delta p}{L} = \frac{250 \mu V S_v^2}{36} \frac{(1-\epsilon)^2}{\epsilon^3} + 1.69 \left[\frac{(1-\epsilon) \mu S_v}{\rho V 6} \right]^{0.071} \frac{\rho V^2 S_v}{6} \frac{(1-\epsilon)}{\epsilon^3} \quad (2.5-8)$$

$$\text{for } 0.5 < \frac{Re}{(1-\epsilon)} < 9.85 \times 10^4 \text{ and } 0.602 < \epsilon < 0.919$$

Using equations (2.5-1) and (2.5-2), the pressure drop across a plain square metal screen can be written as:

$$\Delta p = k' [1.3 (1 - A_{screen} / A) + (A / A_{screen} - 1)^2] \rho V^2 / 2 \quad \text{for } 50 < Re_{screen} < 10^3 \quad (2.5-9)$$

$$\Delta p = [1.3 (1 - A_{screen} / A) + (A / A_{screen} - 1)^2] \rho V^2 / 2 \quad \text{for } Re_{screen} \geq 10^3 \quad (2.5-10)$$

As seen in Table 2.5-1, the value for k' is very close to 1.0 for Reynolds numbers greater than 400. Therefore, the general equation for pressure drop across a plain square metal screen can be approximated using the form of equation (2.5-10). Specifically, the following equation could be used.

$$\Delta p \approx [1.3 (1 - A_{screen} / A) + (A / A_{screen} - 1)^2] \rho V^2 / 2 \quad \text{for } Re_{screen} \geq 400 \quad (2.5-11)$$

2.5.1 Screen Pressure Drop for LANL/UNM Tests

NUREG/CR-6874 does not provide a detailed description of the debris screen or the underlying support screen used during debris sump screen testing performed at the University of New Mexico (UNM) for LANL. The report states that the debris screen was a 1/8-inch rectangular mesh and describes the support screen as a perforated sheet of metal. The flow area fraction through the debris screen was estimated to be about 55 percent, and the flow area fraction through the support screen under the debris screen was estimated to be about 44 percent. If the support screen is assumed to be about 1/32-inch (0.794 mm) thick, the support screen is defined as a thick plate. For the range of test temperatures from 70 to 142 °F (21.2 to 61.1 °C), and the range of approach velocities from 0.1 to 2.0 ft/s (0.0305 to 0.61 m/s), the Reynolds number for flow through the screen (Re_{screen}) is calculated to range from 177 to 7680. This Reynolds number range results in a form loss coefficient multiplier (k') for equation (2.5-2) ranging from about 1.1 for the low Reynolds number to 1.0 for Re_{screen} greater than 1000. Using a form loss coefficient multiplier of 1.0, the loss coefficient for the debris screen is calculated to be 1.25, and the loss coefficient for the supporting screen is calculated to be 6.95. Therefore, if the total loss coefficient for this test facility in an unclogged condition is assumed to be the sum of the loss coefficients for the debris and support screens, the total head loss across both screens can be calculated using the following equation.

$$\Delta p_{screen} = (K_{screen} + K_{plate}) \rho V^2 / 2 \approx 8.2 \rho V^2 / 2 \quad (2.5-12)$$

Consequently, the total head loss across a debris screen is the sum of the pressure drop across the debris

bed and the pressure drop across the clean unclogged sump screen given by equation (2.5-12).

2.5.2 Pressure Drops for PNNL Tests with a Woven Metal Screen or Perforated Plate

The Pacific Northwest National Laboratory (PNNL) performed debris head loss tests for flow through a woven metal screen and a perforated plate. PNNL conducted the tests to obtain the pressure drop through a clean unclogged metal screen and a clean unclogged perforated plate in order to verify the irreversible loss coefficient relations provided in Section 2.5. Table 2.5-4 provides descriptions of the woven metal screen and the perforated plate used in the PNNL tests. Figure 2.5-1 shows pictures of the screen and plate used for the PNNL tests.

Table 2.5-4 Dimensions of Wire Screen and Perforated Plate Used in PNNL Head Loss Testing

Description	Percent Open Area (%)	Dimension and Shape of Open Area ((inch) / (m) / shape)	Center to Center Pitch of Open Area (inch) / (m)
5 Mesh Woven Metal Wire Screen	41	0.128 / 0.00325 / square	0.200 / 0.00508
Perforated Plate with 60° Staggered Centers	40	0.125 / 0.00318 diameter / circle	0.188 / 0.00478



Wire Screen Welded In Support Ring



Woven Metal Wire Screen



Perforated Metal Plate

Figure 2.5-1 Wire Screen and Perforated Plate Used in PNNL Head Loss Testing

Tests performed to obtain the pressure drop and irreversible loss coefficient across the clean unclogged wire mesh screen verified the acceptability of the Idelchik (Ref. 22) loss coefficient relation for a mesh

Equation (2.6-2) can also be written in the following form, which matches the viscous term to the form of the Darcy equation as shown in equation (2.2-13).

$$\frac{\Delta p_{\text{debris bed}}}{\Delta L_{\text{debris bed}}} = \underbrace{\frac{\mu V S_v^2}{K(X)} \frac{m_{\text{solid}}}{A \Delta L_{\text{debris bed}} \rho_{\text{solid}}}}_{\text{Viscous Term}} + \underbrace{b \left[\frac{(1-\varepsilon) \mu S_v}{\rho V 6} \right]^c \frac{\rho V^2 S_v}{6} \frac{(1-\varepsilon)}{\varepsilon^3}}_{\text{Kinetic Term}} \quad (2.6-3)$$

where

A debris bed cross-sectional surface area
 m_{solid} mass of solid material in the debris bed
 ρ_{solid} density of solid material in the debris bed

The following equations account for the presence of two debris types, Nukon and CalSil, in the debris bed. These equations use the viscous pressure drop term from equation (2.2-12) and the kinetic term from equation (2.4-2) to account for the varying proportions of Nukon and CalSil in the debris bed.

$$\frac{\Delta p_{\text{debris bed}}}{\Delta L_{\text{debris bed}}} = \left[\frac{S_{\text{Nukon}}^2 X_{\text{Nukon}}^3}{K(X_{\text{Nukon}}) (1+X_{\text{Nukon}})^2} \frac{(1-\varepsilon_{\text{Nukon}})^2}{\varepsilon_{\text{Nukon}}^3} + \frac{S_{\text{CalSil}}^2 X_{\text{CalSil}}^3}{K(X_{\text{CalSil}}) (1+X_{\text{CalSil}})^2} \frac{(1-\varepsilon_{\text{CalSil}})^2}{\varepsilon_{\text{CalSil}}^3} \right] \mu V + \left[S_{\text{Nukon}} 1.95 \left[\frac{(1-\varepsilon_{\text{Nukon}}) \mu S_{\text{Nukon}}}{\rho V 6} \right]^{0.071} \frac{(1-\varepsilon_{\text{Nukon}})}{\varepsilon_{\text{Nukon}}^3} + S_{\text{CalSil}} 3.89 \left[\frac{(1-\varepsilon_{\text{CalSil}}) \mu S_{\text{CalSil}}}{\rho V 6} \right]^{0.13} \frac{(1-\varepsilon_{\text{CalSil}})}{\varepsilon_{\text{CalSil}}^3} \right] \frac{\rho V^2}{6} \quad (2.6-4)$$

for Nukon with $0.5 < \frac{Re}{(1-\varepsilon)} < 9.85 \times 10^4$ and $0.564 < \varepsilon < 0.919$

for CalSil with $440 < Re < 7.92 \times 10^4$ and $0.38 < \varepsilon < 0.44$

For a cylindrical fibrous bed with flow perpendicular to the fibers and ($X > 1.0 \times 10^{-4}$ and $\varepsilon < 0.995$):

$$K(X_{\text{Nukon}}) = -0.5 + 0.5 \ln(1+X_{\text{Nukon}}) + \frac{1}{(2 + 2 X_{\text{Nukon}} + X_{\text{Nukon}}^2)} \quad (2.2-7)$$

For a spherical particle bed with ($X > 1.0 \times 10^{-4}$ and $\varepsilon < 0.995$):

$$K(X_{\text{CalSil}}) = 2 - \frac{3}{(1+X_{\text{CalSil}})^{1/3}} + \frac{5}{3(1+X_{\text{CalSil}})^{5/3} + 2} \quad (2.2-9)$$

where

S_{Nukon} Nukon specific surface area in debris bed
 S_{CalSil} CalSil specific surface area in debris bed
 X_{Nukon} Nukon void ratio in debris bed (equals $\text{Vol}_{\text{void}} / \text{Vol}_{\text{Nukon}}$)
 X_{CalSil} CalSil void ratio in debris bed (equals $\text{Vol}_{\text{void}} / \text{Vol}_{\text{CalSil}}$)
 $\varepsilon_{\text{Nukon}}$ porosity of Nukon in debris bed
 $\varepsilon_{\text{CalSil}}$ porosity of CalSil in debris bed
 μ fluid absolute viscosity
 ρ fluid density
b 1.95 for a cylindrical fibrous bed, 3.89 for a spherical particle bed
c 0.071 for a cylindrical fibrous bed, 0.13 for a spherical particle bed

It should again be emphasized that the indicated values for the empirical multipliers and exponents (1.95, 3.89, 0.071, and 0.13) in the turbulent term of the pressure drop equation for the debris bed are initial starting values that will be refined using test data. Additionally, the values of S_{Nukon} and S_{CalSil} will be reassessed by using the test data. These items will be addressed in Section 4.

For a debris bed, the pressure drop resulting from a sudden contraction at the debris bed entrance and a sudden expansion at the debris bed exit can be calculated using the following equations.

$$\Delta p_{irreversible\ loss} = \Delta p_{contr} + \Delta p_{expexit} \quad (2.6-5)$$

$$\Delta p_{contr} = \{ 0.5 (1 - \epsilon_{debris}) \rho / 2 \} (V / \epsilon_{debris})^2 \quad (2.6-6)$$

$$\Delta p_{expexit} = \{ (1 - f \epsilon_{debris})^2 \rho / 2 \} [V / (f \epsilon_{debris})]^2 \quad (2.6-7)$$

$$f = A_{screen} / A \quad (2.6-8)$$

where

A_{screen}	flow area through screen or perforated plate
A	debris bed cross-sectional surface area
Δp_{contr}	irreversible contraction pressure drop at debris bed entrance
$\Delta p_{expexit}$	irreversible expansion pressure drop for the part of the debris bed exit with flow
ϵ_{debris}	debris bed porosity (equals Vol_{void} / Vol_{tot})

The pressure drop across a clean unclogged, thin ($L_{screen}/d_h < 0.015$), plain square screen fabricated using circular metal wires can be calculated using the following equation.

$$\Delta p_{total} = \Delta p_{debrisbed} + \Delta p_{screen} \quad (2.6-9)$$

$$\Delta p_{screen} = [1.3 (1 - f) + (f - 1)^2] \rho V^2 / 2 \quad \text{for } Re_{screen} \geq 400 \quad (2.6-10)$$

where

L_{screen}	screen thickness
d_h	hydraulic diameter of flow area through a screen
Δp_{screen}	pressure drop (head loss) across a clean unclogged screen
Re_{screen}	Reynolds number using screen flow area and screen hydraulic diameter

If a thin perforated flat plate ($L_{sheet}/d_h < 0.015$) is used instead of a metal screen, the pressure drop across a clean unclogged thin debris bed and perforated plate can be calculated using the following equations.

$$\Delta p_{total} = \Delta p_{debrisbed} + \Delta p_{plate} \quad (2.6-11)$$

$$\Delta p_{plate} = \{ [0.707 (1 - f)^{1/2} + 1 - f]^2 / f^2 \} \rho V^2 / 2 \quad \text{for } Re_{plate} > 10^5 \quad (2.6-12)$$

$$f = A_{plate} / A \quad (2.6-13)$$

where

A_{plate}	flow area through perforated plate
L_{sheet}	sheet thickness

d_h	hydraulic diameter of flow area through the perforated plate
Δp_{plate}	pressure drop (head loss) across a clean unclogged perforated plate
Re_{plate}	Reynolds number using plate flow area A_{plate} and hydraulic diameter

2.7 Temperature Upper Limit

The head loss calculation method was developed to predict the pressure drop across a sump screen under single-phase flow conditions, and it has not been validated—and cannot be applied—for two-phase flow conditions. Two-phase flow conditions can occur if sufficient pressure drop occurs across a sump screen. As pressure decreases downstream of the screen, noncondensable gas dissolved in water can come out of solution, and hot water can flash into steam. Either one or a combination of these phenomena can result in two-phase flow, which can significantly increase pressure drop.

A release of air from solution can produce nucleation sites, which can increase the possibility of steam formation and flashing. To prevent water from flashing into steam, the pressure downstream of the sump screen must always remain above the saturation pressure at the sump water temperature. Consequently, a sensitivity analysis was performed using a series of calculations to estimate the point at which a significant void fraction is created downstream of the sump screen as a result of air coming out of solution or liquid flashing into steam. This sensitivity analysis included the conservative assumption that the water upstream of the sump screen contained the maximum amount of dissolved air for a range of water temperatures and total containment pressures. (The total containment pressure equals the containment pressure plus the static water head above the screen.) The maximum equilibrium concentration of dissolved air mass in subcooled water was obtained from information in Reference 20. The void fraction downstream of the screen was then calculated for different sump screen pressure drops and upstream temperature and pressure conditions. In so doing, it was assumed that the excess air above the saturated dissolved air condition downstream of the sump screen would immediately be released as gas. Figures 2.7-1 to 2.7-4 graphically depict the results of this sensitivity analysis. Specifically, Figures 2.7-1 and 2.7-2 plot the downstream void fraction as a function of water temperature for two total containment pressures and three assumed sump screen pressure drops. Figures 2.7-3 and 2.7-4 plot the downstream void fraction versus the sump screen pressure drop for a range of water temperatures at two total containment pressures. These plots also reflect the requirement that the pressure downstream of the screen must remain above the saturation pressure at the sump water temperature. The plots depicted in Figures 2.7-1 to 2.7-4 indicate that ***the condition at which a significant void fraction occurs downstream of the sump screens depends on the sump screen pressure drop, total containment pressure, and sump water temperature.***

The software package described in Reference 23, which determines the head loss across a debris-covered PWR sump screen using the NUREG/CR-6224 (Ref. 2) calculational method, incorporates the calculational approach described in this section, which determines the point at which two-phase conditions exist downstream of a PWR sump screen.

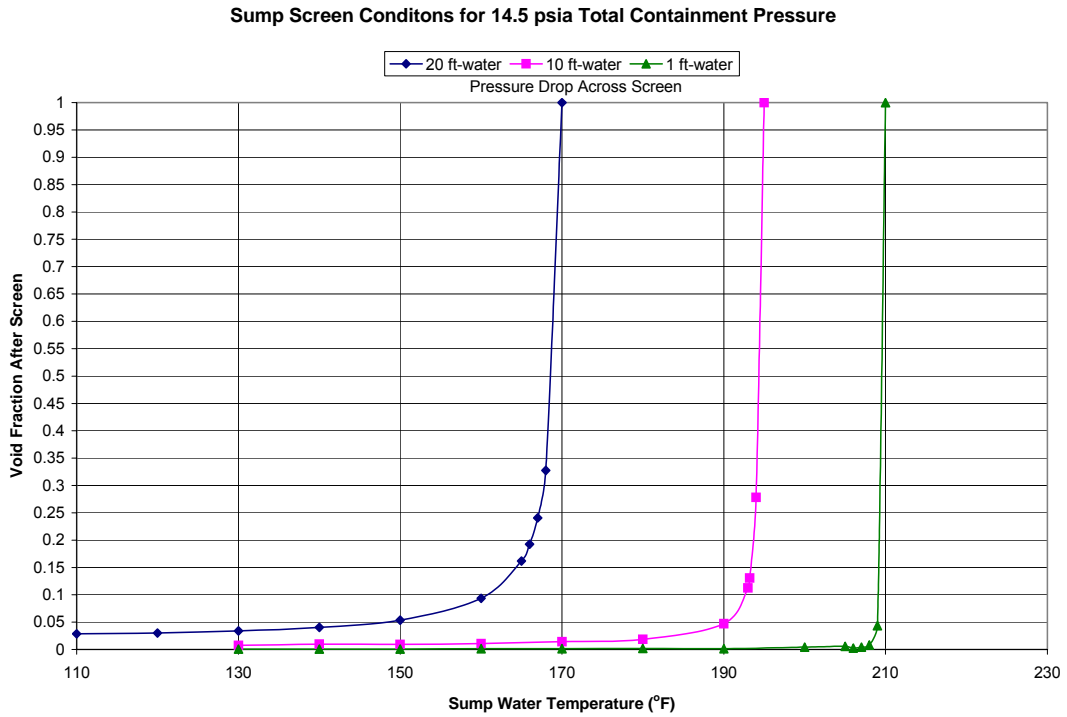


Figure 2.7-1 Downstream Void Fraction Versus Water Temperature at 14.5 psia (1.0×10^5 Pa)

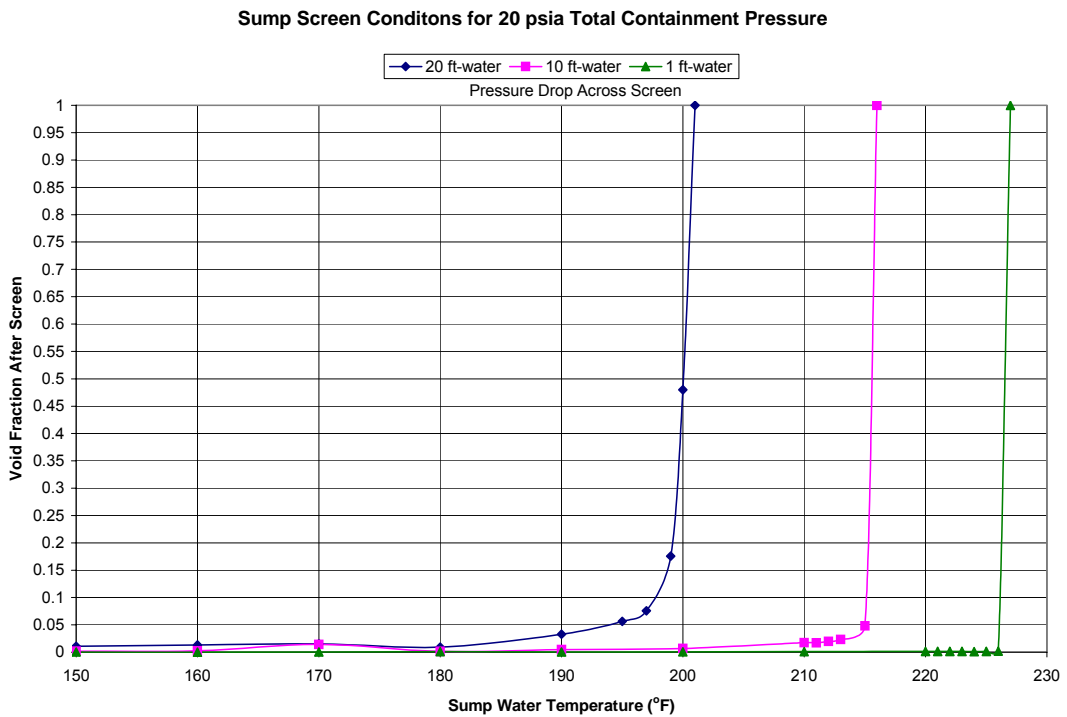


Figure 2.7-2 Downstream Void Fraction Versus Water Temperature at 20 psia (1.38×10^5 Pa)

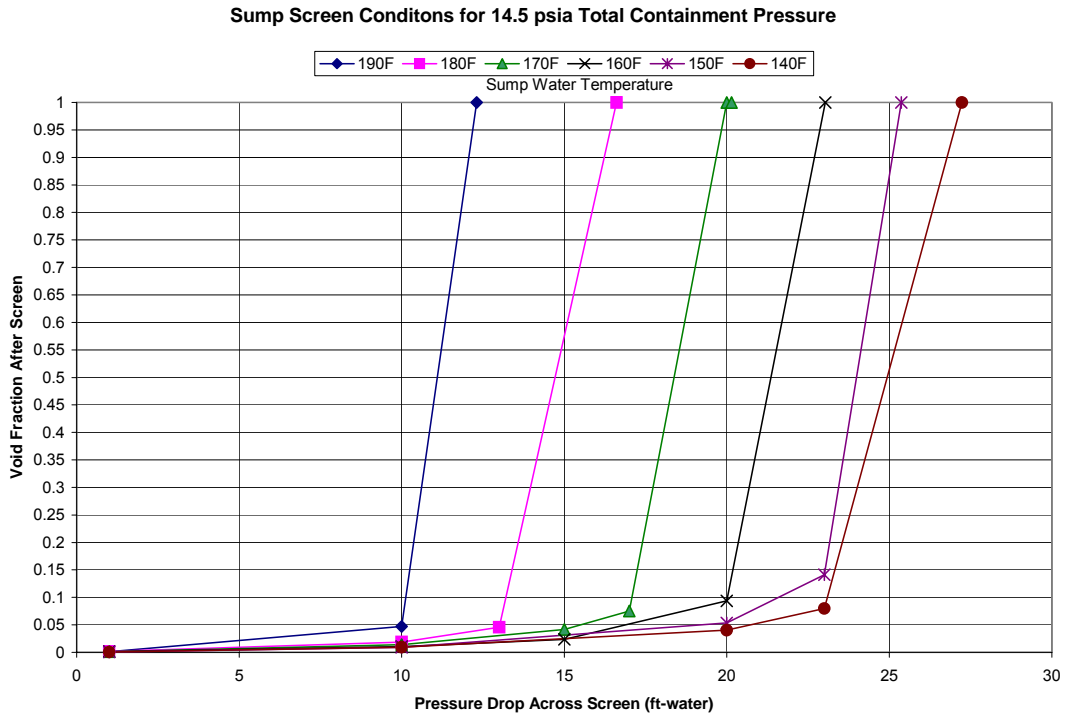


Figure 2.7-3 Downstream Void Fraction Versus Screen Pressure Drop at 14.5 psia (1.0×10^5 Pa)

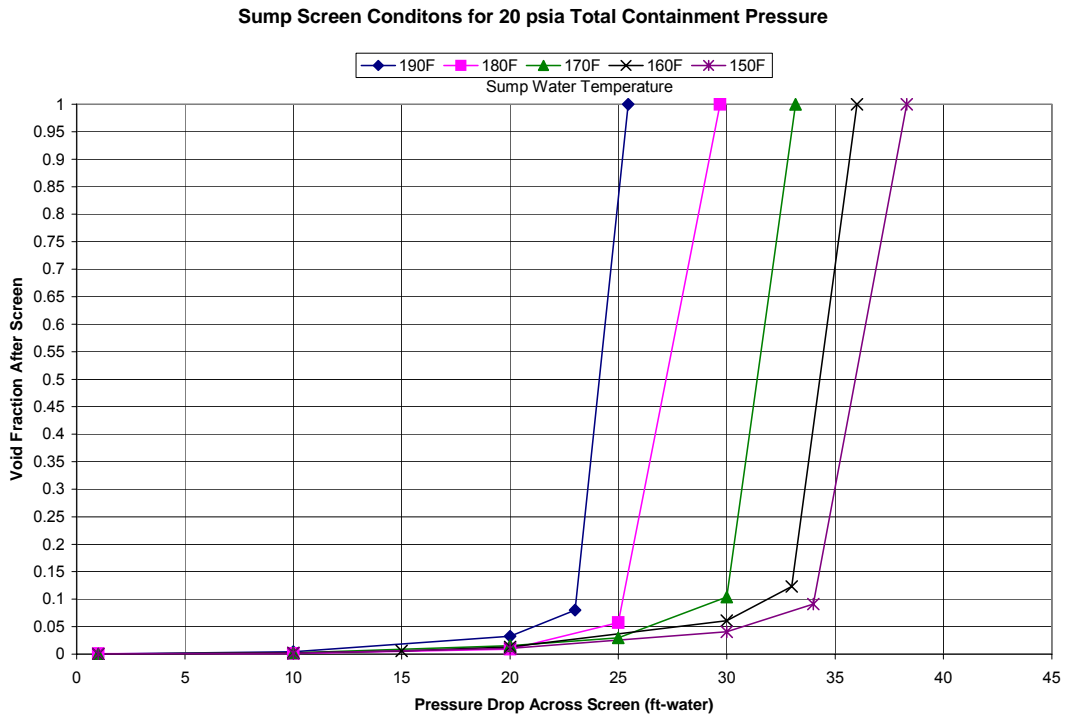


Figure 2.7-4 Downstream Void Fraction Versus Screen Pressure Drop at 20 psia (1.38×10^5 Pa)

Neither the head loss correlation developed in this report nor the NUREG/6224 correlation is appropriate for calculating pressure drops that result in large downstream void fractions. However, the void fraction that can result in pump cavitation problems is very low and within the range of application of the correlation and testing. Specifically, the NRC and the industry generally accept that a pump will experience cavitation problems when its inlet void fraction exceeds about 0.03 (3 percent), as indicated in Reference 21. Using a void fraction limit of 3 percent for conditions downstream of the sump screens, the acceptable operating range for sump pool temperature can be determined. Table 2.7-1 and Figure 2.7-5 show the conservatively obtained recommended maximum allowable sump pool temperature as a function of sump screen pressure drop and total containment pressure. These recommended temperature values reflect the inclusion of a conservative margin of at least 5 °F (2.8 °C). Because the void fraction assessment was performed for a range of assumed sump screen pressure drops, the results provided in Table 2.7-1 and Figure 2.7-5 can be applied to any sump screen pressure drop calculation method.

Table 2.7-1 Acceptable Range of Sump Pool Water Temperature

Total Containment Pressure (psia) / (Pa)	Pressure Drop Across Sump Screen (ft-water) / (m-water)	Acceptable Sump Pool Water Temperature (°F) / (°C)
14.5 / 1.0×10^5	1 / 0.3048	< 200 / 93.3
14.5 / 1.0×10^5	10 / 3.048	< 180 / 82.2
14.5 / 1.0×10^5	20 / 6.096	< 120 / 48.9
20 / 1.38×10^5	1 / 0.3048	< 220 / 104.4
20 / 1.38×10^5	10 / 3.048	< 210 / 98.9
20 / 1.38×10^5	20 / 6.096	< 180 / 82.2

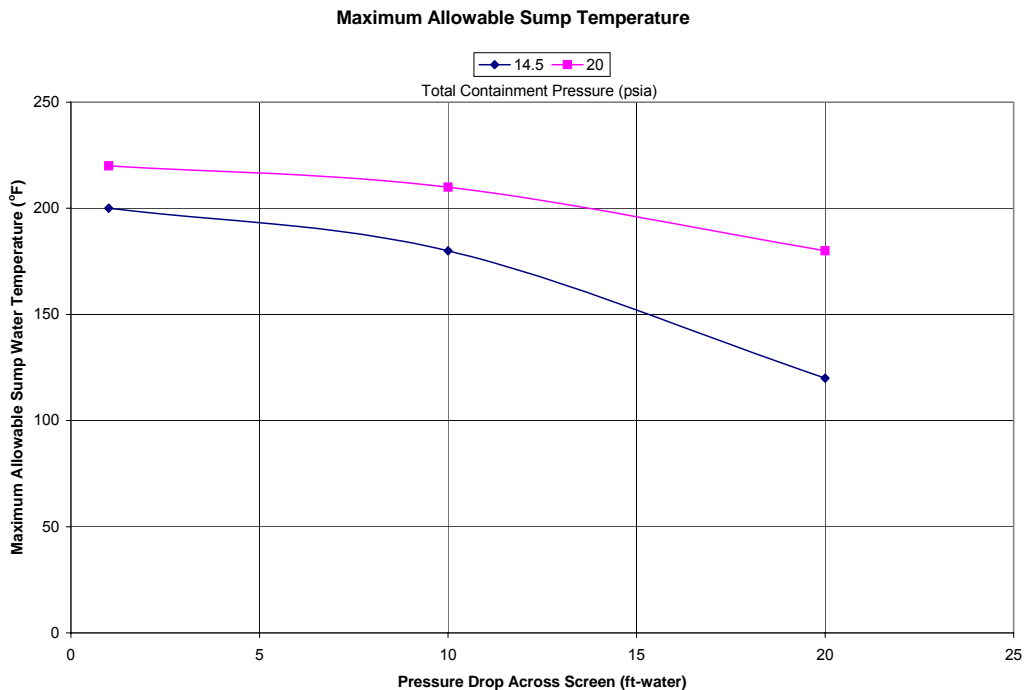
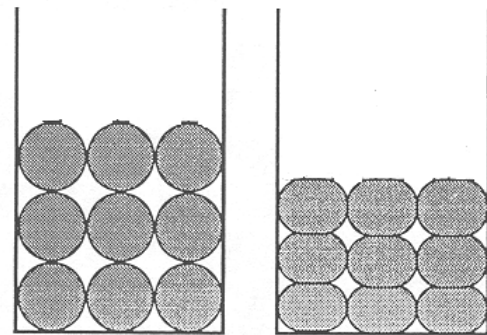


Figure 2.7-5 Maximum Allowable Sump Pool Water Temperature and Total Containment Pressure Versus Sump Screen Pressure Drop

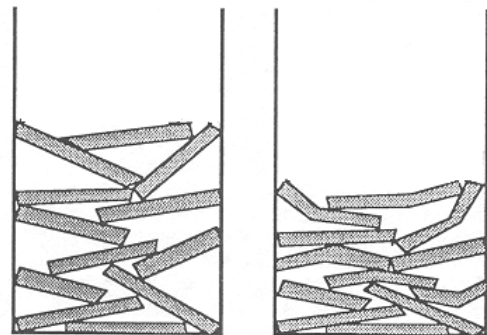
3. COMPRESSIBILITY OF A DEBRIS BED ON A SUMP SCREEN

The material compressibility, a measure of the mechanical strength of the material, affects fluid flow in a porous medium. Reference 10 states that compressible media forms of gels and fibers present unique problems in relating fluid flow and applied pressure because the bed porosity can change throughout the bed as conditions vary. Reference 10 indicates that the porosity change in a porous, compressible medium that is subjected to fluid drag forces can be attributed to several mechanisms, as illustrated in Figure 3.0-1. Specifically, the geometry of a porous medium can change because of (1) deformation of the solid matter, (2) rearrangement of the individual particles or fibers as a result of movement, bending, or slipping, and (3) disintegration and subsequent rearrangement of the solid material. Bending, slipping, and disintegration are essentially irreversible processes. Therefore, these deformation mechanisms produce nonrecoverable volume reductions. The degree of nonrecoverable deformation is especially pronounced during an initial compression and decreases as the deformation is repeated.

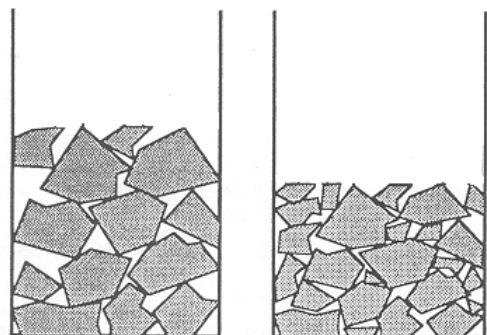
Reference 10 indicates that a porous medium composed of material such as fibers, particles, or gel exhibits hysteresis during compression recovery cycles. The amount of nonrecoverable deformation decreases as the deformation is repeated until no more nonrecoverable deformation is observed. The compressibility model described here is semiempirical, and the solid material in the porous medium is assumed to be incompressible. The influence of pressure on the compressibility of the porous medium may be addressed numerically by varying a multiplier for the compressibility relation until nonrecoverable deformation is negligible. This approach is difficult to implement in a numerical calculation; therefore, the assumption is made that the first compression is an irreversible process and that, after the first compression, the porous medium is elastic with constant compressibility.



Deformation



Rearrangement (Movement, Bending, Slipping)



Disintegration and Rearrangement

Figure 3.0-1 Volume Reduction Mechanisms for Granular and Fibrous Materials (Ref. 10)

3.1 Pressure Forces Through a Porous Medium with Flowing Liquid

The total pressure, P_{tot} , in a porous medium undergoing flow and compression can be separated into two pressure components—the hydraulic pressure of the fluid, P_h , and the mechanical stress exerted on the medium, P_m . The values of the pressures vary along the flow position in the porous medium; however, the sum of the two components is constant throughout the medium. Therefore, the following equation is valid along the flow length of the porous medium (Refs. 11, 16, and 17).

$$P_{tot} = P_m + P_h \quad (3.1-1)$$

where

P_{tot} total applied pressure on a porous medium
 P_m mechanical stress exerted on the porous medium
 P_h hydraulic pressure of the fluid flow

If a porous medium of thickness t is defined, Figure 3.1-1 shows the relationship between the pressure components along the flow length in a porous medium.

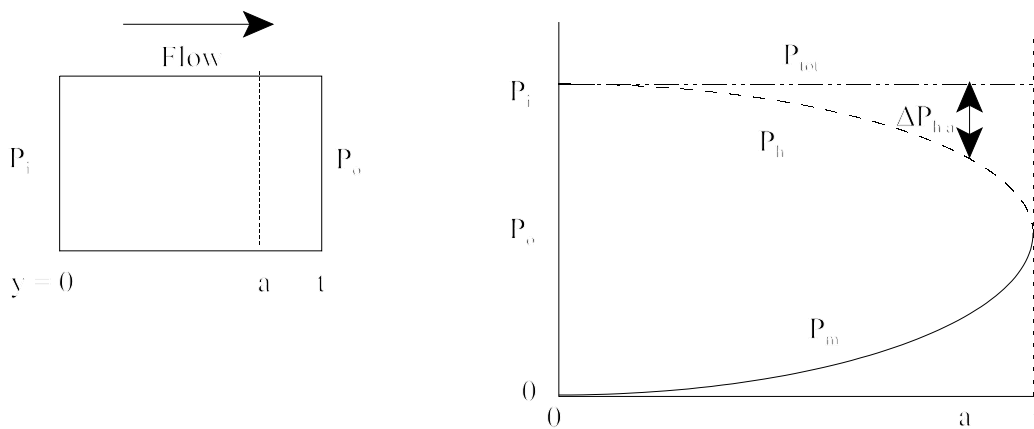


Figure 3.1-1 Pressure Distribution in a Porous Medium

Using Figure 3.1-1, the following relationships can be defined.

At the entrance, $y = 0$:

$$P_h = P_i, \quad \Delta P_h = 0, \quad P_m = 0 \quad (3.1-2)$$

At the exit, $y = t$:

$$P_h = P_o, \quad \Delta P_h = P_i - P_o, \quad P_m = P_i - P_o \quad (3.1-3)$$

At $y = a$:

$$P_h = P_i - \Delta P_{ha}, \quad P_m = \Delta P_{ha} \quad (3.1-4)$$

where

P_i inlet pressure upstream of the porous medium
 P_o outlet pressure downstream of the porous medium

ΔP_h pressure drop across the porous medium
 ΔP_{ha} pressure drop across the porous medium at $y = a$

3.2 Compressibility of a Porous Medium During the First Compression

As previously stated, the compressibility of a porous medium debris bed is assumed to be an irreversible process during the first compression. Equations have been developed that relate the compressibility of the total volume to the pressure across the solid material (Ref. 10).

$$\beta_t = N P_m^{-b_c} \quad (3.2-1)$$

where

β_t compressibility of the total volume
 N material-specific parameter
 P_m mechanical stress exerted on the porous medium
 b_c material-specific parameter ($b_c = 1$)

When b_c is assumed to be 1, the following relationship correlates the concentration density of fibrous material in a porous bed to the compacting pressure (Refs. 2, 17, 18, and 19).

$$c_m = M P_m^N \quad (3.2-2)$$

where

c_m solid material concentration density
 M material-specific empirical constant

Reference 10 states that equation (3.2-2) has been successfully applied for the low-pressure region, but does not predict a finite value for concentration at higher pressure. Consequently, an approach is used to relate the compressibility to the void volume instead of the total volume.

$$\beta_v = N P_m^{-b_c} \quad (3.2-3)$$

where

β_v compressibility of the void volume
 N material-specific parameter

If the volume of the solid material is assumed to be incompressible, which indicates that the compressibility is related entirely to the void volume, and b_c is assumed to be equal to 1, Reference 10 provides the following relationship for a debris bed undergoing a nonrecoverable deformation.

$$X = X' (P_m / P_m')^{-N} \quad (3.2-4)$$

where

X' void ratio at P_m' for the first compression at bed formation
 X void ratio at P_m for subsequent compressions
 P_m' mechanical stress for the first compression at bed formation
 P_m mechanical stress exerted on the porous medium for subsequent compressions

The debris bed thickness can be related to the void ratio using the following relations.

$$X = \text{Vol}_{\text{void}} / \text{Vol}_{\text{solid}} = (\text{Vol}_{\text{tot}} - \text{Vol}_{\text{solid}}) / \text{Vol}_{\text{solid}} \quad (3.2-5)$$

$$\text{Vol}_{\text{tot}} = L_{\text{debrisbed}} A \quad (3.2-6)$$

where

$L_{\text{debrisbed}}$ debris bed thickness
 A debris bed cross-sectional surface area

The following expression for debris bed thickness can be derived using the previous two equations.

$$L_{\text{debrisbed}} = \text{Vol}_{\text{solid}} (1 + X) / A \quad (3.2-7)$$

3.3 Compressibility of a Porous Medium After the First Compression

As previously stated, the compressibility of a porous medium debris bed is assumed to be constant after the first compression. If the material is treated as being elastic with constant compressibility:

$$\beta_v = N P_{\text{max}}^{-1} \quad (3.3-1)$$

where

P_{max} highest compressive stress to which the porous material has been exposed
 N material-specific parameter

By using this assumption, for pressures below the maximum applied pressure, Reference 10 relates the compressive stress across the porous medium to the void ratio using the following equation.

$$X = X(P_{\text{max}}) \exp \left[N - \frac{N P_m}{P_{\text{max}}} \right] \quad (3.3-2)$$

where

$X(P_{\text{max}})$ void ratio at P_{max}

The debris bed thickness can be calculated from the void ratio, solid volume of the debris bed, and debris bed surface area using equation (3.2-7).

4. DETERMINATION OF DEBRIS BED AND MATERIAL PROPERTIES

Sections 2 and 3 derive and present the equations for calculating pressure drop across a compressible, porous medium debris bed that can be present on a post-LOCA PWR sump screen. This section describes a method for calculating the pressure drop across a debris bed through which water is flowing and identifies values for the debris bed and material, which are needed to calculate the pressure drop.

The developed calculational approach employs pressure drop calculations across a debris bed composed of either one or two calculational control volumes. The one-volume method should be used for calculating head loss across a debris bed composed of a single debris type. The one-volume approach does not represent the best calculational method for beds with multiple debris types and nonhomogeneous debris distributions because hydraulic and mechanical pressures can vary nonuniformly within the debris bed. Therefore, the two-volume method overcomes this limitation by calculating the debris bed flow and compression by assuming the presence of two compressible calculational control volumes for the debris bed.

The determination to use the one-volume or the two-volume calculational approach depends on the characteristics of the debris bed. Table 4.0-1 identifies the following types of possible debris bed configurations for beds composed of fibers and particles such as Nukon and CalSil:

- Homogeneous unsaturated debris bed—The configuration represents a uniform mixture of fibers and particles in a debris bed. Testing has shown that a bed can be initially formed at an approach velocity of 0.1 ft/s (0.0305 m/s) with conditions close to a uniform Nukon/CalSil distribution. However, the uniform condition was not maintained with flow passing through the debris bed, when the particles tend to redistribute from a uniform condition to one in which the particles are concentrated in the fiber in a portion of the debris bed. Testing has shown that the homogeneous debris bed produces the lower bound head loss. This condition can be modeled using the one-volume calculational approach. The homogeneous debris bed with a uniform distribution of Nukon fibers and CalSil particles can be modeled by using the NUREG/CR-6224 (Ref. 2) equations to calculate debris bed pressure drop.
- Heterogeneous locally saturated debris bed—This condition represents a more stable reconfiguration of particles in a fiber bed. The upstream portion of the debris bed is considered to be composed entirely of fibers, and the downstream end of the debris bed is considered to contain the maximum concentration of particles that the fiber bed can contain under a specific flow condition. (The maximum particle concentration volume can be located anywhere within the debris bed; however, for calculation purposes, the maximum particle concentration volume is assumed to be present at the downstream end of the debris bed.) Testing has shown that this bed configuration typically results in a larger, upper bound head loss. The two-volume calculational method must be used to model this bed configuration to account for the two different debris distributions within the debris bed. Figure 4.0-1 illustrates the plots for PNNL Test 051117_NC_2776_L1, where the initially formed debris bed transitioned from a homogeneous condition to a locally saturated condition. Calculations in Section 6 show the results of the one-volume homogeneous and two-volume calculations to indicate the change in debris configuration from a homogeneous to a locally saturated debris bed and the ability of the two calculational approaches to predict the lower and upper bound pressure drops.
- Homogeneous saturated debris bed—This bed configuration is a subset of the locally saturated debris bed. In this configuration, the fiber bed is completely saturated with particles. In other

words, every part of the fiber bed contains particles. The one-volume method can be used to model this configuration because the saturated debris bed is closest to a true homogeneous condition with uniform distribution of fiber and particles. However, the two-volume approach may be needed to determine the presence of a homogeneous saturated debris bed. The saturated debris bed can be modeled by using the NUREG/CR-6224 (Ref. 2) equations to calculate debris bed pressure drop.

- Heterogeneous oversaturated debris bed—This condition represents the case when the debris bed contains more particles than required to saturate the fiber bed. It is postulated that the downstream portion of the bed is composed of fiber saturated with particles. The upstream portion of the bed is composed entirely of particles. The two-volume calculational method must be used to solve for this condition because of the different debris distributions in the bed. PNNL tests with oversaturated conditions have resulted in large pressure drops that can essentially be called a “clogged” condition because of the overabundance of CalSil particles in the Nukon fiber debris bed.

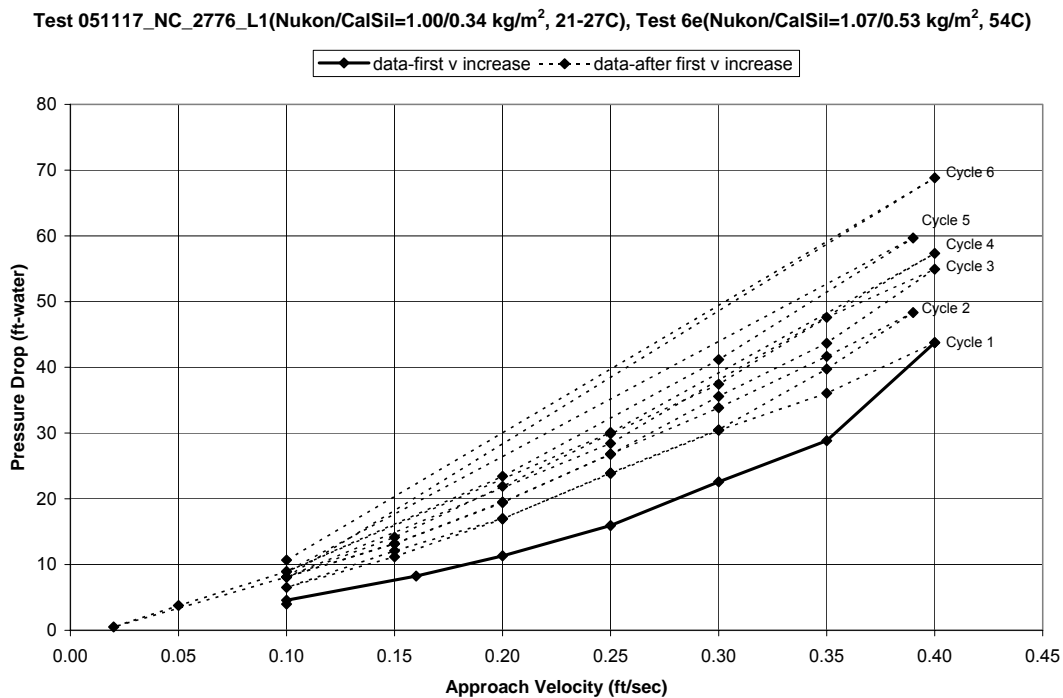


Figure 4.0-1 Transition from Homogeneous to Local Saturation Condition for PNNL Nukon/CalSil Test 051117_NC_2776_L1

To apply the calculational approach, several debris bed initial conditions, parameters, and material parameters must be known. The following specific information is needed to calculate the pressure drop across a porous medium debris bed:

- constituent masses of the material in the test debris beds

- initial thickness of the debris bed at bed formation
- debris material properties such as density and specific surface area as well as the multipliers and exponents in the kinetic term of the porous medium pressure drop equation
- maximum concentration of particulate debris in a fibrous debris bed, a condition called the maximum particle concentration
- material-specific compression parameter, necessary to predict the porous media debris bed compression and expansion

The values for these parameters can be obtained by comparing (1) the predictions obtained using the calculational approach with (2) the test data from the PNNL (Ref. 24), LANL/UNM (Ref. 3), and Argonne National Laboratory (ANL) (Ref. 25) tests. The following sections describe the approaches used to obtain values or relations for the required parameters.

Table 4.0-1 Conditions for a Fiber/Particle (e.g., Nukon/CalSil) Debris Bed

	Flow Direction ↓ Homogeneous Unsaturated Particle/Fiber Bed	Flow Direction ↓ Homogeneous Saturated Particle/Fiber Bed	Flow Direction ↓ Fiber Bed Saturated Particles in Fiber Bed	Flow Direction ↓ Particle Bed Saturated Particles in Fiber Bed
Description	Homogeneous Unsaturated Bed	Homogeneous Saturated Bed	Heterogeneous Locally Saturated Bed	Heterogeneous Oversaturated Bed
Calculational Method	One-Volume	One-Volume	Two-Volume	Two-Volume
Condition	$\text{dens}_{\text{fiber}}$ is uniform $\text{dens}_{\text{particle}} < \text{dens}_{\text{particlesatmax}}$	$\text{dens}_{\text{fiber}}$ is uniform $\text{dens}_{\text{particle}} = \text{dens}_{\text{particlesatmax}}$	<u>Inlet Volume:</u> $\text{dens}_{\text{fiber}}$ is uniform $\text{dens}_{\text{particle}} = 0.0$ <u>Outlet Volume:</u> $\text{dens}_{\text{fiber}}$ is uniform $\text{dens}_{\text{particle}} = \text{dens}_{\text{particlesatmax}}$	<u>Inlet Volume:</u> $\text{dens}_{\text{fiber}} = 0.0$ $\text{dens}_{\text{particle}} > 0.0$ <u>Outlet Volume:</u> $\text{dens}_{\text{fiber}}$ is uniform $\text{dens}_{\text{particle}} = \text{dens}_{\text{particlesatmax}}$
Comments	<ul style="list-style-type: none"> • Best estimate Δp for bed with one debris type • Lower bound Δp for bed with two debris types • Condition not stable for two debris types and will probably revert to a heterogenous locally saturated bed • Condition modeled with NUREG/CR-6224 equation 	<ul style="list-style-type: none"> • Best estimate Δp for saturated bed with two debris types • Condition modeled with NUREG/CR-6224 equation 	<ul style="list-style-type: none"> • Upper bound Δp for unsaturated bed with two debris types • Homogeneous unsaturated bed transforms to this state 	<ul style="list-style-type: none"> • Upper bound Δp for oversaturated bed with two debris types • Test with oversaturated bed at PNNL resulted in high head loss with essentially clogged condition

Note: dens is bed density for debris type (mass/bed volume)

4.1 Mass of Debris Bed Constituents During Testing

4.1.1 Constituent Debris Bed Masses for PNNL Tests

The PNNL Series 1 tests used a metal screen, and the PNNL Series 2 and benchmark tests used a perforated plate for testing. Section 2.5 describes the metal screen and perforated plate used for testing. The mass of the insulation debris accumulated on the metal screen or perforated plate was obtained from actual post-test measurements. Table 4.1-1 compares the Nukon and CalSil masses added to the loop with the actual masses deposited on the metal screen. The Nukon and CalSil masses added to the loop were obtained by weighing, as was the total debris mass on the metal screen. The CalSil mass in the Nukon/CalSil debris beds was obtained by using a chemical dissolution method developed by PNNL, which is described in NUREG/CR-6917 (Ref. 24). The Nukon mass in the Nukon/CalSil debris bed was obtained by subtracting the CalSil mass from the total debris bed mass. The chemical dissolution method used to determine the mass of CalSil in the debris bed had an uncertainty of ± 15 percent.

Table 4.1-1 provides the ratios of the debris bed mass of the Nukon, CalSil, and the total mass to the added masses. As shown in Table 4.1-1, the Nukon mass exceeds the added mass in five cases (in other words, the Nukon ratio exceeds 1.0 in five cases). For the Nukon-only bed created for the Series 1 tests, the discrepancy could be the result of metal or rust particles added to the loop from a temporary gate valve that was used in place of a new but defective gate valve. Five of the tests listed in Table 4.1-1 used this temporary valve, but a new valve was installed for the last two tests in Series 1.

Table 4.1-2 lists the debris bed masses used in the predictions cited in this report. For the Nukon-only Test 051108_NO_3067_L1, calculations assumed that the mass of the metal or rust present in the debris bed possessed the same properties as Nukon because the volume occupied by the metal or rust is about 3.1 percent of the Nukon volume.

$$\text{Metal/rust volume} = (33.32-30.67) / 1000 \text{ kg} / 7870 \text{ kg/m}^3 = 3.37 \times 10^{-7} \text{ m}^3$$

$$\text{Nukon volume} = 30.67 / 1000 \text{ kg} / 2803 \text{ kg/m}^3 = 1.09 \times 10^{-5} \text{ m}^3$$

The report calculations assume that the construction debris mass in the debris bed for the Nukon-only Test 060125_NO_3067_L1 possesses Nukon properties. The volume percentage of this debris is about 1.6 percent, which is less than the metal/rust volume fraction for Test 051108_NO_3067_L1.

$$\text{Construction debris volume} = (32.05-30.67) / 1000 \text{ kg} / 7870 \text{ kg/m}^3 = 1.75 \times 10^{-7} \text{ m}^3$$

For the other three tests in which the calculated Nukon debris bed mass exceeded the added Nukon mass, the Nukon debris bed mass was assumed to possess fibers from the CalSil insulation, which possess properties similar to those of Nukon. CalSil insulation is primarily composed of calcium silicate particles, but as much as 12 percent can be other materials such as fibers of various types (e.g., glass, cellulose)

Mass was lost during retrieval of the Nukon/CalSil debris bed for Test 051110_NC_0595_L1, which was the smallest debris bed tested in Series 1. Consistent with the trends shown by the other Nukon/CalSil tests—especially Test 051121_NC_1586_L1, which had the next smallest debris bed—100 percent of the added Nukon mass and 50 percent of the added CalSil mass were assumed to be present in the debris bed.

Debris bed mass was lost from Series 2 Tests 060404_NC_2698_LP1 and 050517_NC_0808_LP1 and LP2 during retrieval. Consequently, the total bed mass has been estimated using mass retrieval trends from similar tests. In addition, the calculated Nukon mass in the debris bed is larger than the mass added to the loop for Series 2 Tests 060807_NC_0708_LP1 and LP2, and 060517_NC_0808_LP1 and LP2. As previously mentioned, predictive calculations used the calculated Nukon masses because the debris bed fibers were assumed to be composed of Nukon fibers and the fibers present in CalSil insulation.

Table 4.1-1 Debris Mass Summary for PNNL Tests

Test	Mass Added to Test Loop			Debris Bed Mass			Debris Bed Mass / Added Mass		
	Nukon Mass (g)	CalSil Mass (g)	Total Mass (g)	Calculated Nukon Mass ³ (g)	Measured CalSil Mass ² (g)	Total Weighed Mass ¹ (g)	Nukon	CalSil	Total
Series 1 Tests (Using Metal Screen)									
051108_NO_3067_L1 ^{4,6}	30.67	0.0	30.67	≤ 30.67	0.0	33.32 ^{4,6}	1.086 ^{4,6}	NA	1.086 ^{4,6}
060125_NO_3067_L1 ⁷	30.67	0.0	30.67	≤ 30.67	0.0	32.05 ⁷	1.045 ⁷	NA	1.045 ⁷
051110_NC_0595_L1 ^{5,6}	3.97	1.98	5.95	3.18 ⁵	0.86 ⁵	4.04 ⁵	0.801 ^{5,6}	0.434 ^{5,3}	0.679 ^{5,6}
051115_NC_4098_L1 ⁶	26.44	14.54	40.98	22.28	13.58	35.86	0.843	0.934	0.875
051117_NC_2776_L1 ⁶	18.51	9.25	27.76	18.43	6.44	24.87	0.996	0.696	0.896
051121_NC_1586_L1 ⁶	10.58	5.29	15.87	10.45	3.13	13.58	0.988	0.592	0.856
051123_NC_2181_L1	14.54	7.27	21.81	14.65	4.63	19.28	1.008	0.637	0.884
051128_NC_2776_L2	18.51	9.25	27.76	17.23	6.26	23.49	0.931	0.677	0.846
Series 2 Tests (Using Perforated Plate)									
060321_NO_0405_LP1 (BM-1) ⁹	4.05	0.0	4.05	3.18	0.0	3.18	0.785	NA	0.785
060313_NO_1349_LP1 (BM-2) ⁹	13.49	0.0	13.49	10.74	0.0	10.74	0.796	NA	0.796
060425_NO_2703_LP1, LP2, LP3	27.03	0.0	27.03	23.19	0.0	23.19	0.858	NA	0.858
060731_NO_2703_LP1, LP2	27.03	0.0	27.03	23.3	0.0	23.3	0.862	NA	0.862
060802_NO_2703_LP1, LP2	27.03	0.0	27.03	22.19	0.0	22.19	0.821	NA	0.821
060512_CO_8108_LP1, LP2, LP3	0.0	81.08	81.08	0.0	8.09	8.09 ⁸	Bed	Incomplete	0.100
060323_NC_1619_LP1 (BM-3) ⁹	13.49	2.70	16.19	11.663	0.377	12.04	0.865	0.140	0.744
060331_NC_2024_LP1	13.49	6.75	20.24	11.179	2.461	13.64	0.829	0.365	0.6739
060817_NC_2024_LP1, LP2	13.49	6.75	20.24	12.881	2.229	15.11	0.955	0.330	0.747
060404_NC_2698_LP1	13.49	13.49	26.98	9.754	6.316	16.07 ⁵	0.723	0.468	0.5956 ⁵
060509_NC_0505_LP1	4.04	1.01	5.05	3.427	0.463	3.89	0.848	0.458	0.770
060426_NC_0708_LP1, LP2	4.04	3.04	7.08	3.881	0.089	3.97	0.961	0.029	0.561
060807_NC_0708_LP1, LP2	4.04	3.04	7.08	4.518	0.342	4.86	1.118	0.113	0.686
060809_NC_0708_LP1, LP2	4.04	3.04	7.08	2.89	0.09	2.98	0.715	0.030	0.421
060517_NC_0808_LP1, LP2	4.04	4.04	8.08	4.054	1.486	5.54 ⁵	1.003	0.368	0.686 ⁵
060427_NC_0252_LP1	2.01	0.5	2.51	NA	NA	1.05 ⁸	Bed	Incomplete	0.418
060428_NC_0453_LP1	2.01	2.52	4.53	NA	NA	1.76 ⁸	Bed	Incomplete	0.389

- ¹ Total weighed debris bed mass
- ² CalSil mass in debris bed obtained using chemical dissolution method has an uncertainty of ±15 percent
- ³ Nukon mass in debris bed calculated using the equation $mass_{Nukon} = mass_{Total} - mass_{CalSil}$
- ⁴ Metal/rust particles from a temporary gate valve are visible in debris bed
- ⁵ Mass lost from debris bed because the bed ruptured during retrieval
- ⁶ Debris beds for these Series 1 tests possibly suffered from contamination by metal/rust particles from a temporary gate valve
- ⁷ Construction debris present in bed
- ⁸ Incomplete bed (The masses used in these tests were insufficient to form a complete, continuous debris bed.)
- ⁹ Benchmark test labeled with BM

Table 4.1-2 Debris Bed Masses Used for the PNNL Test Calculations

Test	Nukon Mass (g)	CalSil Mass (g)	Total Mass (g)
Series 1 Tests (Using Metal Screen)			
051108_NO_3067_L1	33.32 ¹	0.0	33.32 ¹
060125_NO_3067_L1	32.05 ⁵	0.0	32.05 ⁵
051110_NC_0595_L1	3.97 ²	0.99 ³	4.96 ^{2,3}
051115_NC_4098_L1	22.28	13.58	35.86
051117_NC_2776_L1	18.43	6.44	24.87
051121_NC_1586_L1	10.45	3.13	13.58
051123_NC_2181_L1	14.65 ⁴	4.63	19.28
051128_NC_2776_L2	17.23	6.26	23.49
Series 2 Tests (Using Perforated Plate)			
060321_NO_0405_LP1 (BM-1) ⁷	3.18	0.0	3.18
060313_NO_1349_LP1 (BM-2) ⁷	10.74	0.0	10.74
060425_NO_2703_LP1, LP2, LP3	23.19	0.0	23.19
060731_NO_2703_LP1, LP2	23.3	0.0	23.3
060802_NO_2703_LP1, LP2	22.19	0.0	22.19
060512_CO_8108_LP1, LP2, LP3 ⁸	0.0 ⁸	8.09 ⁸	8.09 ⁸
060323_NC_1619_LP1 (BM-3) ⁷	11.663	0.377	12.04
060331_NC_2024_LP1	11.179	2.461	13.64
060817_NC_2024_LP1, LP2	12.881	2.229	15.11
060404_NC_2698_LP1	12.0 ⁶	4.7 ⁶	16.7 ⁶
060509_NC_0505_LP1	3.427	0.463	3.89
060426_NC_0708_LP1, LP2	3.881	0.089	3.97
060807_NC_0708_LP1, LP2	4.518 ⁴	0.342	4.86
060809_NC_0708_LP1, LP2	2.89	0.09	2.89
060517_NC_0808_LP1, LP2	4.16 ^{4,6}	1.52 ⁶	5.68 ⁶
060427_NC_0252_LP1	NA ⁸	NA ⁸	1.05 ⁸
060428_NC_0453_LP1	NA ⁸	NA ⁸	1.76 ⁸

¹ Metal/rust particles in debris bed are assumed to have Nukon properties

² Because debris bed mass was lost during retrieval, 100 percent of the added Nukon mass is assumed to be present in the debris bed

³ Because debris bed mass was lost during retrieval, 50 percent of the added CalSil mass is assumed to be present in the debris bed, consistent with the CalSil fraction present in the next-lowest-concentration Nukon/CalSil debris bed (Test 051121_NC_1586_L1)

⁴ Nukon mass in the debris bed is assumed to contain fibers from the CalSil insulation

⁵ Construction debris in bed is assumed to have Nukon properties

⁶ Corrected for mass that was lost from debris bed when the bed ruptured during retrieval

⁷ Benchmark tests labeled with BM

⁸ Incomplete bed (The masses used in these tests were insufficient to form a complete, continuous debris bed.)

4.1.2 Constituent Debris Bed Masses for LANL/UNM Tests

The masses of the debris beds for the LANL/UNM tests (Ref. 3) were not measured. Only the masses of Nukon and CalSil added to the test loop were measured. For these tests, the assumption was that all of the Nukon added to the test loop accumulated in the debris bed. Additionally, almost all of the CalSil added to the test loop was assumed to be present in the debris bed; however, a small correction for the CalSil accumulated mass was made by considering turbidity measurements of the test water. Table 4.1-3 compares the bed masses per projected test screen area tabulated for the LANL/UNM tests with the similar PNNL Series 1 tests. Both the LANL/UNM tests and the PNNL Series 1 tests used similarly sized metal screens for testing. In this comparison, the LANL/UNM tests used a screen area of 0.0656 m² (0.70572 ft²). In a January 4, 2006, email, C. Shaffer of ARES Corporation, who was directly involved with the LANL/UNM testing, indicated that this area was the appropriate value to use for the LANL/UNM test facility; however, this value differs from the analysis screen flow area of 0.06899 m² (0.7426 ft²) specified in NUREG/CR-6874 (Ref. 3). By design, the PNNL screen area of 0.01863 m² (0.2005 ft²) equals the inner diameter of the test section. By comparing the estimate LANL/UNM bed masses to those measured by PNNL, the conclusion can be reached that the LANL/UNM assumption—that all of the Nukon and almost all of the CalSil added to the test loop were deposited in the debris bed—may not be correct. The mass accumulation assumption used for the LANL/UNM test could adversely affect the development and verification of a head loss calculational method. Consequently, the LANL/UNM test pressure drop predictions, which depend on the debris masses, are not expected to provide a good assessment of the calculational model.

Table 4.1-3 Debris Bed Mass Comparison for Similar PNNL and LANL/UNM Tests

LANL Test*	Added Nukon kg/m ²	Added CalSil kg/m ²	Estimated Bed CalSil kg/m ²	Bed CalSil / Nukon	Total Debris kg/m ²	PNNL Series 1 Tests [#]						
						Added Nukon kg/m ²	Added CalSil kg/m ²	Bed Nukon kg/m ²	Bed CalSil kg/m ²	Bed CalSil / Nukon	Total Debris kg/m ²	
						051114_SO_0000_L1	0.0	0.0	0.0	0.0	NA	0.0
						051128_SO_0000_L1	0.0	0.0	0.0	0.0	NA	0.0
1a	1.77	0.00	0.00	0.0	1.77	051108_NO_3067_L1 ^{&}	1.65	0.0	1.79	0.00	0.0	1.79
						060125_NO_3067_L1 ⁺	1.65	0.0	1.72	0.00	0.0	1.72
6b	1.53	0.84	0.83	0.544	2.36	051115_NC_4098_L1	1.42	0.78	1.20	0.73	0.610	1.92
6e	1.07	0.53	0.53	0.497	1.60	051117_NC_2776_L1	0.99	0.50	0.99	0.35	0.349	1.33
6e2	1.07	0.53	0.53	0.500	1.60	051128_NC_2776_L2	0.99	0.50	0.92	0.34	0.363	1.26
6f	0.61	0.31	0.30	0.493	0.91	051121_NC_1586_L1	0.57	0.28	0.56	0.17	0.300	0.73
6h	0.23	0.11	0.11	0.460	0.33	051110_NC_0595_L1 [^]	0.21	0.11	0.21	0.05	0.249	0.27
6i	0.84	0.42	0.41	0.495	1.25	051123_NC_2181_L1	0.78	0.39	0.79	0.25	0.316	1.03

* Pipe id= 11-3/8 inch, Pipe Area = 0.06556 m²

[#] Area = 0.01863 m²

[&] Metal/rust particles present in bed.

⁺ Construction debris present in bed.

[^] Best estimate bed masses; bed ruptured during retrieval.

4.2 Reference Debris Bed Thickness at Low-Velocity Formation

To use the compressibility approach outlined in Sections 3.2 and 3.3, a reference debris bed thickness for bed formation at a low approach velocity is required. A correlation to calculate a reference debris bed thickness for low-velocity bed formation was developed, using the data obtained by employing test data from PNNL and the Series 6 tests (Ref. 3) performed by LANL/UNM.

4.2.1 Low-Velocity Reference Debris Bed Thickness Using PNNL Test Data

Data from the PNNL Series 1 tests were used to determine the relationship between initial debris bed thickness and debris mass per area. The debris bed thicknesses for most of the Series 1 tests were approximated by visual measurement, using a ruler, of the debris bed during testing. Only the debris bed thicknesses for the Nukon-only test, Test 060125_NO_3067_L1, were obtained by using the optical triangulation technique described in NUREG/CR-6917 (Ref. 24). Similar to the LANL tests, most of the Series 1 debris beds were built at an approach velocity of about 0.0305 m/s (0.1 ft/s). However, some of the initial Series 1 tests built the debris beds at about 0.061 m/s (0.2 ft/s). Figure 4.2-1 plots the initial bed thicknesses for Nukon/CalSil debris beds at steady-state conditions as a function of total debris surface concentration (bed debris mass/surface area). This figure indicates that only a relatively small difference in initial debris bed thickness existed for the debris beds built at approach velocities of 0.0305 m/s and 0.061 m/s. Test data can be used to develop a relation between initial debris bed thickness and Nukon/CalSil debris bed surface concentration.

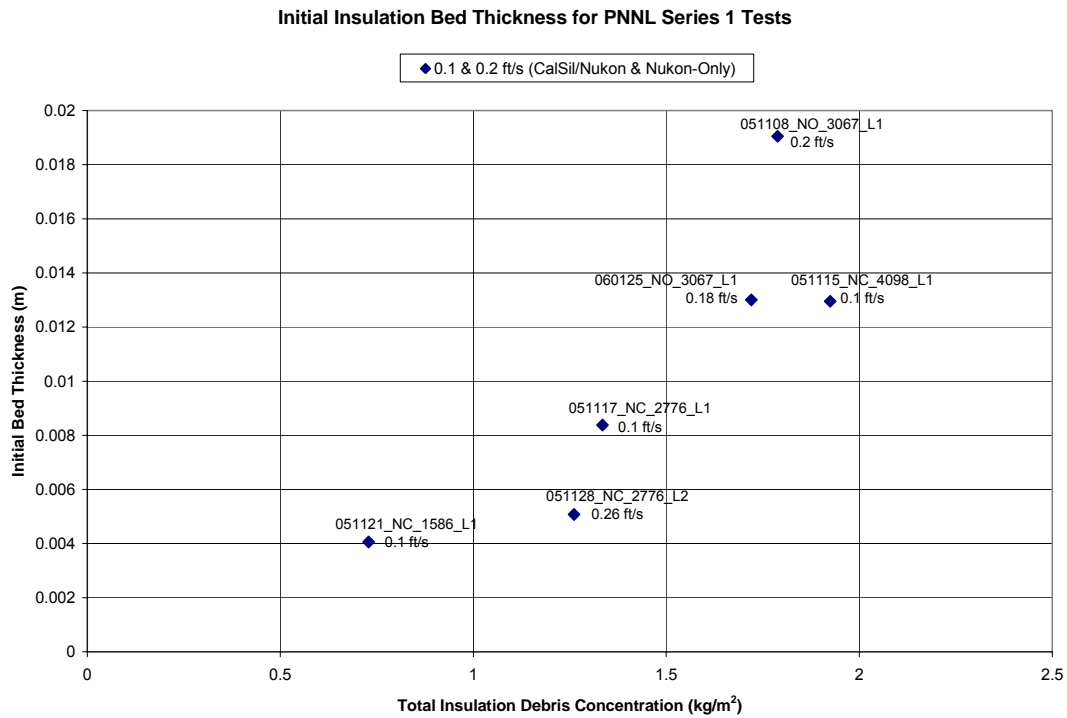


Figure 4.2-1 Initial Low-Velocity Debris Bed Thickness Using PNNL Series 1 Test Data

The void ratio of the debris bed constituents can be used to develop a relation between the bed thickness and the constituent concentrations. As indicated in equation (2.2-4), the void ratio is defined in the following equation.

$$X = \text{Vol}_{\text{void}} / \text{Vol}_{\text{solid}} \quad (2.2-4)$$

As indicated in equation (2.2-11), if a debris bed is composed of a single debris type, the void ratio definition can be written to provide a relation for thickness.

$$X = \frac{A \Delta L \rho_{\text{solid}}}{m_{\text{solid}}} - 1 \quad (2.2-11)$$

where

ΔL thickness for a debris bed composed of a single debris type

Equation (2.2-11) can be algebraically manipulated to provide a relation for debris bed thickness.

$$\Delta L = \frac{(X + 1)}{A} \frac{m_{\text{solid}}}{\rho_{\text{solid}}} \quad (4.2-1)$$

Using this relation, the debris bed thickness at bed formation can be obtained by correlating the value of void ratio, X , at bed formation to data. In addition, the initial thickness at formation for a debris bed composed of more than one debris type can be related to the sum of the thickness of each debris bed solid constituent. Therefore, the initial debris bed thickness for a Nukon/CalSil debris bed can be written as follows.

$$\Delta L_{\text{initial}} = \frac{(X_{\text{Nukon}} + 1)}{A} \frac{m_{\text{Nukon}}}{\rho_{\text{Nukon}}} + \frac{(X_{\text{CalSil}} + 1)}{A} \frac{m_{\text{CalSil}}}{\rho_{\text{CalSil}}} \quad (4.2-2)$$

where

$\Delta L_{\text{initial}}$ debris bed thickness at a reference bed formation approach velocity of about 0.0305 m/s (0.1 ft/s)

A debris bed cross-sectional surface area

X_{Nukon} Nukon void ratio in debris bed

X_{CalSil} CalSil void ratio in debris bed

m_{Nukon} Nukon mass in the debris bed

m_{CalSil} CalSil mass in the debris bed

ρ_{Nukon} Nukon material density

ρ_{CalSil} CalSil material density

The values for the void ratio of the solid constituents at bed formation can be determined from test data. Using the PNNL Series 1 test data, the values of X_{Nukon} and X_{CalSil} at the initial bed formation velocities are indicated in the following equation.

$$\Delta L_{\text{initial}} = \frac{(12.5 + 1)}{A} \frac{m_{\text{Nukon}}}{\rho_{\text{Nukon}}} + \frac{(19.1 + 1)}{A} \frac{m_{\text{CalSil}}}{\rho_{\text{CalSil}}} \quad (4.2-3)$$

Figure 4.2-2 compares the measured initial debris bed thicknesses for the PNNL Series 1 tests to the values calculated using equation (4.2-3). This figure plots initial debris bed thickness versus total Nukon/CalSil mass per surface area. The optical triangulation method was used to record the bed thickness for Test 060125_NO_3067_L1; the measured thicknesses for the other tests were made using visual measurements. This figure shows agreement between three of the measured data and calculations. Three data points do not match calculations; two are for the Nukon-only tests, Tests 051108_NO_3067_L1 and 060125_NO_3067_L1, and the third is for the Nukon/CalSil test, Test 051128_NC_2776_L2. The debris beds for the two Nukon-only tests were formed at 0.061 m/s (0.2 ft/s). The measurements for the Nukon-only test (Test 051108_NO_3067_L1) are not fully acceptable because metal and rust debris was observed in the test debris bed. Consequently, this test was rerun; however, the data for the retest (Test 060125_NO_3067_L1) still do not match calculations. The calculation

comparisons with data for these two tests are not considered to be appropriate because the two beds were formed at 0.061 m/s (0.2 ft/s), and thickness measurements were not made at 0.0305 m/s (0.1 ft/s). The Nukon/CalSil test, Test 051128_NC_2776_L2, is not considered a good check for the debris bed thickness calculation because bed thickness measurements were recorded only at a higher velocity of 0.079 m/s (0.26 ft/s). Moreover, the data at bed formation for this test are in question because steady-state conditions at bed formation could not be achieved.

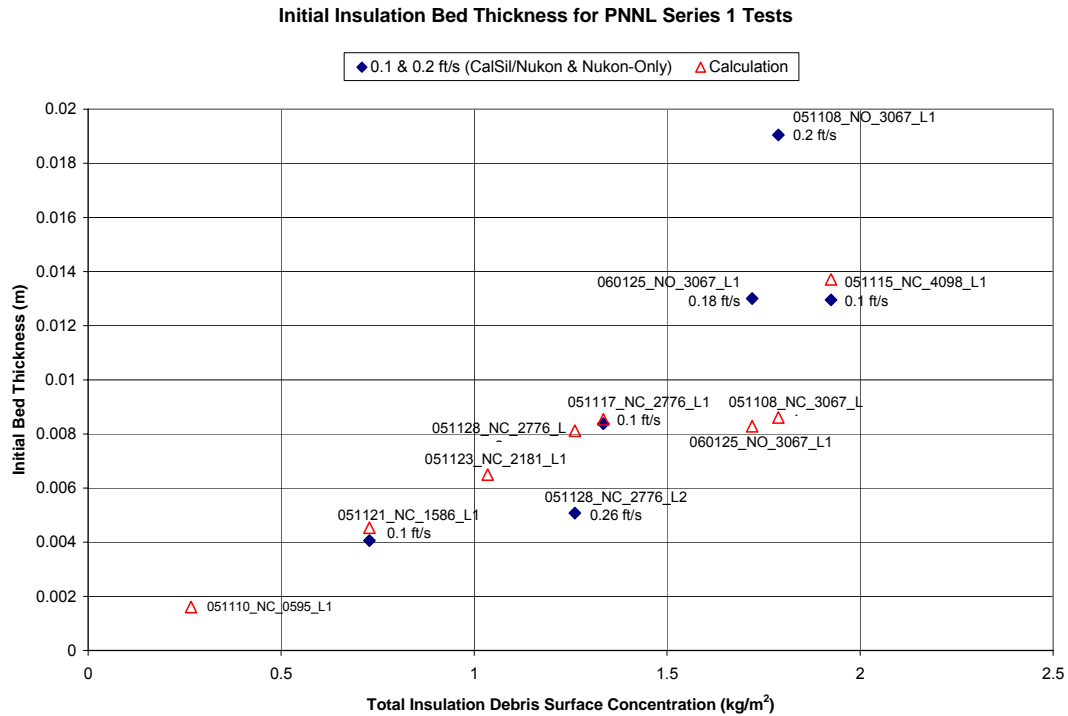


Figure 4.2-2 Comparison of Initial Low-Velocity Debris Bed Thickness Using PNNL Series 1 Test Data

The debris bed thicknesses for the Series 2 Nukon-only and Nukon/CalSil tests and for the Series 1 Nukon-only test, Test 060125_NO_3067_L1, were in situ measurements using the optical triangulation technique described in NUREG/CR-6917 (Ref. 24). This technique can provide measurements of the center body of the debris bed, the thickness of the debris bed rim, and the surface contour of the debris bed. The visual measurement technique used for the bulk of the Series 1 tests is not as accurate as the optical triangulation technique. The visual method is subject to human inaccuracies because it is difficult to measure the debris bed body thickness by using the visual method if a rim is present. Consequently, the debris bed measurement obtained using the optical triangulation method provides more accurate debris bed thickness measurements than any method previously employed for this type of testing.

Figure 4.2-3 plots the average debris bed thickness for all Series 2 tests and Series 1 Test 060125_NO_3067_L1 obtained using the optical triangulation technique versus debris mass divided by the screen or perforated plate surface area. The average debris bed thickness was obtained by using an area weighted average of the debris bed rim and body thicknesses. The debris beds for all of the Series 2 tests were formed at an approach velocity of 0.0305 m/s (0.1 ft/s); the debris bed for Series 1 Test 060125_NO_3067_L1 was formed at an approach velocity of 0.061 m/s (0.2 ft/s). The Series 2 test data covered a wide range of debris bed CalSil to Nukon mass ratios ranging from 0.02 to 0.46. In addition,

the Series 2 tests studied the effect of fluid temperature on debris bed behavior. Consequently, the Series 2 tests present data for debris beds formed at three different temperatures, about 25, 50, and 80 °C (25, 122, and 176 °F); in contrast, the debris beds for the PNNL Series 1 tests and the LANL/UNM tests were formed at ambient temperatures, about 25 °C (77 °F).

Figure 4.2-3 shows that the debris bed formation thickness is relatively insensitive to fluid temperature. However, the formation debris bed thickness for Series 1 Test 060125_NO_3067_L1, which was created at an approach velocity of 0.061 m/s (0.2 ft/s), results in an initial debris bed thickness that is substantially different from those of the Series 2 tests, which used an approach velocity of 0.0305 m/s (0.1 ft/s) for bed formation. The following equation to calculate initial debris bed thickness results from using the average formation bed thickness obtained from optical triangulation data for only the Series 2 tests and Series 1 Test 060125_NO_3067_L1.

$$\Delta L_{\text{initial}} = \frac{(30 + 1)}{A} \frac{m_{\text{Nukon}}}{\rho_{\text{Nukon}}} + \frac{(6.2 + 1)}{A} \frac{m_{\text{CalSil}}}{\rho_{\text{CalSil}}} \quad (4.2-4)$$

Figure 4.2-3 provides a comparison between the measured formation debris bed thicknesses with the predictions using equation (4.2-4). This equation provides a reasonable prediction of formation debris bed thickness for Nukon-only and Nukon/CalSil debris beds for an approach velocity of 0.0305 m/s (0.1 ft/s) over the range of temperatures from about 19 to 82 °C (66.2 to 179.6 °F).

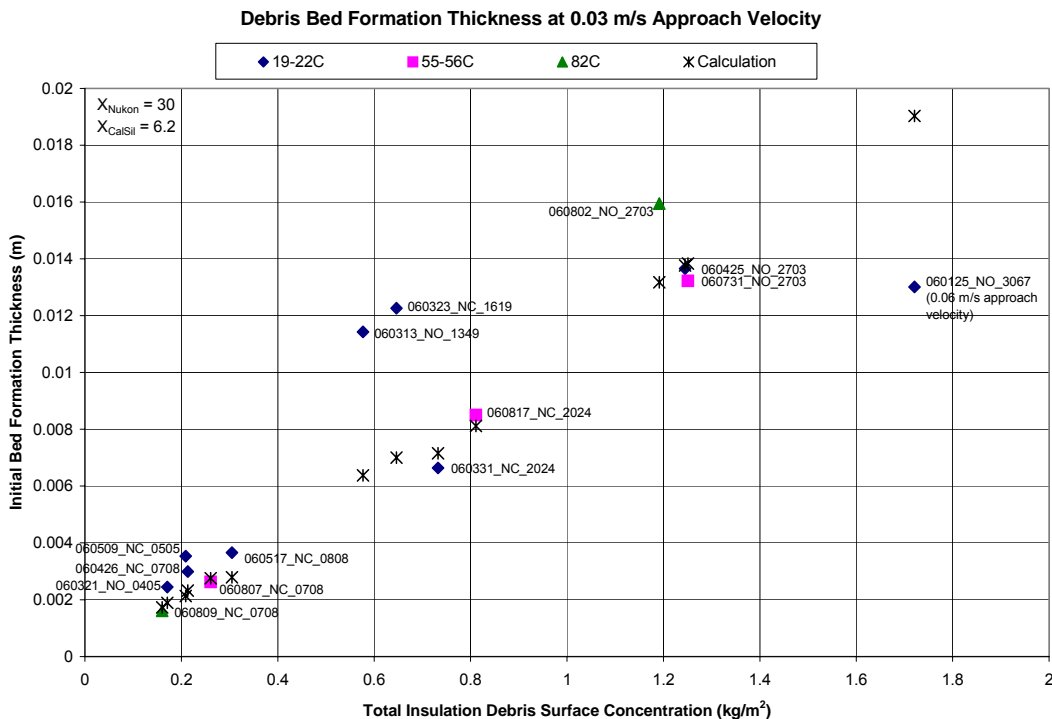


Figure 4.2-3 Comparison of Initial Low-Velocity Debris Bed Thickness Using PNNL Series 2 Test Data

4.2.2 Low-Velocity Reference Debris Bed Thickness Using LANL/UNM Series 6 Test Data

Tests performed at LANL/UNM provide data for pressure drop across a debris bed consisting of Nukon, CalSil, and other materials. The debris bed thicknesses for the LANL/UNM tests were obtained through visual measurement, using a ruler. Debris bed thickness was only measured for Series 6 tests, which provided pressure drops across debris beds composed of various masses of mixtures of Nukon and CalSil. All of the Series 6 tests began measurements at a water approach velocity of about 0.0305 m/s (0.1 ft/s). Figure 4.2-4 plots the debris bed thicknesses from this test series formed at about 0.0305 m/s (0.1 ft/s) against the total Nukon and CalSil mass surface concentration of the debris bed. This figure indicates that a linear relation exists between the low-velocity debris bed thickness at formation and the total mass concentration of the Nukon and CalSil. Only one data point for Test 6c falls outside the range of a linear fit through the remainder of the test data. The following linear equation was developed to relate the initial low-velocity debris bed thickness to debris mass density. This equation must use the indicated units.

$$L'_{\text{debrisbed}} = 0.006010 \text{ dens}_{\text{debris}} + 0.003884 \quad (4.2-5)$$

$$\text{dens}_{\text{debris}} = (m_{\text{Nukon}} + m_{\text{CalSil}}) / A \quad (4.2-6)$$

where

- $L'_{\text{debrisbed}}$ debris bed thickness (m) at an approach velocity of about 0.0305 m/s (0.1 ft/s)
- $\text{dens}_{\text{debris}}$ total debris bed mass divided by total debris bed area (kg/m^2), a value that should reflect the mass covering the flow area of the debris bed
- A debris bed cross-sectional surface area (m^2)

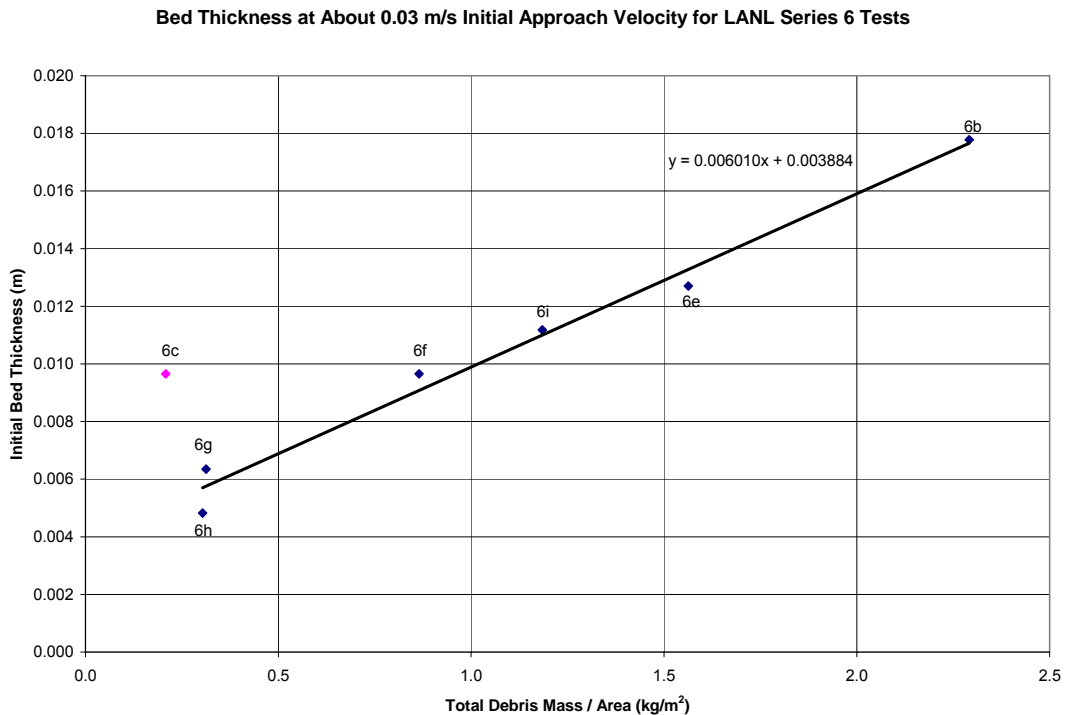


Figure 4.2-4 Initial Low-Velocity Debris Bed Thickness Using LANL Series 6 Test Data

4.2.3 Low-Velocity Reference Debris Bed Thickness Using LANL/UNM and PNNL Test Data

The relation developed using the PNNL Series 2 data differs from those developed using the PNNL Series 1 test data or the LANL/UNM Series 6 test data. Because of the uncertainties relating to the actual insulation mass accumulated in the debris bed for the LANL/UNM tests, as discussed further in Section 4.1, the curve fit developed by using the LANL/UNM data is not recommended for general application. In addition, the curve fit developed by using the LANL/UNM data does not pass through the (0,0) point where the bed thickness equals zero when the bed mass equals zero.

Figure 4.2-5 shows the relationship between the initial debris bed thicknesses from the LANL/UNM Series 6 Nukon/CalSil data and the PNNL data for the Nukon-only and Nukon/CalSil beds built at 0.0305 m/s (0.1 ft/s) and 0.061 m/s (0.2 ft/s). The variances in recorded data can be related to (1) discrepancies regarding the actual masses in the debris bed for the LANL Series 6 tests and (2) uncertainties regarding the actual bed thickness obtained using a visual ruler measurement for the LANL/UNM Series 6 and PNNL Series 1 data.

Because of these considerations, equation (4.2-4) in Section 4.2.1, obtained by using the PNNL Series 2 data, is recommended for general use. The Series 2 tests have the most accurate measurements of the Nukon and CalSil masses in the debris bed and of the debris bed thickness. Figure 4.2-6 compares the results of the recommended relation for calculating the initial debris bed thickness with all test data for Nukon and Nukon/CalSil debris beds formed at an approach velocity of 0.0305 m/s (0.1 ft/s). This plot also presents four additional data points obtained for Nukon-only benchmark tests, performed at ANL and documented in NUREG/CR-6913, "Chemical Effects Head-Loss Research in Support of Generic Issue 191," issued September 2006 (Ref. 25). For the ANL tests, the debris bed thickness was measured using a visual ruler method. Section 6.3 more fully discusses the ANL tests.

Equation (4.2-4) appears to better match these accumulated test data at lower debris bed surface concentrations (kg/m^2). At higher surface concentrations, the predictions are slightly greater than the measurements. However, the data at the higher surface concentrations were obtained from the LANL Series 6 and PNNL Series 1 data points, which probably exhibit the greatest measurement inaccuracies.

The comparisons of the data readings also illustrate the insensitivity of the initial formation debris bed thickness to the type of collecting surface screen and perforated plate. The PNNL Series 1 and LANL/UNM Series 6 tests used similar metal screens for testing, and the PNNL Series 2 and ANL benchmark tests used similar perforated plates. The screens and perforated plates used during these tests had similar ratios of flow area per total surface area, similar opening diameters, and similar hole spacing. Thus, the characteristics of an initially formed bed appear to be insensitive to whether a screen or perforated plate is used as long as the ratios of flow area per total surface area are similar.

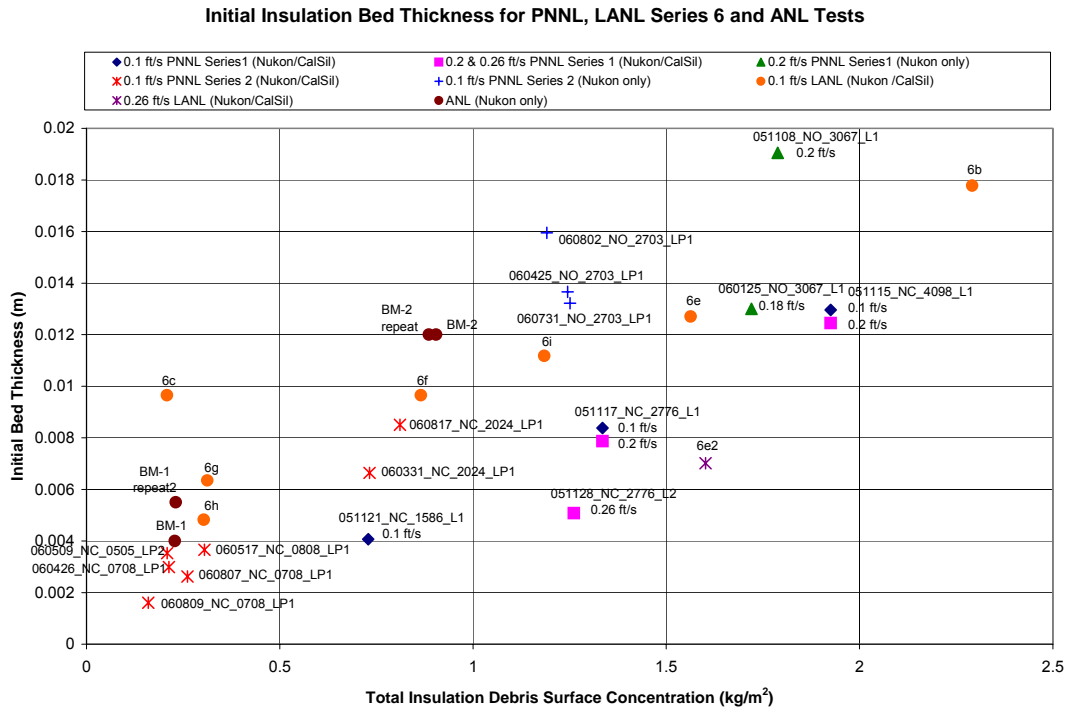


Figure 4.2-5 Initial Low-Velocity Debris Bed Thickness Using PNNL, LANL and ANL Test Data

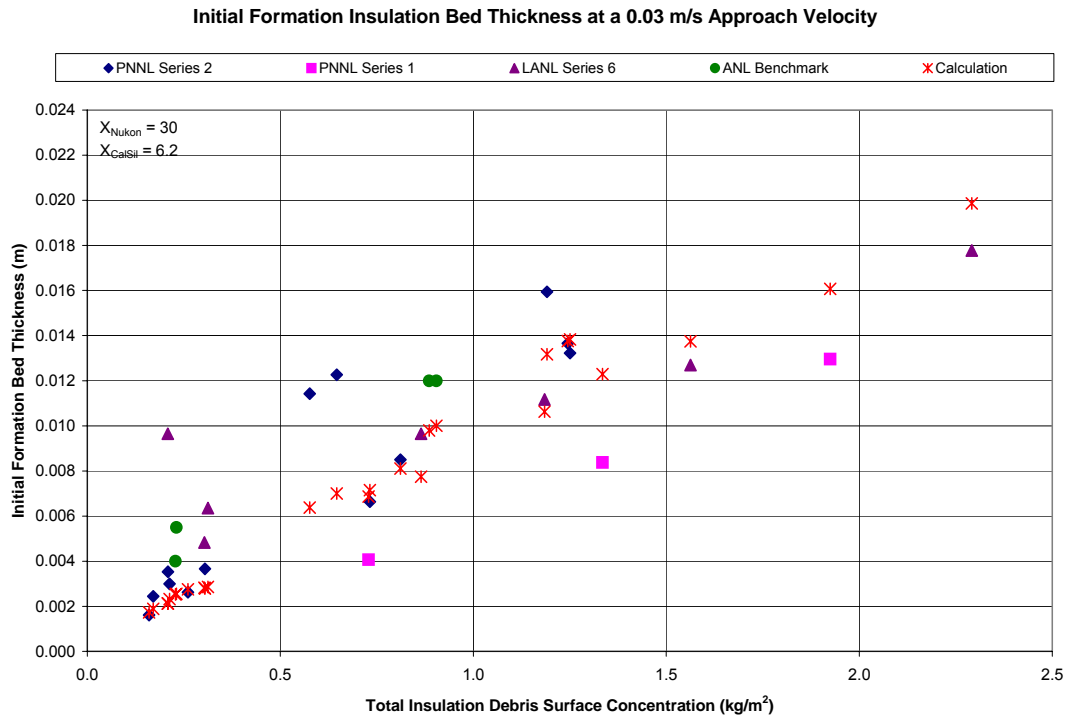


Figure 4.2-6 Initial Formation Debris Bed Thickness Test Data for a 0.03 m/s Approach Velocity

4.3 Material Properties and Empirical Values for the Head Loss Equation

4.3.1 Determination of Material Properties

Table 4.3-1 shows the material density of the Nukon fibers and the CalSil particles recommended in NUREG/CR-6874 (Ref. 3) for predictive calculations. PNNL verified the appropriateness of these density values in Reference 24. Consequently, these Nukon and CalSil material densities are recommended for predictive calculations. CalSil insulation can include fiber material such as fiberglass and cellulose. The CalSil fibers are assumed to possess the same material density as fiberglass.

Table 4.3-1 Debris Properties for Head Loss Calculations

Debris	NUREG/CR-6874 (Ref. 3) Recommended Material Density (ρ_{solid}) (kg/m ³) / (lbm/ft ³)	NUREG/CR-6874 (Ref. 3) Recommended Specific Surface Area (S_v) (m ⁻¹) / (ft ⁻¹)	Current Recommended Specific Surface Area (S_v) (m ⁻¹) / (ft ⁻¹)
Nukon Fibers	2803 / 175 ¹	561,024 / 171,000 ²	984,252 / 300,000
CalSil Particles	1842 / 115 ³	1,968,504 / 600,000 ⁴ 2,887,139 / 880,000 ⁵	2,132,546 / 650,000
Fiberglass Fibers in CalSil	2803 / 175 ⁶	561,024 / 171,000 ⁷	984,252 / 300,000

¹ Nukon fiberglass material density reported in NUREG/CR-6874

² Nukon fiber specific surface area recommended in NUREG/CR-6874

³ CalSil material density obtained from a particle density test reported in NUREG/CR-6874

⁴ CalSil particle specific surface area recommended in NUREG/CR-6874 for mixed debris beds

⁵ CalSil particle specific surface area recommended in NUREG/CR-6874 for thin debris beds

⁶ CalSil fiber material density assumed for debris bed calculations

⁷ CalSil fiber specific surface area assumed in NUREG/CR-6874

Table 4.3-1 lists the specific surface area recommended in NUREG/CR-6874 for performing calculations with Nukon fibers. The manufacturer of Nukon has indicated that the diameter of the Nukon fibers is 0.00026 ± 0.0002 inch ($6.6 \times 10^{-6} \text{ m} \pm 5.1 \times 10^{-6} \text{ m}$) without binder material on the fibers and 0.00028 ± 0.0002 inch ($7.1 \times 10^{-6} \text{ m} \pm 5.1 \times 10^{-6} \text{ m}$) with binder material. If the specific surface area is calculated using the manufacturer-specified fiber diameter and the geometric definition for a packed bed composed of cylindrical fibers oriented perpendicular to the flow direction in equation (2.1-5), the following values result.

$$S_v = 4 / 0.00026 \text{ inch} = 605,694 \text{ m}^{-1} = 184,615 \text{ ft}^{-1} \text{ without binder material}$$

$$S_v = 4 / 0.00028 \text{ inch} = 562,430 \text{ m}^{-1} = 171,429 \text{ ft}^{-1} \text{ with binder material}$$

PNNL performed independent measurements of the Nukon fiber diameters. These measurements indicated that the fiber diameters range between 5 and 15 microns. The diameters result in the following range of S_v values when using the geometrical relation in equation (2.1-5).

$$S_v = 4 / 5 \times 10^{-6} \text{ m} = 800,000 \text{ m}^{-1} = 243,840 \text{ ft}^{-1} \quad \text{for 5-micron-diameter fibers}$$

$$S_v = 4 / 15 \times 10^{-6} \text{ m} = 266,667 \text{ m}^{-1} = 81,280 \text{ ft}^{-1} \quad \text{for 15-micron-diameter fibers}$$

The values for S_v calculated by using the manufacturer-supplied diameters are similar to, and may be the basis for, the values recommended in NUREG/CR-6874 (Ref. 3). However, not all of the fibers in a Nukon debris bed are expected to be oriented perpendicular to flow. Consequently, the S_v value that results from assessment of test data and is recommended for application in the developed calculational method can differ from the theoretical value calculated by using equation (2.1-5). In addition, the values for S_v calculated by using the PNNL-measured diameter range indicate a wider variation for S_v . In fact, as illustrated in several references (e.g., Ref. 15), the values for S_v that are recommended for calculating pressure drop across debris beds can differ substantially from the values calculated by using the geometrical equations for perpendicularly oriented fibers or spherical particles, specifically equations (2.1-3) and (2.1-5).

As shown in the comparisons of predictions and test data discussed in Section 6, the Nukon specific surface area listed in Table 4.3-1 is appropriate for use in predictive calculations. Using the PNNL Nukon-only test data, the value for the Nukon specific surface area necessary in calculations to match the measured pressure drop ranged from about 803,806 to 967,848 m^{-1} (245,000 to 295,000 ft^{-1}) with an average and median value both about 820,210 m^{-1} (250,000 ft^{-1}). The recommended value of 984,252 m^{-1} (300,000 ft^{-1}) is an upper limit that envelops the range of Nukon S_v . In addition, PNNL test data show that the Nukon specific surface area is not strongly dependent on fluid temperature. Because CalSil insulation can include fiberglass fibers, using the Nukon specific surface area for the fibers present in CalSil insulation is appropriate.

NUREG/CR-6874 recommends different values for the CalSil particle-specific surface area, depending on whether the debris bed is thin or thick. In fact, the predicted CalSil specific surface area obtained by using the LANL/UNM test data described in NUREG/CR-6874 varied from about 984,252 to 2,887,139 m^{-1} (300,000 to 880,000 ft^{-1}). This variance appears inappropriate because the value for the specific surface area of a particulate should primarily depend on the properties of the material.

As indicated in Section 4.1, the PNNL testing included an attempt to build a CalSil-only debris bed in the PNNL large loop. A complete, continuous CalSil debris bed could not be developed despite the addition of 81.08 grams of CalSil to the test loop. Before testing in the large loop, PNNL did perform a series of CalSil-only tests in its benchtop loop to determine the CalSil loading that could build a complete, continuous debris bed. These tests were also unsuccessful. Consequently, attempts were made to determine the CalSil particle-specific surface area by accounting for the bed bypass holes in performing pressure drop analysis of the tested debris beds. Attempts were also made to calculate the CalSil particle-specific surface area by assessing the data for the Nukon-CalSil tests listed in Section 4.1. As a result, the best estimate of the CalSil particle specific surface area is about 2,132,546 m^{-1} (650,000 ft^{-1}). This value is recommended for predictive calculations.

4.3.2 Determination of Multiplier and Exponent Values for the Kinetic Term of the Head Loss Equation

As indicated in equations (2.6-2) and (2.6-4), the kinetic term for the pressure drop equation includes material-dependent empirical multipliers and exponents. Section 2.3 provides the basis for these values. Empirical values b and c must be defined for two types of debris materials, spherical particles and cylindrical fibers. Reference 16 notes the values of b and c —3.89 and 0.13, respectively, which were developed for spherical particles—are appropriate for calculations for CalSil particle debris beds. However, the values of b and c suggested for the Nukon cylindrical fibers were developed from pressure drop data for woven metal screen with different types of weaves (Ref. 15). These values may not be

generally appropriate for a bed of Nukon fibers. However, the expected values should be of the same order of magnitude.

The viscous term of the head loss equation is the dominant contributor to pressure drop for sump screen approach velocities that are less than 0.061 m/s (0.2 ft/s). The viscous term contributes more than 90 percent of the total pressure drop for all of the calculational results provided in Section 6. At approach velocities less than 0.0305 m/s (0.1 ft/s), the viscous term contributes an even larger percentage of the pressure drop. Consequently, it can be argued that the kinetic term could be omitted from the head loss calculation. Because the empirical multipliers b and c for the kinetic term do not produce a major impact on the sump screen debris bed pressure drop, the current suggested values of b and c may be used for the cylindrical fibers with the current range of expected PWR sump screen approach velocities.

4.4 Particulate Maximum Concentration Model for Nukon/CalSil Debris Beds

In NUREG/CR-6874 (Ref. 3), the NUREG/CR-6224 (Ref. 2) head loss calculational method was correlated to test data by varying the specific surface area of the CalSil particles in a Nukon/CalSil debris bed as a function of bed thickness. This approach led to the “thin bed” effect, which employed a larger specific surface area value for debris beds below a specified thickness. A major objective of the current derivation is to develop a theoretically consistent approach that can be applied over all ranges of debris bed thickness without the need to vary the value of specific surface area.

Test data will be used to identify a maximum particle concentration or saturation condition for a debris bed composed of small particles such as CalSil mixed with a fiber such as Nukon. This condition represents the maximum mass concentration of CalSil particles in a fibrous Nukon bed that results in the maximum pressure drop increase because of particle clogging. This effect was observed in previous testing for thin debris beds and was called the “thin bed” effect. In actuality, a thin layer of concentrated particles in a fiber bed can exist in debris beds of any thickness. This section discusses the approach to determine the particle concentration limit.

Experts recognize that the limiting debris bed pressure drop condition exists for a completely clogged bed. This condition results in a no-flow condition with the maximum pressure drop. PNNL test data will be used to identify debris bed conditions that result in a practical maximum upper bound pressure drop. As indicated in Section 4.1, the masses of Nukon and CalSil in the debris beds tested at the LANL/UNM facility are in question. Consequently, using the LANL/UNM head loss data to determine the maximum CalSil concentration conditions in a Nukon debris bed is not appropriate.

4.4.1 Nukon/CalSil Maximum Concentration Model Developed Using PNNL Test Data

To identify the maximum CalSil concentration in a Nukon bed, PNNL test data were used to develop a relationship between head loss, the mass of each of the debris constituents, the porosity of the debris bed, and the debris bed thickness. To enable the application of this approach to screens with different areas, the proposed method relates parameters that are independent of the surface area of the tested debris beds.

The two-volume calculational model was used to estimate the maximum CalSil concentration in a Nukon bed. The initial bed thickness for a specific test was calculated by using the calculational model described in Section 4.2. The assumptions were that (1) the Nukon mass in the debris bed was uniformly distributed throughout the debris bed, (2) the upstream portion of the bed was composed almost entirely of Nukon fibers, with only 0.01 percent of the CalSil in the bed located in the upstream volume, and (3) the downstream volume located next to the screen was composed of Nukon that was concentrated with

CalSil particles. Using these assumptions, the initial thickness of the downstream particle saturated volume at the bed formation approach velocity of 0.0305 m/s (0.1 ft/s) could be determined by applying the following relations.

$$Y = \frac{\text{dens}_{\text{CalSilmax}}}{\text{dens}_{\text{Nukon}}} = \frac{m_{\text{CalSil}} / A / \Delta L_{\text{min}}}{m_{\text{Nukon}} / A / \Delta L_{\text{total}}} = \frac{m_{\text{CalSil}} \Delta L_{\text{total}}}{m_{\text{Nukon}} \Delta L_{\text{min}}} \quad (4.4-1)$$

$$\Delta L_{\text{min}} = \frac{m_{\text{CalSil}} \Delta L_{\text{total}}}{m_{\text{Nukon}} Y} = \frac{m_{\text{CalSil}}}{A \text{ dens}_{\text{Nukon}} Y} \quad (4.4-2)$$

where

$\text{dens}_{\text{CalSilmax}}$	maximum saturated CalSil debris bed density (mass per debris bed volume)
$\text{dens}_{\text{Nukon}}$	Nukon debris bed density (mass per debris bed volume)
m_{CalSil}	CalSil mass in debris bed
m_{Nukon}	Nukon mass in debris bed
A	debris bed cross-sectional surface area
ΔL_{total}	total bed thickness
ΔL_{min}	thickness of debris bed saturated with CalSil particles

The value of Y used in the two-volume calculational method is varied until the pressure drop predictions for the modeled test match the test data. Table 4.4-1 shows the values of Y determined by using data from all the PNNL tests that recorded bed thickness. This table also provides the value of the particle concentrated volume within the debris bed. Figures 4.4-4 to 4.4-15 illustrate the ability to determine the value of Y by using PNNL Series 1 and 2 test data.

Several approaches were attempted to identify a practical maximum particle concentration limit. One approach used test data to relate the particle concentration density in the particle concentrated volume of the debris bed to the fiber density in the debris bed. Figure 4.4-1 plots the CalSil particle debris bed density in the particle concentrated volume against the Nukon fiber debris bed density. For comparison, this figure also plots the porosity of the particle concentrated end volume as a function of fiber bed density. A relationship between CalSil particle concentrated density and the Nukon fiber bed density could not be obtained from Figure 4.4-1; thus, this approach could not be used for predictive calculations.

Another approach used test data to relate the CalSil particle porosity in the particle concentrated volume to Y, the ratio of the particle density in the particle concentrated volume and the fiber bed density. Figure 4.4-2 plots the CalSil particle concentration porosity against Y. A relationship for the maximum CalSil porosity in a Nukon fiber bed can be obtained from Figure 4.4-2. The following relation can be used to calculate the particle porosity in the particle concentrated volume.

$$\epsilon_{\text{CalSilSat}} = 0.00322934 Y^2 - 0.06740456 Y + 1.00108928 \quad (4.4-3)$$

where

$\epsilon_{\text{CalSilSat}}$	CalSil particle saturation porosity in end Nukon/CalSil volume
-------------------------------	--

Assuming that the Nukon is evenly distributed in the debris bed, the thickness of the end volume can be calculated from the maximum CalSil concentration porosity in the end volume by using the definition of porosity.

$$\epsilon_{\text{CalSilSat}} = \frac{\text{Vol}_{\text{CalSilvoid}}}{\text{Vol}_{\text{tot}}} = \frac{\text{Vol}_{\text{total}} - \text{Vol}_{\text{CalSil}}}{\text{Vol}_{\text{tot}}} \quad (4.4-4)$$

$$\epsilon_{\text{CalSilSat}} = \frac{A \Delta L_{\text{min}} - m_{\text{CalSil}} / \rho_{\text{CalSil}}}{A \Delta L_{\text{min}}} \quad (4.4-5)$$

$$\Delta L_{\text{min}} = \frac{m_{\text{CalSil}}}{\rho_{\text{CalSil}} A (1 - \epsilon_{\text{CalSilSat}})} \quad (4.4-6)$$

A third calculational approach used test data to relate the ratio of the thickness of the particle concentrated volume and the total bed thickness to the ratio of the particle and fiber masses in the debris bed. Figure 4.4-3 shows the resultant plot. The following equations relate the thickness ratio to the ratio of the particle and fiber masses.

$$\Delta L_{\text{min}} / \Delta L_{\text{initial}} = 0.00768499 e^{8.36430232 \left(\frac{m_{\text{CalSil}}}{m_{\text{Nukon}}} \right)} \quad (4.4-7)$$

The thickness ratio of the particle concentrated volume can be used to predict the characteristics of a particle/fiber debris bed and the resultant pressure drop. This approach provided the best predictive capabilities when compared to other considered approaches, including the other two presented approaches. Consequently, Section 6 compares the results obtained using this third approach to Nukon/CalSil debris bed test data.

Notably, the recommended approach for calculating the maximum pressure drop across a Nukon/CalSil debris bed assumes that the pressure drop measurements from the PNNL Series 1 and 2 test data represent the maximum practical pressure drop across a Nukon/CalSil debris bed for the range of tested conditions. If future test data indicate that this assumption is incorrect, modification of the relation to obtain the maximum particle concentration thickness would be necessary.

Table 4.4-1 CalSil End Volume Concentration Conditions Determined from PNNL Test Data

Test	Test Temperature (°C) / (°F)	Velocity at Initial Measured Thickness (m/s) / (ft/s)	Nukon Bed Density (kg/m ³)	CalSil End Vol Bed Density (kg/m ³)	$\frac{\text{dens}_{\text{CalSilmax}}}{\text{dens}_{\text{Nukon}}}$	Thickness of Particle Concentrated Vol (m) / (in)	CalSil Concentrated in End Vol of Debris Bed
Series 1 Tests							
051115_NC_4098_L1	21–27 / 69.8–80.6	0.0305 / 0.1	92.34	60.94	0.6600	0.01196 / 0.4709	Yes
051117_NC_2776_L1	16–27 / 60.8–80.6	0.0305 / 0.1	118.04	161.82	1.3710	0.002136 / 0.08409	Yes
051121_NC_1586_L1	21–25 / 60.8–77	0.0305 / 0.1	138.05	267.03	1.9345	0.0006292 / 0.02477	Yes
051123_NC_2181_L1	21–27 / 60.8–80.6	0.076 / 0.25	90.20	418.15	4.6360	0.0005945 / 0.02341	Yes
051128_NC_2776_L2	22–32 / 71.6–89.6	0.079 / 0.26	148.00	288.58	1.9500	0.001164 / 0.04583	Yes
Series 2 Tests							
060323_NC_1619_LP1	21–22 / 60.8–71.6	0.0305 / 0.1	51.04	1.65	0.03232	0.0	Homogeneous Bed
060331_NC_2024_LP1	21–24 / 60.8–75.2	0.0305 / 0.1	90.53	157.42	1.7390	0.0008392 / 0.03304	Yes
060817_NC_2024_LP1	53–56 / 127.4–132.8	0.0305 / 0.1	81.27	454.59	5.5940	0.0002632 / 0.01036	Yes
060509_NC_0505_LP1	20–22 / 68–71.6	0.0305 / 0.1	52.11	28.14	0.5400	0.0008833 / 0.03478	Yes
060426_NC_0708_LP1	21–24 / 60.8–75.2	0.0305 / 0.1	69.52	688.16	9.9000	0.000006943 / 0.0002733	Yes
060807_NC_0708_LP1	54–56 / 129.2–132.8	0.0305 / 0.1	92.71	463.52	5.0000	0.00003961 / 0.001559	Yes
060809_NC_0708_LP1	79–83 / 174.2–181.4	0.0305 / 0.1	96.96	682.53	7.0400	0.000007079 / 0.0002787	Yes
060517_NC_0453_LP1	25 / 77	0.0305 / 0.1	61.06	523.43	8.5730	0.0001559 / 0.006138	Yes

The analyses that developed this table used the following assumptions:

- All calculations used a bed formation velocity of 0.0305 m/s (0.1 ft/s); test velocities do not exceed about 0.15 m/s (0.5 ft/s).
- Calculations used the debris masses identified in Table 4.1-2.
- The calculations used measured bed thicknesses. The Series 1 tests used visually measured bed thicknesses; the Series 2 tests used thicknesses measured by optical triangulation.
- $S_{v\text{Nukon}} = 984,252 \text{ m}^{-1}$ (300,000 ft⁻¹); $S_{v\text{CalSil}} = 2,132,546 \text{ m}^{-1}$ (650,000 ft⁻¹).
- 99.99 percent of all CalSil mass is present in the Nukon/CalSil volume.
- Nukon is homogeneously distributed in the debris bed.

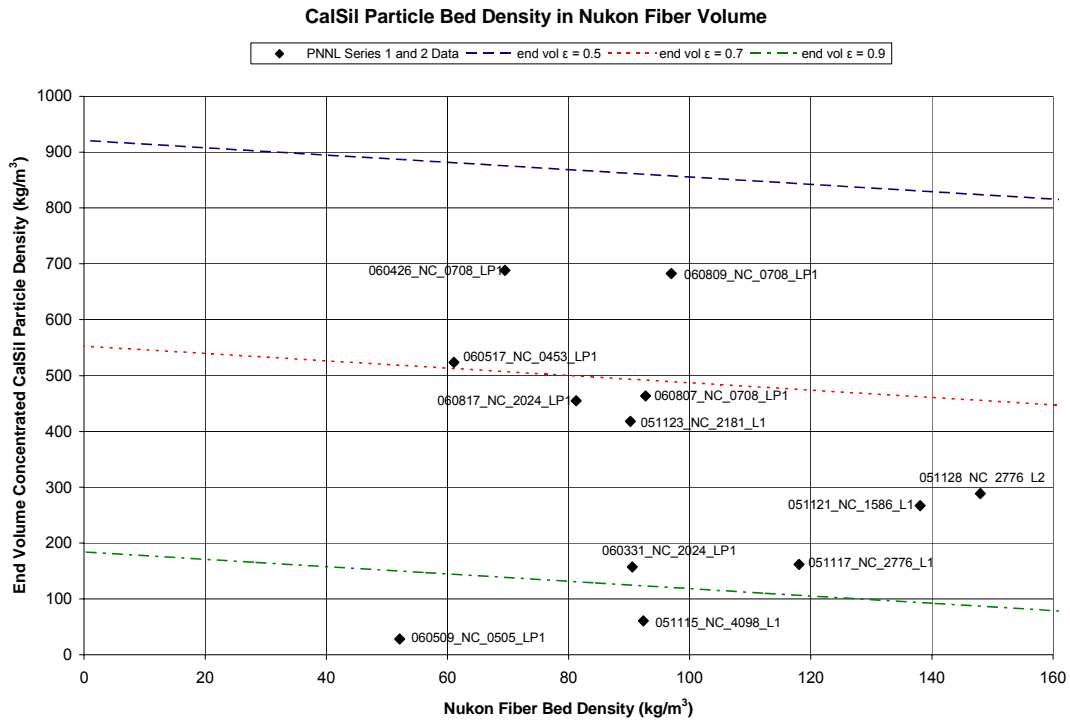


Figure 4.4-1 CalSil Particle End Volume Bed Density in a Nukon/CalSil Debris Bed

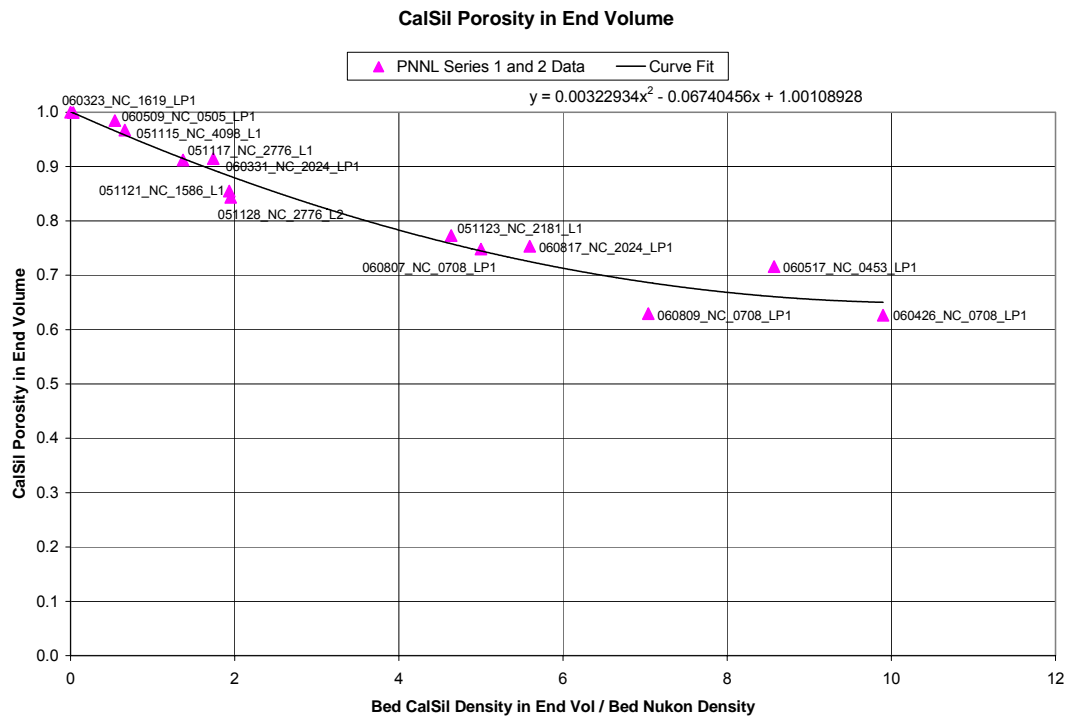


Figure 4.4-2 CalSil End Volume Porosity in a Nukon/CalSil Debris Bed

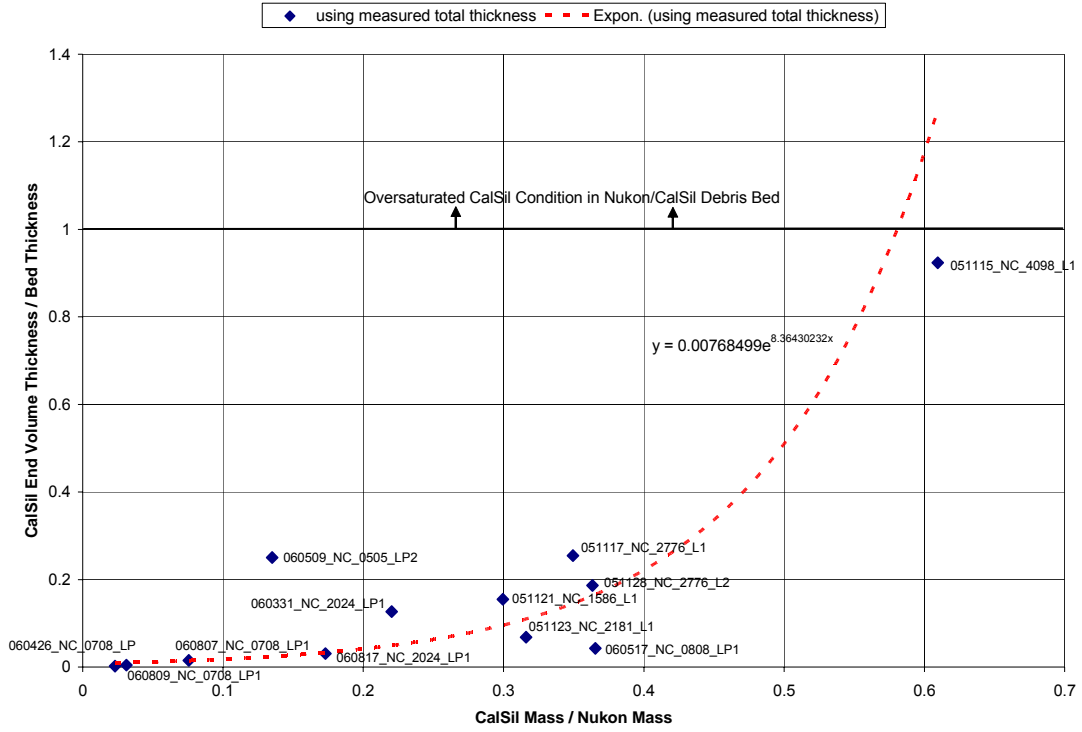


Figure 4.4-3 CalSil End Volume Bed Thickness in a Nukon/CalSil Debris Bed

Test 051115_NC_4098_L1(Nukon/CalSil=1.20/0.73 kg/m², 21-25C) - Two Volume Model

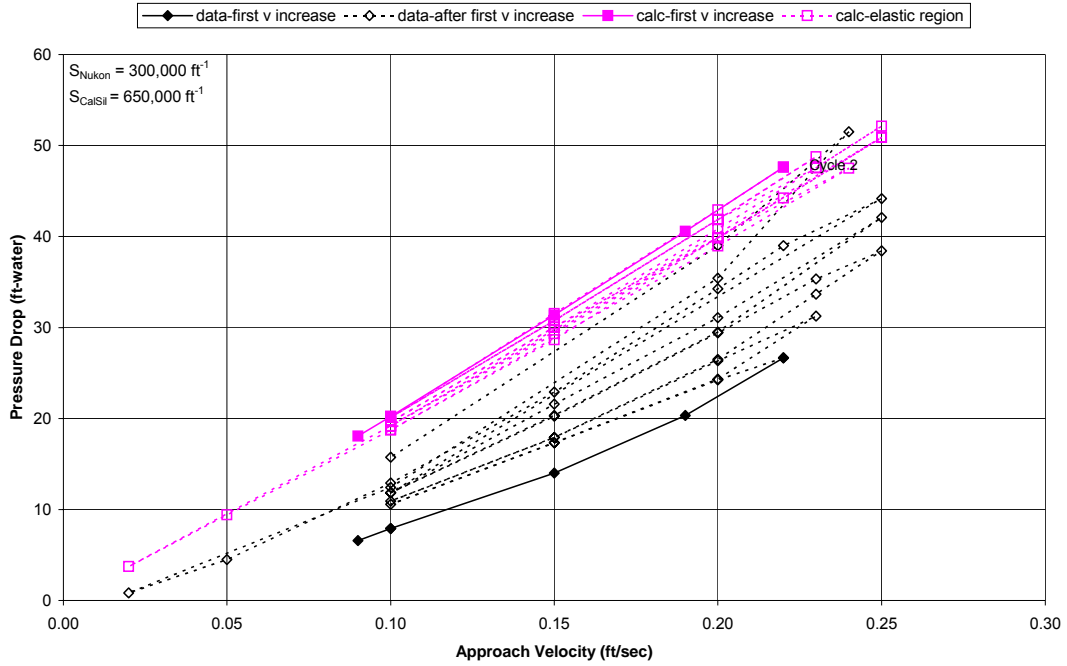


Figure 4.4-4 Head Loss Comparisons for PNNL Test 051115_NC_4098_L1 to Determine Y

Test 051117_NC_2776_L1(Nukon/CalSil=0.99/0.35 kg/m², 21-27C) - Two Volume Model

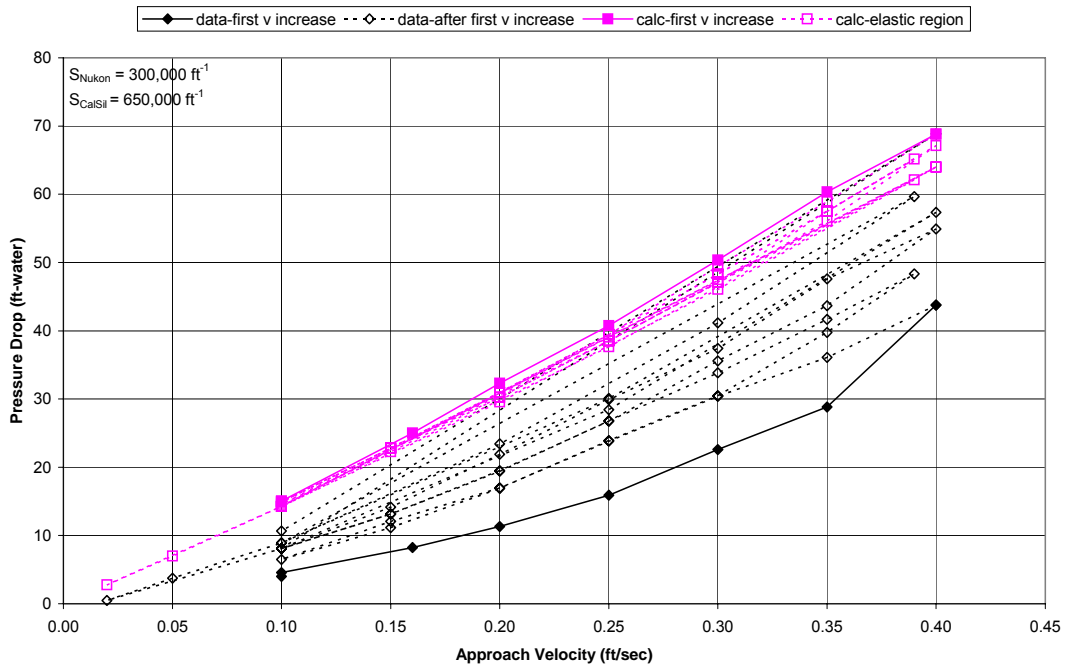


Figure 4.4-5 Head Loss Comparisons for PNNL Test 051117_NC_2776_L1 to Determine Y

Test 051121_NC_1586_L1(Nukon/CalSil=0.56/0.17 kg/m², 16-27C) - Two Volume Model

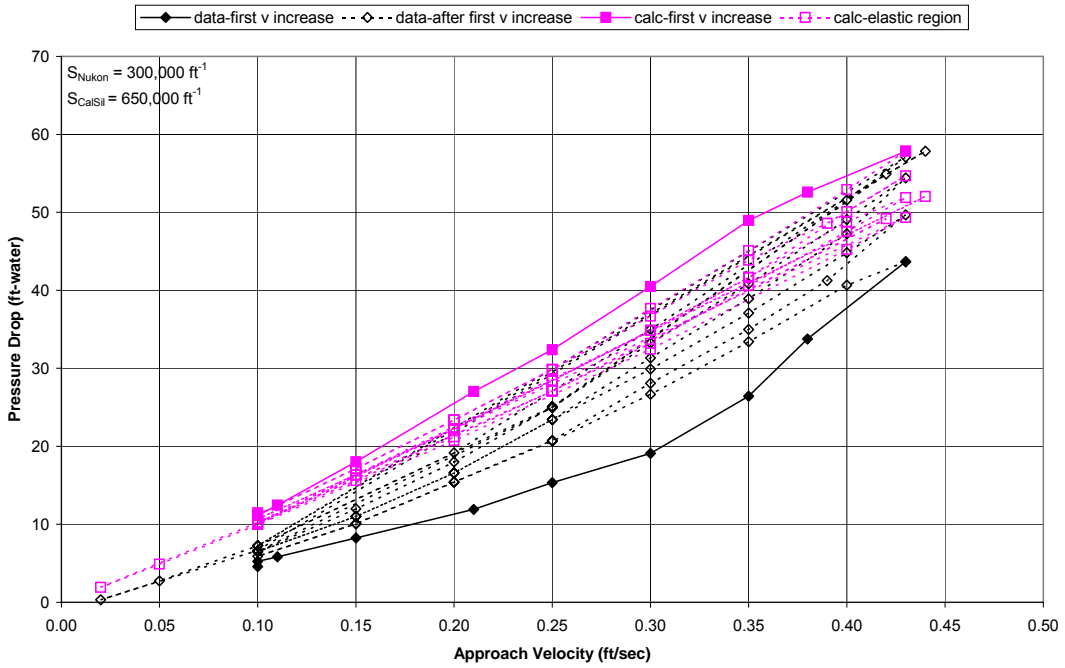


Figure 4.4-6 Head Loss Comparisons for PNNL Test 051121_NC_1586_L1 to Determine Y

Test 051123_NC_2181_L1(Nukon/CalSil=0.79/0.25 kg/m², 22-32C) - Two Volume Model

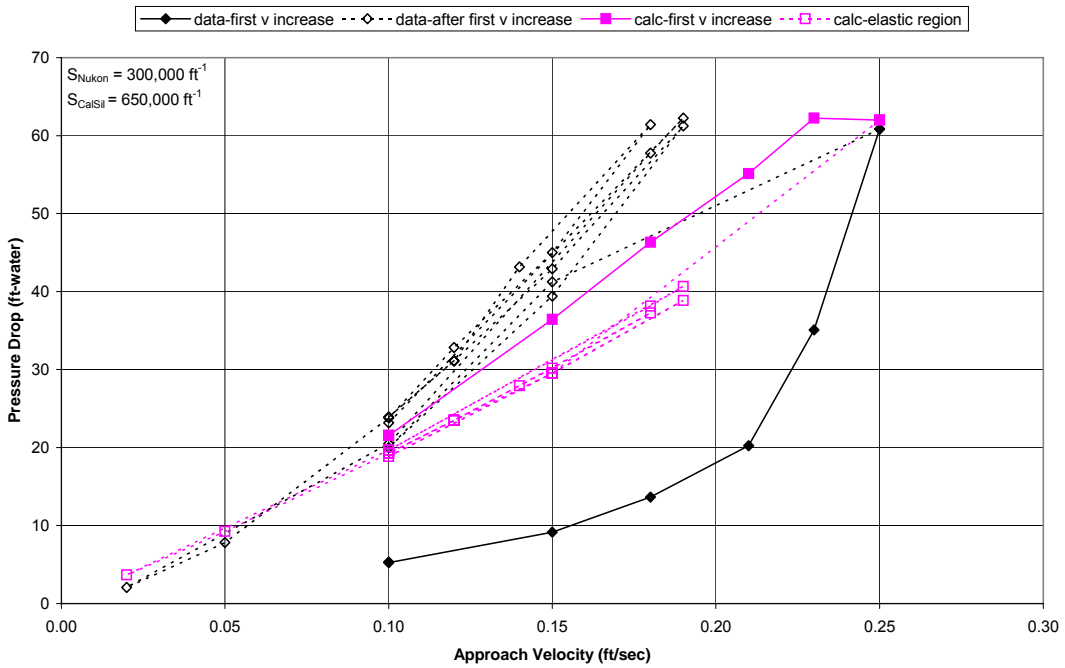


Figure 4.4-7 Head Loss Comparisons for PNNL Test 051123_NC_2181_L1 to Determine Y

Test 051128_NC_2776_L2(Nukon/CalSil=0.93/0.34 kg/m², 21-27C) - Two Volume Model

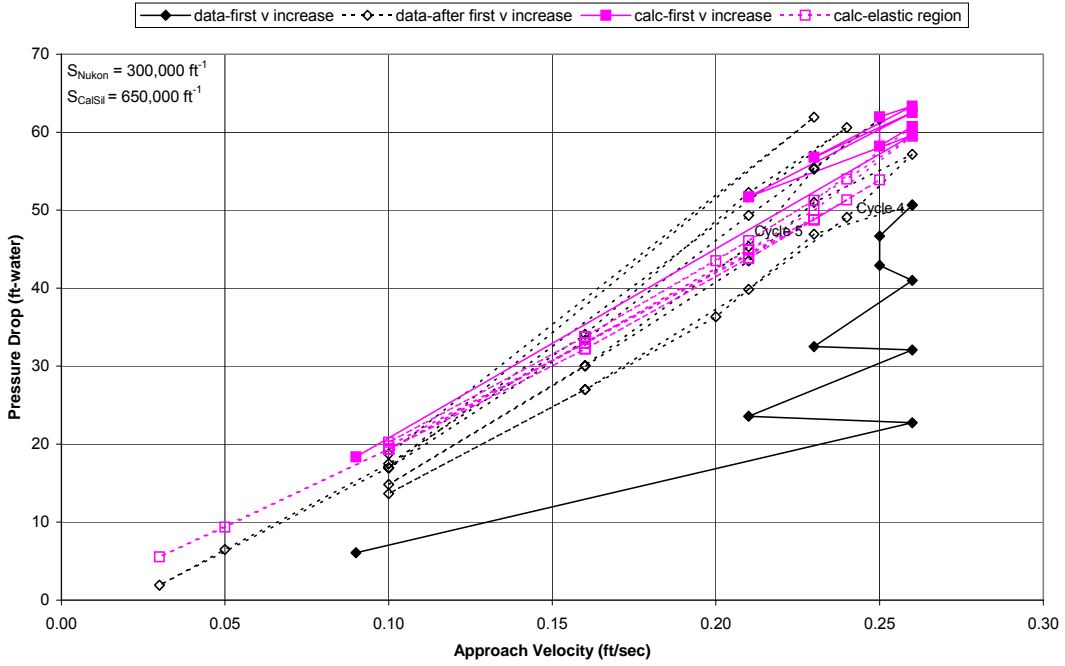


Figure 4.4-8 Head Loss Comparisons for PNNL Test 051128_NC_2776_L2 to Determine Y

PNNL Series 2 060331_NC_2024_LP1(Nukon/CalSil=0.60/0.13 kg/m², 21-24C)-Two Vol Model

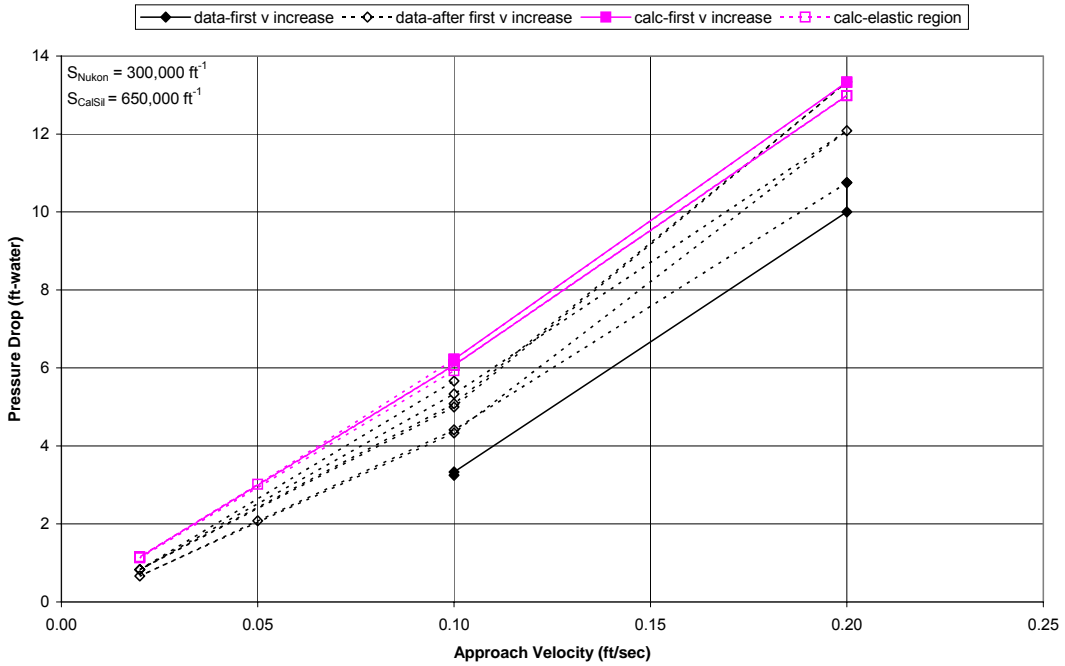


Figure 4.4-9 Head Loss Comparisons for PNNL Test 060331_NC_2024_LP1 to Determine Y

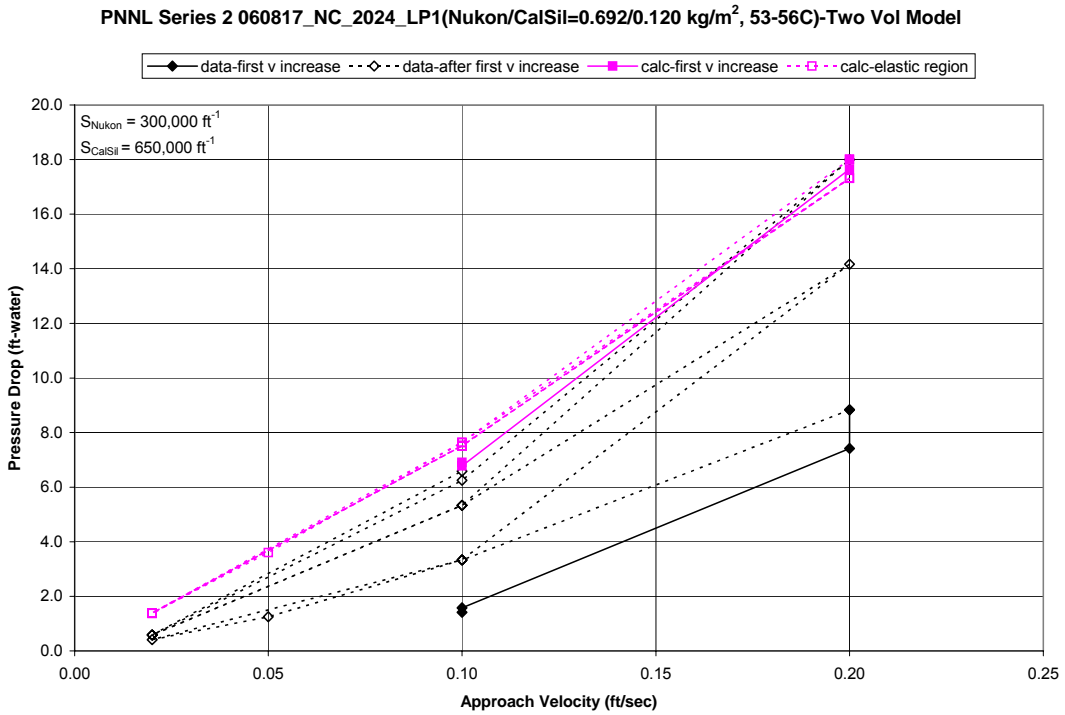


Figure 4.4-10 Head Loss Comparisons for PNNL Test 060817_NC_2024_LP1 to Determine Y

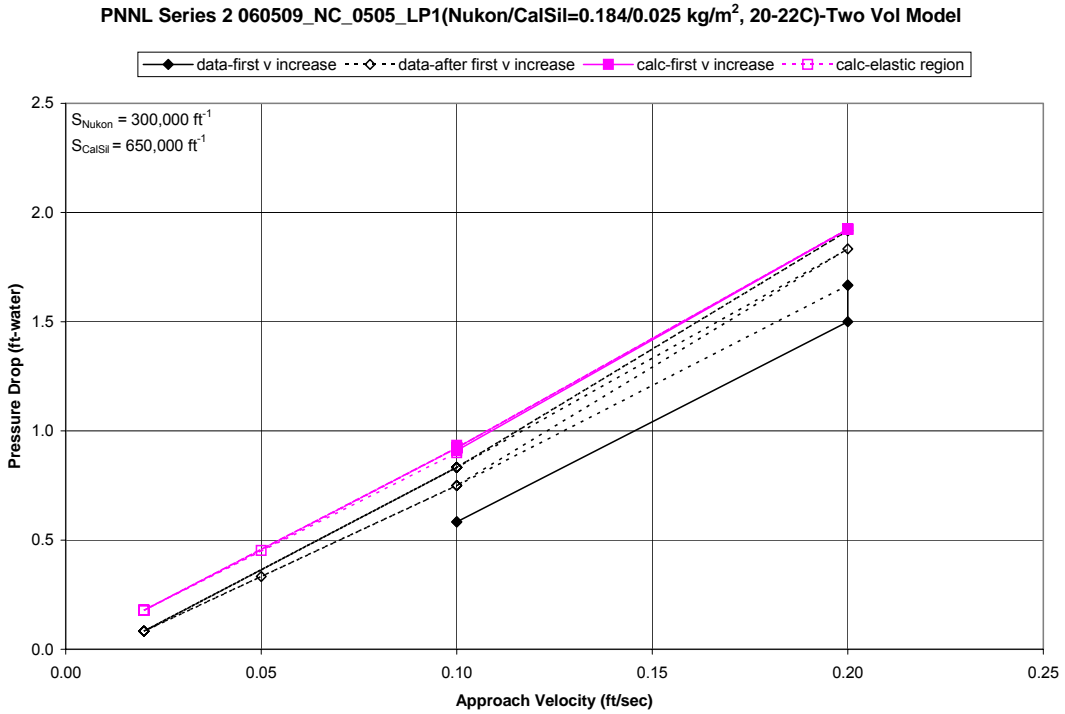


Figure 4.4-11 Head Loss Comparisons for PNNL Test 060509_NC_0505_LP1 to Determine Y

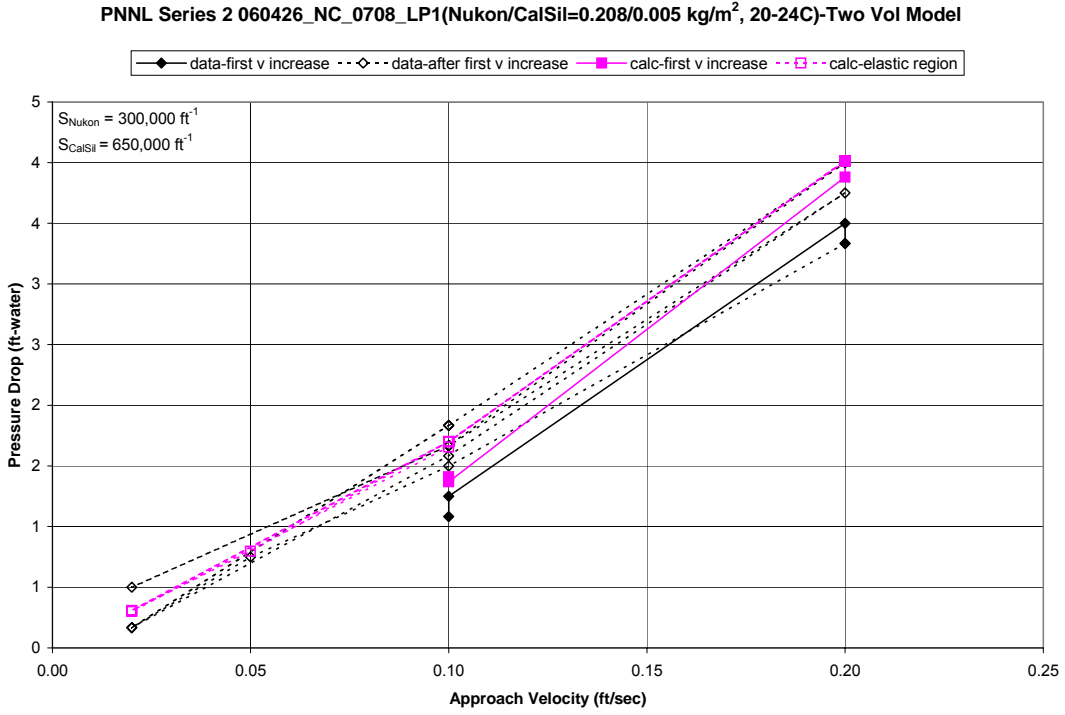


Figure 4.4-12 Head Loss Comparisons for PNNL Test 060426_NC_0708_LP1 to Determine Y

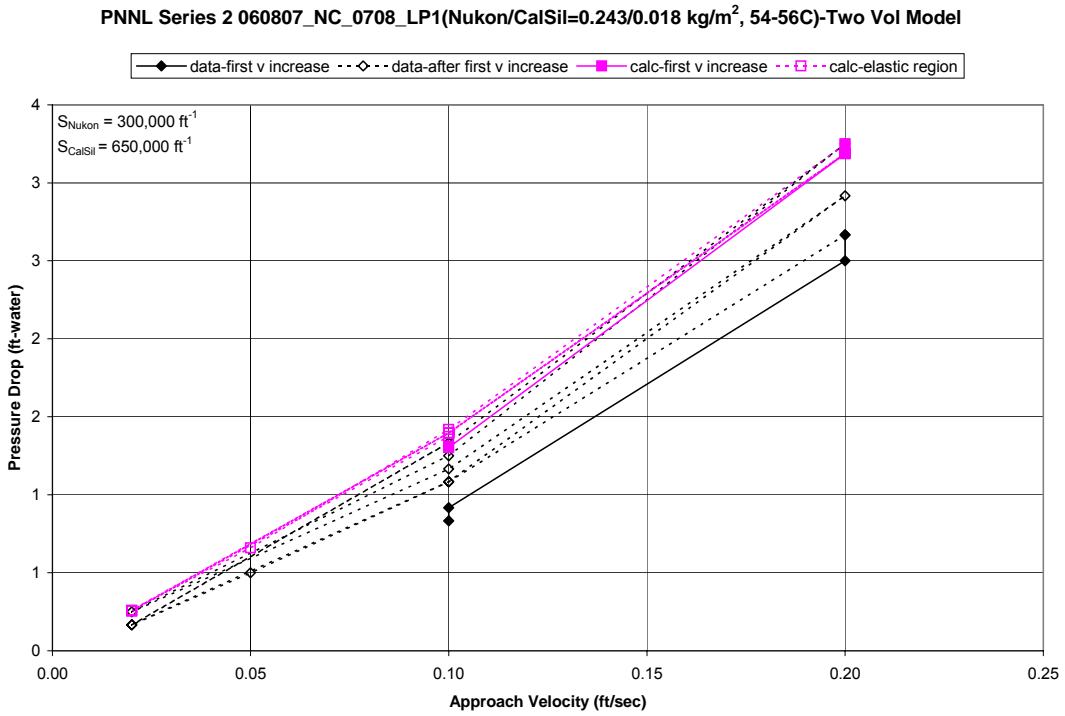


Figure 4.4-13 Head Loss Comparisons for PNNL Test 060807_NC_0708_LP1 to Determine Y

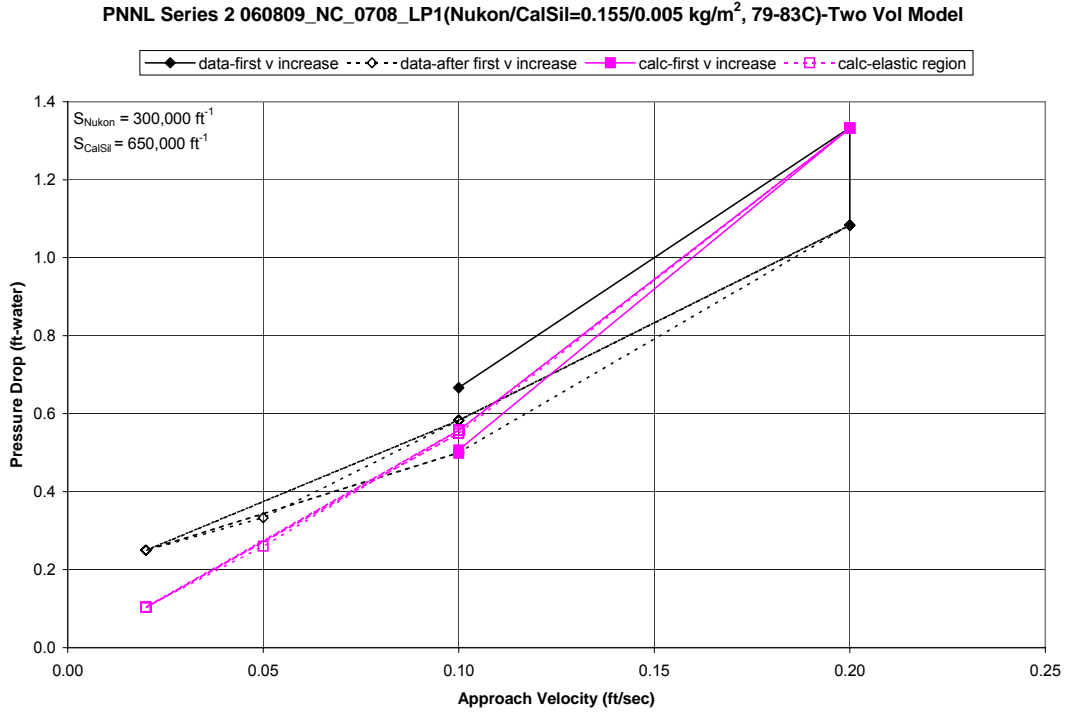


Figure 4.4-14 Head Loss Comparisons for PNNL Test 060809_NC_0708_LP1 to Determine Y

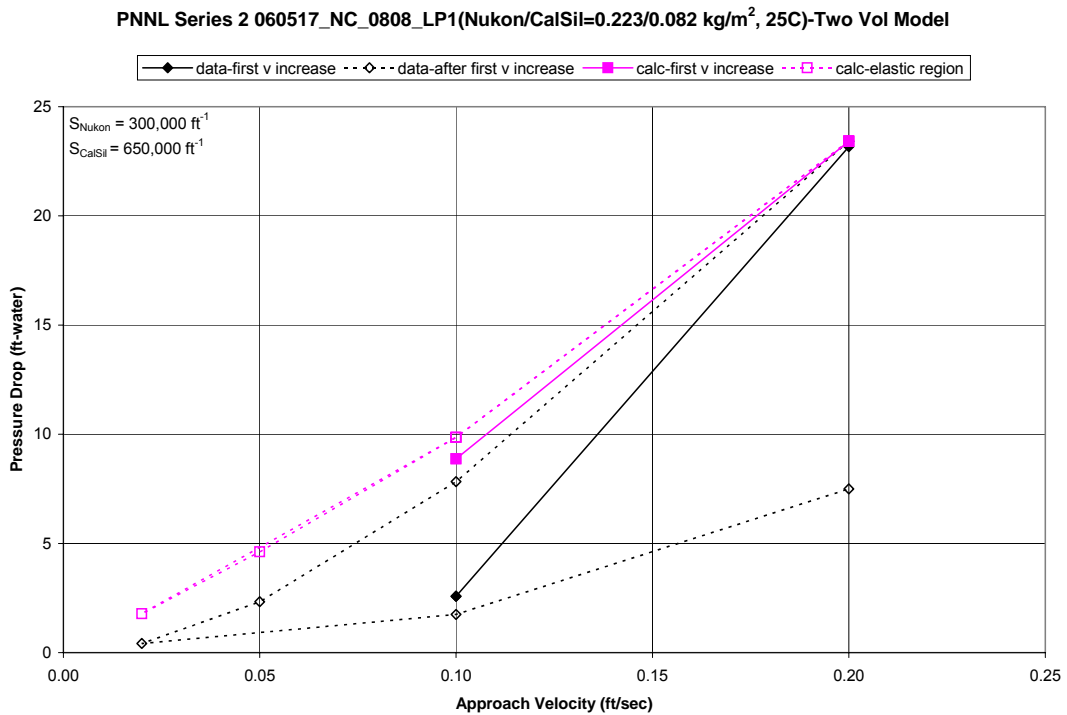


Figure 4.4-15 Head Loss Comparisons for PNNL Test 060517_NC_0808_LP1 to Determine Y

4.5 Material-Specific Compression Parameter Determination

The equations used for determining the first irreversible compression of the debris bed equation (3.2-4) and the elastic relaxation of the debris bed after the first compression equation (3.3-2) employ a material-specific parameter, N . The value of the parameter must be determined from test data. The value for N has been determined by using data obtained from testing at PNNL (Ref. 24), from the Series 6 tests performed by LANL at UNM (Ref. 3), and from the ANL testing (Ref. 25).

4.5.1 Determination of Material-Specific Parameter Using PNNL Test Data

Data from the Series 1 and Series 2 debris bed head loss testing at PNNL have been used to determine the material-specific compression parameter for the plastic equation (3.2-4) and elastic equation (3.3-2) behavior of the tested Nukon and Nukon/CalSil debris beds. Figure 4.5-1 plots the values of X/X' versus P_m/P_m' obtained from the PNNL Series 1 and Series 2 test measurements. This plot indicates that the best values to use for the plastic material-specific parameter for the Series 1 and Series 2 tests are about 0.238 and 0.236, respectively. Because the Series 2 tests provided more accurate measurements of the debris bed height by using the optical triangulation method, a value of 0.236 for the material-specific parameter is appropriate to model the plastic behavior of the debris bed during the first compression equation (3.2-4). Figure 4.5-2 plots $X/X(P_{max})$ versus P_m/P_{max} for the PNNL Series 1 and Series 2 tests. The data from some tests fall outside the range of the bulk of the data and therefore are not considered in the determination of the material-specific parameter. This plot indicates a value of about 0.236 for the material-specific parameter for the elastic behavior equation (3.3-2), which as expected is close to the value resulting from the plastic behavior plotted in Figure 4.5-1. (As indicated in Section 3, it is expected that the same value for the material-specific parameter would be used for the both the plastic and elastic compression.) Consequently, a value of 0.236 is recommended for the material-specific parameter in both the plastic and elastic compression regions.

For completeness, Figures 4.5-3 and 4.5-4 include experimental data for the plastic and elastic compression of a Nukon debris bed, obtained from testing at ANL. Section 6.3 more fully discusses these test results. The ANL data fall within the range of the PNNL test data and provide additional justification for the recommended material-specific parameter of 0.236.

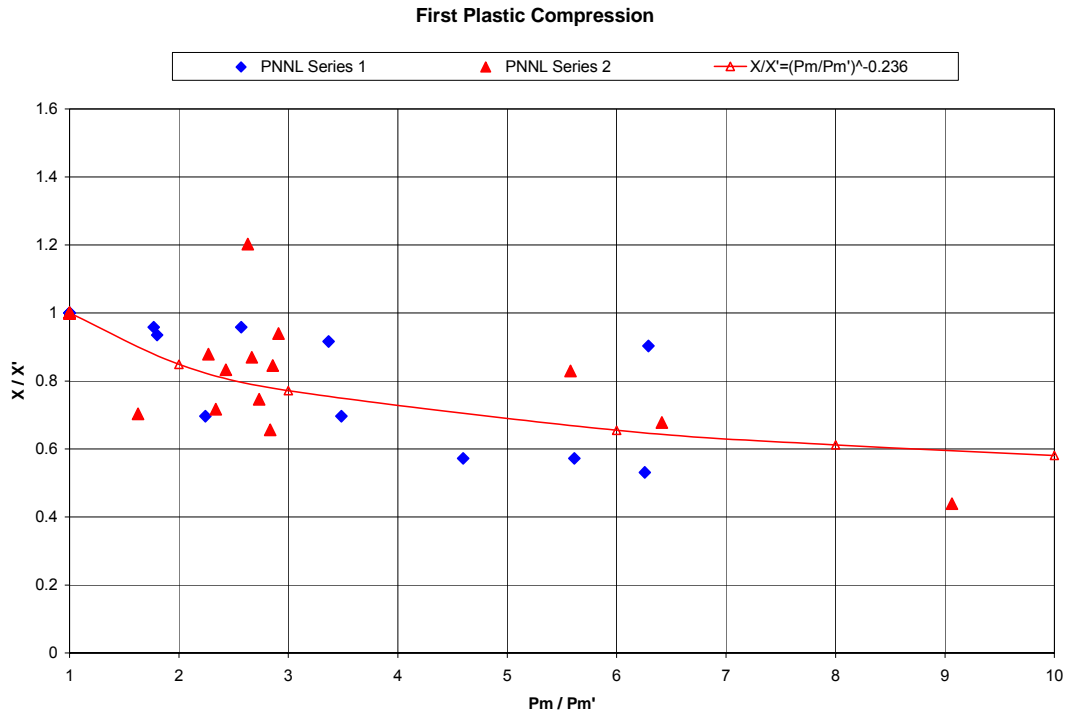


Figure 4.5-1 Debris Bed Plastic First Compression Parameter Using PNNL Test Data

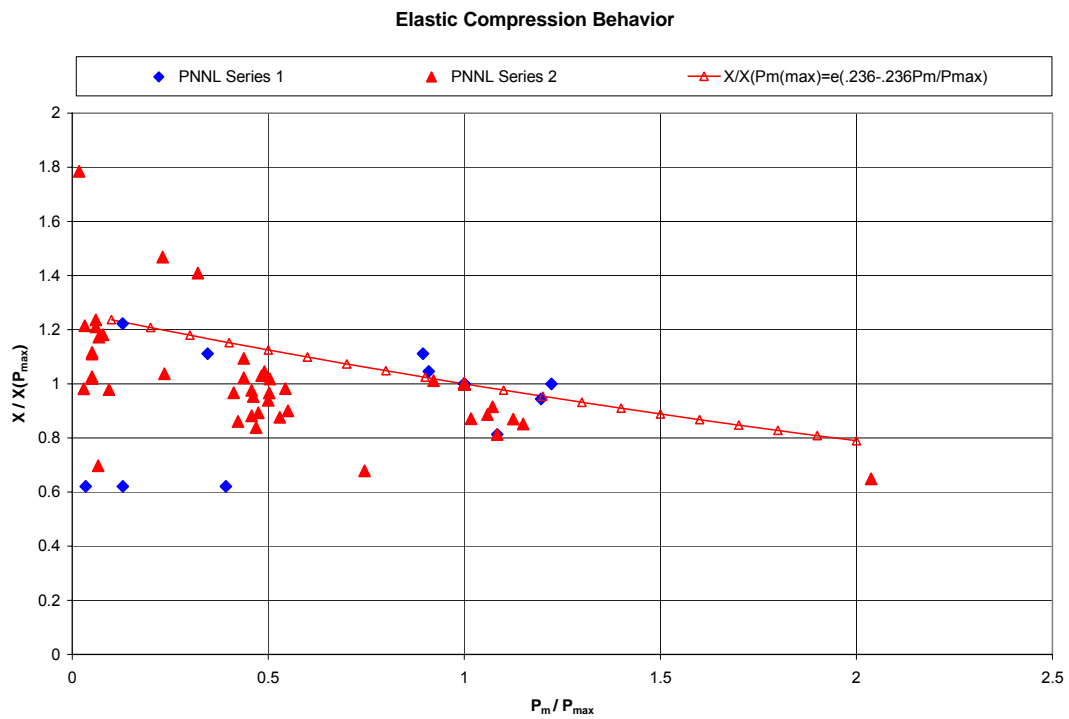


Figure 4.5-2 Debris Bed Elastic Compression Parameter Using PNNL Test Data

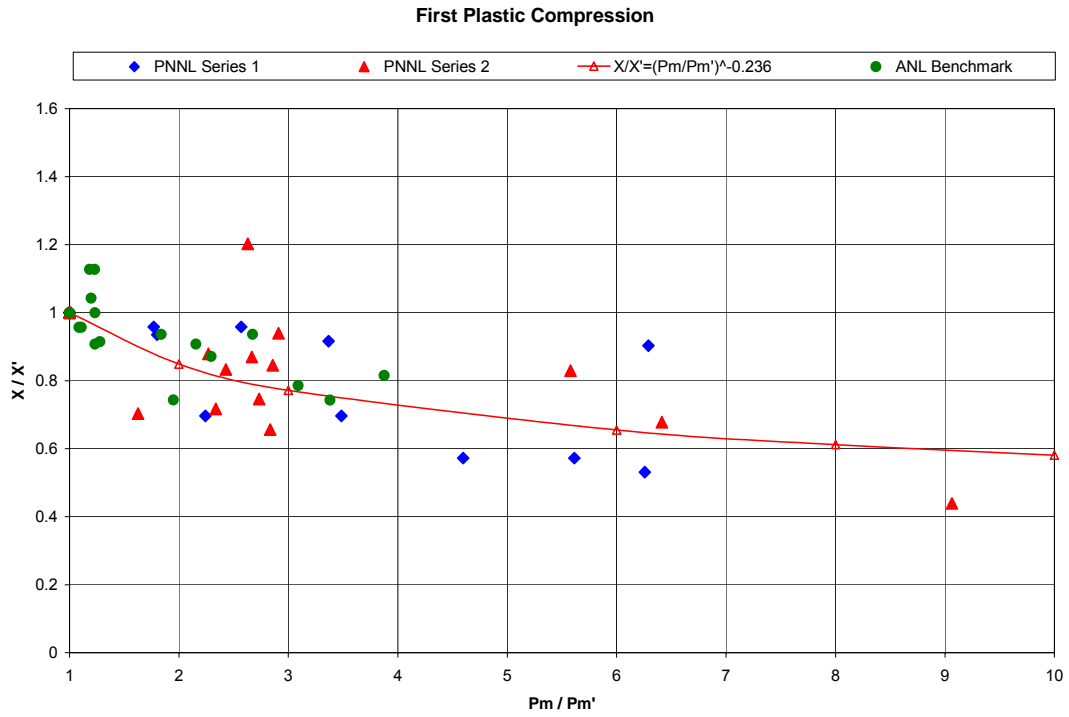


Figure 4.5-3 Debris Bed Plastic First Compression Parameter Using PNNL and ANL Test Data

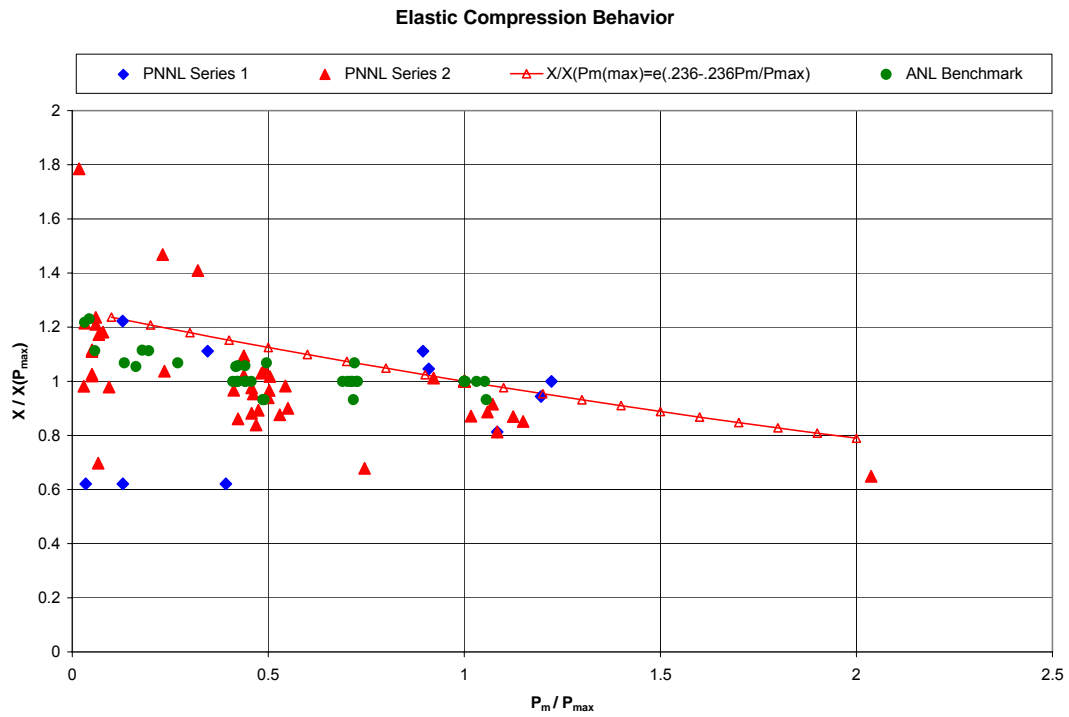


Figure 4.5-4 Debris Bed Elastic Compression Parameter Using PNNL and ANL Test Data

4.5.2 Determination of Material-Specific Parameter Using LANL/UNM Series 6 Test Data

Several tests were performed for LANL at UNM to provide data for pressure drop across a debris bed consisting of Nukon, CalSil, and other materials. Debris bed thickness was only measured for the Series 6 tests, which measured pressure drop across debris beds composed of various masses of mixtures of Nukon and CalSil. Consequently, only the Series 6 tests can be used to determine the values of the material-specific compression parameter, N . As indicated in Section 4.1, the accuracy of the debris bed mass measurements for the LANL/UNM tests is also in question. The debris bed mass is used to calculate the void ratio, X , which is used in the compressibility relations. Despite the problem, this section presents the results of the effort to determine the material-specific parameter by using the Nukon and CalSil masses added to the loop as the bed masses.

Figure 4.5-5 plots data for the Series 6 tests that represent the first irreversible plastic compression of the debris bed after formation. As previously indicated in Section 3.1, the mechanical stress across a debris bed equals the hydraulic pressure drop across the debris bed. The pressure drop ratio ($\Delta p/\Delta p'$) for each test data point has been obtained by dividing the measured pressure drop by the pressure drop measured at the initial approach velocity of about 0.0305 m/s (0.1 ft/s). The void ratio (X/X') was obtained by dividing the void ratio for each test data point by the void ratio measured at the initial approach velocity of about 0.0305 m/s (0.1 ft/s). This plot shows that the data for Test 6g fall outside the range of the other data. Consequently, these data are not considered in determining the value of N . If all other test data are considered, N equals about 0.165. However, three of the points from Test 6h that are indicated on the figure appear to be outside the range of the other data. If these three data points are not considered in the assessment, the material-specific parameter, N , used in equation (3.2-4) equals about 0.303.

Measurements of the test data for the decreasing velocity conditions following the initial peak velocity should be able to determine the value of N in equation (3.3-2) for the elastic behavior of the debris bed. Unfortunately, data plots of $X/X(P_{\max})$ versus P_m/P_{\max} for the Series 6 tests are too scattered to provide a value for N (see Figure 4.5-6). Consequently, a recommended value of N to describe the elastic behavior of the debris beds could not be determined.

4.5.3 Recommended Material-Specific Parameter Value

Because the masses of the constituents of the LANL/UNM debris beds were not accurately determined and because the bed height measurements were determined by using the less accurate visual ruler measurement, the LANL/UNM data do not provide as good an estimate of the material-specific parameter as the PNNL data. Consequently, the material-specific parameter of 0.236, obtained by using the PNNL data, is recommended for use in predictive analyses. It is encouraging that the value obtained by using data from the less accurately measured LANL/UNM tests still provides a material-specific parameter that is close to the values generated by using the PNNL test data.

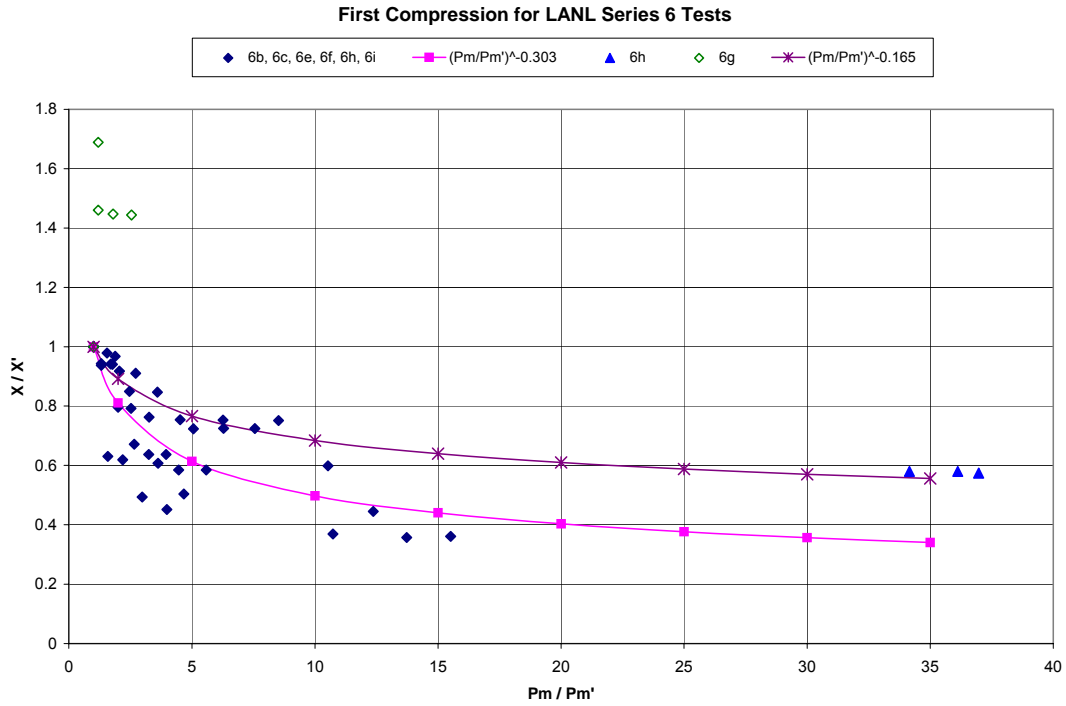


Figure 4.5-5 Bed Plastic First Compression Parameter Using LANL/UNM Series 6 Test Data

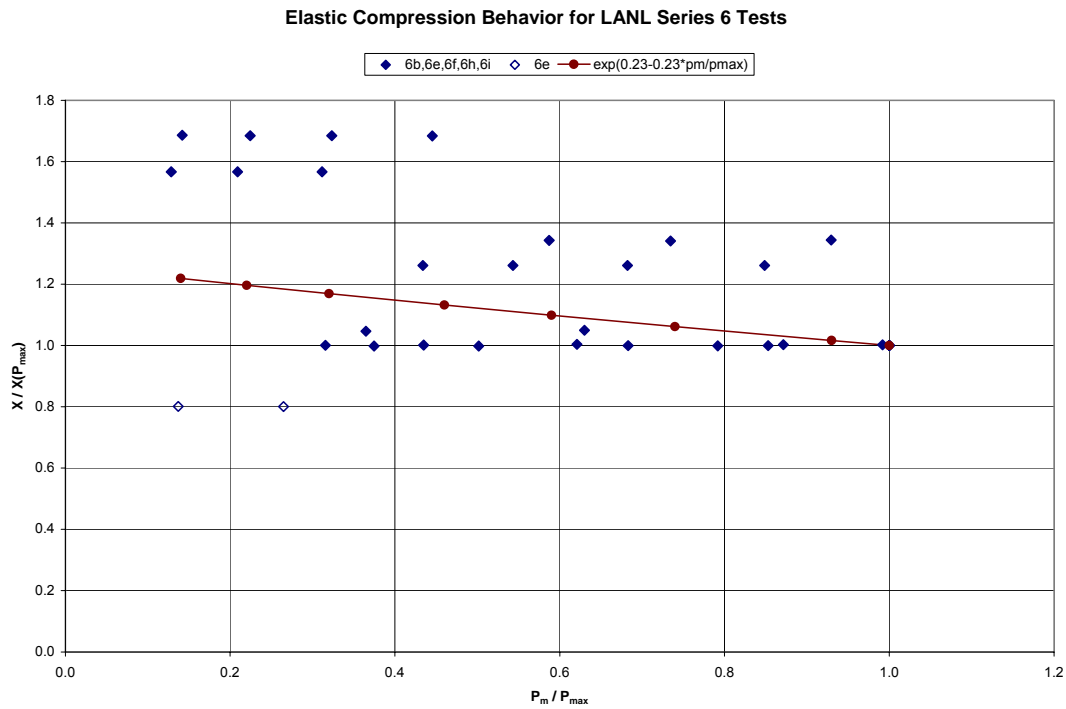


Figure 4.5-6 Debris Bed Elastic Compression Parameter Using LANL/UNM Series 6 Test Data

5. GUIDELINES FOR CALCULATING HEAD LOSS THROUGH A DEBRIS BED

Sections 2 and 3 derive the steady-state flow and compression equations that solve for head loss across a sump screen debris bed. Section 4 describes the method for calculating pressure drop across a debris bed and identifies the values for the debris bed and the material properties that should be used in performing the calculations. This section details the procedure that should be used in applying the correlations listed in Sections 2 and 3 to calculate head loss across a debris-covered sump screen by using the methods, parameters, and constants identified in Section 4. Section 5.1 summarizes the values for the material-specific parameters for calculating head loss. Sections 5.2 and 5.3 describe the analytical procedure for calculating the debris bed pressure drop and compression. Section 5.2 describes the method to calculate the flow and compression for a homogeneous debris bed by using one calculational volume. The one-volume calculational method should be used for calculating head loss across a debris bed composed of a single debris type. The one-volume approach does not represent the best calculational method for beds with multiple debris types and nonhomogeneous debris distributions because hydraulic and mechanical pressures can vary nonuniformly through the debris bed. Therefore, Section 5.3 describes the method for calculating the debris bed flow and the bed compression by assuming the presence of two compressible calculational control volumes for the debris bed.

5.1 Application Limits

5.1.1 Approach Velocity Limit

The approach velocities ranged between approximately 0.01534 and 0.3048 m/s (0.05 to 1.0 ft/s) for the LANL/UNM tests. Some tests were also performed with higher velocities up to about 0.488 m/s (1.6 ft/s). The approach velocities for the PNNL tests did not exceed 0.305 m/s (1.0 ft/s), and most of the test points were less than 0.15 m/s (0.5 ft/s). Therefore, the developed pressure drop methods have been verified for approach velocities up to about 0.488 m/s (1.6 ft/s).

For the tested range of velocities, the viscous term of the pressure drop equation contributes more than 90 percent of the pressure drop. Consequently, it can be argued that calculations of pressure drop, especially at the lower approach velocities, only need to consider the viscous term.

5.1.2 Temperature Limit

The LANL/UNM tests were performed at water temperatures between about 21 and 60 °C (70 and 140 °F). The PNNL tests were performed at water temperatures between about 21 and 85 °C (70 and 185 °F). The head loss correlation depends on water properties, flow velocity, and debris properties. The water density and viscosity exhibit large changes in value as a function of temperature. Reference 7 includes head loss calculations for Nukon and Nukon/CalSil debris beds with different approach velocities and water temperatures. This study concluded that the calculated pressure drop (head loss) decreases with increasing temperature, primarily because water viscosity decreases with increasing temperature. Therefore, assuming that the head loss relation correctly accounts for the fluid properties and that the debris bed properties and characteristics do not change with temperature, analysts should be able to apply the head loss correlation to a wide range of water temperatures as long as the appropriate fluid properties are used. The PNNL testing has verified this conclusion. Consequently, the pressure drop methods are appropriate for water temperatures between about 21 and 85 °C (70 and 185 °F).

As indicated in Section 2, the head loss correlation assumes the presence of single-phase flow conditions in the debris bed. Consequently, the correlation cannot be applied to two-phase flow conditions. In Section 2.7, Table 2.7-1 and Figure 2.7-5 specify the upper temperature limits for maintaining one-phase flow through the sump screen.

5.2 Pressure Drop and Compressibility Across a One-Volume Debris Bed

The following sections provide the recommended characteristic values for Nukon and CalSil debris and the application procedure for calculating head loss across a debris-covered sump screen. Section 5.2 specifically describes the calculational procedure for a one-volume debris bed. This approach is appropriate for homogeneous debris beds, especially debris beds composed of one debris type.

5.2.1 Debris Characteristic Values

Table 5.2-1 notes the recommended bounding Nukon and CalSil debris properties for use in head loss calculations. Section 4 provides the basis for choosing these values.

Table 5.2-1 Recommended Bounding Debris Properties for Head Loss Calculations

Debris	Material Density (ρ_{solid}) (kg/m ³) / (lbm/ft ³)	Specific Surface Area (S_v) (m ⁻¹) / (ft ⁻¹)
Nukon Fibers	2803 / 175 (ρ_{Nukon})	984,252 / 300,000 (S_{Nukon})
CalSil Particles	1842 / 115 (ρ_{CalSil})	2,132,546 / 650,000 (S_{CalSil})
Fiberglass Fibers in CalSil	2803 / 175 (ρ_{CalSil})	984,252 / 300,000 (S_{CalSil})

5.2.2 Head Loss Application Procedure for a One-Volume Nukon/CalSil Debris Bed

The head loss calculation across a debris-covered sump screen is obtained by using an iterative procedure. The following steps should be taken to calculate the head loss across a sump screen with a debris bed composed of a homogeneous mixture of Nukon fibers and CalSil particles. The equations require the use of consistent metric or English units. Typical units for the equations are specified.

Step 1. Identify the total containment pressure; water temperature and properties, water absolute viscosity (μ_{water}), and water density (ρ_{water}); debris properties (ρ_{Nukon} , ρ_{CalSil} , S_{Nukon} , S_{CalSil}) from Table 5.2-1; debris mass (m_{Nukon} , m_{CalSil}); screen or perforated plate cross-sectional surface area (A) and area ratio (f); and flow area (A_{screen}) and velocity (V) approaching the sump screen.

where

μ_{water}	water absolute viscosity (kg/(m-s), lbm/(ft-s))
ρ_{water}	water density (kg/m ³ , lbm/ft ³)
ρ_{Nukon}	Nukon (fiber) material density (kg/m ³ , lbm/ft ³)
ρ_{CalSil}	CalSil (particle) material density (kg/m ³ , lbm/ft ³)
S_{Nukon}	Nukon (fiber) specific surface area in debris bed (m ⁻¹ , ft ⁻¹)
S_{CalSil}	CalSil (particle) specific surface area in debris bed (m ⁻¹ , ft ⁻¹)
m_{Nukon}	Nukon mass in the debris bed
m_{CalSil}	CalSil mass in the debris bed
A	debris bed cross-sectional surface area (m ² , ft ²)
A_{screen}	flow area through screen or perforated plate (m ² , ft ²)

- f flow area of screen or perforated plate divided by the total screen or plate area (equals A_{screen} / A)
- V approach velocity through the cross-sectional area of solid plus fluid, upstream of sump screen (m/s, ft/s)

Step 2. Calculate the debris bed thickness at a reference bed formation approach velocity using the following relation. A reference bed formation approach velocity of 0.0305 m/s (0.1 ft/s) was used in this report.

$$\Delta L_{\text{initial}} = \frac{(X_{\text{Nukon}} + 1)}{A} \frac{m_{\text{Nukon}}}{\rho_{\text{Nukon}}} + \frac{(X_{\text{CalSil}} + 1)}{A} \frac{m_{\text{CalSil}}}{\rho_{\text{CalSil}}} \quad (4.2-2)$$

where

- $\Delta L_{\text{initial}}$ debris bed thickness at the reference bed formation approach velocity (m, ft)
- X_{Nukon} Nukon void ratio in debris bed (Nukon layer at formation = 30)
- X_{CalSil} CalSil void ratio in debris bed (CalSil layer at formation = 6.2)
- m_{Nukon} Nukon mass in the debris bed (kg, lbm)
- m_{CalSil} CalSil mass in the debris bed (kg, lbm)

Step 3. Calculate the debris porosity, void ratio, and effective dimensionless permeability function $K(X)$ at the reference bed formation approach velocity using the following relations.

$$\text{Vol}_{\text{total}} = \Delta L_{\text{initial}} A \quad (5.2-1)$$

$$\text{Vol}_{\text{Nukon}} = m_{\text{Nukon}} / \rho_{\text{Nukon}} \quad (5.2-2)$$

$$\text{Vol}_{\text{CalSil}} = m_{\text{CalSil}} / \rho_{\text{CalSil}} \quad (5.2-3)$$

$$\text{Vol}_{\text{solid}} = \text{Vol}_{\text{Nukon}} + \text{Vol}_{\text{CalSil}} \quad (5.2-4)$$

$$\text{Vol}_{\text{void}} = \text{Vol}_{\text{total}} - \text{Vol}_{\text{solid}} \quad (5.2-5)$$

$$\varepsilon'_{\text{debris}} = (\text{Vol}_{\text{total}} - \text{Vol}_{\text{solid}}) / \text{Vol}_{\text{total}} \quad (5.2-6)$$

$$\varepsilon_{\text{Nukon}} = (\text{Vol}_{\text{total}} - \text{Vol}_{\text{Nukon}}) / \text{Vol}_{\text{total}} \quad (5.2-7)$$

$$\varepsilon_{\text{CalSil}} = (\text{Vol}_{\text{total}} - \text{Vol}_{\text{CalSil}}) / \text{Vol}_{\text{total}} \quad (5.2-8)$$

$$X'_{\text{debris}} = \text{maximum} (\text{Vol}_{\text{void}} / \text{Vol}_{\text{solid}}, 0.0001) \quad (5.2-9)$$

$$X_{\text{Nukon}} = \text{maximum} (\text{Vol}_{\text{void}} / \text{Vol}_{\text{Nukon}}, 0.0001) \quad (5.2-10)$$

$$X_{\text{CalSil}} = \text{maximum} (\text{Vol}_{\text{void}} / \text{Vol}_{\text{CalSil}}, 0.0001) \quad (5.2-11)$$

$$K(X_{\text{Nukon}}) = -0.5 + 0.5 \ln(1 + X_{\text{Nukon}}) + \frac{1}{(2 + 2 X_{\text{Nukon}} + X_{\text{Nukon}}^2)} \quad \text{for a bed of cylindrical fibers} \\ (X > 1.0 \times 10^{-4}, \varepsilon < 0.995) \quad (2.2-7)$$

$$K(X_{\text{CalSil}}) = 2 - \frac{3}{(1 + X_{\text{CalSil}})^{1/3}} + \frac{5}{3(1 + X_{\text{CalSil}})^{5/3} + 2} \quad \text{for a bed of spherical particles} \\ (X > 1.0 \times 10^{-4}, \varepsilon < 0.995) \quad (2.2-9)$$

where

$\text{Vol}_{\text{total}}$	total debris bed volume (m^3, ft^3)
$\text{Vol}_{\text{Nukon}}$	volume of Nukon in porous medium (debris bed) (m^3, ft^3)
$\text{Vol}_{\text{CalSil}}$	volume of CalSil in porous medium (debris bed) (m^3, ft^3)
$\text{Vol}_{\text{solid}}$	volume of solid material in porous medium (Nukon and CalSil in debris bed) (m^3, ft^3)
Vol_{void}	void volume of porous medium (debris bed) (m^3, ft^3)
$\varepsilon'_{\text{debris}}$	debris bed porosity at the reference bed formation approach velocity
$\varepsilon_{\text{Nukon}}$	effective porosity of Nukon in debris bed
$\varepsilon_{\text{CalSil}}$	effective porosity of CalSil in debris bed
X'_{debris}	void ratio at the reference bed formation approach velocity
X_{Nukon}	effective Nukon void ratio in debris bed (equals $\text{Vol}_{\text{void}} / \text{Vol}_{\text{Nukon}}$)
X_{CalSil}	effective CalSil void ratio in debris bed (equals $\text{Vol}_{\text{void}} / \text{Vol}_{\text{CalSil}}$)

Step 4. Calculate viscous (laminar) and kinetic (turbulent) components of pressure drop through the debris bed by using equation (2.6-4). The values of the water density (ρ_{water}) and water absolute viscosity (μ_{water}) should be adjusted to reflect the correct thermodynamic conditions (e.g., temperature) at each calculation point.

$$\Delta p'_{\text{debris bed}} = \left[\frac{S_{\text{Nukon}}^2 X_{\text{Nukon}}^3 (1 - \varepsilon_{\text{Nukon}})^2}{K(X_{\text{Nukon}}) (1 + X_{\text{Nukon}})^2 \varepsilon_{\text{Nukon}}^3} + \frac{S_{\text{CalSil}}^2 X_{\text{CalSil}}^3 (1 - \varepsilon_{\text{CalSil}})^2}{K(X_{\text{CalSil}}) (1 + X_{\text{CalSil}})^2 \varepsilon_{\text{CalSil}}^3} \right] \mu_{\text{water}} V \Delta L_{\text{initial}} + \\ \left[S_{\text{Nukon}} 1.95 \left[\frac{(1 - \varepsilon_{\text{Nukon}}) \mu_{\text{water}} S_{\text{Nukon}}}{\rho_{\text{water}} V 6} \right]^{0.071} \frac{(1 - \varepsilon_{\text{Nukon}})}{\varepsilon_{\text{Nukon}}^3} + S_{\text{CalSil}} 3.89 \left[\frac{(1 - \varepsilon_{\text{CalSil}}) \mu_{\text{water}} S_{\text{CalSil}}}{\rho_{\text{water}} V 6} \right]^{0.13} \frac{(1 - \varepsilon_{\text{CalSil}})}{\varepsilon_{\text{CalSil}}^3} \right] \frac{\rho_{\text{water}} V^2 \Delta L_{\text{initial}}}{6} \\ + 0.5 (1 - \varepsilon_{\text{debris}}) \rho_{\text{water}} / 2 (V / \varepsilon_{\text{debris}})^2 + (1 - f \varepsilon_{\text{debris}})^2 \rho_{\text{water}} / 2 [V / (f \varepsilon_{\text{debris}})]^2 \quad (2.6-4)$$

$$\text{for Nukon with } 0.5 < \frac{\text{Re}}{(1 - \varepsilon)} < 9.85 \times 10^4 \text{ and } 0.564 < \varepsilon < 0.919$$

$$\text{for CalSil with } 440 < \text{Re} < 7.92 \times 10^4 \text{ and } 0.38 < \varepsilon < 0.44$$

where

$\Delta p'_{\text{debrisbed}}$	debris pressure drop at the reference bed formation approach velocity (Pa, psi)
$\varepsilon_{\text{debris}}$	debris bed porosity (equals $\text{Vol}_{\text{void}} / \text{Vol}_{\text{tot}}$)

The last two terms of equation (2.5-2) are the irreversible entrance and exit pressure drops.

Step 5. Steps 1 through 4 provide initial information regarding the debris bed that will be used to calculate the debris bed compression and pressure drop conditions at higher approach velocities. Steps 5 through 8 calculate the debris bed conditions from the initial low-velocity point to higher approach velocities, assuming irreversible compression of the debris bed.

Step 6. For the next higher approach velocity condition, if applicable, assume a debris bed thickness. The first assumed value should be close to the initial thickness $\Delta L_{\text{initial}}$. Use Steps 3 and 4 to calculate the total pressure drop ($\Delta p_{\text{debrisbed}}$) for the assumed debris bed thickness.

Step 7. Using the new calculated values, calculate updated values for X_{debris} and $\Delta L_{\text{debrisbed}}$ accounting for bed compression.

$$X_{\text{debris}} = X'_{\text{debris}} (\Delta p_{\text{debrisbed}} / \Delta p'_{\text{debrisbed}})^{-N} \quad (3.2-4)$$

$$\Delta L_{\text{debrisbed}} = \text{Vol}_{\text{solid}} (1 + X_{\text{debris}}) / A \quad (3.2-7)$$

where

X_{debris}	void ratio
X'_{debris}	void ratio at the reference bed formation approach velocity
$\Delta p_{\text{debrisbed}}$	debris bed pressure drop (Pa, psi)
$\Delta p'_{\text{debrisbed}}$	debris pressure drop at the reference bed formation approach velocity (Pa, psi)
N	material-specific parameter for porous medium compression (= 0.236)
$\Delta L_{\text{debrisbed}}$	debris bed thickness (m, ft)

The solution is converged if the calculated debris bed thickness equals the assumed debris bed thickness in Step 6. If convergence is reached, proceed to the next step. If the convergence criteria are not met, repeat Steps 6 through 7, using the new calculated values for debris bed thickness ($\Delta L_{\text{debrisbed}}$).

Step 8. Repeat Steps 5 through 7 for the next higher approach velocity, if applicable. At the highest approach velocity, define the converged values for debris bed void ratio, pressure drop, and debris bed thickness as X_{pmax} , Δp_{pmax} , and ΔL_{pmax} .

Step 9. The following steps calculate the debris bed decompression and pressure drop if the approach velocity falls below the highest approach velocity. This approach assumes elastic behavior of the debris bed.

Step 10. For the next lower approach velocity condition, if applicable, assume a debris bed thickness. The first assumed value should be close to the maximum thickness ΔL_{pmax} . Use Steps 3 and 4 to calculate the total pressure drop ($\Delta p_{\text{debrisbed}}$) for the assumed debris bed thickness.

Step 11. Using the new calculated values, calculate updated values for X_{debris} and $\Delta L_{\text{debrisbed}}$ accounting for bed compression.

$$X_{\text{debris}} = X_{\text{pmax}} \exp \left[N - \frac{N \Delta p_{\text{debrisbed}}}{\Delta p_{\text{pmax}}} \right] \quad (3.3-2)$$

$$\Delta L_{\text{debrisbed}} = \text{Vol}_{\text{solid}} (1 + X_{\text{debris}}) / A \quad (3.2-7)$$

where

X_{pmax}	void ratio at Δp_{pmax}
Δp_{pmax}	pressure drop at highest approach velocity (Pa, psi)

The solution is converged if the calculated debris bed thickness equals the assumed debris bed thickness in Step 10. If convergence is reached, proceed to the next step. If the convergence criteria are not met, repeat Steps 10 through 11, using the new calculated values for debris bed thickness ($\Delta L_{\text{debrisbed}}$).

Step 12. Repeat Steps 9 through 11 for the next lower approach velocity.

Step 13. Perform this check for each calculated pressure drop. Using the containment pressure and calculated sump screen head loss (pressure drop), read the maximum allowable sump water temperature from Figure 2.7-5.

If the actual sump water temperature is lower than the maximum allowable temperature, acceptable pump inlet conditions exist, and the sump screen pressure drop calculation is one-phase and acceptable.

If the actual sump water temperature is higher than the maximum allowable temperature, the void fraction at the sump screen exit exceeds 3 percent, which indicates that pump cavitation is possible. This condition indicates that the sump screen pressure drop calculation is inapplicable because two-phase flow exists.

5.2.3 Head Loss Application Procedure for a One-Volume Nukon Debris Bed

The compression relation for a Nukon debris bed is similar to that for a Nukon/CalSil debris bed. Therefore, the iterative calculation procedure outlined in Section 5.2.2 to calculate the head loss across a debris bed can be used for a Nukon debris bed by ignoring the CalSil mass, solid volume, and pressure drop. Use the following equation, which replaces equation (2.5-2) in Step 4, to calculate the pressure drop across a Nukon-only debris bed.

$$\Delta p'_{\text{debrisbed}} = \left[\frac{S_{\text{Nukon}}^2 X_{\text{Nukon}}^3}{K(X_{\text{Nukon}})(1 + X_{\text{Nukon}})^2} \right] \mu_{\text{water}} V \frac{(1 - \epsilon'_{\text{debris}})^2}{\epsilon'_{\text{debris}}^3} \Delta L_{\text{initial}} + S_{\text{nukon}} 1.95 \left[\frac{(1 - \epsilon_{\text{Nukon}}) \mu_{\text{water}} S_{\text{Nukon}}}{\rho_{\text{water}} V 6} \right]^{0.071} \frac{\rho_{\text{water}} V^2}{6} \frac{(1 - \epsilon'_{\text{debris}})}{\epsilon'_{\text{debris}}^3} \Delta L_{\text{initial}} + \Delta p_{\text{irreversible}} \quad (5.2-12)$$

$$\text{for Nukon with } 0.5 < \frac{\text{Re}}{(1-\epsilon)} < 9.85 \times 10^4 \text{ and } 0.564 < \epsilon < 0.919$$

The irreversible pressure drop equals the sum of the abrupt entrance and exit pressure drops.

$$\Delta p_{\text{irreversible}} = 0.5 (1 - \epsilon_{\text{debris}}) \rho_{\text{water}} / 2 (V / \epsilon_{\text{debris}})^2 + (1 - f \epsilon_{\text{debris}})^2 \rho_{\text{water}} / 2 [V / (f \epsilon_{\text{debris}})]^2 \quad (5.2-13)$$

5.2.4 Head Loss Application Procedure for a One-Volume CalSil Debris Bed

Because building a debris bed composed entirely of CalSil is very difficult, no complete test data record the head loss and thickness of a CalSil bed. Measurements of both parameters are necessary to determine the compression behavior of a CalSil debris bed. Consequently, the general procedure outline in Section 5.2.2 can be used with some modifications for CalSil-only debris bed calculations. As indicated in NUREG/CR-6874 (Ref. 3), CalSil is primarily composed of particles, but does possess some fibers. To apply the developed calculational procedure to a debris bed composed entirely of CalSil, the assumption is that a fraction of the bed is composed of fiberglass fibers. This approach requires a knowledge of the CalSil fiber mass, the CalSil fiber material density, and the CalSil fiber-specific surface area; unfortunately, specific information on these factors is not available. Consequently, as shown in Table 5.2-1, the values of the CalSil reference fiber mass, fiber material density, and fiber-specific surface area for calculations with a CalSil-only debris bed are assumed equal to the Nukon fiberglass values. The use of a Nukon specific surface area for the CalSil fibers is reasonable because both fiber debris types are

fiberglass fibers, and the specific surface area depends on the shape of the debris. Similarly, use of the Nukon fiberglass material density for the fiberglass fibers in CalSil is also reasonable.

NUREG/CR-6874 estimates that about 90 percent of CalSil insulation is composed of particles, implying that about 10 percent is fiber. However, manufacturer information indicates that CalSil used in the PNNL testing is composed of 4 to 5 percent cellulose and glass fiber. Consequently, when employing the head loss calculational procedure outlined in Section 5.2.2 for a debris bed composed entirely of CalSil, about 4 to 10 percent of the total added CalSil mass should be assumed to be fiber with the properties indicated in Table 5.2-1. However, the fiber fractions for the specific CalSil being considered should be used if known. This requires the addition of Step 1a in Section 5.2.2 to include the calculation of the CalSil particle and fiber masses.

Step 1a. Identify the CalSil fiber mass in the system and calculate the saturated CalSil particle mass in the debris bed, using the total CalSil system mass.

$$m_{\text{CalSilfiber}} = m_{\text{fract}_{\text{fiber}}} m_{\text{CalSiltotal}} \quad (5.2-14)$$

$$m_{\text{CalSil}} = (1 - m_{\text{fract}_{\text{fiber}}}) m_{\text{CalSiltotal}} \quad (5.2-15)$$

where

$m_{\text{fract}_{\text{fiber}}}$	fiber mass fraction in total CalSil mass
$m_{\text{CalSilfiber}}$	CalSil fiber mass in debris bed (kg, lbm)
$m_{\text{CalSiltotal}}$	total fiber and particle CalSil mass (kg, lbm)
m_{CalSil}	CalSil (particle) mass in debris bed (kg, lbm)

In the remainder of the calculation steps in Section 5.2.2, replace the value for m_{Nukon} with that for $m_{\text{CalSilfiber}}$.

5.3 Pressure Drop and Compressibility Across a Two-Volume Debris Bed

The calculational procedure outlined in Section 5.2 assumes that the solid material in a debris bed is uniformly distributed throughout the entire volume thickness. This condition may not exist for a debris bed composed of small granular particles that can redistribute in the bed or for a deformable debris bed that can exhibit a larger concentration of solid material at the downstream exit portion of the debris bed. This section describes a calculational method that was developed to estimate the solid material assumed to be concentrated at the downstream portion of a debris bed.

5.3.1 Description of a Two-Volume Nukon/CalSil Debris Bed Model

References 10 and 11 discuss a calculational procedure for determining the pressure drop and compression (or expansion) of a debris bed that is divided into several control volumes along the direction of flow. This section uses these references as a starting point for developing an analytical approach to calculate the pressure drop and compression (or expansion) of a debris bed.

The current approach assumes that a debris bed can be adequately analyzed by using two nodes or control volumes along the flow direction of a debris bed. To develop the control volume calculational method, the following six assumptions apply:

- (1) Calculations start after bed formation. At that time, each of the two control volumes is initially assumed to possess a uniform distribution of debris material within each control volume, but the two volumes may have different debris concentrations. Both control volumes are allowed to compress or expand, using the calculational theories discussed in Sections 2 and 3.
- (2) Consistent with the assumptions of Sections 2 and 3, the solid material in a debris bed is assumed to be incompressible. Therefore, the solid volume in each control volume remains unchanged during a compression or expansion process. Only the fluid volume of each control volume can change; however, as indicated in Section 3, the solid material can deform, move, bend, or slip.
- (3) The fibrous material (e.g., Nukon) is initially assumed to possess the same initial concentration in each control volume.
- (4) At the start of calculations after bed formation, all the CalSil particle material is assumed to be present only in the downstream exit volume. During bed formation, the granular material (e.g., CalSil) flows across control volume surfaces and achieves a maximum concentration in the downstream exit volume. No particle mass is present in the upstream entrance volume after bed formation unless the saturation condition of the bed is exceeded. This assumption provides an upper limit for the head loss calculation across a saturated Nukon/CalSil debris bed.

If the particle mass exceeds the saturation condition in the fiber volume, the excess particle mass is assumed to occupy the entrance volume, and the exit volume possesses a saturated particle/fiber mixture.

- (5) The thickness of the downstream control volume is calculated from the maximum concentration conditions of the granular material in the fibrous material.
- (6) During the flow and compression/expansion calculations, the solid material in a control volume is assumed to remain in that control volume and cannot transport between volumes or across the

debris bed upstream and downstream surfaces. This assumption is probably valid for fibrous material or large solid particles, and may not be completely appropriate or realistic for small granular materials, but is probably appropriate and conservative for calculations.

The assumption of no solid mixing across control volume boundaries permits the calculation of changes in the thickness of the control volumes in the debris bed. Figure 5.3-1 illustrates how an initially uncompressed debris bed is assumed to compress as the result of an increase of flow through the debris bed.

For calculational purposes, the initial debris bed thickness is computed by using the method described in Section 4.2. The maximum concentrated particle thickness and the resultant particle concentration in a fibrous debris bed are determined by using the approach described in Section 4.4.

The developed calculational procedure also accounts for the presence of a woven metal screen or perforated plate that reduces the flow area at the downstream exit of the debris bed. The two-volume calculational approach accounts for the irreversible pressure drop caused by the flow area sudden contraction at the debris bed entrance and by the flow area sudden expansion at the debris bed exit.

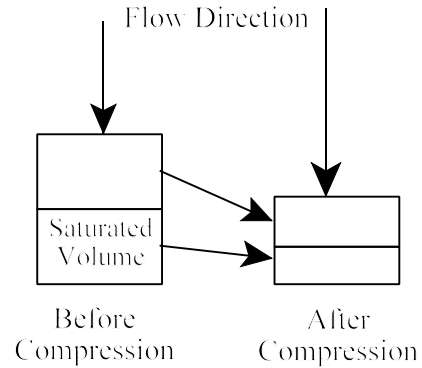


Figure 5.3-1 Debris Bed Compression

$$\Delta p_{\text{contr}} = 0.5 (1 - \epsilon_{\text{debrisentr}}) \rho_{\text{water}} / 2 (V / \epsilon_{\text{debrisentr}})^2 \quad (5.3-1)$$

$$\Delta p_{\text{expexit}} = (1 - f \epsilon_{\text{debrisexit}})^2 \rho_{\text{water}} / 2 (V / (f \epsilon_{\text{debrisexit}}))^2 \quad (5.3-2)$$

$$f = A_{\text{screen}} / A \quad (5.3-3)$$

where

- A_{screen} flow area through screen or perforated plate
- A debris bed cross-sectional surface area (upstream and downstream of screen)
- Δp_{contr} irreversible contraction pressure drop at debris bed entrance
- $\Delta p_{\text{expexit}}$ irreversible expansion pressure drop for the part of the debris bed exit with flow
- $\epsilon_{\text{debrisentr}}$ porosity at debris bed entrance
- $\epsilon_{\text{debrisexit}}$ porosity at debris bed exit
- ρ_{water} water density

5.3.2 Head Loss Application Procedure for a Two-Volume Nukon/CalSil Debris Bed

The head loss calculation across a debris-covered sump screen is performed using an iterative procedure. The following steps should be taken to calculate the head loss across the two control volumes of a sump screen covered with a debris bed composed of Nukon fibers and CalSil particles. The equations require the use of consistent English or metric units.

Step 1. Identify the total containment pressure; water temperature and properties, water absolute viscosity (μ_{water}), and water density (ρ_{water}); debris properties (ρ_{Nukon} , ρ_{CalSil} , S_{Nukon} , S_{CalSil}) from Table 5.2-1; debris mass (m_{Nukon} , m_{CalSil}); screen or perforated plate cross-sectional surface area (A) and area ratio (f); flow area (A_{screen}) and velocity approaching the sump screen (V).

where

μ_{water}	water absolute viscosity (kg/(m-s), lbm/(ft-s))
ρ_{water}	water density (kg/m ³ , lbm/ft ³)
ρ_{Nukon}	Nukon (fiber) material density (kg/m ³ , lbm/ft ³)
ρ_{CalSil}	CalSil (particle) material density (kg/m ³ , lbm/ft ³)
S_{Nukon}	Nukon (fiber) specific surface area in debris bed (m ⁻¹ , ft ⁻¹)
S_{CalSil}	CalSil (particle) specific surface area in debris bed (m ⁻¹ , ft ⁻¹)
m_{Nukon}	Nukon mass in the debris bed
m_{CalSil}	CalSil mass in the debris bed
A	debris bed cross-sectional surface area (m ² , ft ²)
A_{screen}	flow area through screen or perforated plate (m ² , ft ²)
f	flow area of screen or perforated plate divided by the total screen or plate area (equals A_{screen} / A)
V	approach velocity through cross-sectional area of solid plus fluid, upstream of sump screen (m/s, ft/s)

Step 2. Calculate the debris bed thickness at a reference bed formation approach velocity using the following relation. A reference bed formation approach velocity of 0.0305 m/s (0.1 ft/s) was used in this report.

$$\Delta L_{\text{initial}} = \frac{(X_{\text{Nukon}} + 1)}{A} \frac{m_{\text{Nukon}}}{\rho_{\text{Nukon}}} + \frac{(X_{\text{CalSil}} + 1)}{A} \frac{m_{\text{CalSil}}}{\rho_{\text{CalSil}}} \quad (4.2-2)$$

where

$\Delta L_{\text{initial}}$	debris bed thickness at the reference bed formation approach velocity (m, ft)
X_{Nukon}	Nukon void ratio in debris bed (Nukon layer at formation = 30) (equals $\text{Vol}_{\text{void}} / \text{Vol}_{\text{Nukon}}$)
X_{CalSil}	CalSil void ratio in debris bed (CalSil layer at formation = 6.2) (equals $\text{Vol}_{\text{void}} / \text{Vol}_{\text{CalSil}}$)
m_{Nukon}	Nukon mass in the debris bed (kg, lbm)
m_{CalSil}	CalSil mass in the debris bed (kg, lbm)

Step 3. Calculate the thickness of the concentrated saturated CalSil particle section in the debris bed, using equation (4.4-7).

$$\Delta L'_{\text{exit}} = \Delta L_{\text{initial}} 0.00768499 e^{8.36430232 (m_{\text{CalSil}} / m_{\text{Nukon}})} \quad (4.4-7)$$

$$\Delta L'_{\text{entr}} = \max(\Delta L_{\text{initial}} - \Delta L'_{\text{exit}}, 0) \quad (5.3-4)$$

where

$\Delta L'_{entr}$ thickness (m) of control volume at debris bed entrance at the reference bed formation approach velocity (m, ft)

$\Delta L'_{exit}$ thickness (m) of particle saturated control volume at debris bed exit at the reference bed formation approach velocity (m, ft)

If $\Delta L'_{entr}$ equals zero, the following calculations are equivalent to the one-volume model and should only consider the exit control volume. If the calculated $\Delta L'_{exit} > \Delta L_{initial}$, an oversaturated condition exists, and the procedures in Section 5.3.3 should be implemented.

Step 4. Consistent with the assumption that debris mass cannot enter or leave the debris bed or move between control volumes, the debris masses and volumes in each control volume are defined.

$$Vol_{totalentr} = \Delta L'_{entr} A \quad (5.3-5)$$

$$Vol_{totalexit} = \Delta L'_{exit} A \quad (5.3-6)$$

$$Vol_{Nukonentr} = L'_{entr} / (L'_{entr} + L'_{exit}) m_{Nukon} / \rho_{Nukon} \quad (5.3-7)$$

$$Vol_{Nukonexit} = L'_{exit} / (L'_{entr} + L'_{exit}) m_{Nukon} / \rho_{Nukon} \quad (5.3-8)$$

$$Vol_{CalSilentr} = L'_{entr} / (L'_{entr} + L'_{exit}) 0.0001 m_{CalSil} / \rho_{CalSil} \quad (5.3-9)$$

$$Vol_{CalSilexit} = L'_{exit} / (L'_{entr} + L'_{exit}) 0.9999 m_{CalSil} / \rho_{CalSil} \quad (5.3-10)$$

$$Vol_{solidentr} = Vol_{Nukonentr} + Vol_{CalSilentr} \quad (5.3-11)$$

$$Vol_{solidexit} = Vol_{Nukonexit} + Vol_{CalSilexit} \quad (5.3-12)$$

where

m_{Nukon} Nukon mass in debris bed (kg, lbm)

m_{CalSil} CalSil mass in debris bed (kg, lbm)

$Vol_{Nukonsubscript}$ Nukon volume in debris bed control volume (m^3 , ft^3)

$Vol_{CalSilsubscript}$ CalSil volume in debris bed control volume (m^3 , ft^3)

$Vol_{solidsubscript}$ Nukon and CalSil volume in debris bed control volume (m^3 , ft^3)

and subscripts

entr entrance control volume

exit exit control volume

Step 5. Calculate the debris porosity, void ratio, and effective dimensionless permeability function $K(X)$ for each control volume, using the following relations.

$$Vol_{voidentr} = Vol_{totalentr} - Vol_{solidentr} \quad (5.3-13)$$

$$Vol_{voidexit} = Vol_{totalexit} - Vol_{solidexit} \quad (5.3-14)$$

$$\epsilon_{debrisentr} = Vol_{voidentr} / Vol_{totalentr} \quad (5.3-15)$$

$$\varepsilon_{\text{debrisexit}} = \text{Vol}_{\text{voidexit}} / \text{Vol}_{\text{totalexit}} \quad (5.3-16)$$

$$\varepsilon_{\text{Nukonentr}} = (\text{Vol}_{\text{totalextr}} - \text{Vol}_{\text{Nukonentr}}) / \text{Vol}_{\text{totalextr}} \quad (5.3-17)$$

$$\varepsilon_{\text{Nukonexit}} = (\text{Vol}_{\text{totalexit}} - \text{Vol}_{\text{Nukonexit}}) / \text{Vol}_{\text{totalexit}} \quad (5.3-18)$$

$$\varepsilon_{\text{CalSilentr}} = (\text{Vol}_{\text{totalextr}} - \text{Vol}_{\text{CalSilentr}}) / \text{Vol}_{\text{totalextr}} \quad (5.3-19)$$

$$\varepsilon_{\text{CalSilexit}} = (\text{Vol}_{\text{totalexit}} - \text{Vol}_{\text{CalSilexit}}) / \text{Vol}_{\text{totalexit}} \quad (5.3-20)$$

$$X'_{\text{debrisentr}} = \text{maximum} (\text{Vol}_{\text{voidentr}} / \text{Vol}_{\text{solidentr}}, 0.0001) \quad (5.3-21)$$

$$X'_{\text{debrisexit}} = \text{maximum} (\text{Vol}_{\text{voidexit}} / \text{Vol}_{\text{solidexit}}, 0.0001) \quad (5.3-22)$$

$$X_{\text{Nukonentr}} = \text{maximum} (\text{Vol}_{\text{voidentr}} / \text{Vol}_{\text{Nukonentr}}, 0.0001) \quad (5.3-23)$$

$$X_{\text{Nukonexit}} = \text{maximum} (\text{Vol}_{\text{voidexit}} / \text{Vol}_{\text{Nukonexit}}, 0.0001) \quad (5.3-24)$$

$$X_{\text{CalSilentr}} = \text{maximum} (\text{Vol}_{\text{voidentr}} / \text{Vol}_{\text{CalSilentr}}, 0.0001) \quad (5.3-25)$$

$$X_{\text{CalSilexit}} = \text{maximum} (\text{Vol}_{\text{voidexit}} / \text{Vol}_{\text{CalSilexit}}, 0.0001) \quad (5.3-26)$$

For a bed of cylindrical fibers ($X > 1.0 \times 10^{-4}$, $\varepsilon < 0.995$):

$$K(X_{\text{Nukonentr}}) = -0.5 + 0.5 \ln(1 + X_{\text{Nukonentr}}) + \frac{1}{(2 + 2 X_{\text{Nukonentr}} + X_{\text{Nukonentr}}^2)} \quad (5.3-27)$$

$$K(X_{\text{Nukonexit}}) = -0.5 + 0.5 \ln(1 + X_{\text{Nukonexit}}) + \frac{1}{(2 + 2 X_{\text{Nukonexit}} + X_{\text{Nukonexit}}^2)} \quad (5.3-28)$$

For a bed of spherical particles ($X > 1.0 \times 10^{-4}$, $\varepsilon < 0.995$):

$$K(X_{\text{CalSilentr}}) = 2 - \frac{3}{(1 + X_{\text{CalSilentr}})^{1/3}} + \frac{5}{3(1 + X_{\text{CalSilentr}})^{5/3} + 2} \quad (5.3-29)$$

$$K(X_{\text{CalSilexit}}) = 2 - \frac{3}{(1 + X_{\text{CalSilexit}})^{1/3}} + \frac{5}{3(1 + X_{\text{CalSilexit}})^{5/3} + 2} \quad (5.3-30)$$

where

$\text{Vol}_{\text{totalsubscript}}$	total debris bed volume of control volume (m^3 , ft^3)
$\text{Vol}_{\text{voidsubscript}}$	void volume in debris bed control volume (m^3 , ft^3)
$\varepsilon_{\text{debris subscript}}$	control volume porosity
$\varepsilon_{\text{Nukon subscript}}$	effective porosity of Nukon in debris bed control volume
$\varepsilon_{\text{CalSil subscript}}$	effective porosity of CalSil in debris bed control volume
$X'_{\text{debris subscript}}$	control volume void ratio at a reference bed formation approach velocity
$X_{\text{Nukon subscript}}$	effective void ratio of Nukon in debris bed control volume
$X_{\text{CalSil subscript}}$	effective void ratio of CalSil in debris bed control volume

and subscripts

entr entrance control volume
 exit exit control volume

Step 6. Calculate the viscous (laminar) and kinetic (turbulent) components of pressure drop through the debris bed by using equation (2.5-2) for both the entrance and exit control volumes. The values of the water density (ρ_{water}) and water absolute viscosity (μ_{water}) should be adjusted to reflect the correct thermodynamic conditions (e.g., temperature) at each calculation point.

The pressure drop for the entrance control volume also includes an irreversible pressure loss for flow entering the debris bed.

$$\Delta p'_{\text{debrisbedentr}} = \left[\frac{S_{\text{Nukon}}^2 X_{\text{Nukonentr}}^3 (1-\epsilon_{\text{Nukonentr}})^2}{K(X_{\text{Nukonentr}}) (1 + X_{\text{Nukonentr}})^2 \epsilon_{\text{Nukonentr}}^3} + \frac{S_{\text{CalSil}}^2 X_{\text{CalSilenr}}^3 (1-\epsilon_{\text{CalSilenr}})^2}{K(X_{\text{CalSilenr}}) (1 + X_{\text{CalSilenr}})^2 \epsilon_{\text{CalSilenr}}^3} \right] \mu_{\text{water}} V \Delta L'_{\text{entr}} +$$

$$\left[S_{\text{Nukon}} 1.95 \left[\frac{(1-\epsilon_{\text{Nukonentr}}) \mu_{\text{water}} S_{\text{Nukon}}}{\rho_{\text{water}} V 6} \right]^{0.071} \frac{(1-\epsilon_{\text{Nukonentr}})^2}{\epsilon_{\text{Nukonentr}}^3} + S_{\text{CalSil}} 3.89 \left[\frac{(1-\epsilon_{\text{CalSilenr}}) \mu_{\text{water}} S_{\text{CalSil}}}{\rho_{\text{water}} V 6} \right]^{0.13} \frac{(1-\epsilon_{\text{CalSilenr}})^2}{\epsilon_{\text{CalSilenr}}^3} \right] \rho_{\text{water}} \frac{V^2 \Delta L'_{\text{entr}}}{6} +$$

$$0.5 (1 - \epsilon_{\text{debrisentr}}) \rho_{\text{water}} / 2 (V / \epsilon_{\text{debrisentr}})^2 \quad (5.3-31)$$

where

$\Delta p'_{\text{debrisbedsubscript}}$ debris pressure drop at the reference bed formation approach velocity (Pa, psi)
 V approach velocity through cross-sectional area of solid plus fluid, upstream of sump screen (m/s, ft/s)

The pressure drop for the exit control volume also includes an irreversible pressure loss for flow exiting the debris bed through holes in the screen or perforated plate.

$$\Delta p'_{\text{debrisbedexit}} = \left[\frac{S_{\text{Nukon}}^2 X_{\text{Nukonexit}}^3 (1-\epsilon_{\text{Nukonexit}})^2}{K(X_{\text{Nukonexit}}) (1 + X_{\text{Nukonexit}})^2 \epsilon_{\text{Nukonexit}}^3} + \frac{S_{\text{CalSil}}^2 X_{\text{CalSilexit}}^3 (1-\epsilon_{\text{CalSilexit}})^2}{K(X_{\text{CalSilexit}}) (1 + X_{\text{CalSilexit}})^2 \epsilon_{\text{CalSilexit}}^3} \right] \mu_{\text{water}} V \Delta L'_{\text{exit}} +$$

$$\left[S_{\text{Nukon}} 1.95 \left[\frac{(1-\epsilon_{\text{Nukonexit}}) \mu_{\text{water}} S_{\text{Nukon}}}{\rho_{\text{water}} V 6} \right]^{0.071} \frac{(1-\epsilon_{\text{Nukonexit}})^2}{\epsilon_{\text{Nukonexit}}^3} + S_{\text{CalSil}} 3.89 \left[\frac{(1-\epsilon_{\text{CalSilexit}}) \mu_{\text{water}} S_{\text{CalSil}}}{\rho_{\text{water}} V 6} \right]^{0.13} \frac{(1-\epsilon_{\text{CalSilexit}})^2}{\epsilon_{\text{CalSilexit}}^3} \right] \rho_{\text{water}} \frac{V^2 \Delta L'_{\text{exit}}}{6} +$$

$$(1 - f \epsilon_{\text{debrisexit}}) \rho_{\text{water}} / 2 [V / (f \epsilon_{\text{debrisexit}})]^2 \quad (5.3-32)$$

At the reference bed formation approach velocity, define the values for debris bed void ratio, pressure drop, and debris bed thickness of each control volume as $X'_{\text{debrisbedentr}}$, $\Delta p'_{\text{debrisbedentr}}$, $\Delta L'_{\text{debrisbedentr}}$, $X'_{\text{debrisbedexit}}$, $\Delta p'_{\text{debrisbedexit}}$, and $\Delta L'_{\text{debrisbedexit}}$.

Step 7. Steps 1 through 6 provide initial information regarding the two control volumes of the debris bed that will be used to calculate the debris bed compression and pressure drop conditions at higher approach velocities. Steps 7 through 10 calculate the debris bed conditions from the initial low-velocity point at higher approach velocities, assuming irreversible compression of the debris bed.

For the next higher approach velocity condition, if applicable, assume debris bed thicknesses for the two control volumes. It is recommended that the first assumed values be the initial thicknesses, $\Delta L'_{\text{debrisbedentr}}$ and $\Delta L'_{\text{debrisbedexit}}$ of the two control volumes.

Step 8. Use the methods outlined in Steps 4 through 6 to calculate the total pressure drops ($\Delta p_{\text{debrisbedentr}}$ and $\Delta p_{\text{debrisbedexit}}$) for the assumed debris bed thicknesses of the two control volumes.

Step 9. Using the new calculated values, compute updated values for $X_{\text{debrisentr}}$, $X_{\text{debrisexit}}$, $\Delta L_{\text{debrisbedentr}}$ and $\Delta L_{\text{debrisbedexit}}$, accounting for irreversible bed compression. Consistent with the equations in Section 3.1, the mechanical stress for the exit control volume should account for the stress transmitted by the entrance control volume.

$$X_{\text{debrisentr}} = X'_{\text{debrisentr}} (\Delta p_{\text{debrisbedentr}} / \Delta p'_{\text{debrisbedentr}})^{-N} \quad (5.3-33)$$

$$\Delta L_{\text{debrisbedentr}} = \text{Vol}_{\text{solidentr}} (1 + X_{\text{debrisentr}}) / A \quad (5.3-34)$$

$$X_{\text{debrisexit}} = X'_{\text{debrisexit}} [(\Delta p_{\text{debrisbedentr}} + \Delta p_{\text{debrisbedexit}}) / (\Delta p'_{\text{debrisbedentr}} + \Delta p'_{\text{debrisbedexit}})]^{-N} \quad (5.3-35)$$

$$\Delta L_{\text{debrisbedexit}} = \text{Vol}_{\text{solidexit}} (1 + X_{\text{debrisexit}}) / A \quad (5.3-36)$$

where

$X_{\text{debrisbedsubscript}}$	control volume void ratio
$X'_{\text{debrisbedsubscript}}$	control volume void ratio at a reference bed formation approach velocity
$\Delta p_{\text{debrisbedsubscript}}$	debris bed control volume pressure drop (Pa, psi)
$\Delta p'_{\text{debrisbedsubscript}}$	control volume pressure drop at the reference bed formation approach velocity (Pa, psi)
N	material-specific parameter for porous medium compression (= 0.236)
$\Delta L_{\text{debrisbedsubscript}}$	control volume bed thickness (m, ft)

The solution is converged if the calculated debris bed thickness for each control volume equals the control volume debris bed thicknesses assumed in Step 7. If convergence is reached, proceed to the next step. If the convergence criteria are not met, repeat Steps 8 through 9, using the new calculated values for debris bed thicknesses ($\Delta L_{\text{debrisbedentr}}$, $\Delta L_{\text{debrisbedexit}}$).

Step 10. Repeat Steps 7 through 9 for the next higher approach velocity, if applicable. At the highest approach velocity, define the converged values for debris bed void ratio, pressure drop, and debris bed thickness of each control volume as X_{pmaxentr} , $\Delta p_{\text{pmaxentr}}$, $\Delta L_{\text{pmaxentr}}$, X_{pmaxexit} , $\Delta p_{\text{pmaxexit}}$, and $\Delta L_{\text{pmaxexit}}$.

Step 11. The following steps calculate the debris bed decompression and pressure drop if the approach velocity drops below the highest approach velocity. This approach assumes elastic behavior of the debris bed. For the next lower approach velocity condition, if applicable, assume a debris bed thickness for each control volume. It is recommended that the first assumed value be close to the maximum thicknesses, $\Delta L_{\text{pmaxentr}}$ and $\Delta L_{\text{pmaxexit}}$.

Step 12. Use Steps 4 through 6 to calculate the pressure drops ($\Delta p_{\text{debrisbedentr}}$ and $\Delta p_{\text{debrisbedexit}}$) for the assumed debris bed thickness of each control volume.

Step 13. Using the new calculated values, compute updated values for $X_{\text{debrisbedsubscript}}$ and $\Delta L_{\text{debrisbedsubscript}}$, accounting for bed expansion.

$$X_{\text{debrisentr}} = X_{\text{pmaxentr}} \exp \left[N - \frac{N \Delta p_{\text{debrisbedentr}}}{\Delta p_{\text{pmaxentr}}} \right] \quad (5.3-37)$$

$$\Delta L_{\text{debrisbedentr}} = \text{Vol}_{\text{solidentr}} (1 + X_{\text{debrisentr}}) / A \quad (5.3-38)$$

$$X_{\text{debrisexit}} = X_{\text{pmaxexit}} \exp \left[N - \frac{N (\Delta p_{\text{debrisbedentr}} + \Delta p_{\text{debrisbedexit}})}{(\Delta p_{\text{pmaxentr}} + \Delta p_{\text{pmaxexit}})} \right] \quad (5.3-39)$$

$$\Delta L_{\text{debrisbedexit}} = \text{Vol}_{\text{solidexit}} (1 + X_{\text{debrisexit}}) / A \quad (5.3-40)$$

where

$X_{\text{pmaxsubscript}}$ control volume void ratio at Δp_{pmax}
 $\Delta p_{\text{pmaxsubscript}}$ control volume pressure drop at highest approach velocity (Pa, psi)

The solution is converged if the calculated debris bed thicknesses equal the assumed debris bed thicknesses in Step 11. If convergence is reached, proceed to the next step. If the convergence criteria are not met, repeat Steps 12 and 13, using the new calculated values for debris bed thicknesses ($\Delta L_{\text{debrisbedentr}}$ and $\Delta L_{\text{debrisbedexit}}$).

Step 14. Repeat Steps 11 through 13 for the next lower approach velocity.

Step 15. Perform this check for each calculated pressure drop. The acceptability of the total pressure drop across the two volumes calculated at each approach velocity should be assessed to ensure that single-phase flow exists downstream of the debris bed. Using the total containment pressure and calculated total sump screen head loss (pressure drop), read the maximum allowable sump water temperature from Figure 2.7-5.

If the actual sump water temperature is lower than the maximum allowable temperature, acceptable pump inlet conditions exist, and the sump screen pressure drop calculation is one-phase and acceptable.

If the actual sump water temperature is higher than the maximum allowable temperature, the void fraction at the sump screen exit exceeds 3 percent, which indicates that pump cavitation is possible. This condition indicates that the sump screen pressure drop calculation is inapplicable because two-phase flow exists.

5.3.3 Head Loss Application Procedure for a Two-Volume Oversaturated CalSil Debris Bed

As previously indicated, a condition can exist where the CalSil mass in a Nukon/CalSil debris bed will exceed the saturated CalSil conditions of Nukon. This condition is called an oversaturated CalSil debris bed.

For this condition, the exit volume is assumed to be composed of all of the Nukon mass and the saturated mass of CalSil, and the entrance volume is assumed to be almost entirely composed of CalSil. The procedure outlined in Section 5.3.2 can be applied to the exit volume. However, the approach outlined in Section 5.2 for a one-volume CalSil bed should be applied to the entrance volume. This approach recognizes that CalSil is composed of particles and fibers. Consistent with Section 5.2.4, 4 to 10 percent of the CalSil mass is assumed to be fiberglass fibers, and the remainder is assumed to be particles.

Consequently, the following modifications are suggested if $\Delta L'_{\text{exit}} > \Delta L_{\text{initial}}$ as determined using the information calculated in Step 3. This procedure has not been verified using test data because tests have not been run for a Nukon/CalSil debris bed with an oversaturated CalSil particle concentration. Figure 4.4-3 indicates that the maximum value for the ratio of the concentrated CalSil particle mass to

Nukon mass in a debris bed is about 0.6. Therefore, the thickness of the CalSil/Nukon exit volume and the CalSil-only entrance volume can be approximated using the following modifications to Steps 3 and 4.

Step 3. Calculate the CalSil fiber mass and CalSil particle mass in the entrance and exit volumes.

$$m_{\text{Nukonexit}} = m_{\text{Nukon}} + m_{\text{fract}_{\text{fiber}}} m_{\text{CalSil}} \quad (5.3-41)$$

$$m_{\text{CalSilexit}} = \text{minimum}[0.6 (m_{\text{Nukon}} + m_{\text{fract}_{\text{fiber}}} m_{\text{CalSil}}), (1 - m_{\text{fract}_{\text{fiber}}}) m_{\text{CalSil}}] \quad (5.3-42)$$

$$\Delta L'_{\text{exit}} = \frac{(X_{\text{Nukon}} + 1)}{A} \frac{m_{\text{Nukonexit}}}{\rho_{\text{Nukon}}} + \frac{(X_{\text{CalSil}} + 1)}{A} \frac{m_{\text{CalSilexit}}}{\rho_{\text{CalSil}}} \quad (5.3-43)$$

$$\Delta L'_{\text{entr}} = \max(\Delta L_{\text{initial}} - \Delta L'_{\text{exit}}, 0) \quad (5.3-44)$$

$$m_{\text{Nukonentr}} = 0.0 \quad (5.3-45)$$

$$m_{\text{CalSilentr}} = m_{\text{CalSil}} - m_{\text{CalSilexit}} \quad (5.3-46)$$

where

$m_{\text{fract}_{\text{fiber}}}$	fiber mass fraction in total CalSil mass
$m_{\text{Nukonexit}}$	Nukon mass in exit control volume (kg, lbm)
$m_{\text{CalSilexit}}$	CalSil mass in exit control volume (kg, lbm)
$m_{\text{Nukonentr}}$	fiber mass in entrance control volume (kg, lbm)
$m_{\text{CalSilentr}}$	CalSil particle mass in entrance control volume (kg, lbm)

Therefore, the debris volumes of each control volume are defined in Step 4.

$$\text{Vol}_{\text{totalentr}} = \Delta L'_{\text{entr}} A \quad (5.3-47)$$

$$\text{Vol}_{\text{totalexit}} = \Delta L'_{\text{exit}} A \quad (5.3-48)$$

$$\text{Vol}_{\text{Nukonentr}} = m_{\text{Nukonentr}} / \rho_{\text{Nukon}} \quad (5.3-49)$$

$$\text{Vol}_{\text{Nukonexit}} = m_{\text{Nukonexit}} / \rho_{\text{Nukon}} \quad (5.3-50)$$

$$\text{Vol}_{\text{CalSilentr}} = m_{\text{CalSilentr}} / \rho_{\text{CalSil}} \quad (5.3-51)$$

$$\text{Vol}_{\text{CalSilexit}} = m_{\text{CalSilexit}} / \rho_{\text{CalSil}} \quad (5.3-52)$$

$$\text{Vol}_{\text{solidentr}} = \text{Vol}_{\text{Nukonentr}} + \text{Vol}_{\text{CalSilentr}} \quad (5.3-53)$$

$$\text{Vol}_{\text{solidexit}} = \text{Vol}_{\text{Nukonexit}} + \text{Vol}_{\text{CalSilexit}} \quad (5.3-54)$$

It should again be emphasized that the procedure for calculating a CalSil oversaturation condition has not been verified with test data. The suggested procedure represents a reasonable initial approach for calculating properties of debris beds with oversaturation conditions.

6. COMPARISONS OF HEAD LOSS PREDICTIONS WITH TEST DATA

This section compares the head loss test data obtained from the PNNL tests, given in NUREG/CR-6917 (Ref. 24), and the ANL tests, given in NUREG/CR-6913 (Ref. 25), with predictions obtained using the methods described in this report and the methodology described in NUREG/CR-6224 (Ref. 2). This discussion also compares the recommended calculational method to data from tests performed at the LANL/UNM facility, given in NUREG/CR-6874 (Ref. 3).

6.1 PNNL Large Head Loss Test Facility

Figure 6.1-1 shows a schematic of the PNNL large head loss test facility. The PNNL large head loss test facility consisted of a vertical water circulation loop with a downward-flowing vertical flow channel with a horizontally mounted metal screen or perforated plate to simulate a PWR sump screen surface on which debris is collected. Test debris was added to the loop upstream of the test screen location. The test facility used a pump to circulate water and debris in the test loop until a stable debris bed was formed. Ports for differential pressure transducers were located at various positions upstream and downstream of the debris bed at the test location. The test section was fabricated from clear polycarbonate material so that it was possible to observe and measure the test debris bed. The test loop was equipped with heaters to permit testing at elevated temperatures. A bypass filtering system was also installed in the loop to permit filtering of debris material to prevent recirculated debris from affecting the debris bed stability and to allow test measurements for a stable debris bed. NUREG/CR-6917 provides a more detailed description of the PNNL head loss test facility and test results (Ref. 24).

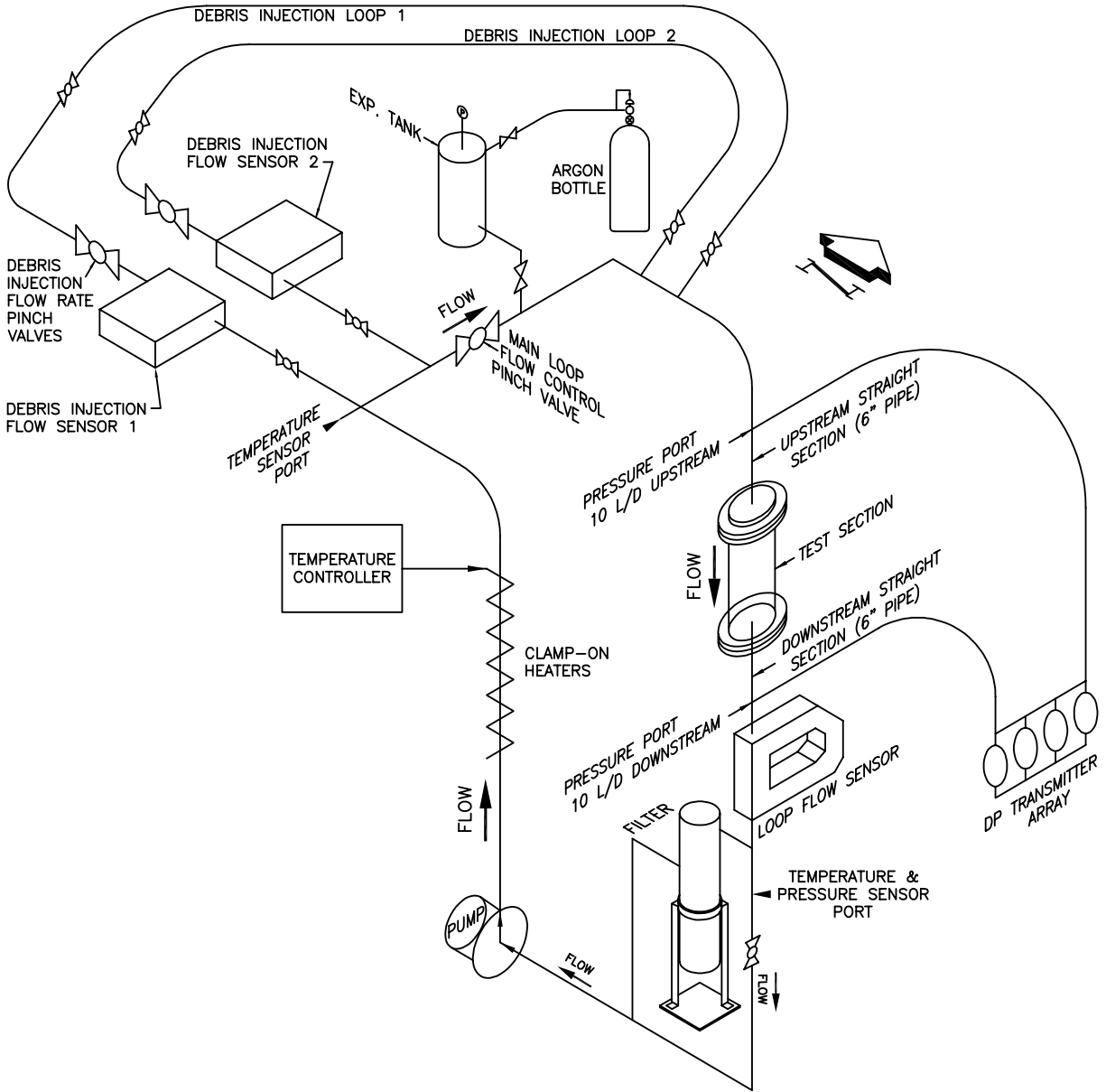


Figure 6.1-1 Schematic of PNNL Large Head Loss Test Facility

6.2 Comparisons of Head Loss Predictions with PNNL Test Data

PNNL performed testing in the large loop in two series, Series 1 and Series 2, which included benchmark tests. The benchmark tests served to compare results from similar tests performed at PNNL and ANL.

PNNL performed the Series 1 tests using the metal screen described in Section 2.5, which was similar to the one used for the LANL/UNM tests. The test matrix for the PNNL Series 1 tests attempted to match the conditions of several of the LANL/UNM Nukon/CalSil Series 6 tests and one Nukon-only LANL/UNM Series 1 test.

The PNNL Series 2 tests provided test measurements using the perforated plate described in Section 2.5 with Nukon/CalSil or Nukon-only debris beds.

The PNNL benchmark tests consisted of three tests specifically performed to match tested conditions at the ANL head loss test facility (Ref. 25) in order to investigate the ability of the two loops to produce similar test results. The benchmark tests were performed using the perforated plate described in Section 2.5 with two Nukon-only debris beds and one Nukon/CalSil debris bed.

The PNNL testing provided better measurements of debris masses on the test screen than did the LANL tests at UNM. The PNNL tests achieved better mass measurement accuracy as well as more repeatable and reliable test results for the following six reasons:

- (1) As indicated in Section 4, PNNL measured debris mass on the screen; in the UNM tests, LANL assumed that essentially all debris mass added to the loop accumulated on the screen. The PNNL tests accounted for the difference between the CalSil mass added and collected on the screen by using a chemical dissolution technique to measure the mass of CalSil collected in the debris bed. Additionally, the Series 2 tests improved bed mass assessments by removing circulating loop debris mass using a filtration system that collected debris mass not deposited on the screen. Consequently, the PNNL test procedure provided measurements of the Nukon and CalSil masses collected on the screen.
- (2) The LANL/UNM test facility appeared to have significant bypass flow around the debris bed and screen; the PNNL test facility was designed to prevent bypass flow around the screen.
- (3) PNNL performed a study to identify the sensitivity of blender processing operation time for debris preparation and developed a debris processing procedure that resulted in consistently prepared Nukon and CalSil debris. The processing time used for the LANL debris preparation was not as rigorously determined and was somewhat arbitrarily set. Consequently, the PNNL test results would generally be expected to provide more repeatable pressure drop measurements.
- (4) An optical laser triangulation system was installed in the PNNL test loop to measure the debris bed thickness and to provide the surface contour of the debris bed for all the Series 2 tests and one Series 1 test.
- (5) The PNNL staff continuously measured and recorded the temperature of the loop water during testing. Additionally, after the Series 1 tests, PNNL installed a temperature control system with loop heaters to maintain a constant water temperature.

- (6) PNNL developed a method to section and study the structure of a debris bed. The PNNL staff applied this procedure to several debris beds to obtain information regarding the concentration gradient of the debris in the bed and to provide information regarding debris bed compression.

Tests performed for Series 1 had the following four limitations:

- (1) All testing was performed at ambient temperature because the loop temperature control was not yet installed.
- (2) An older pinch valve was used in the loop because the as-delivered new valve was defective and had to be replaced. Unfortunately, the older valve had a tendency to introduce rust and metal debris into the debris bed for several of the early Series 1 tests before being replaced.
- (3) The loop filtering system was not installed for the Series 1 tests.
- (4) The debris bed thickness was estimated visually because the optical laser triangulation system, which could measure the debris bed thickness and contour, was not installed and calibrated until just before the last Series 1 test.

The PNNL Series 2 tests, including the benchmark tests, addressed the limitations of the Series 1 tests.

Section 2.5.2 describes the woven metal screen and perforated plate used in the PNNL head loss tests. The assessments reported in this section used this information.

6.2.1 Comparison of Head Loss Predictions to PNNL Series 1 Tests

Table 6.2-1 lists the PNNL Series 1 head loss tests performed using a metal screen. This table also lists most of the LANL/UNM tests and identifies comparative PNNL Series 1 and LANL/UNM tests. Two PNNL Series 1 tests were performed to measure the pressure drop for water flow through an unobstructed metal screen. Two tests were performed for a debris bed composed entirely of Nukon, and six tests were performed using Nukon/CalSil debris beds. For the Nukon/CalSil tests, the Nukon and CalSil debris masses were premixed before addition to the test loop.

Table 6.2-1 PNNL Series 1 and LANL/UNM Head Loss Tests Using a Metal Screen

LANL Test*	Added Nukon kg/m ²	Added CalSil kg/m ²	Estimated Bed CalSil kg/m ²	Bed CalSil / Nukon	Bed Total Debris kg/m ²	Loop Temperature °C	PNNL Test [#]	Bed Nukon kg/m ²	Bed CalSil kg/m ²	Bed CalSil / Nukon	Bed Total Debris kg/m ²	Loop Temperature °C
							051114_SO_0000_L1	0.0	0.0	NA	0.0	17-24
							051128_SO_0000_L1	0.0	0.0	NA	0.0	16-19
2a	0.0	0.110	0.110	Infinity	0.110	21						
2d	0.0	0.110	0.110	Infinity	0.110	52						
2b	0.0	0.885	0.885	Infinity	0.885	21						
2e	0.0	0.885	0.885	Infinity	0.885	52						
2c	0.0	1.769	1.769	Infinity	1.769	21						
2f	0.0	1.769	1.769	Infinity	1.769	52						
3a	0.111	0.056	0.056	0.500	0.167	21						
3b	0.111	0.111	0.111	1.000	0.223	21						
3c	0.111	0.223	0.223	2.000	0.334	21						
6h	0.229	0.114	0.105	0.460	0.334	44	051110_NC_0595_L1	0.213	0.053	0.249	0.266	21-25
1a'	0.885	0.0	0.0	0.0	0.885	21						
6f	0.610	0.305	0.300	0.493	0.911	60	051121_NC_1586_L1	0.561	0.168	0.300	0.729	16-27
6i	0.839	0.419	0.415	0.495	1.254	60	051123_NC_2181_L1	0.786	0.249	0.316	1.035	22-32
3d	0.885	0.442	0.442	0.500	1.327	21						
3j	0.885	0.442	0.442	0.500	1.327	52						
6e	1.068	0.534	0.531	0.497	1.599	54	051117_NC_2776_L1	0.989	0.346	0.349	1.335	21-27
6e2	1.068	0.534	0.534	0.500	1.602	38	051128_NC_2776_L2	0.925	0.336	0.363	1.261	21-27
3e	0.885	0.885	0.885	1.000	1.769	21						
3k	0.885	0.885	0.885	1.000	1.769	52						
3f	0.885	1.769	1.769	2.000	2.654	21						
3l	0.885	1.769	1.769	2.000	2.654	52						
1a	1.769	0.0	0.0	0.0	1.769	21	051108_NO_3067_L1 ^{&}	1.789	0.0	0.0	1.789	20-30
							060125_NO_3067_L1 ⁺	1.720	0.0	0.0	1.720	22-26
1b	1.769	0.0	0.0	0.0	1.769	21						
3g	1.769	0.885	0.885	0.500	2.654	21						
3h	1.769	1.769	1.769	1.000	3.539	21						
3i	1.769	3.539	3.539	2.000	5.308	21						
6b	1.525	0.839	0.830	0.544	2.355	44	051115_NC_4098_L1	1.196	0.729	0.610	1.925	21-25

* Pipe id= 11-3/8 inch, Pipe Area = 0.06556 m²

[#] Area = 0.01863 m²

[&] Metal/rust particles present in bed.

⁺ Construction debris present in bed.

6.2.1.1 PNNL Series 1 Tests of a Clean Unclogged Metal Screen

As indicated in Table 6.2-1, two of the PNNL Series 1 tests measured pressure drop across a clean unclogged metal screen. Figures 6.2-1 and 6.2-2 compare the measured irreversible loss coefficient across the unobstructed metal screen with the values calculated using the Idelchik correlation (Ref. 22) described in Section 2.5. The irreversible loss coefficient across the unobstructed screen was calculated from pressure drop and velocity measurements using the Bernoulli equation.

$$K_{\text{screen}} = 2 \Delta p_{\text{screen}} / (\rho_{\text{water}} V^2) \quad (6.2-1)$$

where

K_{screen}	irreversible loss coefficient for clean unclogged screen
Δp_{screen}	pressure drop (head loss) across a clean unclogged screen
ρ_{water}	water density
V	approach velocity upstream of screen

Figure 6.2-3 indicates the magnitude of pressure drop measurements for Test 051128_SO_0000_L1. Figures 6.2-1 and 6.2-2 plot only the loss coefficient values for Test 051128_SO_0000_L1 because the 0–5-inch differential pressure transducer used for this test was more accurate at lower pressure drop measurements. Measurements for Test 051114_SO_0000_L1 used a 0–30-inch pressure transducer, which was less accurate at lower pressure drop measurements. The loss coefficients obtained from measurements generally agree with the Idelchik correlation except at low approach velocities where the pressure drop is small. The Idelchik correlation for a circular wire metal screen as described in Section 2.5 is indicated to be applicable to the range of tested screen Reynolds numbers. The discrepancies at lower velocity could be attributed to inaccuracies in very low pressure drop measurements.

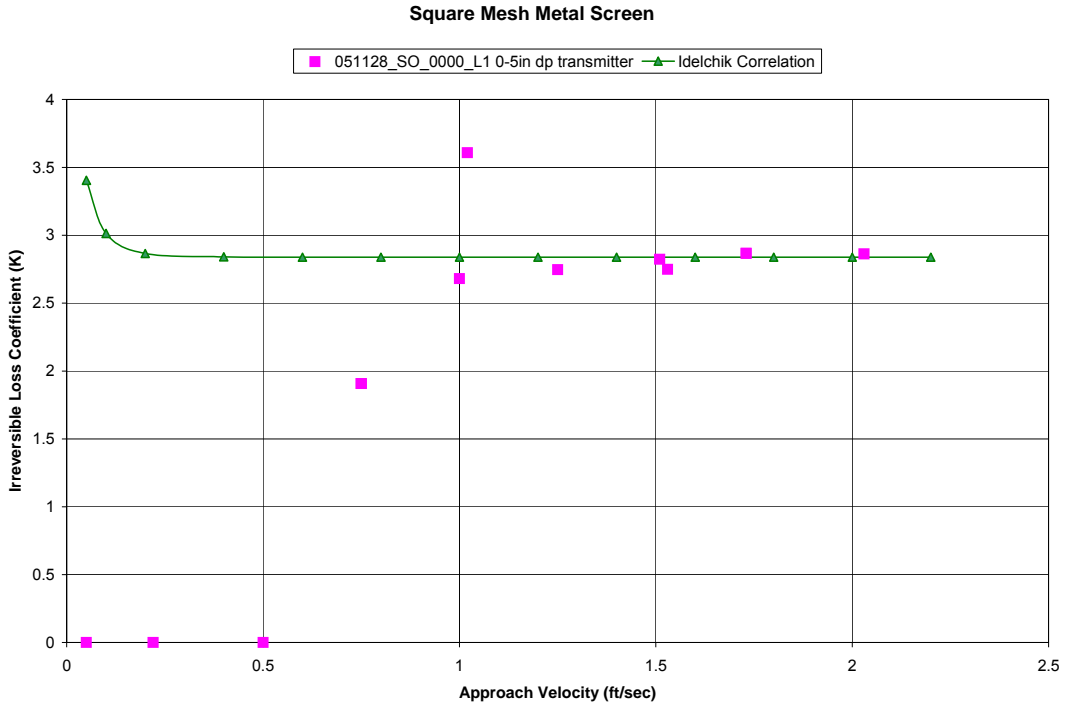


Figure 6.2-1 Comparison of Measured and Correlation Loss Coefficient Versus Approach Velocity

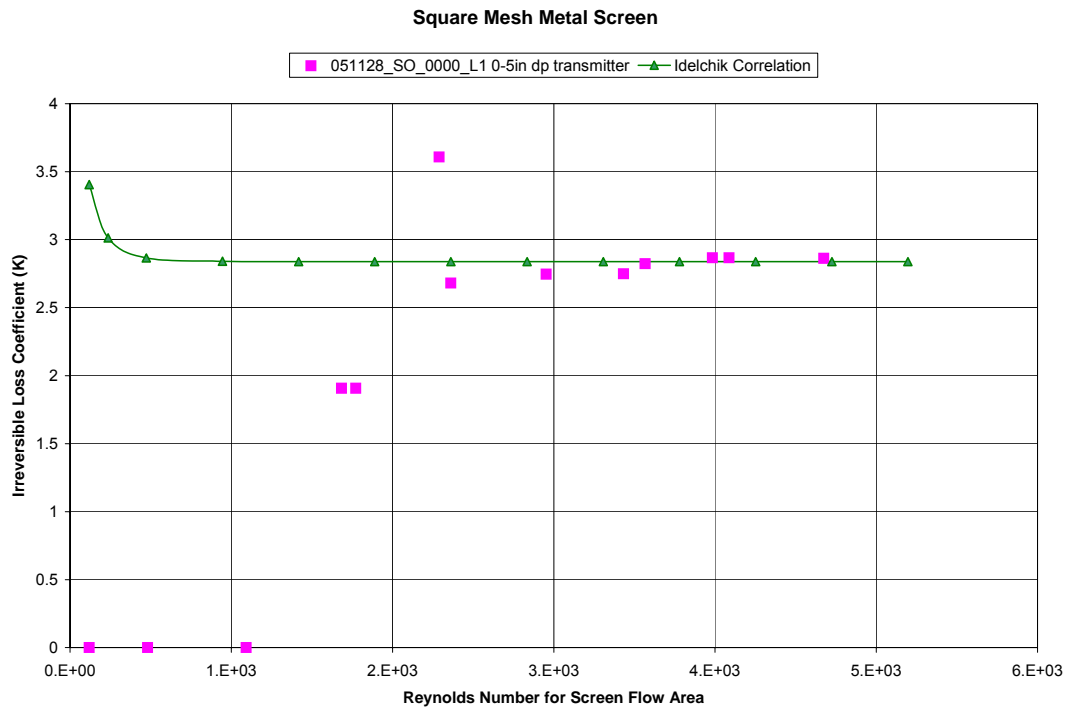


Figure 6.2-2 Comparison of Measured and Correlation Loss Coefficient Versus Reynolds Number

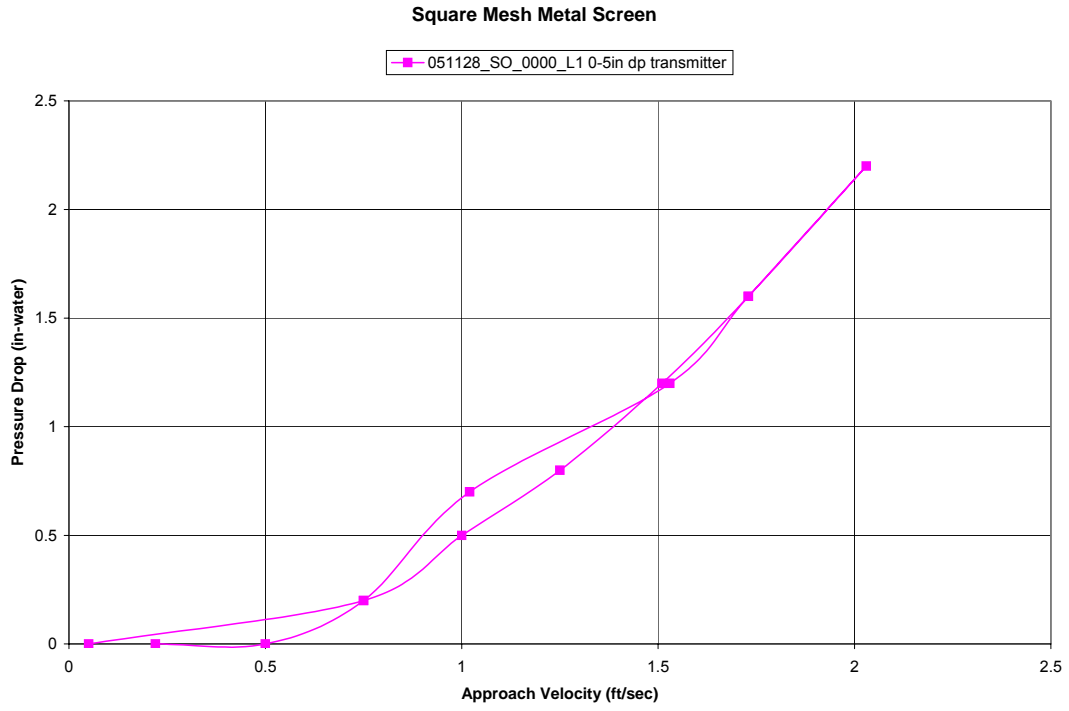


Figure 6.2-3 Measured Pressure Drop Used for Irreversible Loss Coefficient Calculation

6.2.1.2 PNNL Series 1 Tests with Nukon and CalSil Debris on a Metal Screen

Test results and information for the PNNL debris bed head loss testing presented in NUREG/CR-6917 (Ref. 24) indicate that the pressure drop across a debris bed depends on the debris composition and distribution in the bed. Figure 6.2-4 from NUREG/CR-6917 presents test data for a target debris loading of 1.10 kg/m² Nukon and 0.51 kg/m² of CalSil on a metal screen that illustrate the head loss dependence on the debris distribution in a bed. The target debris loading uses the mass added to the test loop, not the actual mass deposited in the debris bed. A debris bed that is built using premixed Nukon/CalSil resulted in the lowest head loss for a given approach velocity. This condition is closest to a homogeneous debris bed, which possesses uniform distribution of Nukon and CalSil debris. The other data points present test results for beds that were formed with staggered-time addition of Nukon and CalSil debris. The staggered debris addition resulted in a nonuniform distribution of debris in the bed.

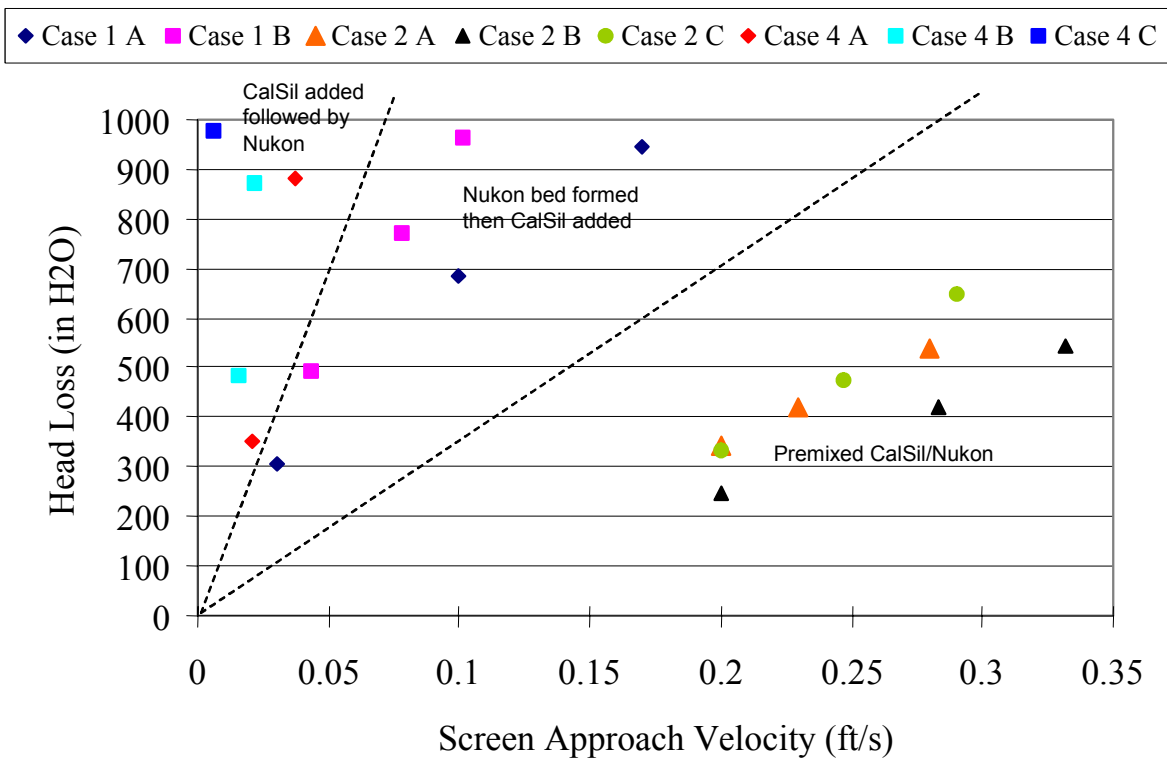


Figure 6.2-4 PNNL Test Data Showing Head Loss Dependence on Debris Distribution in Bed

Section 5 describes two methods for calculating head loss across a debris bed. The first method performs calculations using a one-volume debris bed with uniform debris distribution. The second method uses a two-volume approach in which the fibrous debris such as Nukon is uniformly distributed in the bed and the particulate debris is concentrated in a maximum saturated layer at the debris bed exit. The one-volume method has been shown to provide results that match the pressure drop measurements for a homogeneous bed composed of one debris type or a debris bed with more than one debris type and a uniform debris distribution. Therefore, the one-volume method provides a best estimate of pressure drop for a bed composed of one debris type or a lower limit head loss condition for a bed composed of more

than one debris type. The two-volume approach represents a nonuniform debris bed and results in upper limit head losses. As mentioned in Section 4, the methodology for the two-volume approach has been developed using the PNNL data, assuming that the test data represent the practical upper limit bounding pressure drop conditions. Consequently, the two-volume calculational approach should represent a more practical maximum upper head loss condition.

6.2.1.3 Predictions of PNNL Series 1 Nukon-Only Tests Using a One-Volume Model

Figures 6.2-5 to 6.2-8 compare test data from the PNNL Series 1 Nukon-only debris bed tests with predictions using the one-volume calculational method and the calculational method described in NUREG/CR-6224 (Ref. 2). Tables 4.1-2 and 6.2-1 list the debris bed loadings for the plotted cases. The following items list specific assumptions used for the predictive analyses:

- Section 4.1 provides the basis for the debris bed loadings used in the calculations.
- The predictions obtained using the one-volume calculational method use the debris material-specific surface areas and densities listed in Table 5.2-1; the predictions obtained using the NUREG/CR-6224 method employ the material properties specified in NUREG/CR-6874 and listed in Table 4.3-1.
- The initial debris bed thickness used for the one-volume method is calculated according to the approach discussed in Section 4.2. The NUREG/CR-6224 calculations use the NUREG/CR-6224 calculational method to determine initial bed thickness.
- A material-specific compression parameter of 0.236, as described in Section 4.5, was used for the one-volume calculations. The NUREG/CR-6224 calculations use the NUREG/CR-6224 calculational method to determine bed compression.
- The NUREG/CR-6224 calculations use an as-fabricated packing density of 2.4 lbf/ft³ (38.44 kg/m³) for the Nukon fiber beds as recommended in NUREG/CR-6874 (Ref. 3). The one-volume calculation does not employ this parameter in its solution.
- The loop temperature is recorded at each data point during the PNNL tests, and the one-volume and NUREG/CR-6224 calculations employ the recorded temperature at each data point. Consequently, the plotted predictions reflect the changes in loop temperature.

For the Nukon-only Tests 051108_NO_3067_L1 and 060125_NO_3067_L1, the debris beds were formed at an approach velocity of 0.061 m/s (0.2 ft/s). The approach velocities were cycled four times after bed formation from a low value of about 0.0305 m/s (0.1 ft/s) to about 0.305 m/s (1.0 ft/s). As shown in Figures 6.2-5 and 6.2-7, the one-volume model predictions for the Nukon-only tests bound the pressure drop test data. The NUREG/CR-6224 head loss calculations underpredict pressure drop test measurements for both tests. The primary reason for variances in calculated head loss for the different velocity cycles was the change in measured water temperature that affected the liquid viscosity and density. As shown in Figures 6.2-6 and 6.2-8, the NUREG/CR-6224 debris bed calculations overpredict the bed thickness test data for both tests. For both tests, the one-volume calculation predicts debris bed thicknesses that are close to those measured values. The bed thicknesses for Test 051108_NO_3067_L1 were determined using optical measurements; the laser optical triangulation measurement system was used to measure debris bed thicknesses for Test 060125_NO_3067_L1. The favorable comparisons between the one-volume predictions and test measurements qualitatively justify the presence of a uniform

debris distribution for debris beds composed entirely of Nukon fibers. All of the NUREG/CR-6224 bed thickness predictions overpredict measurements and exhibit the unrealistic uncompacted limit illustrated by the constant bed thicknesses predicted at lower approach velocities.

PNNL Series 1 Test 051108_NO_3067_L1 (Nukon Bed, 1.79 kg/m², 20-30 °C)

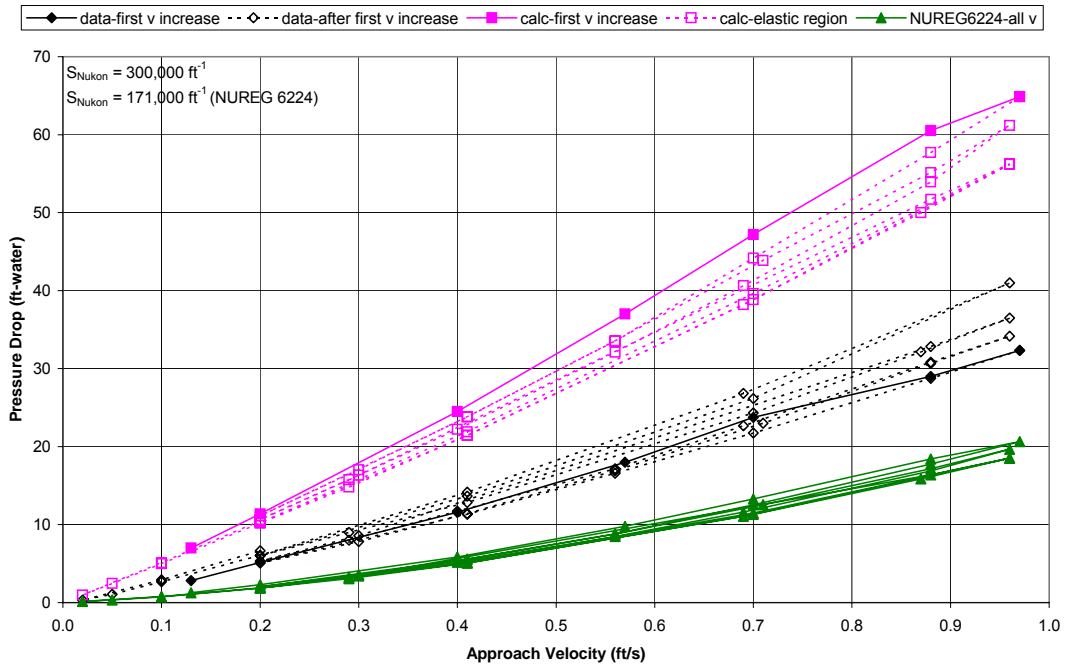


Figure 6.2-5 Head Loss for PNNL Series 1 Nukon-Only Test 051108_NO_3067_L1

PNNL Series 1 Test 051108_NO_3067_L1 (Nukon Bed, 1.79 kg/m², 20-30 °C)

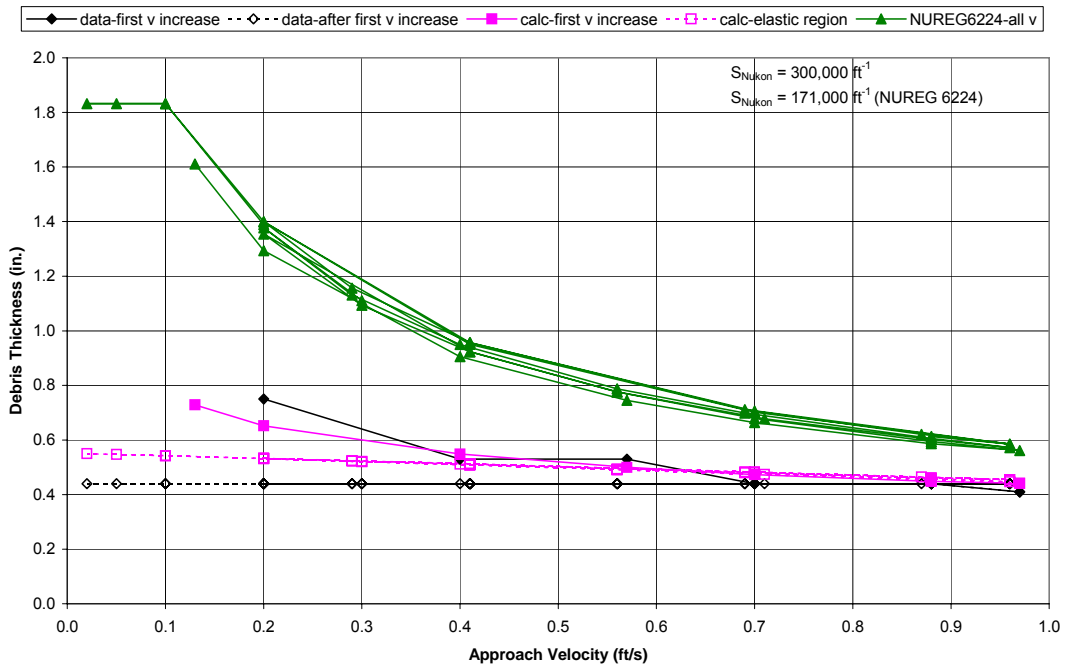


Figure 6.2-6 Bed Thickness for PNNL Series 1 Nukon-Only Test 051108_NO_3067_L1

PNNL Series 1 Test 060125_NO_3067_L1 (Nukon Bed, 1.72 kg/m², 22-26 °C)

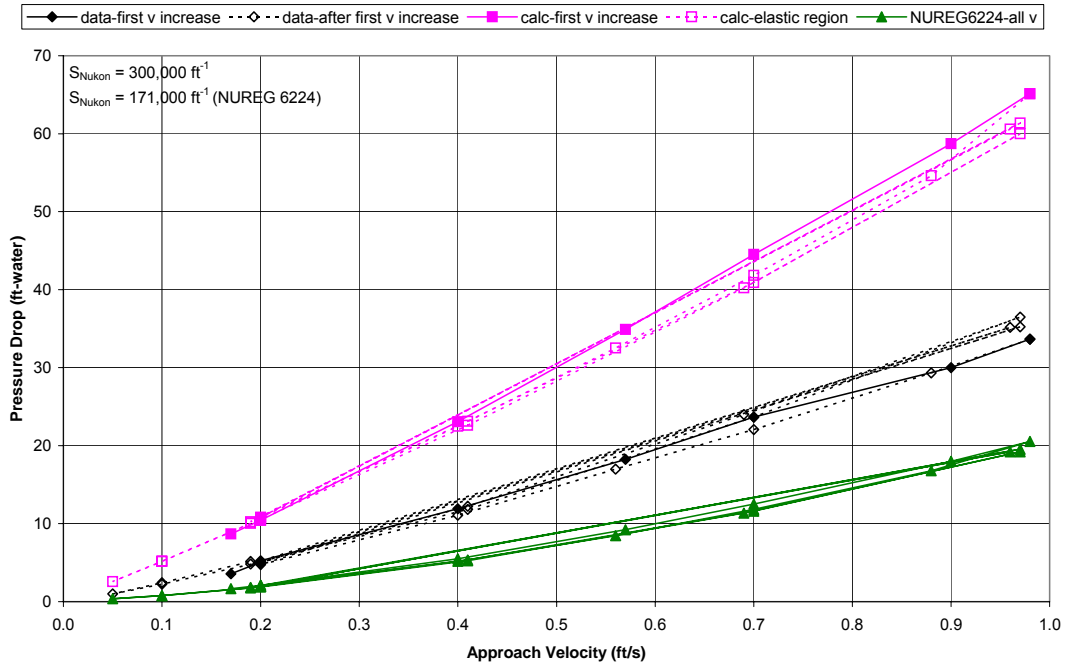


Figure 6.2-7 Head Loss for PNNL Series 1 Nukon-Only Test 060125_NO_3067_L1

PNNL Series 1 Test 060125_NO_3067_L1 (Nukon Bed, 1.72 kg/m², 22-26 °C)

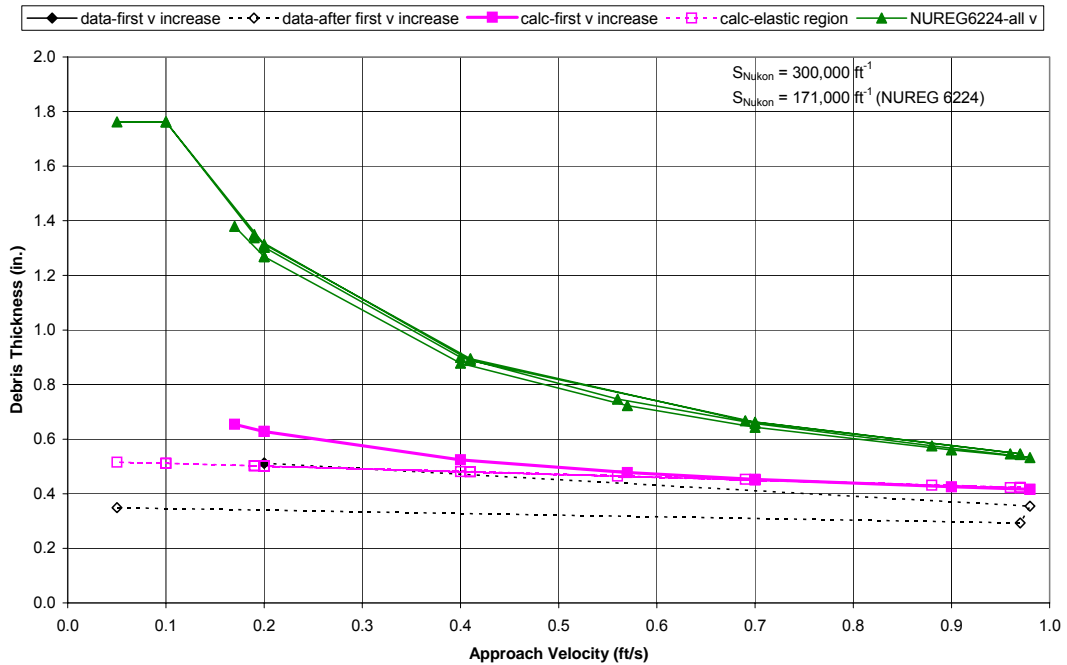


Figure 6.2-8 Bed Thickness for PNNL Series 1 Nukon-Only Test 060125_NO_3067_L1

6.2.1.4 Predictions of PNNL Series 1 Nukon/CalSil Tests Using a Two-Volume Model

This section compares the predictions for the two-volume models with test data from the PNNL Series 1 tests with Nukon/CalSil debris beds. Figures 6.2-9 to 6.2-20 compare the measured pressure drops and bed thicknesses to predictions using the two-volume approach and the NUREG/CR-6224 calculational method. Tables 6.2-1 and 4.1-2 list the debris bed loadings for the plotted cases. The following discusses specific assumptions used for the predictive analyses:

- Section 4.1 provides the basis for the debris bed loadings used in the calculations.
- The predictions obtained using the two-volume calculational method use the debris material-specific surface areas and densities listed in Table 5.2-1; the predictions obtained using the NUREG/CR-6224 method employ the material properties specified in NUREG/CR-6224 and listed in Table 4.3-1.
- The initial debris bed thicknesses used for the two-volume method are calculated according to the approach discussed in Section 4.2. The NUREG/CR-6224 calculations use the NUREG/CR-6224 method to determine initial bed thickness.
- A material-specific compression parameter of 0.236, as described in Section 4.5, is used for the two-volume calculations. The NUREG/CR-6224 calculations use the NUREG/CR-6224 calculational method to determine bed compression.
- The NUREG/CR-6224 calculations use an as-fabricated packing density of 2.4 lbm/ft³ (38.44 kg/m³) for the Nukon fiber beds as recommended in NUREG/CR-6874 (Ref. 3). The two-volume calculation does not employ this parameter in its solution.
- The NUREG/CR-6224 calculations use a particle sludge density of 22 lbm/ft³ (352.4 kg/m³) for the Nukon/CalSil debris beds as recommended in NUREG/CR-6874 (Ref. 3). The two-volume calculation does not employ this parameter in its solution.
- The loop temperature is recorded at each data point during the PNNL tests, and the two-volume and NUREG/CR-6224 calculations employ the recorded temperature at each data point. Consequently, the plotted predictions reflect the changes in loop temperature.

Generally, the two-volume approach provides a better, but not necessarily conservatively bounding, pressure drop prediction than the predictions obtained using the NUREG/CR-6224 method. The bed thickness predictions using the two-volume approach generally match the thickness measurements better than the thicknesses obtained using the NUREG/CR-6224 method.

The two-volume calculational approach assumes the presence of a saturated CalSil volume within the debris bed. As previously stated, the two-volume approach represents a nonuniform debris bed that is intended to provide an upper bound head loss condition. Two-volume calculations are not performed for the Nukon-only tests because a debris bed composed of one debris type is considered to be a homogeneous bed, and, as shown in the previous section, the one-volume approach adequately predicts test data for the Nukon-only tests.

Figure 6.2-9 compares the two-volume head loss predictions for Nukon/CalSil Test 051110_NC_0595_L1. For this test, the bed was formed at an approach velocity of 0.061 m/s (0.2 ft/s).

Six velocity cycles were used during testing. Bed thickness measurements are not recorded for this test. Pressure predictions using the two-volume approach exceed and bound the test data, but predictions obtained using the NUREG/CR-6224 calculational method underpredict test data. Figure 6.2-10 provides predictions of bed thickness.

Figures 6.2-11 and 6.2-12 compare head loss and debris bed thickness predictions using the two-volume model with data for Test 051115_NC_4098_L1. An approach velocity of 0.061 m/s (0.2 ft/s) was used to form the debris bed. Six velocity cycles were used for this test. The head loss predictions using the two-volume and NUREG/CR-6224 models are close to test data. The two-volume bed thickness predictions shown in Figure 6.2-12 are close to test measurements; the NUREG/CR-6224 bed thickness predictions do not match test measurements.

Figures 6.2-13 and 6.2-14 show comparisons of head loss and bed thickness predictions with data for Test 051117_NC_2776_L1. An approach velocity of 0.0305 m/s (0.1 ft/s) was used to form the debris bed. This test was performed using six velocity cycles that were cycled between about 0.0305 m/s (0.1 ft/s) and 0.122 m/s (0.4 ft/s). The two-volume head loss predictions are close to the upper values of the test data measurements. The bed thickness predictions in Figure 6.2-14 are close to test measurements. The NUREG/CR-6224 head loss calculations underpredict measurements, but the bed thickness predictions are closer to test data.

The Nukon and CalSil masses used for Test 051128_NC_2776_L2 were similar to those used in Test 051117_NC_2776_L1. An approach velocity of 0.0305 m/s (0.1 ft/s) was used to form the debris bed. This test was performed using six velocity cycles that were cycled between 0.0305 m/s (0.1 ft/s) and 0.079 m/s (0.26 ft/s). Figures 6.2-15 and 6.2-16 provide the head loss and bed thickness comparisons between test data and predictions for Test 051128_NC_2776_L2. The head loss predictions calculated using the two-volume models match the lower levels of test measurements. This behavior suggests that the CalSil may have redistributed with subsequent cycles. The bed thickness predictions are larger than the measurements. The NUREG/CR-6224 head loss calculations underpredict measurements, and the bed thickness predictions do not match test data.

Figures 6.2-17 and 6.2-18 plot the head loss and bed thickness comparisons for Test 051121_NC_1586_L1. The Nukon/CalSil bed was formed on the metal screen at an approach velocity of 0.0305 m/s (0.1 ft/s). The Nukon and CalSil masses were premixed before addition to the test loop. Test measurements were recorded for six velocity cycles between about 0.0305 m/s (0.1 ft/s) and 0.13 m/s (0.43 ft/s). Figure 6.2-17 indicates that the head loss results from the two-volume calculations are close to test data. The head loss measurements for the first velocity cycle are bounded by the two-volume predictions, but the measured pressure drops for subsequent cycles are close to predictions. This behavior suggests that the CalSil may have redistributed with subsequent cycles. Figure 6.2-18 shows that the initial bed thickness measurements are close to test data. The NUREG/CR-6224 calculations for head loss underpredict test measurements.

The predictions for Test 051123_NC_2181_L1 appear in Figures 6.2-19 and 6.2-20. The Nukon/CalSil debris bed for this test was formed at an approach velocity of 0.0305 m/s (0.1 ft/s). Tests were performed for four velocity cycles. (Each cycle consisted of a velocity increase followed by a velocity decrease.) The pressure drop predictions using the two-volume model are larger than those calculated using the NUREG/CR-6224 approach, but the pressure drop predictions using both models underpredict measurements. The head loss measurements for the first velocity cycle match a part of the two-volume predictions, but the measured pressure drops for subsequent cycles exceed predictions. This behavior

suggests that the CalSil may have redistributed during subsequent cycles. The debris bed thicknesses predicted using the two-volume and NUREG/CR-6224 methods are larger than test measurements.

Test 051110_NO_0595_L1 (Nukon/CalSil=0.213/0.053 kg/m², 21-25C) - Two Volume Model

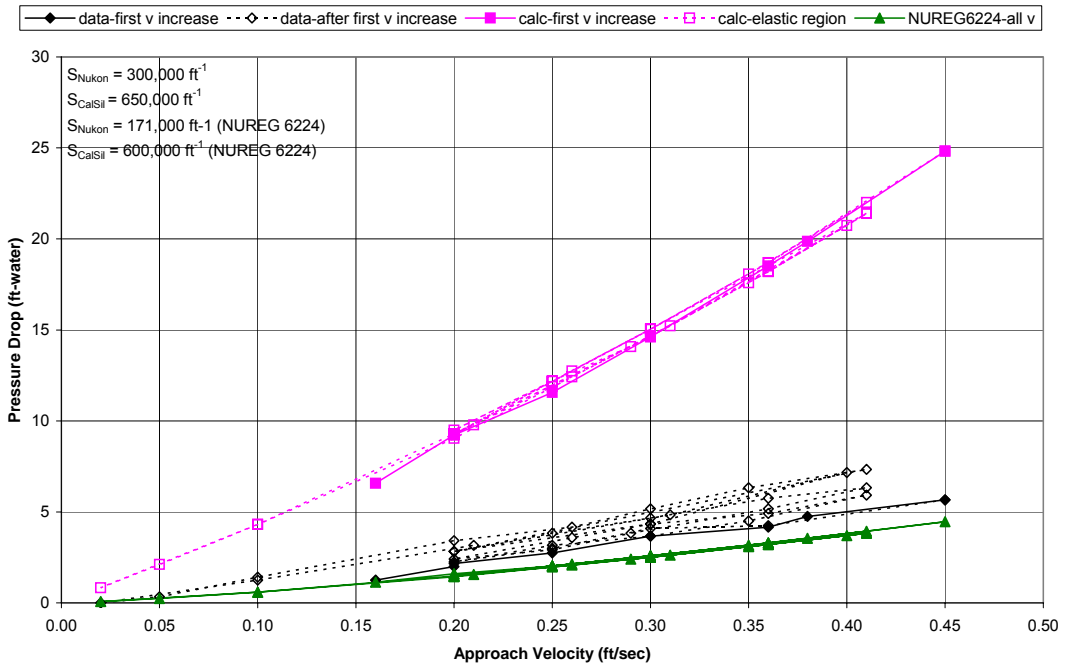


Figure 6.2-9 Head Loss for PNNL Series 1 Nukon/CalSil Test 051110_NC_0595_L1

Test 051110_NO_0595_L1 (Nukon/CalSil=0.213/0.053 kg/m², 21-25C) - Two Volume Model

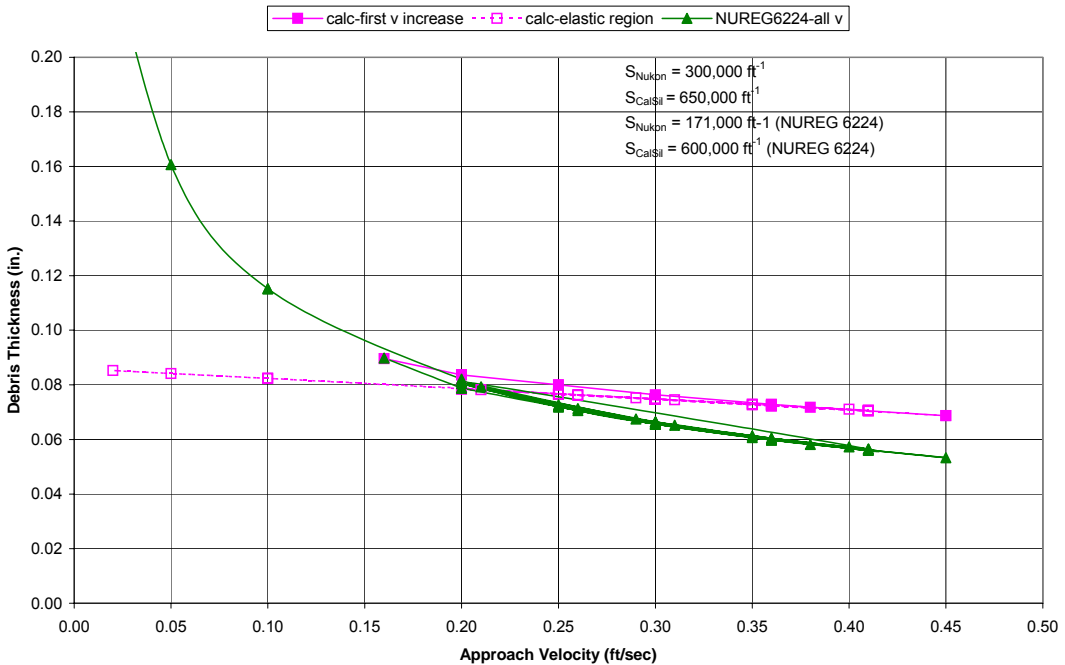


Figure 6.2-10 Bed Thickness for PNNL Series 1 Nukon/CalSil Test 051110_NC_0595_L1

Test 051115_NC_4098_L1(Nukon/CalSil=1.20/0.73 kg/m², 21-25C) - Two Volume Model

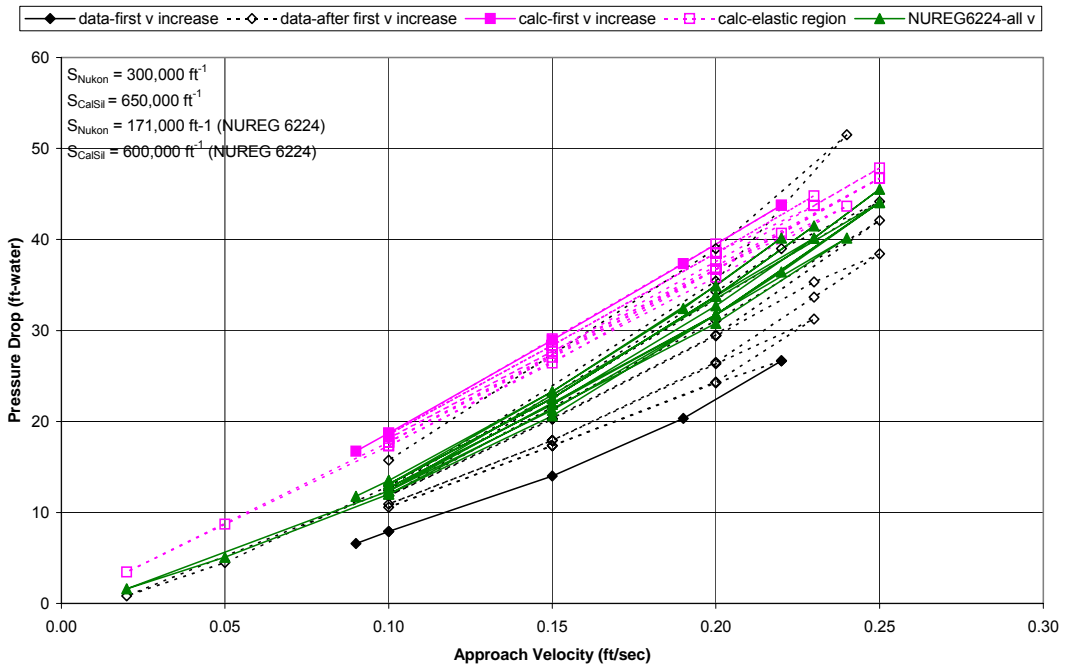


Figure 6.2-11 Head Loss for PNNL Series 1 Nukon/CalSil Test 051115_NC_4098_L1

Test 051115_NC_4098_L1(Nukon/CalSil=1.20/0.73 kg/m², 21-25C) - Two Volume Model

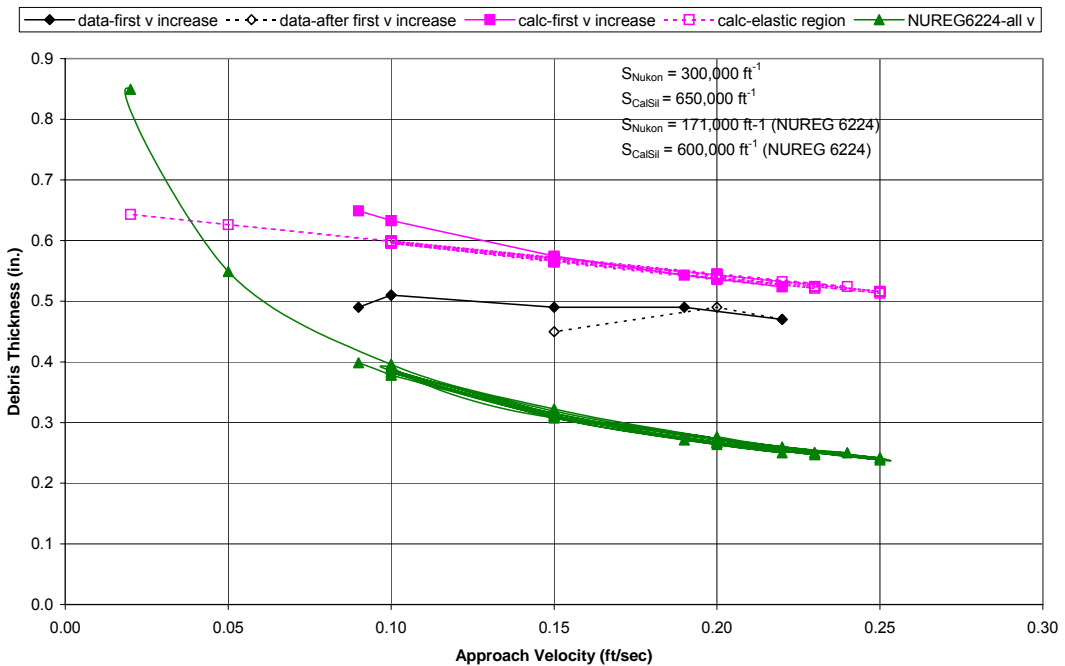


Figure 6.2-12 Bed Thickness for PNNL Series 1 Nukon/CalSil Test 051115_NC_4098_L1

Test 051117_NC_2776_L1(Nukon/CalSil=0.99/0.35 kg/m², 21-27C) - Two Volume Model

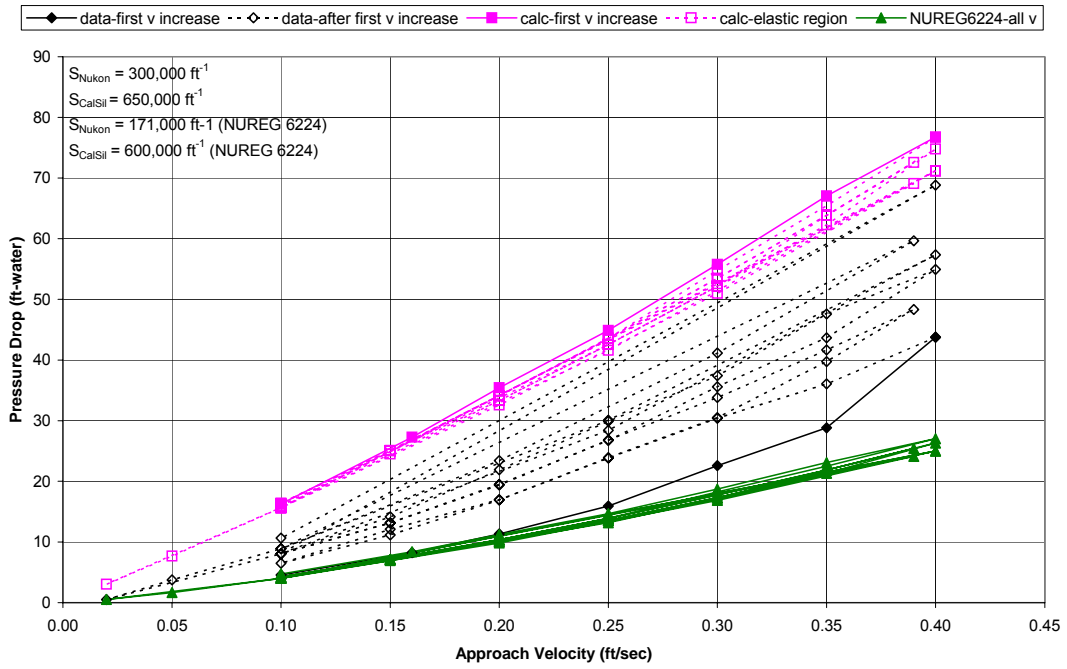


Figure 6.2-13 Head Loss for PNNL Series 1 Nukon/CalSil Test 051117_NC_2776_L1

Test 051117_NC_2776_L1(Nukon/CalSil=0.99/0.35 kg/m², 21-27C) - Two Volume Model

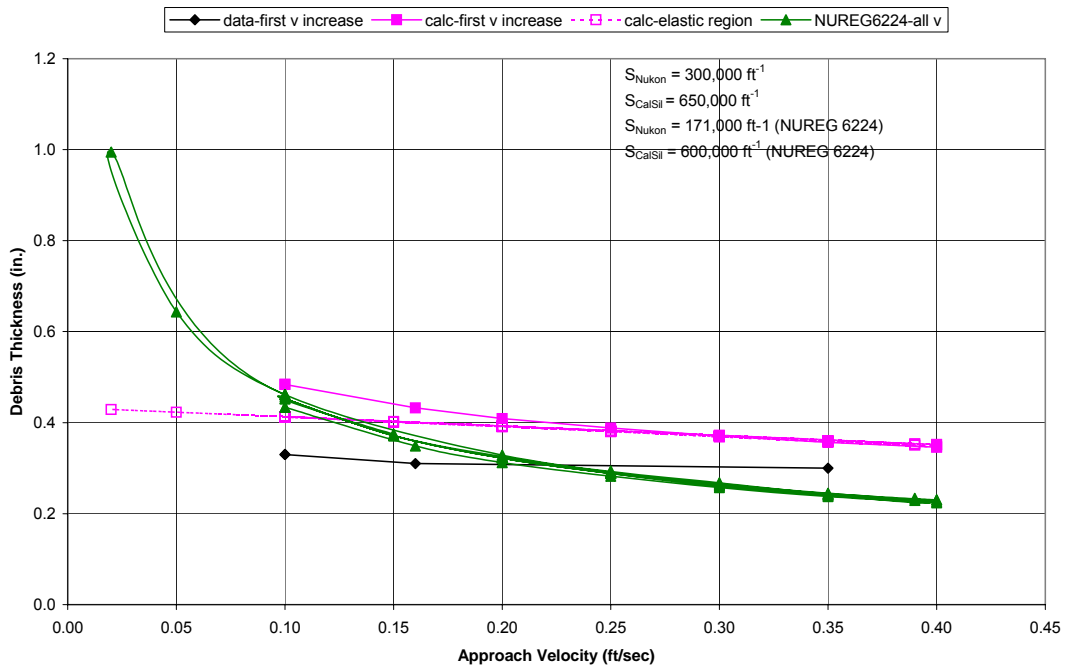


Figure 6.2-14 Bed Thickness for PNNL Series 1 Nukon/CalSil Test 051117_NC_2776_L1

Test 051128_NC_2776_L2(Nukon/CalSil=0.93/0.34 kg/m², 21-27C) - Two Volume Model

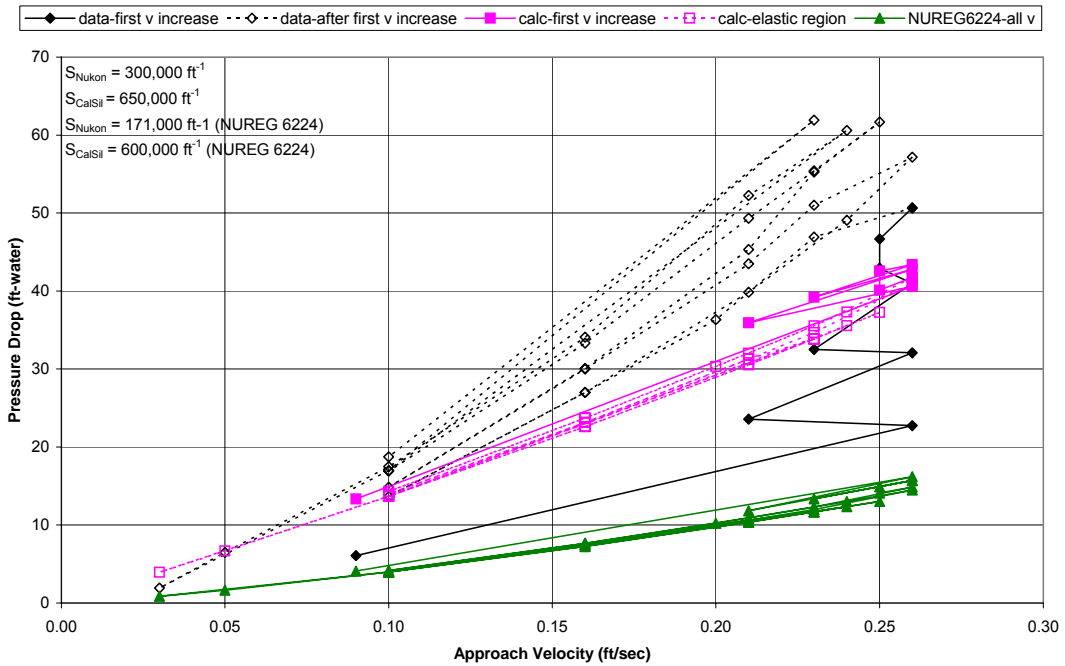


Figure 6.2-15 Head Loss for PNNL Series 1 Nukon/CalSil Test 051128_NC_2776_L2

Test 051128_NC_2776_L2(Nukon/CalSil=0.93/0.34 kg/m², 21-27C) - Two Volume Model

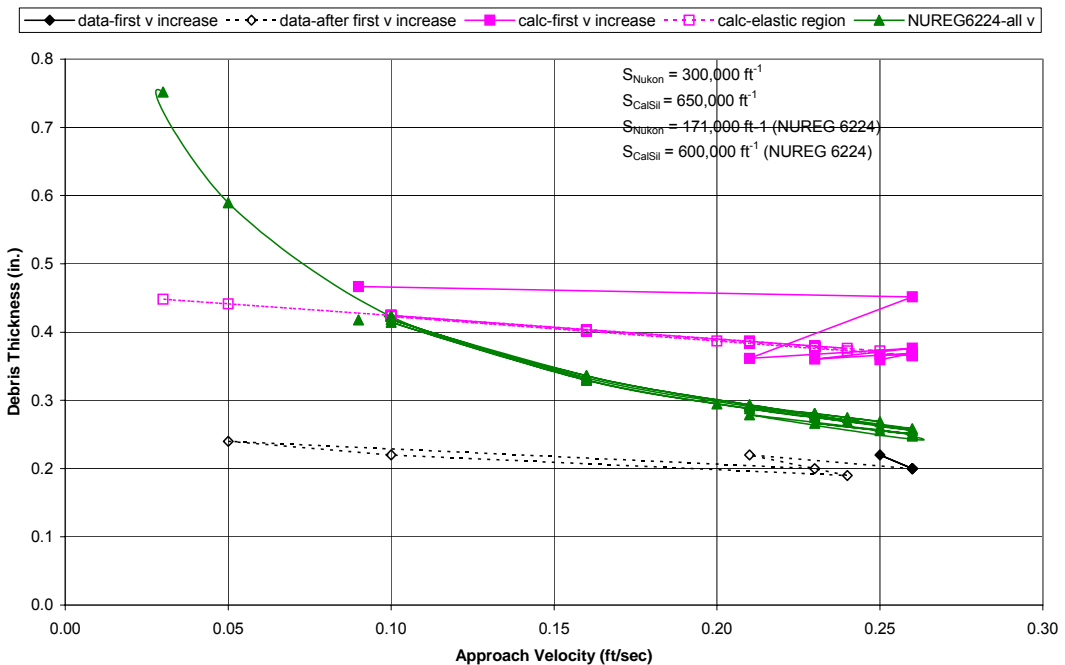


Figure 6.2-16 Bed Thickness for PNNL Series 1 Nukon/CalSil Test 051128_NC_2776_L2

Test 051121_NC_1586_L1(Nukon/CalSil=0.56/0.17 kg/m², 16-27 °C) - Two Volume Model

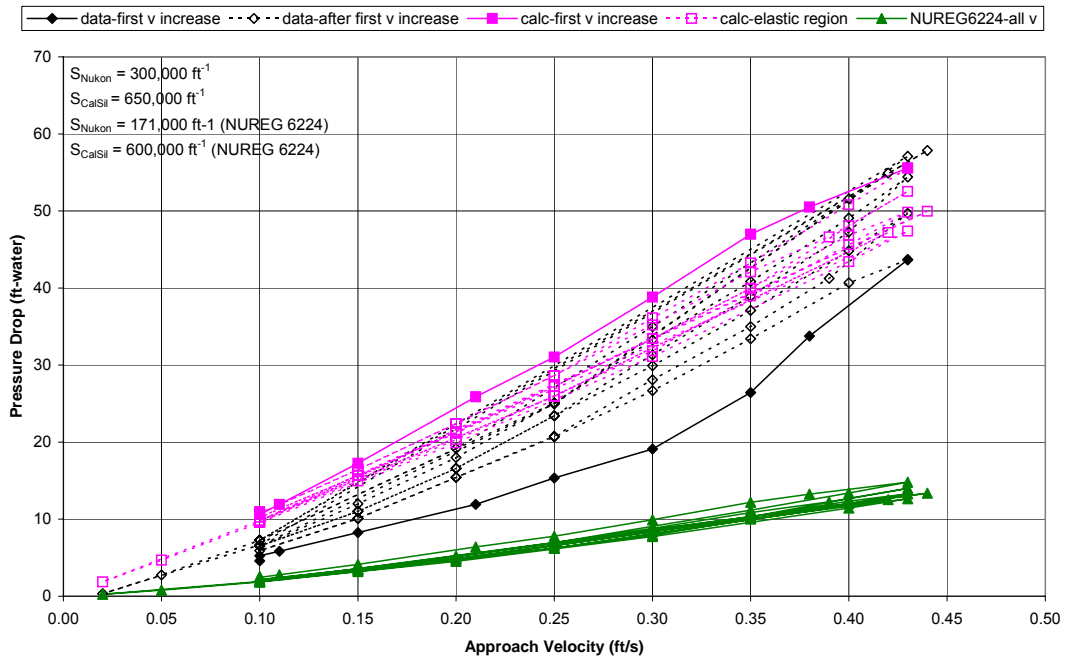


Figure 6.2-17 Head Loss for PNNL Series 1 Nukon/CalSil Test 051121_NC_1586_L1

Test 051121_NC_1586_L1(Nukon/CalSil=0.56/0.17 kg/m², 16-27 °C) - Two Volume Model

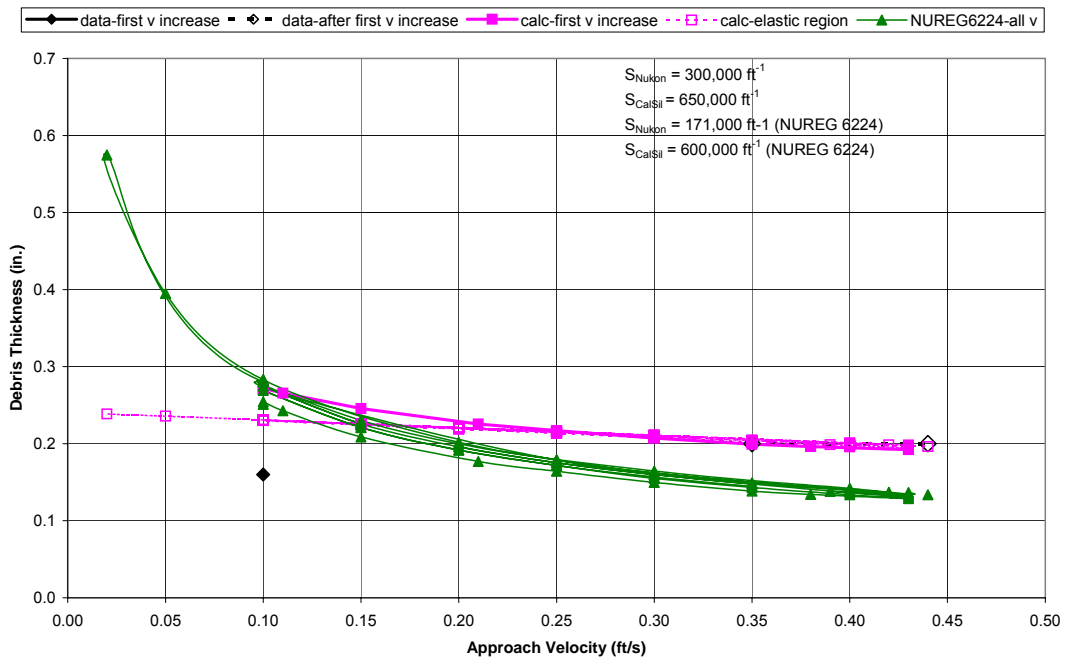


Figure 6.2-18 Bed Thickness for PNNL Series 1 Nukon/CalSil Test 051121_NC_1586_L1

Test 051123_NC_2181_L1(Nukon/CalSil=0.79/0.25 kg/m², 22-32 °C) - Two Volume Model

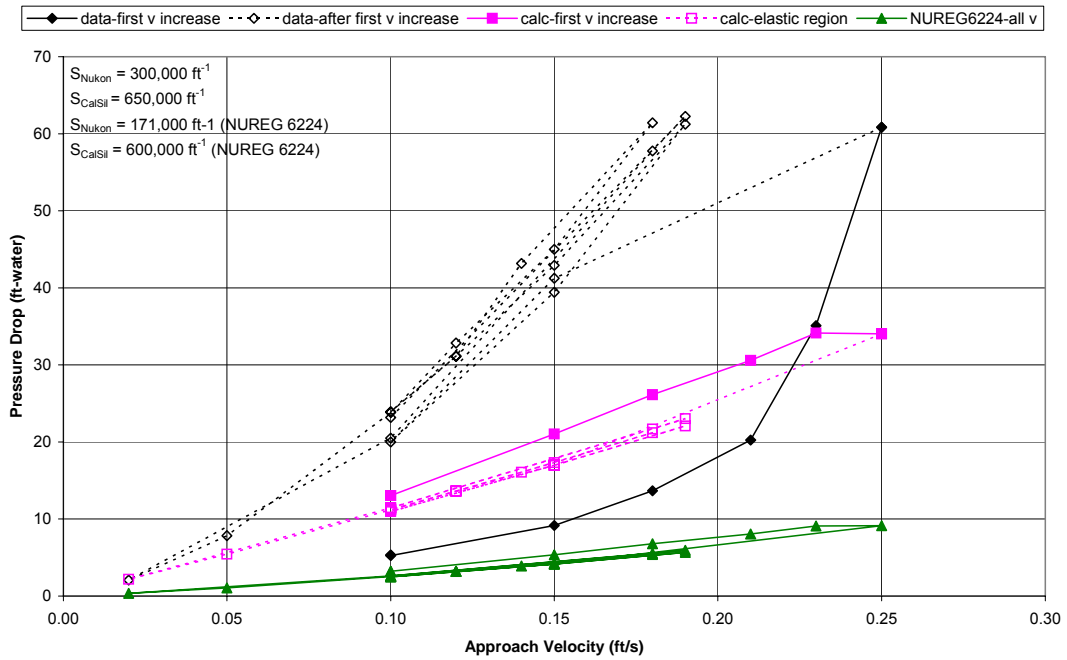


Figure 6.2-19 Head Loss for PNNL Series 1 Nukon/CalSil Test 051123_NC_2181_L1

Test 051123_NC_2181_L1(Nukon/CalSil=0.79/0.25 kg/m², 22-32 °C) - Two Volume Model

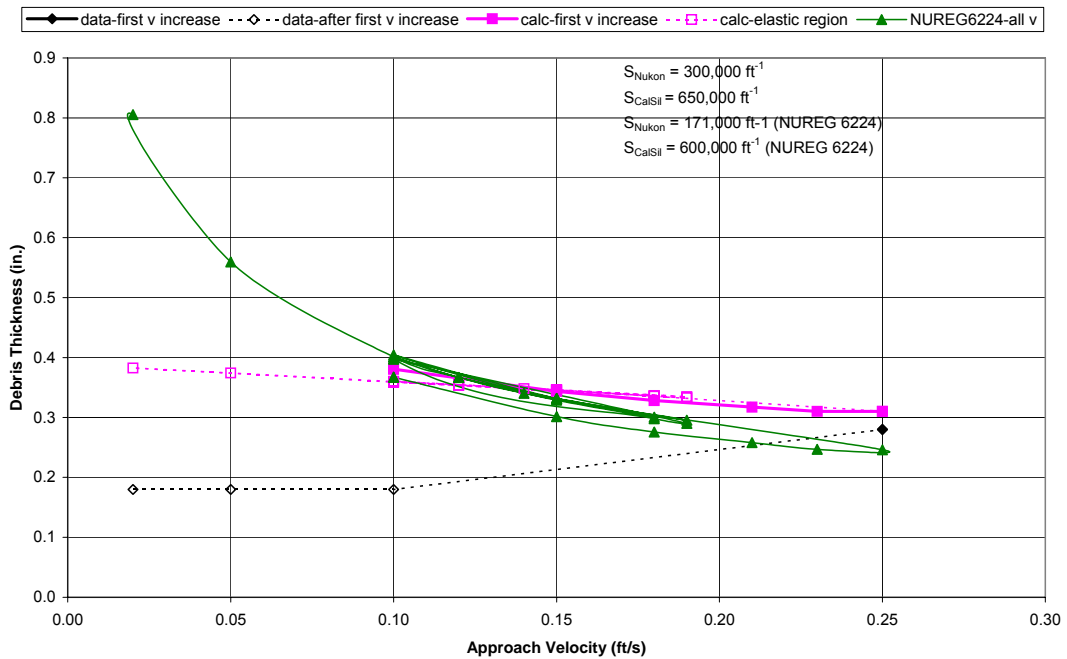


Figure 6.2-20 Bed Thickness for PNNL Series 1 Nukon/CalSil Test 051123_NC_2181_L1

6.2.2 Comparison of Head Loss Predictions to PNNL Series 2 Tests

As previously stated, the Series 2 tests were run using different Nukon and CalSil masses collected on a perforated plate. The head loss measurements are expected to be very close to those obtained using the woven metal sheet because, as indicated in Section 2.5.2, the open flow areas are almost identical. Table 6.2-2 lists the tests that were performed using a perforated plate as part of the PNNL Series 2 tests. This table provides the Nukon and CalSil debris bed loadings using the debris bed masses determined to exist in the debris bed and listed in Table 4.1-2. This section will compare head loss predictions to measurements for the tests that successfully created complete continuous debris beds. The data for all the debris bed thicknesses for the Series 2 tests were measured using the optical triangulation technique.

This section also compares calculational predictions with test results from the PNNL benchmark tests that were performed as part of the Series 2 tests. As indicated in Table 6.2-2, PNNL performed Tests BM-1 (060321_NO_0405_LP1) and BM-2 (060313_NO_1349_LP1) with Nukon-only debris beds. Test BM-3 (060323_NC_1619_LP1) used a Nukon/CalSil debris bed. Table 4.1-1 shows comparisons of the mass added to the test loop and the actual mass present on the perforated test plate.

6.2.2.1 PNNL Series 2 Tests of a Clean Unclogged Perforated Plate

As indicated in Table 6.2-2, the pressure drop across a clean unclogged perforated plate was determined for test conditions at three water temperatures—approximately 28 °C, 55 °C, and 83 °C (82.4 °F, 131 °F, and 181.4 °F). The irreversible loss coefficient across the unobstructed metal screen is calculated using test data in equation (6.2-2).

$$K_{\text{plate}} = 2 \Delta p_{\text{plate}} / (\rho_{\text{water}} V^2) \quad (6.2-2)$$

where

K_{plate}	irreversible loss coefficient for clean unclogged perforated plate
Δp_{plate}	pressure drop (head loss) across a clean unclogged perforated plate
ρ_{water}	water density
V	approach velocity upstream of screen

Figures 6.2-21 and 6.2-22 compare this loss coefficient with the values calculated using the correlation obtained from Idelchik (Ref. 22) using Diagram 8-5 for a perforated plate with the flow holes in a laminar or transitional region ($Re_{\text{plate}} < 10^4$ – 10^5). Figure 6.2-23 shows the measured pressure drop used for calculating the irreversible loss coefficient. This figure also provides the uncertainty bands for the pressure drop measurements. The loss coefficients calculated from test data and obtained using the Idelchik correlation are close in value for all three water temperature ranges except at low velocities. The Idelchik correlation for a perforated plate as described in Section 2.5 is indicated to be applicable to the range of tested Reynolds numbers for the plate flow area. The discrepancies at lower velocities probably result from inaccuracies in measurements of very low pressure drops.

Table 6.2-2 PNNL Series 2 Including Benchmark Head Loss Tests Using a Perforated Plate

PNNL Series 2 Tests [#]	Nukon			CalSil			Bed CalSil / Nukon	Bed Debris kg/m ²	Loop Temperature °C	Comments
	Added kg/m ²	Bed kg/m ²	Bed / Added	Added kg/m ²	Bed kg/m ²	Bed / Added				
060804_PO_0000_L1, L2	0.0	0.0	NA	0.0	0.0	NA	NA	0.0	26-30, 53-57	
060805_PO_0000_L1	0.0	0.0	NA	0.0	0.0	NA	NA	0.0	79-84	
060512_CO_8108_LP1, LP2, LP3	0.0	0.0	NA	4.352	0.434	0.100	NA	0.434	20-22, 54-57, 80-83	Incomplete bed with holes
BM-1, 060321_NO_0405_LP1*	0.217	0.171	0.785	0.0	0.0	NA	NA	0.171	21-22	
BM-2, 060313_NO_1349_LP1	0.724	0.576	0.796	0.0	0.0	NA	NA	0.576	19-22	
060425_NO_2703_LP1, LP2, LP3	1.451	1.245	0.858	0.0	0.0	NA	NA	1.245	22-25, 52-54, 81-84	
060731_NO_2703_LP1, LP2	1.451	1.251	0.862	0.0	0.0	NA	NA	1.251	53-55, 27-28	
060802_NO_2703_LP1, LP2	1.451	1.191	0.821	0.0	0.0	NA	NA	1.191	79-83, 54-57	
BM-3, 060323_NC_1619_LP1	0.724	0.626	0.865	0.145	0.020	0.140	0.032	0.646	21-22	
060331_NC_2024_LP1	0.724	0.600	0.829	0.362	0.132	0.365	0.220	0.732	21-24	
060817_NC_2024_LP1, LP2	0.724	0.691	0.955	0.362	0.120	0.330	0.173	0.811	53-56, 29-30	
060404_NC_2698_LP1 [§]	0.724	0.644	0.890	0.724	0.252	0.348	0.392	0.863	19-24	Bed clogged
060509_NC_0505_LP1	0.217	0.184	0.848	0.054	0.025	0.458	0.135	0.209	20-22	
060426_NC_0708_LP1, LP2	0.217	0.208	0.961	0.163	0.005	0.029	0.023	0.213	21-24, 81-84	
060807_NC_0708_LP1, LP2	0.217	0.243	1.118	0.163	0.018	0.113	0.076	0.261	54-56, 37	
060809_NC_0708_LP1, LP2	0.217	0.155	0.715	0.163	0.005	0.030	0.031	0.160	79-83, 53-54	
060517_NC_0808_LP1, LP2 ^{&}	0.217	0.223	1.030	0.217	0.082	0.376	0.365	0.305	25, 82-84	Holes developed at 0.2 ft/s
060427_NC_0252_LP1	0.108	NA	NA	0.027	NA	NA	NA	0.056	21-22	Incomplete bed with holes
060428_NC_0453_LP1	0.108	NA	NA	0.135	NA	NA	NA	0.094	21-22	Incomplete bed with holes

BM indicates a Benchmark Test

[#] Pipe and Screen Area = 0.01863 m²

* Debris bed ruptured during retrieval; negligible debris material lost.

[&] Debris bed ruptured during retrieval; less than 5% debris material volume lost.

[§] Debris bed disturbed post-retrieval; an unquantifiable mass may have been lost.

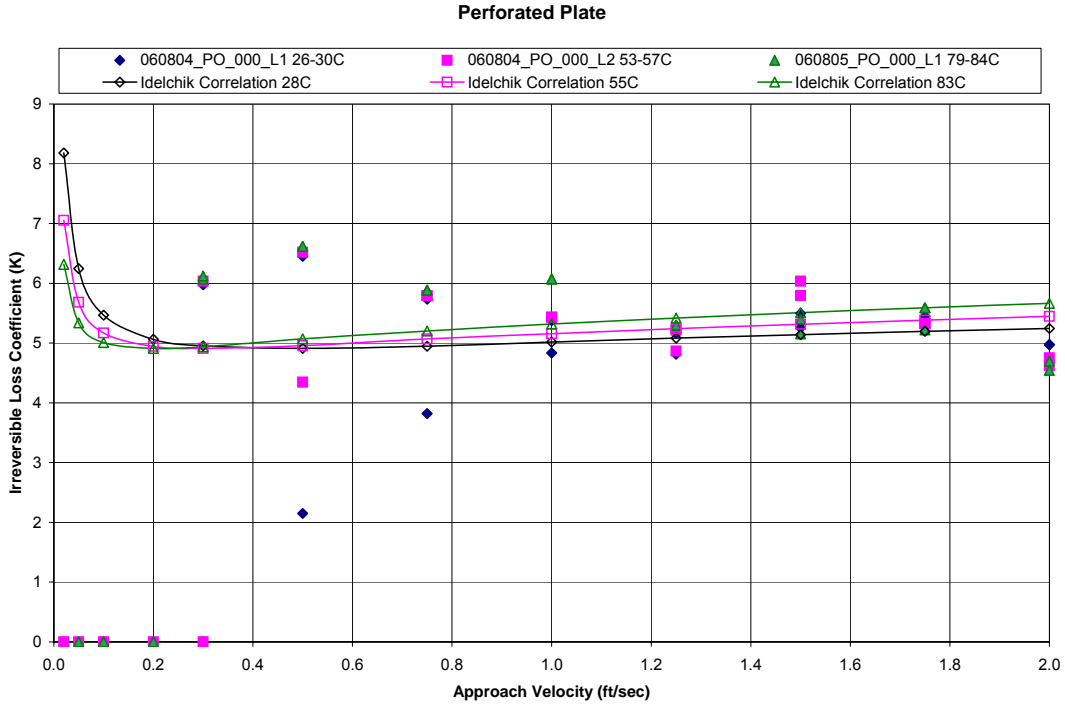


Figure 6.2-21 Measured and Correlation Loss Coefficients Versus Approach Velocity

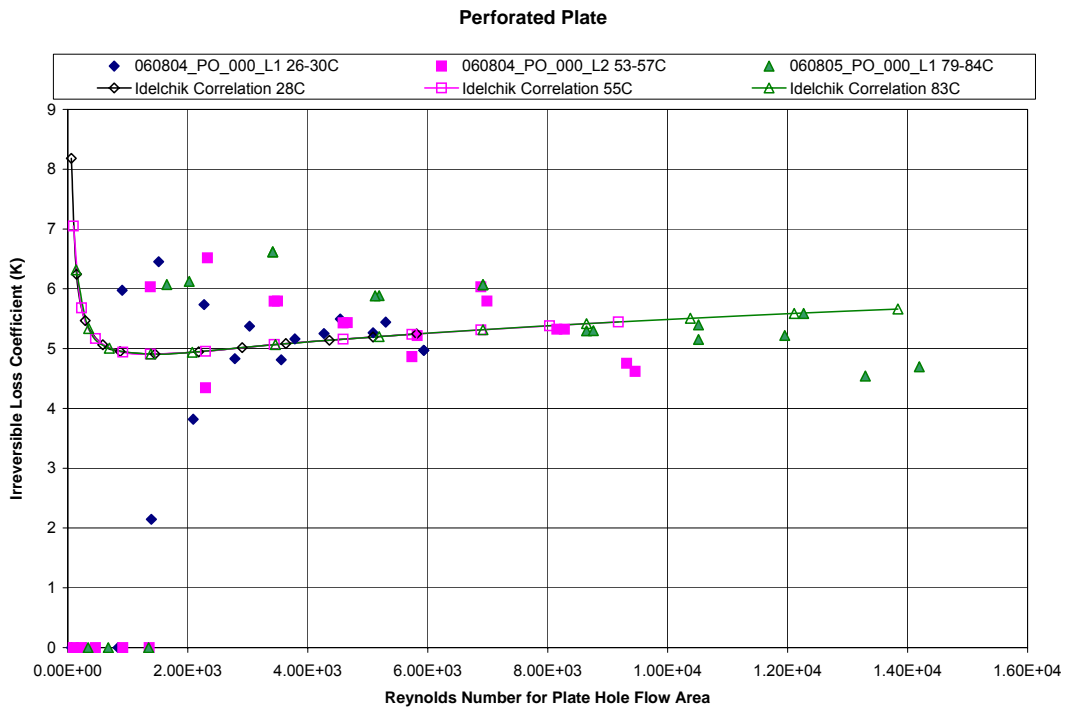


Figure 6.2-22 Measured and Correlation Loss Coefficients Versus Reynolds Number

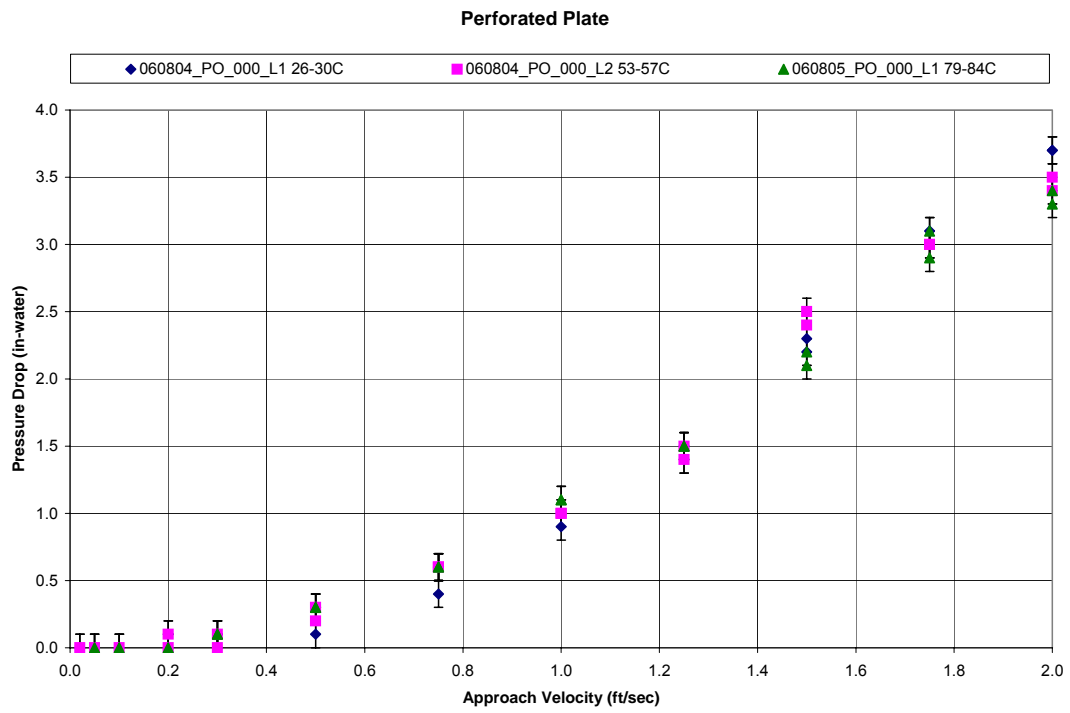


Figure 6.2-23 Measured Pressure Drop Used for Irreversible Loss Coefficient Calculation

6.2.2.2 Predictions of PNNL Series 2 Nukon-Only Tests Using a One-Volume Model

Figures 6.2-24 to 6.2-41 compare test data from the PNNL Series 2 Nukon-only debris bed tests with predictions using the one-volume calculational method and the calculational method described in NUREG/CR-6224. Tables 6.2-2 and 4.1-2 list the debris bed loadings for the plotted cases. The following list notes specific assumptions used for the predictive analyses:

- Section 4.1 provides the basis for the debris bed loadings used in the calculations.
- The predictions obtained using the one-volume calculational method apply the debris material-specific surface areas and densities listed in Table 5.2-1; the predictions obtained using the NUREG/CR-6224 method apply the material properties specified in NUREG/CR-6874 and listed in Table 4.3-1.
- The initial debris bed thickness used for the one-volume method is calculated according to the approach discussed in Section 4.2. The NUREG/CR-6224 calculations use the NUREG/CR-6224 calculational method to determine initial bed thickness.
- A material-specific compression parameter of 0.236, as described in Section 4.5, is used for the one-volume calculations. The NUREG/CR-6224 calculations use the NUREG/CR-6224 method to determine bed compression.
- The NUREG/CR-6224 calculations use an as-fabricated packing density of 2.4 lbm/ft³ (38.44 kg/m³) for the Nukon fiber beds as recommended in NUREG/CR-6874 (Ref. 3). The one-volume calculation does not employ this parameter in its solution.
- The loop temperature is recorded at each data point during the PNNL tests, and the one-volume and NUREG/CR-6224 calculations employ the recorded temperature at each data point. Consequently, the plotted predictions reflect the changes in loop temperature.

Generally, the one-volume calculational approach provides better predictions of test conditions for the Series 2 Nukon-only tests than does the NUREG/CR-6224 calculational method. The pressure drop predictions obtained using the one-volume method are either close to or exceed test data measurements, and all the debris bed thickness predictions are close to test data obtained using the optical triangulation technique. All the NUREG/CR-6224 pressure drop calculations for these Nukon-only tests underpredict test measurements, and all the predictions for the NUREG/CR-6224 bed thickness exceed measurements. All of the NUREG/CR-6224 bed thickness predictions exhibit the unrealistic uncompacted limit illustrated by the constant bed thicknesses predicted at lower approach velocities.

Two Nukon-only benchmark tests were performed as part of the Series 2 testing. The Nukon debris was prepared by using a slightly different procedure than those used for the Series 1 and other Series 2 tests. The preparation difference may cause variances in test trends between the benchmark test data and data from the other tests because changes in debris preparation can affect debris distribution in the debris bed. However, test data do not indicate substantial differences in data trends between the two benchmark tests and the other Series 2 Nukon-only tests.

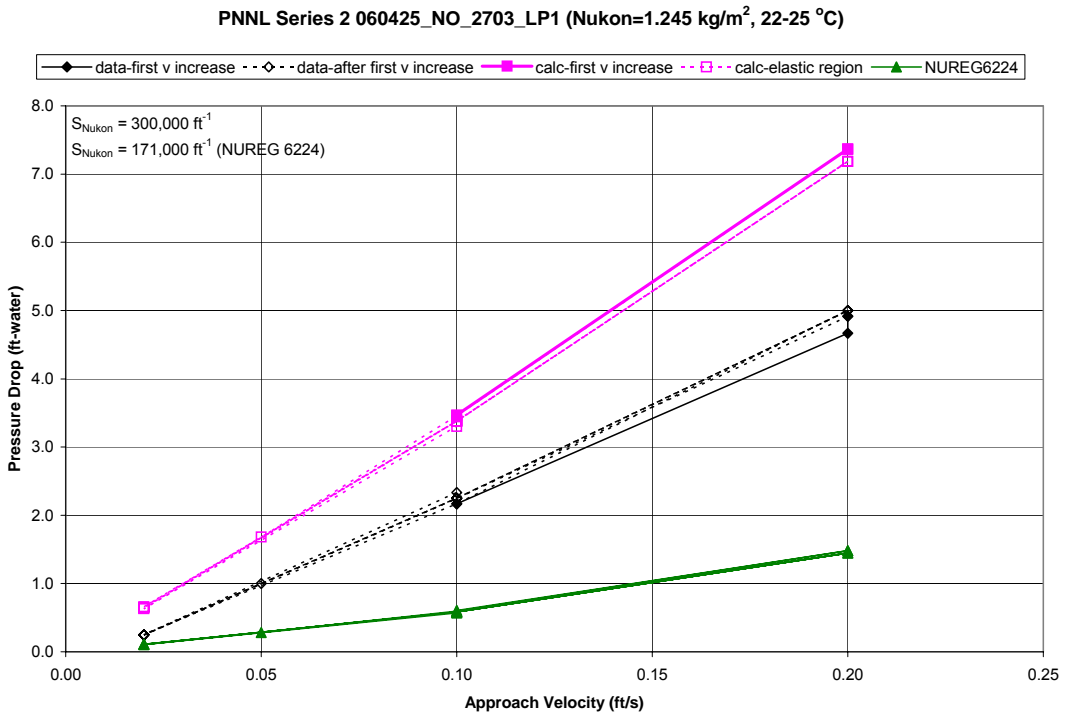


Figure 6.2-24 Head Loss for PNNL Series 2 Nukon-Only Test 060425_NO_2703_LP1

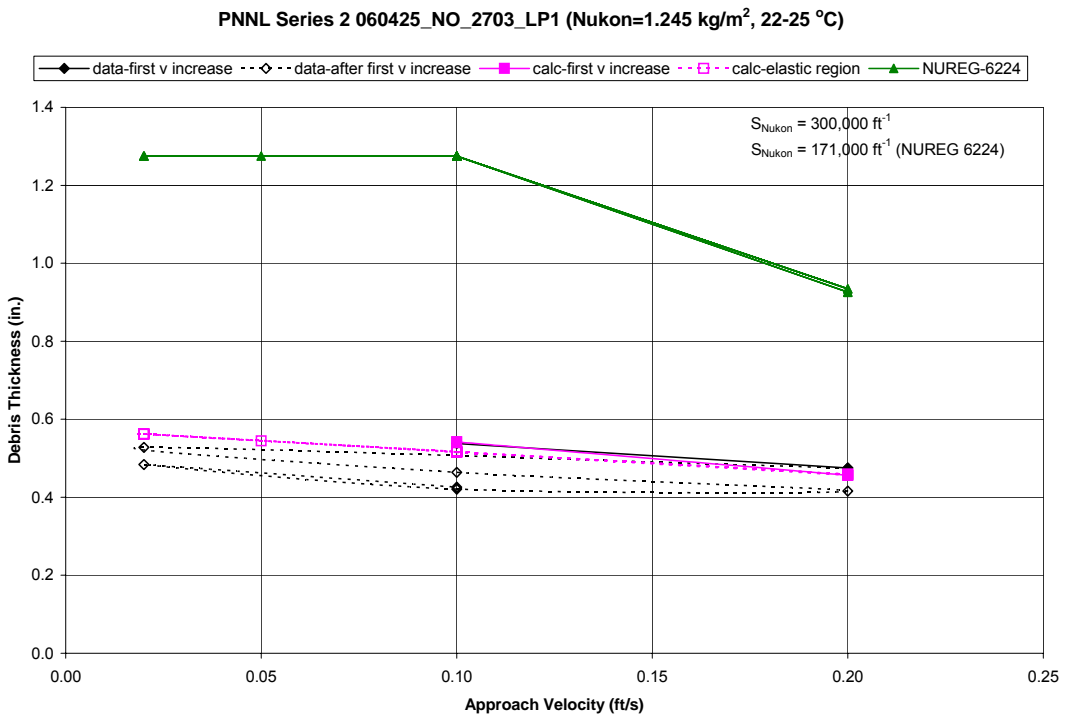


Figure 6.2-25 Bed Thickness for PNNL Series 2 Nukon-Only Test 060425_NO_2703_LP1

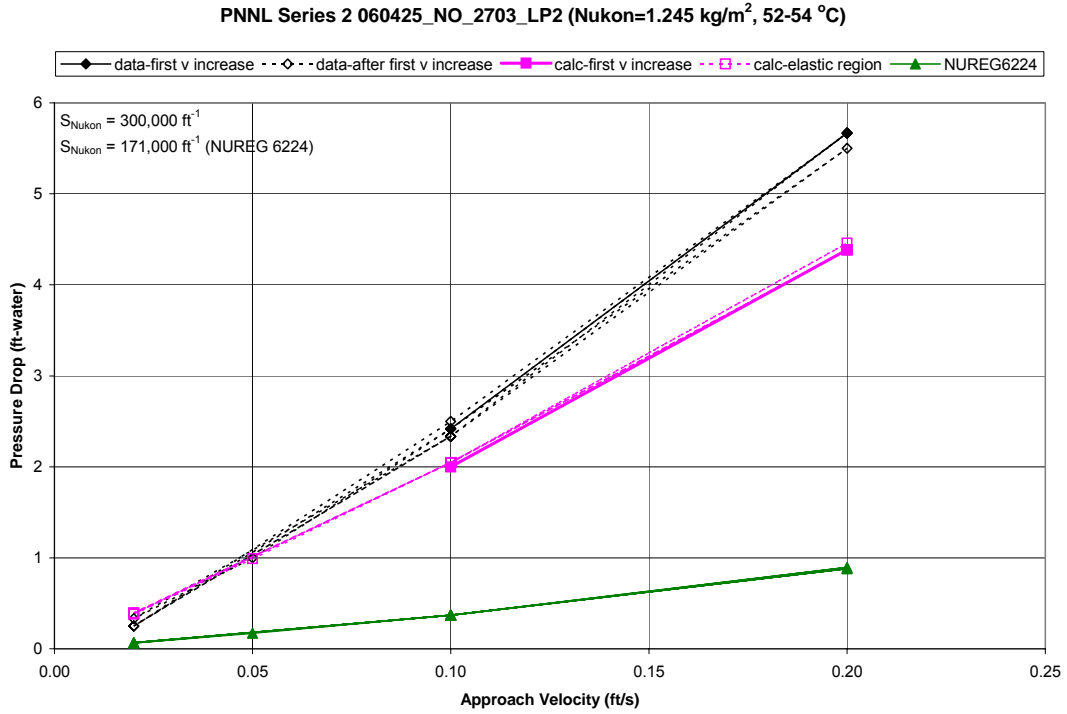


Figure 6.2-26 Head Loss for PNNL Series 2 Nukon-Only Test 060425_NO_2703_LP2

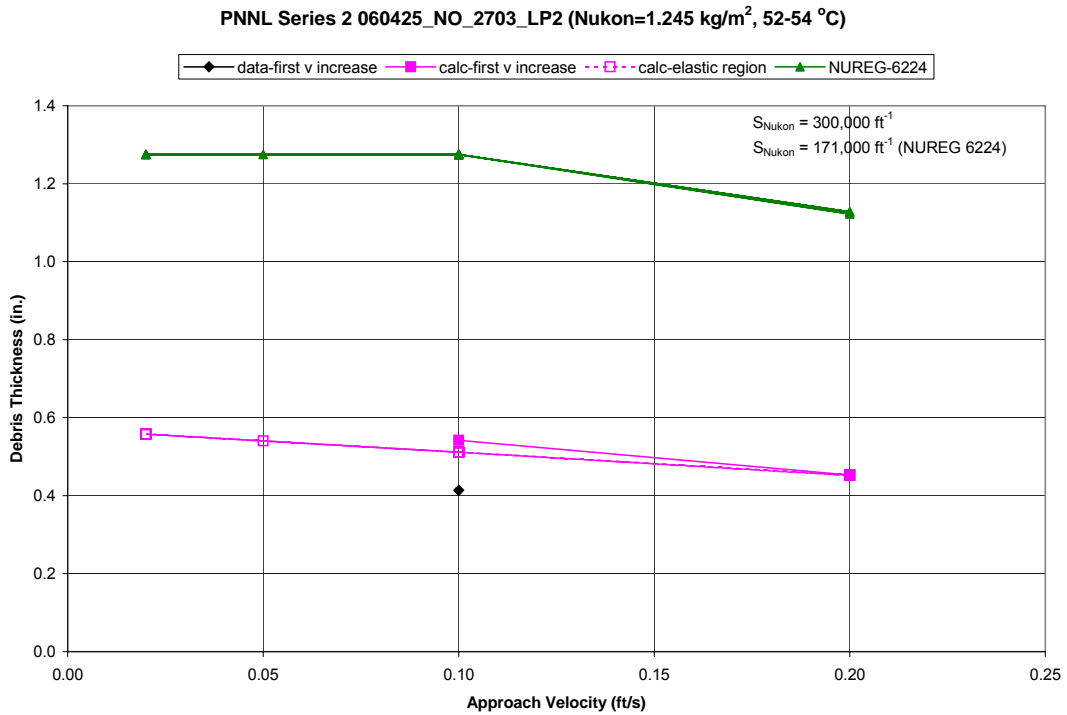


Figure 6.2-27 Bed Thickness for PNNL Series 2 Nukon-Only Test 060425_NO_2703_LP2

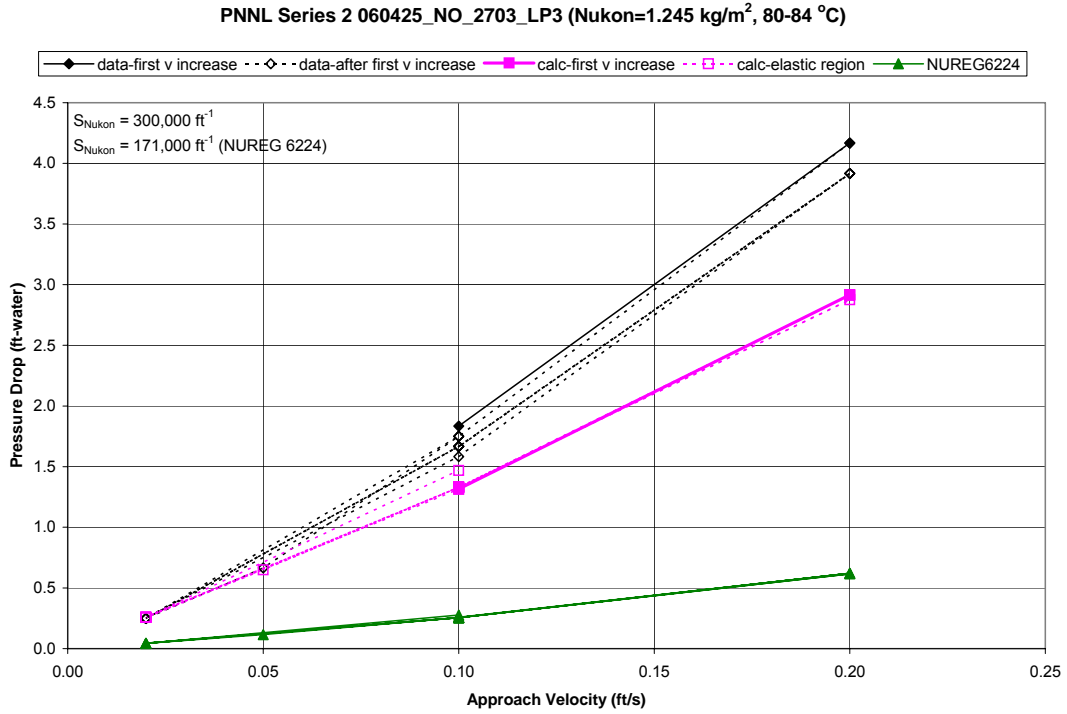


Figure 6.2-28 Head Loss for PNNL Series 2 Nukon-Only Test 060425_NO_2703_LP3

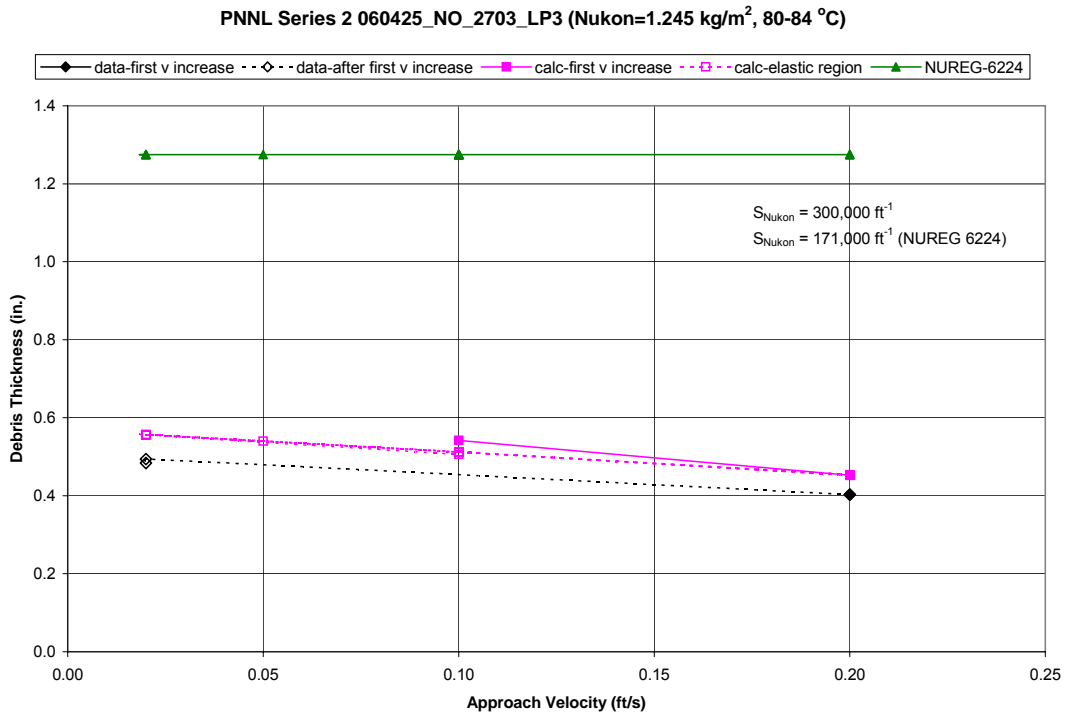


Figure 6.2-29 Bed Thickness for PNNL Series 2 Nukon-Only Test 060425_NO_2703_LP3

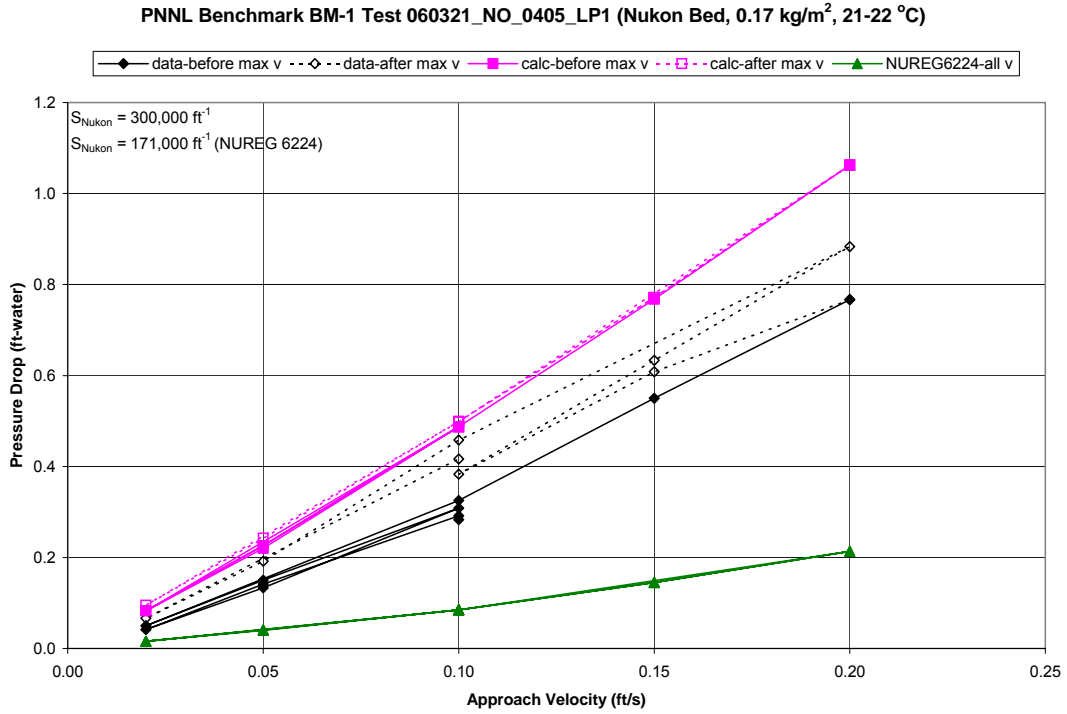


Figure 6.2-30 Head Loss for PNNL Series 2 Benchmark Nukon-Only Test 060321_NO_0405_LP1

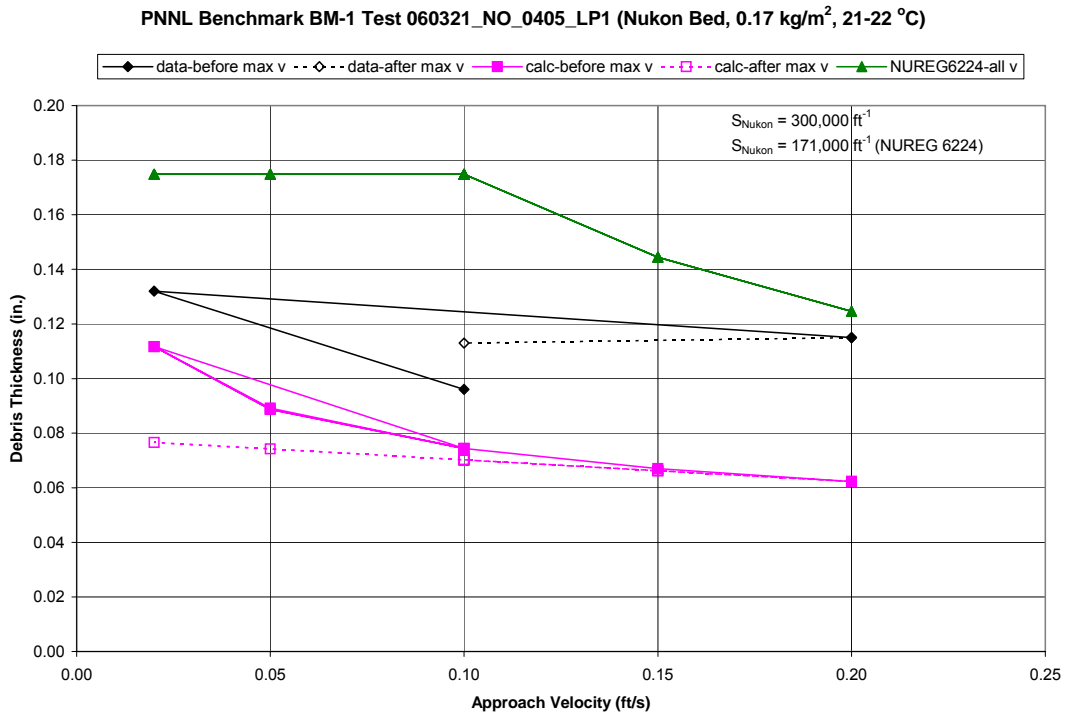


Figure 6.2-31 Bed Thickness for Series 2 Benchmark Nukon-Only Test 060321_NO_0405_LP1

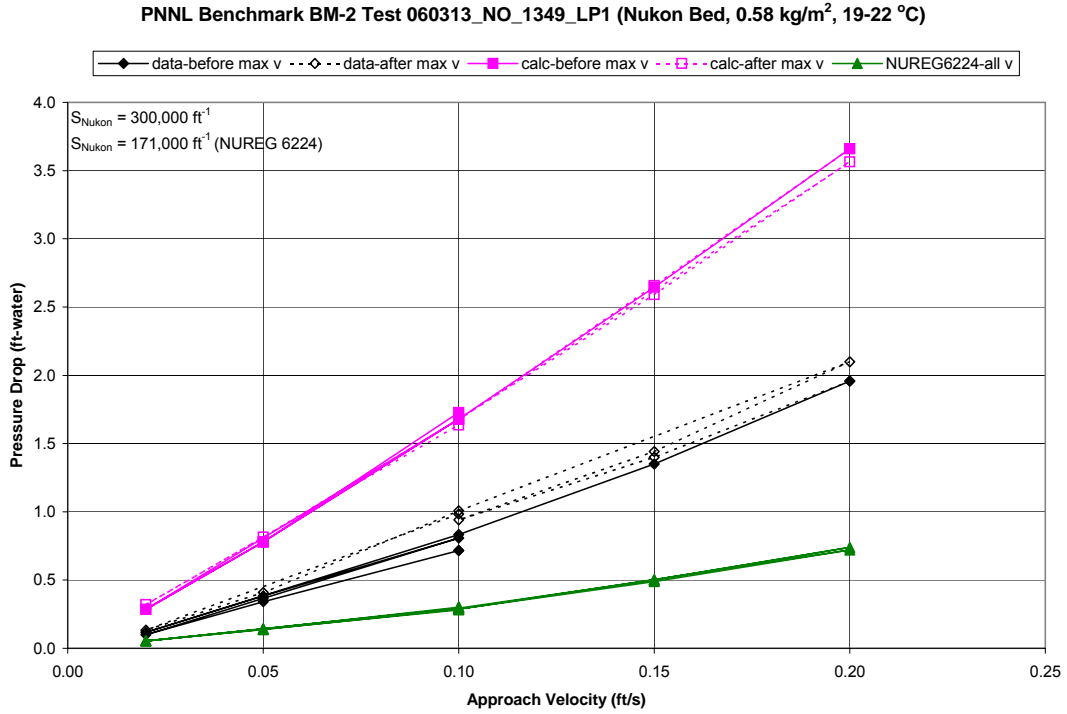


Figure 6.2-32 Head Loss for PNNL Series 2 Benchmark Nukon-Only Test 060313_NO_1349_LP1

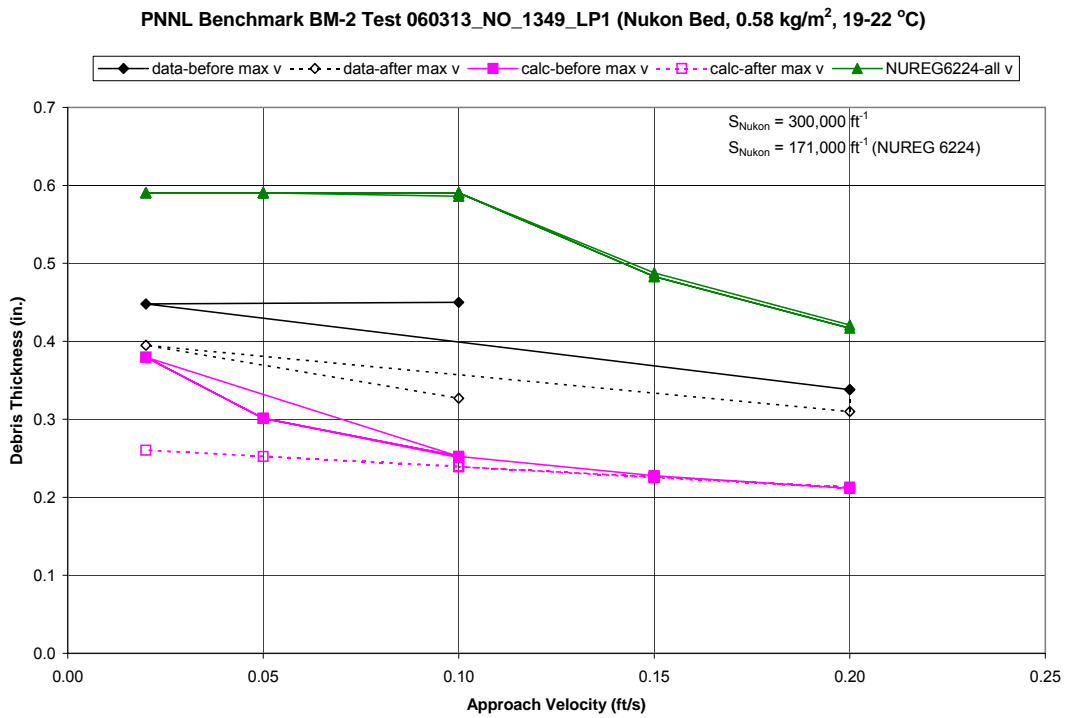


Figure 6.2-33 Bed Thickness for Series 2 Benchmark Nukon-Only Test 060313_NO_1349_LP1

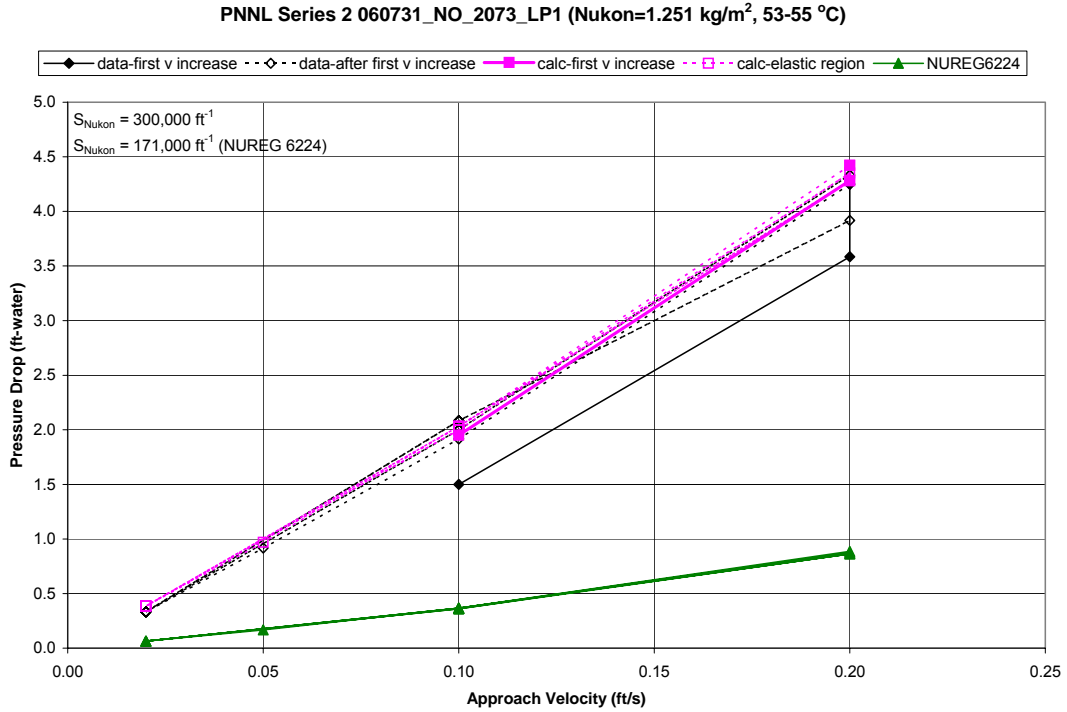


Figure 6.2-34 Head Loss for PNNL Series 2 Nukon-Only Test 060731_NO_2073_LP1

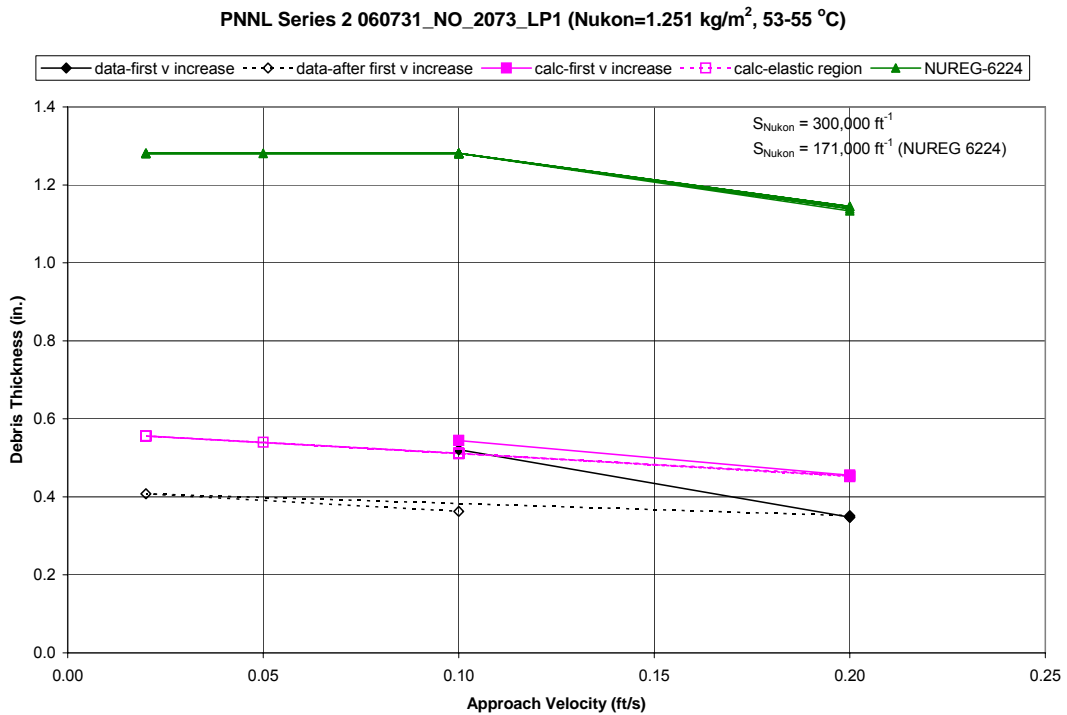


Figure 6.2-35 Bed Thickness for PNNL Series 2 Nukon-Only Test 060731_NO_2073_LP1

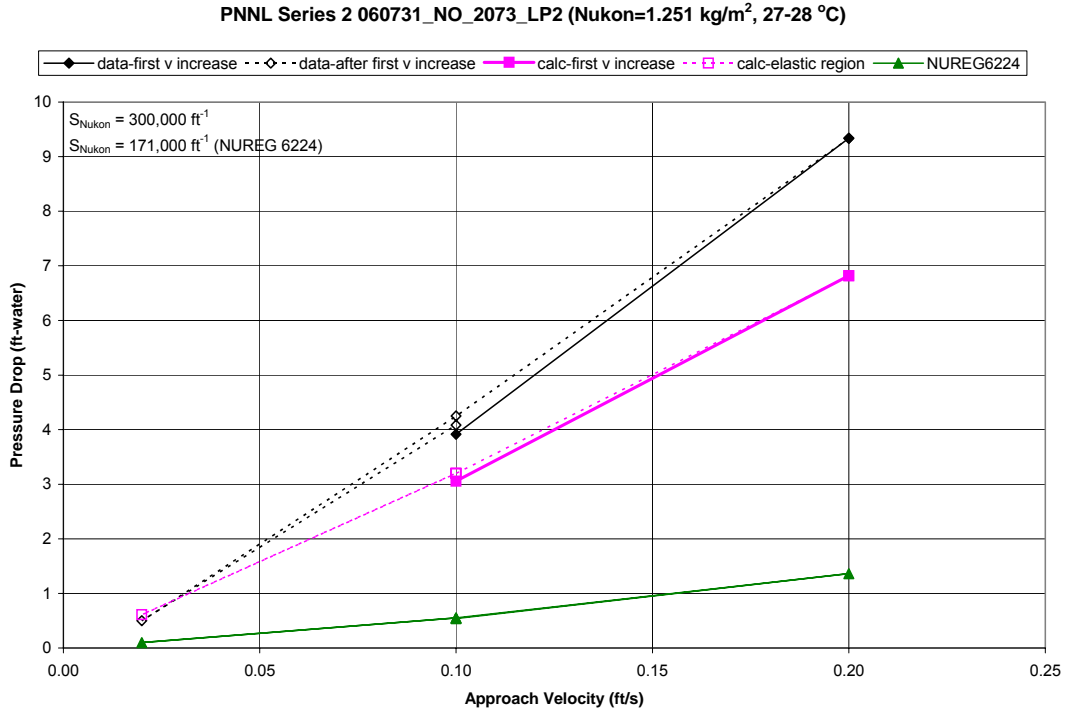


Figure 6.2-36 Head Loss for PNNL Series 2 Nukon-Only Test 060731_NO_2073_LP2

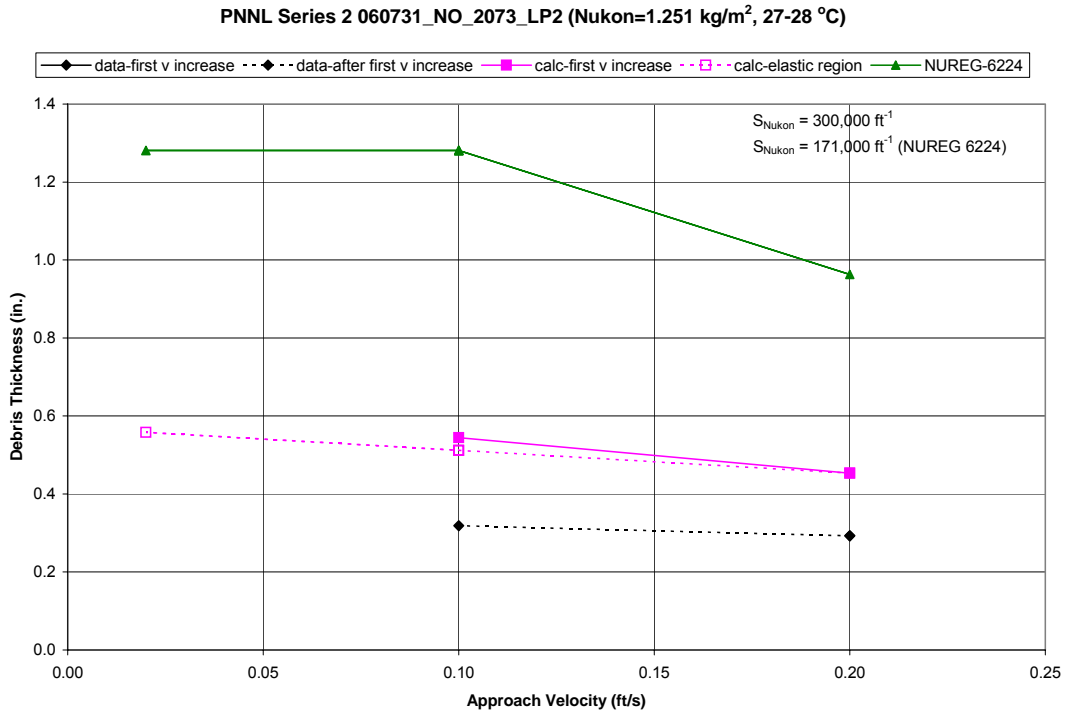


Figure 6.2-37 Bed Thickness for PNNL Series 2 Nukon-Only Test 060731_NO_2073_LP2

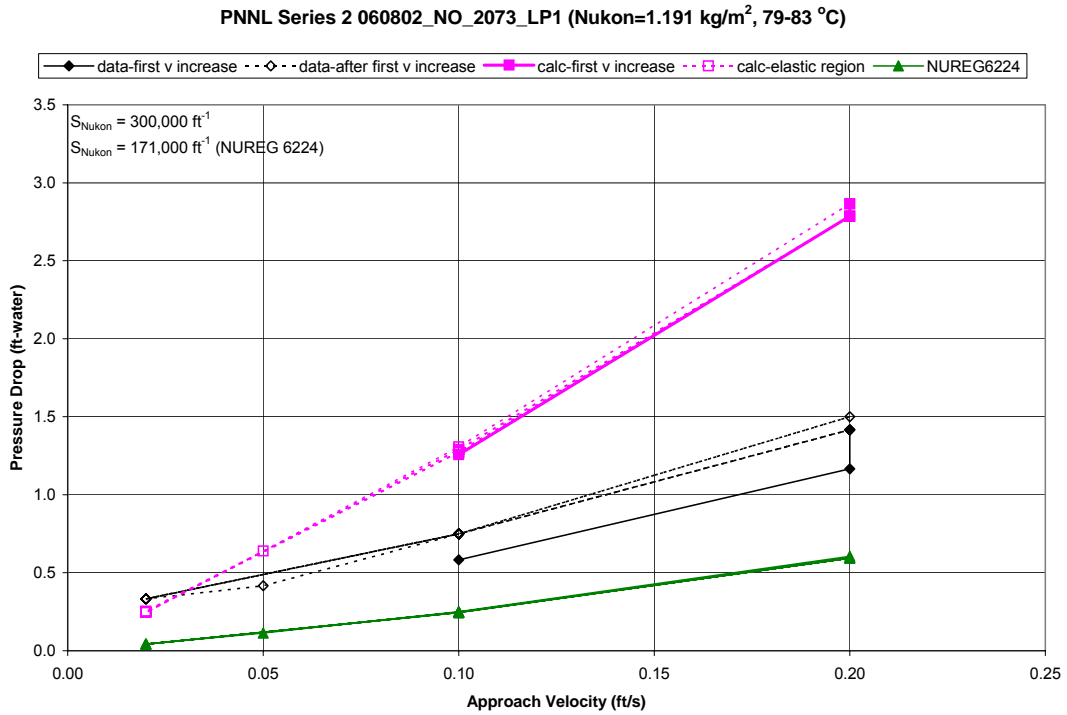


Figure 6.2-38 Head Loss for PNNL Series 2 Nukon-Only Test 060802_NO_2073_LP1

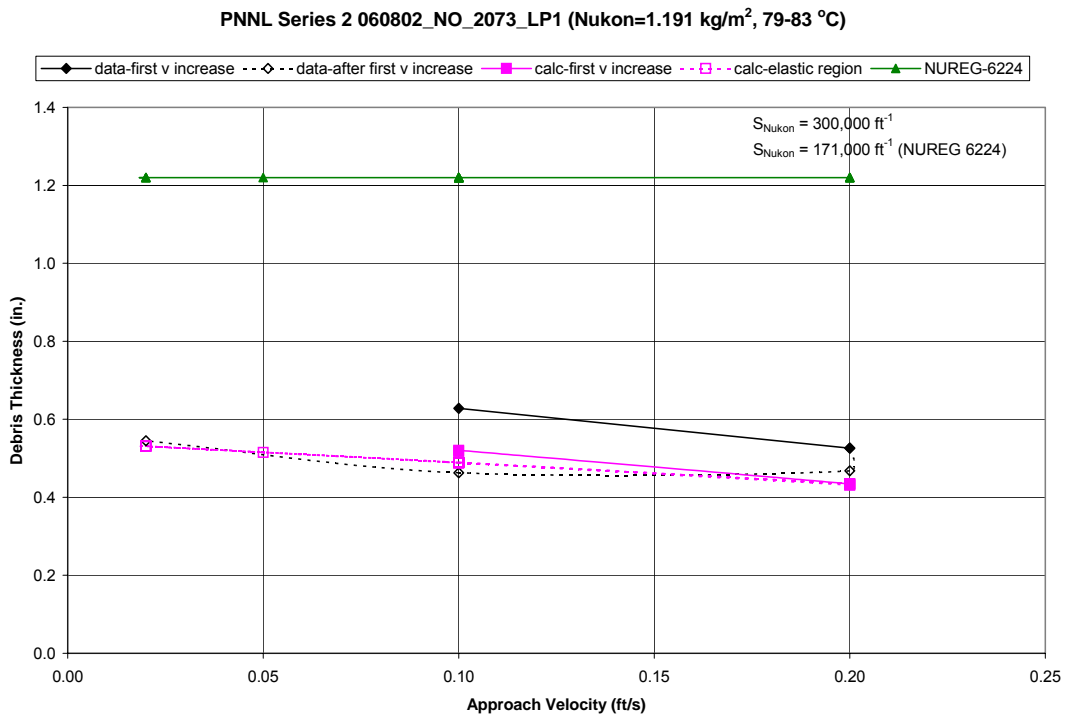


Figure 6.2-39 Bed Thickness for PNNL Series 2 Nukon-Only Test 060802_NO_2073_LP1

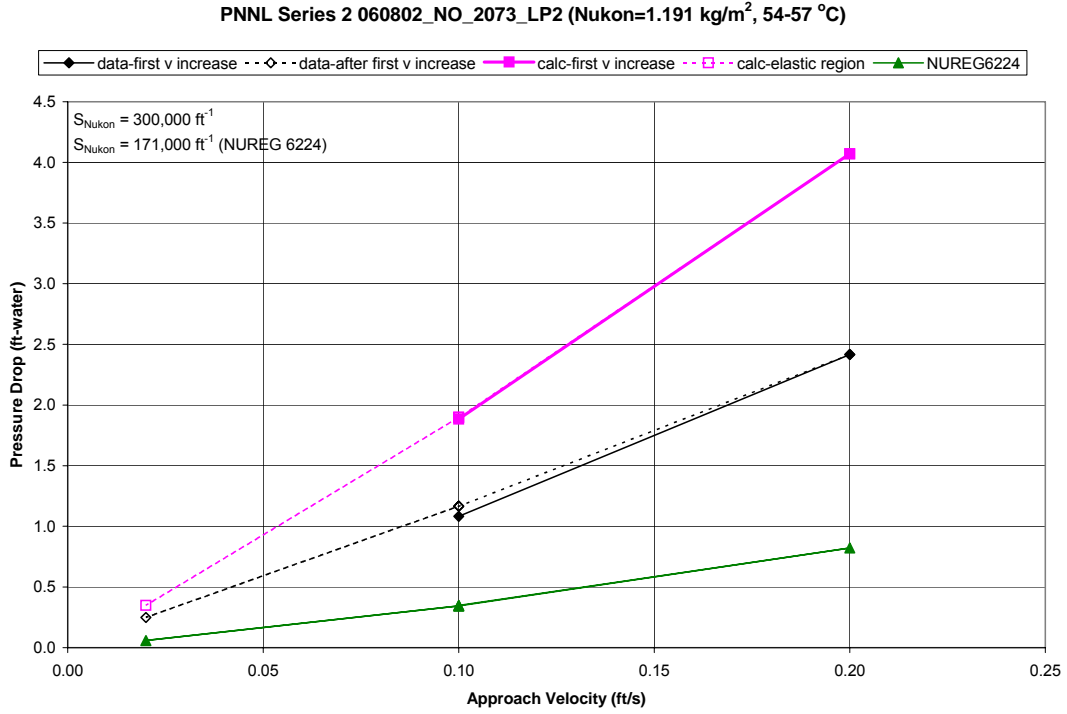


Figure 6.2-40 Head Loss for PNNL Series 2 Nukon-Only Test 060802_NO_2073_LP2

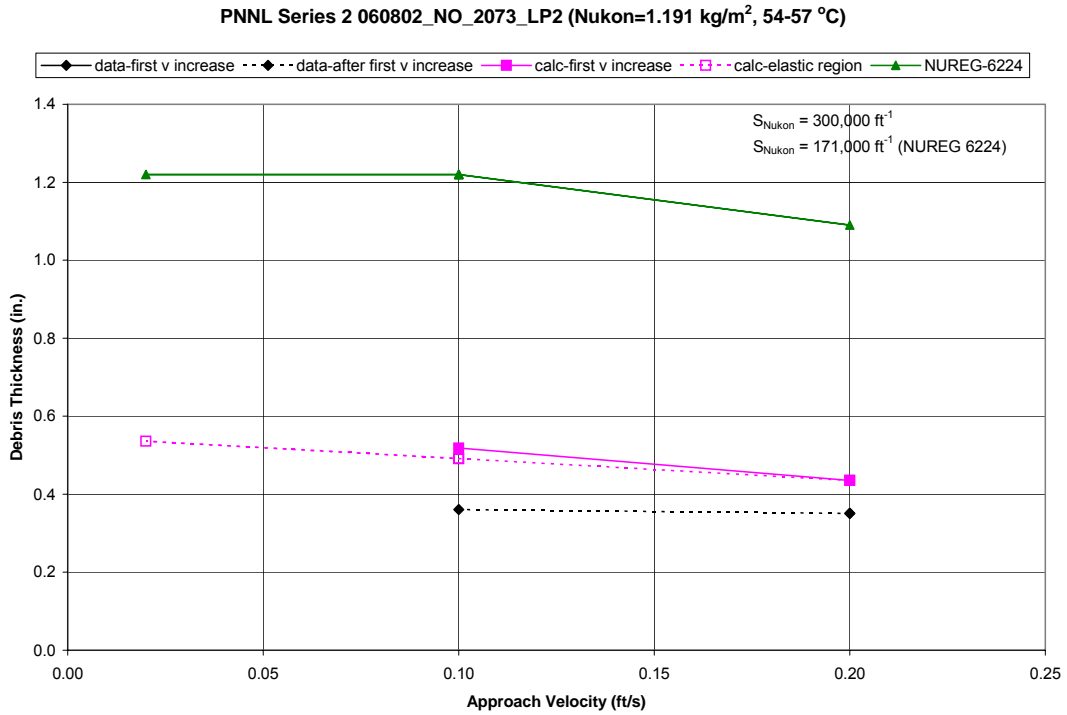


Figure 6.2-41 Bed Thickness for PNNL Series 2 Nukon-Only Test 060802_NO_2073_LP2

6.2.2.3 Predictions of PNNL Series 2 Nukon/CalSil Tests Using a Two-Volume Model

This section compares the predictions for the two-volume model with test data from the PNNL Series 2 tests with Nukon/CalSil debris beds. Figures 6.2-42 to 6.2-65 compare the measured pressure drop and bed thicknesses to predictions made using the two-volume approach and the NUREG/CR-6224 calculational method. Tables 6.2-1 and 4.1-2 list the debris bed loadings for the plotted cases. The Nukon and CalSil debris masses were premixed before addition to the test loop. The following list notes specific assumptions used for the predictive analyses:

- Section 4.1 provides the basis for the debris bed loadings used in the calculations.
- The predictions obtained using the two-volume calculational method apply the debris material-specific surface areas and densities listed in Table 5.2-1; the predictions obtained using the NUREG/CR-6224 method apply the material properties specified in NUREG/CR-6874 and listed in Table 4.3-1.
- The initial debris bed thicknesses used for the two-volume method are calculated according to the approach discussed in Section 4.2. The NUREG/CR-6224 calculations use the NUREG/CR-6224 method to determine initial bed thickness.
- A material-specific compression parameter of 0.236, as described in Section 4.5, is used for the two-volume calculations. The NUREG/CR-6224 calculations use the NUREG/CR-6224 calculational method to determine bed compression.
- The NUREG/CR-6224 calculations use an as-fabricated packing density of 2.4 lbm/ft³ (38.44 kg/m³) for the Nukon fiber beds as recommended in NUREG/CR-6874 (Ref. 3). The two-volume calculation does not employ this parameter in its solution.
- The NUREG/CR-6224 calculations use a particle sludge density of 22 lbm/ft³ (352.4 kg/m³) for the Nukon/CalSil debris beds as recommended in NUREG/CR-6874 (Ref. 3). The two-volume calculation does not employ this parameter in its solution.
- The loop temperature is recorded at each data point during the PNNL tests, and the two-volume and NUREG/CR-6224 calculations employ the recorded temperature at each data point. Consequently, the plotted predictions reflect the changes in loop temperature.

Generally, the two-volume approach provides a better, but not necessarily conservatively bounding, pressure drop prediction than do the predictions obtained by using the NUREG/CR-6224 method. The bed thickness predictions using the two-volume approach generally match the thickness measurements better than the thicknesses obtained using the NUREG/CR-6224 method. Some of the NUREG/CR-6224 bed thickness predictions exhibit the unrealistic uncompacted limit illustrated by the constant bed thicknesses predicted at lower approach velocities.

The pressure drop predictions obtained using the two-volume approach match or exceed test measurements in five of the eight tests. The two-volume approach underpredicts pressure drop measurements in three of the eight test cases. The underpredictions are related to the empirical equation developed to calculate the thickness of the concentrated CalSil particle layer within a Nukon fiber debris bed. Although this empirical equation provides adequate concentration thickness values for large CalSil thicknesses, at lower CalSil thicknesses, small differences in determining concentration thickness can

result in large changes in the calculated pressure drop. The NUREG/CR-6224 calculations underpredict debris bed pressure drop in all Series 2 test cases, and the NUREG/CR-6224 calculations overpredict the bed thickness in almost all test cases.

One of the Series 2 tests, Test 060323_NC_1619_LP1, was a benchmark test. Figures 6.2-42 and 6.2-43 show comparisons between predictions and test data. As previously indicated, test debris was prepared using a slightly different procedure than those used for the Series 1 and other Series 2 tests. The preparation differences may have caused variances in test trends between the benchmark test data and data from the other tests because changes in debris preparation can affect debris distribution in the bed. Test data do not indicate substantial differences in data trends between the benchmark test and the other Series 2 Nukon/CalSil tests. However, as indicated in Section 4.3, calculations seem to indicate that the benchmark test possessed a relatively homogeneous Nukon/CalSil debris bed, whereas the other Nukon/CalSil tests appeared to possess a concentrated CalSil section in the debris beds. Figure 6.2-44, which compares the predictions from the one- and two-volume calculational methods with test data, suggests the presence of a homogeneous bed. Pressure drop predictions using the one-volume approach are closer to, but larger in value, than the test data, and the two-volume pressure drop predictions exceed the one-volume predictions.

It is generally expected that the one-volume homogeneous pressure drop predictions for a Nukon/CalSil bed with a concentrated CalSil section would fall below test measurements. The expectation that the one-volume model would predict pressure drops lower than test data for a debris bed with a concentrated CalSil volume is illustrated in seven of the eight Series 2 tests, as illustrated in Figure 6.2-47 for Test 060331_NC_2024_LP1, Figure 6.2-50 for Test 060817_NC_2024_LP1, Figure 6.2-53 for Test 060509_NC_0505_LP1, Figure 6.2-56 for Test 060426_NC_0708_LP1, Figure 6.2-59 for Test 060807_NC_0708_LP1, Figure 6.2-62 for Test 060809_NC_0708_LP1, and Figure 6.2-65 for Test 060517_NC_0808_LP1. These figures all indicate this trend.

The pressure drop predictions for the two-volume model do not always bound the test measurements. The discrepancies are concentrated for tests with small CalSil masses in the debris bed (Tests 060426_NC_0708_LP1, 060809_NC_0708_LP1, and 060517_NC_0808_LP1). The discrepancies in predictions for small CalSil bed masses can be related to the fact that small errors in the calculation of CalSil concentration thickness using the empirical correlation can dramatically affect the pressure drop calculation. This suggests that improvements in the correlation for concentration CalSil thickness would greatly improve calculational ability. However, the developed calculational approach can still provide an estimate of the range of expected pressure drop for particular debris bed characteristics. Additionally, the calculational ability is an improvement over the method previously used, as described in NUREG/CR-6224.

BM-3 Test 060323_NC_1619_LP1(Nukon/CalSil=0.626/0.02 kg/m²,21-22 °C)-Two Vol Model

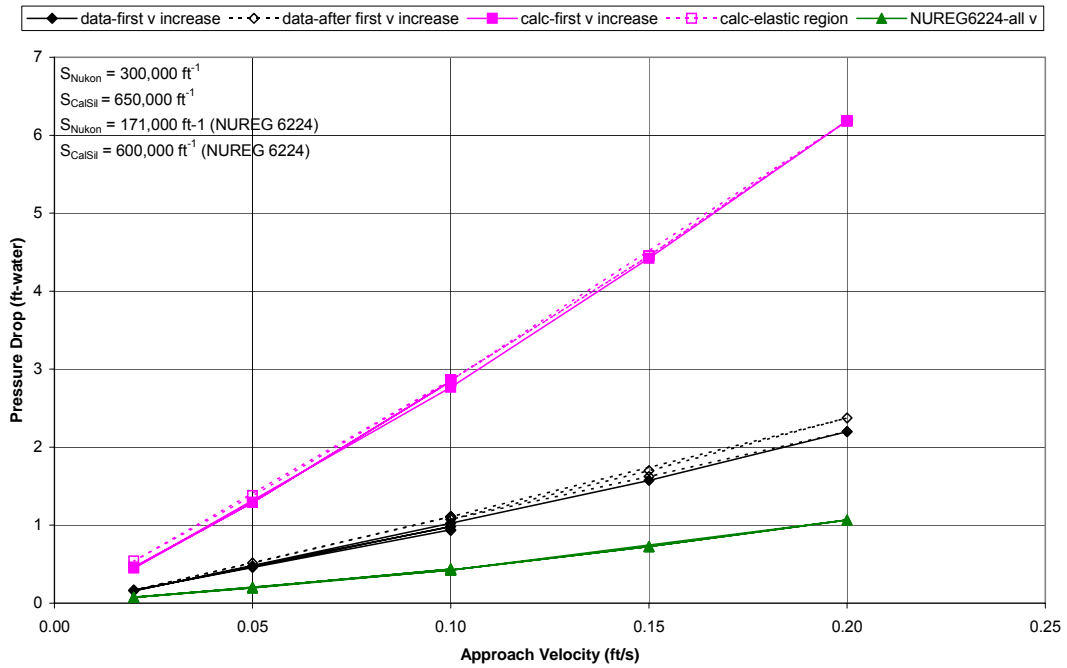


Figure 6.2-42 Head Loss for PNNL Series 2 Benchmark Nukon/CalSil Test 060323_NC_1619_LP1

BM-3 Test 060323_NC_1619_LP1(Nukon/CalSil=0.626/0.02 kg/m²,21-22 °C)-Two Vol Model

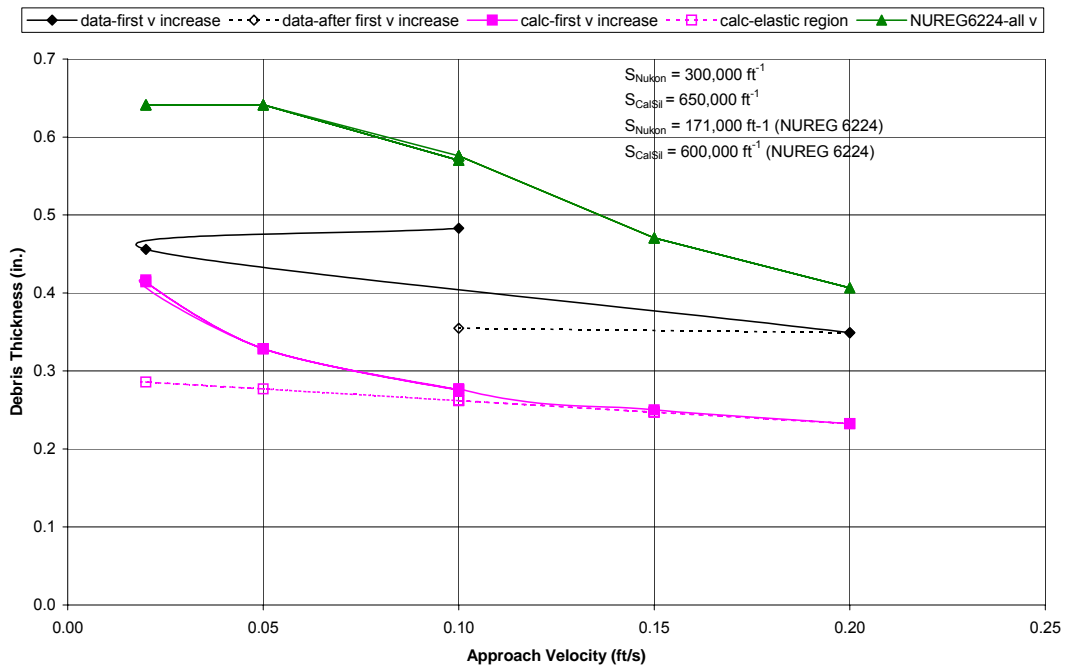


Figure 6.2-43 Bed Thickness for Series 2 Benchmark Nukon/CalSil Test 060323_NC_1619_LP1

PNNL BM-3 Test 060323_NC_1619_LP1(Nukon/CalSil=0.626/0.02 kg/m²,21-22 °C)

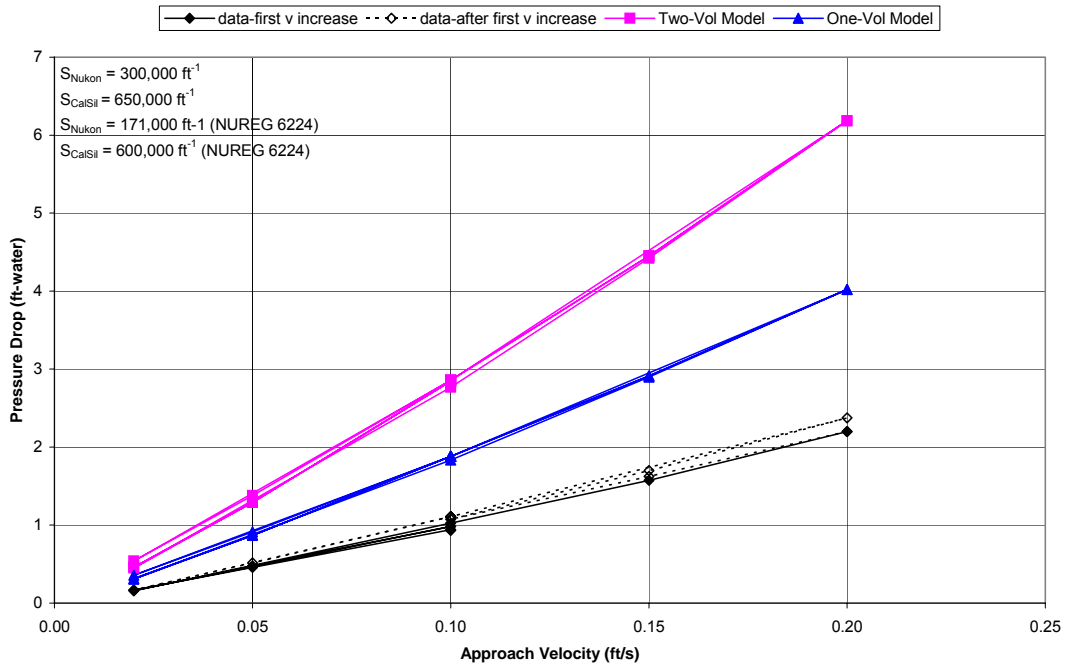


Figure 6.2-44 Head Loss for PNNL Series 2 Benchmark Nukon/CalSil Test 060323_NC_1619_LP1

PNNL Series 2 060331_NC_2024_LP1(Nukon/CalSil=0.60/0.13 kg/m², 21-24 °C)-Two Vol Model

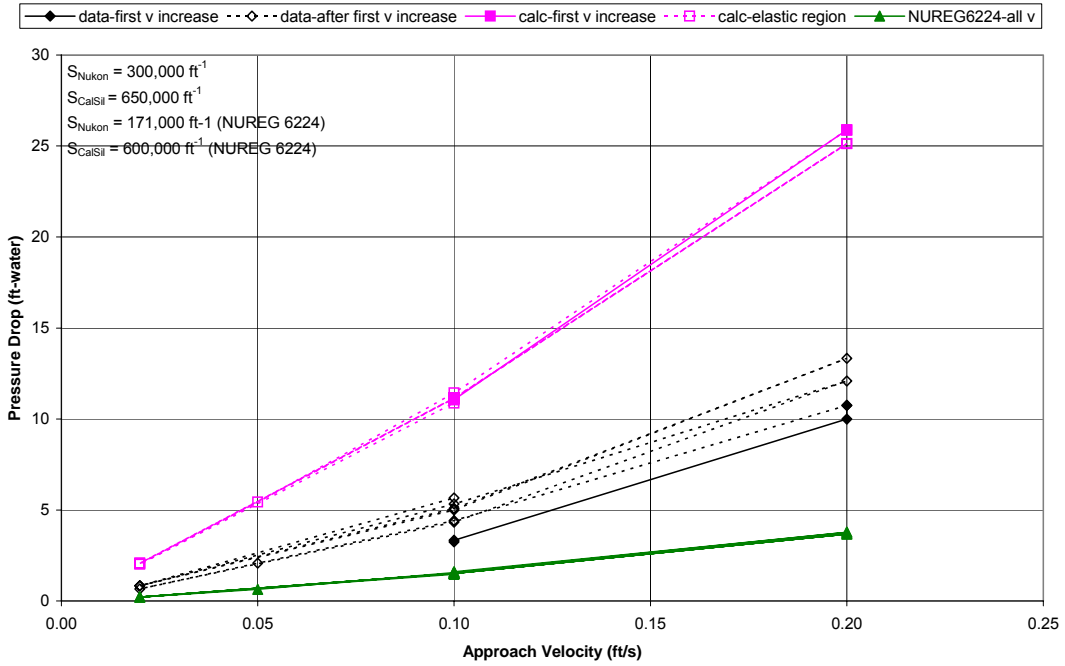


Figure 6.2-45 Head Loss for PNNL Series 2 Nukon/CalSil Test 060331_NC_2024_LP1

PNNL Series 2 060331_NC_2024_LP1(Nukon/CalSil=0.60/0.13 kg/m², 21-24 °C)-Two Vol Model

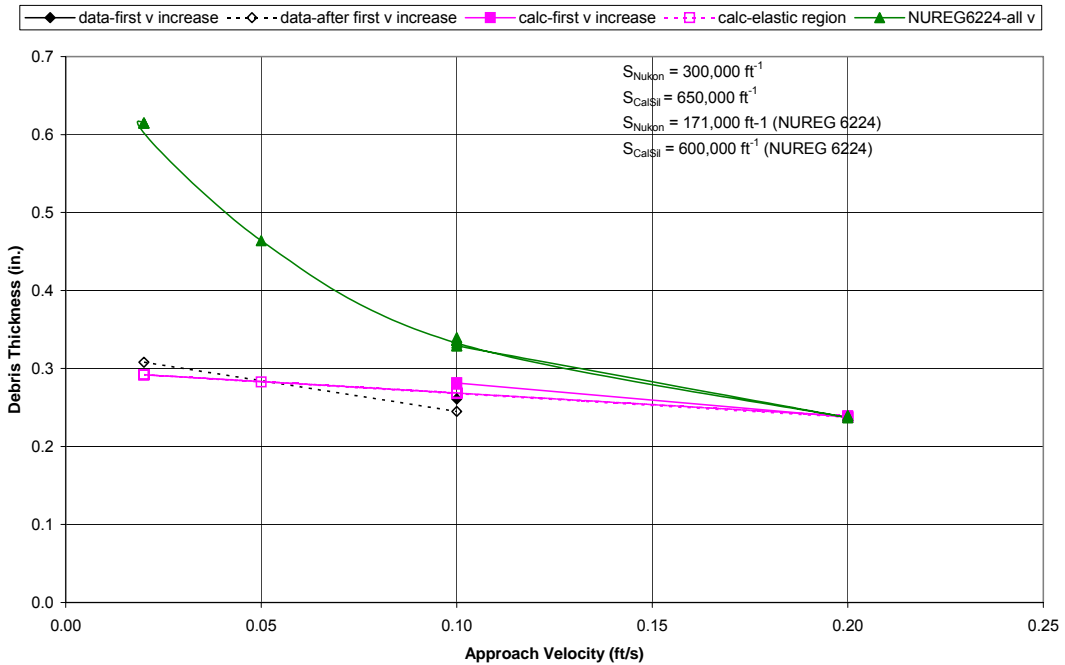


Figure 6.2-46 Bed Thickness for PNNL Series 2 Nukon/CalSil Test 060331_NC_2024_LP1

PNNL Series 2 060331_NC_2024_LP1(Nukon/CalSil=0.60/0.13 kg/m², 21-24 °C)

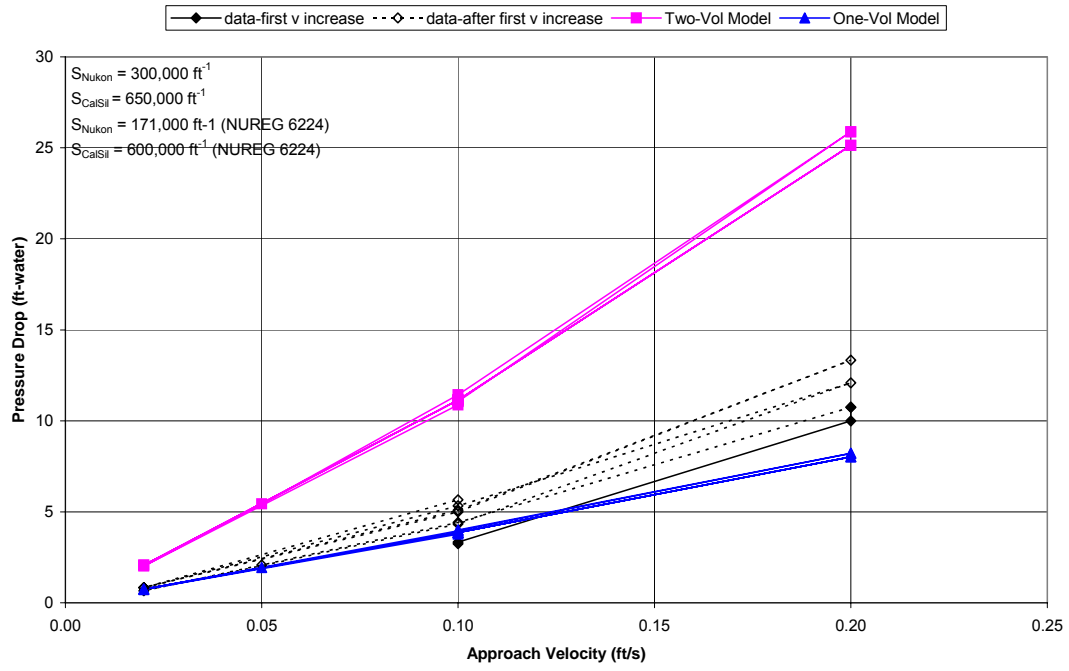


Figure 6.2-47 Head Loss for PNNL Series 2 Nukon/CalSil Test 060331_NC_2024_LP1

Series 2 060817_NC_2024_LP1(Nukon/CalSil=0.692/0.120 kg/m², 53-56 °C)-Two Vol Model

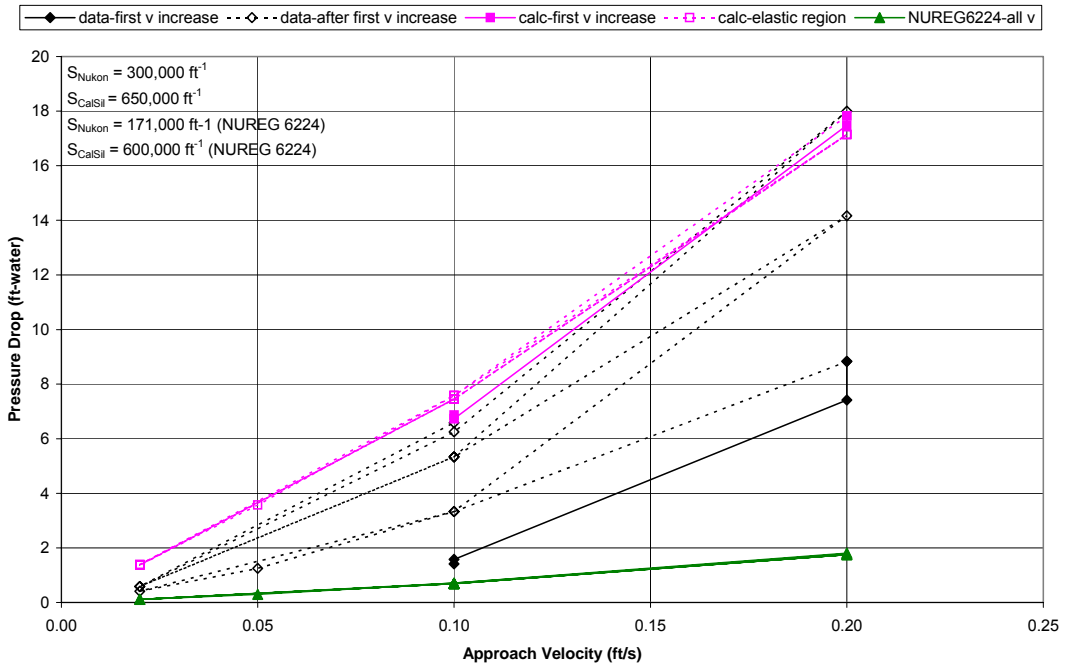


Figure 6.2-48 Head Loss for PNNL Series 2 Nukon/CalSil Test 060817_NC_2024_LP1

Series 2 060817_NC_2024_LP1(Nukon/CalSil=0.692/0.120 kg/m², 53-56 °C)-Two Vol Model

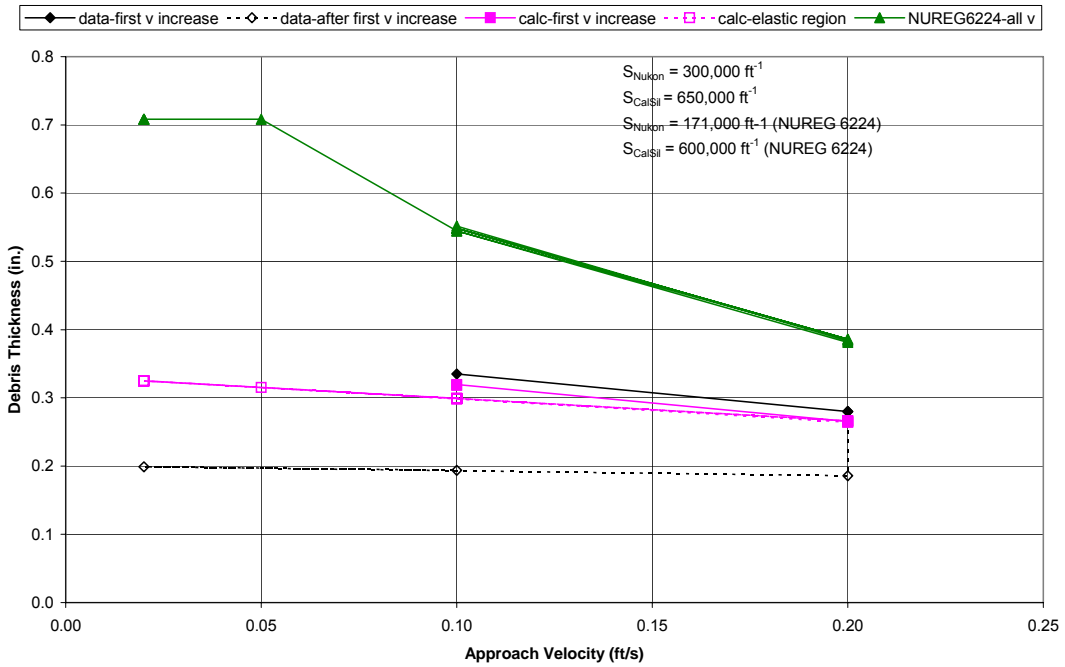


Figure 6.2-49 Bed Thickness for PNNL Series 2 Nukon/CalSil Test 060817_NC_2024_LP1

PNNL Series 2 060817_NC_2024_LP1(Nukon/CalSil=0.692/0.120 kg/m², 53-56 °C)

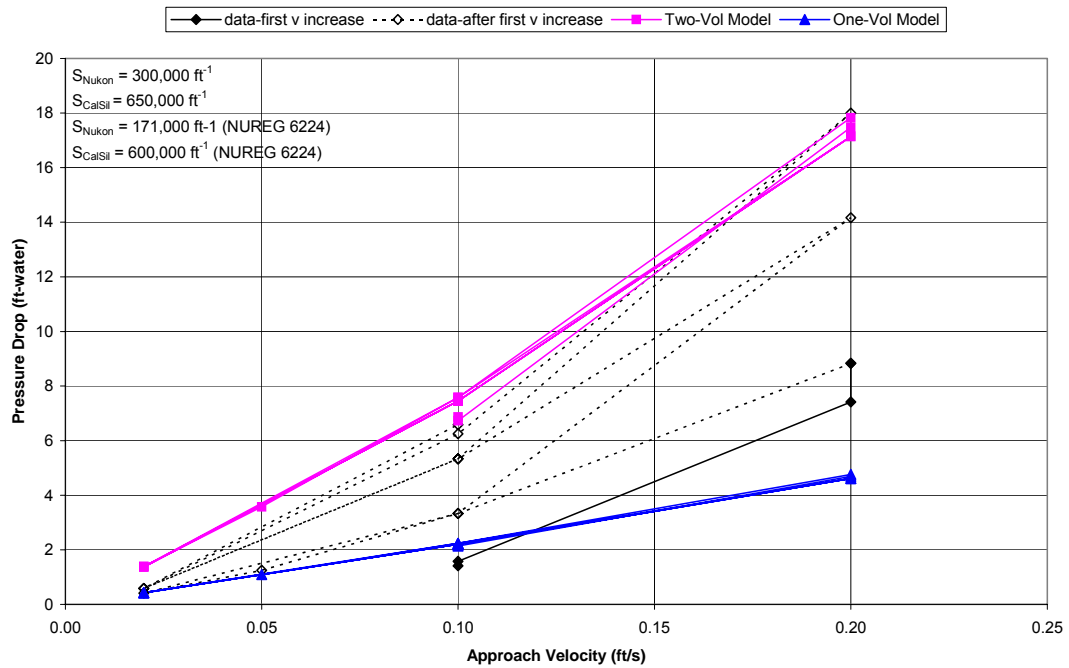


Figure 6.2-50 Head Loss for PNNL Series 2 Nukon/CalSil Test 060817_NC_2024_LP1

Series 2 060509_NC_0505_LP1(Nukon/CalSil=0.184/0.025 kg/m², 20-22 °C)-Two Vol Model

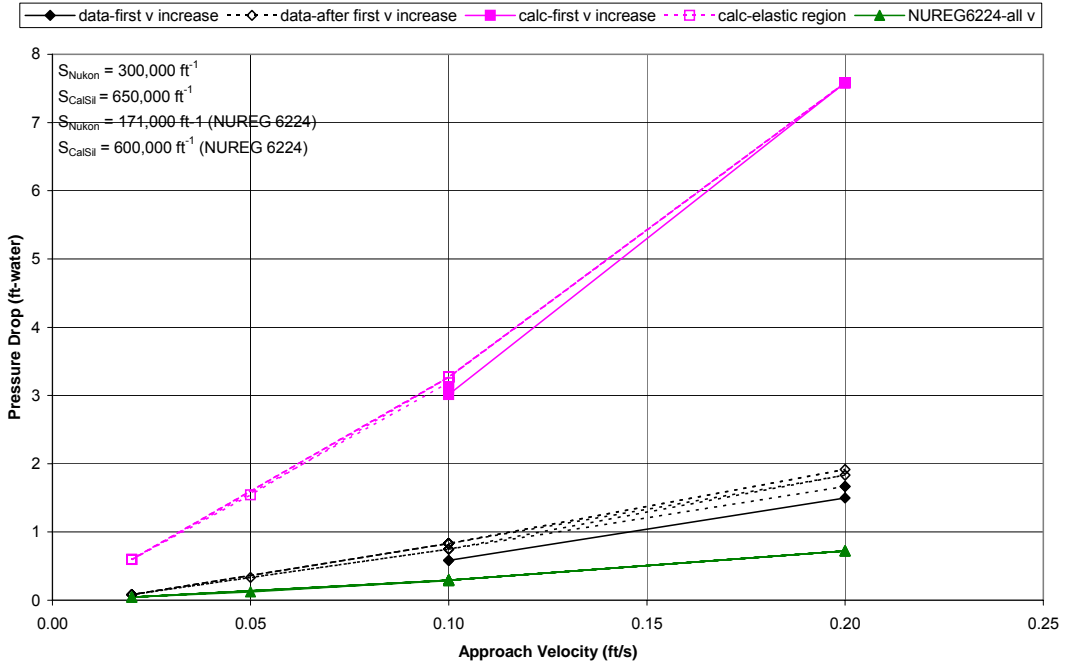


Figure 6.2-51 Head Loss for PNNL Series 2 Nukon/CalSil Test 060509_NC_0505_LP1

Series 2 060509_NC_0505_LP1(Nukon/CalSil=0.184/0.025 kg/m², 20-22 °C)-Two Vol Model

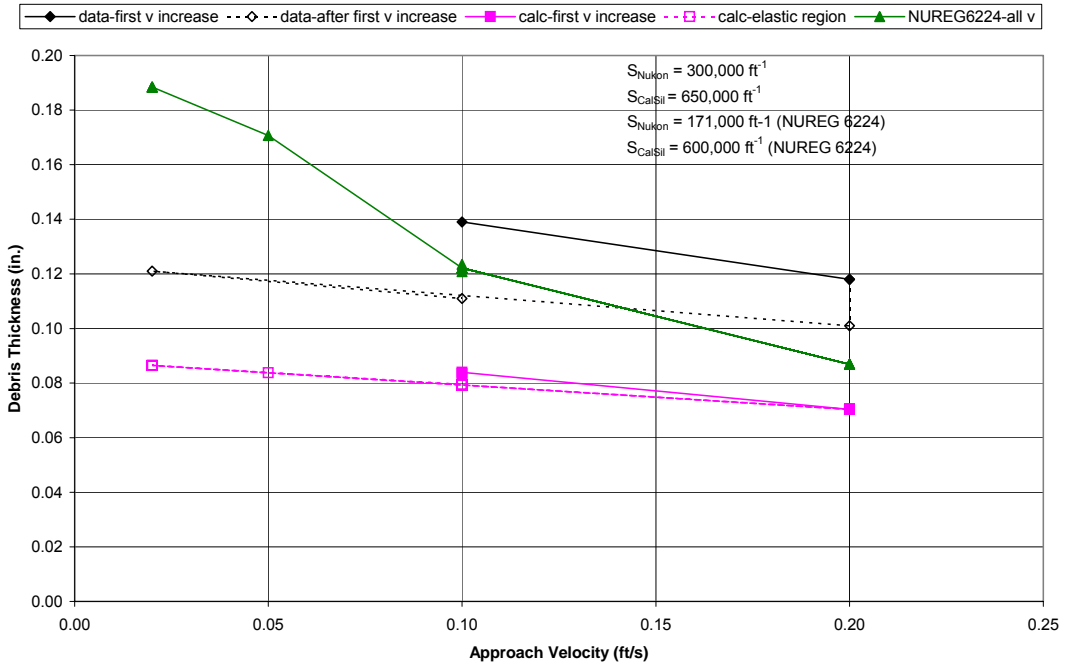


Figure 6.2-52 Bed Thickness for PNNL Series 2 Nukon/CalSil Test 060509_NC_0505_LP1

PNNL Series 2 060509_NC_0505_LP1(Nukon/CalSil=0.184/0.025 kg/m², 20-22 °C)

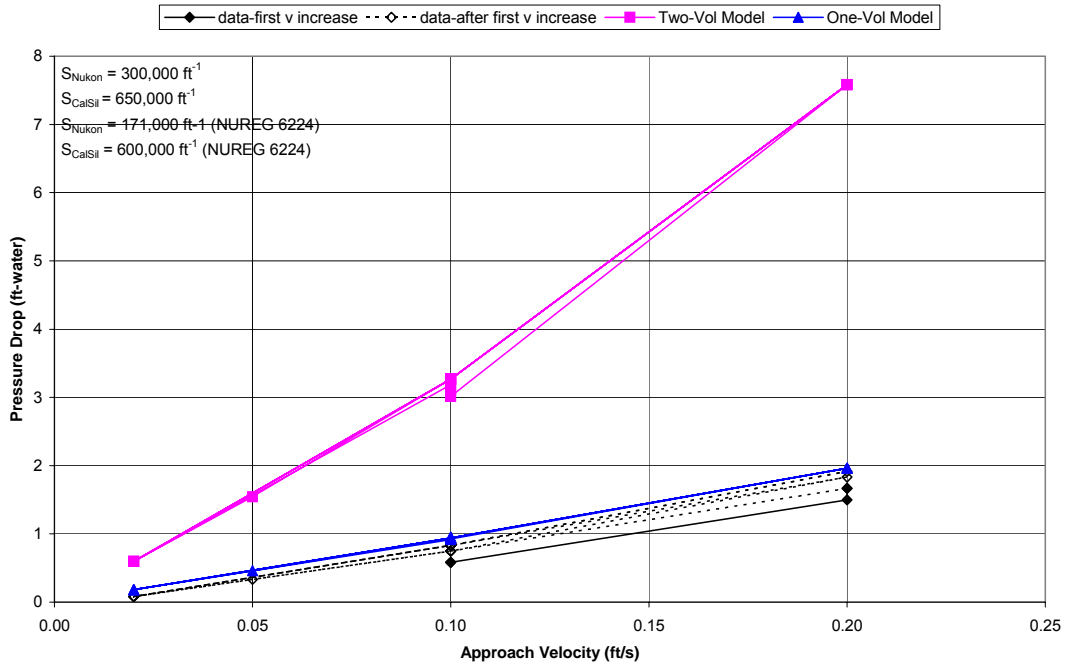


Figure 6.2-53 Head Loss for PNNL Series 2 Nukon/CalSil Test 060509_NC_0505_LP1

Series 2 060426_NC_0708_LP1(Nukon/CalSil=0.208/0.005 kg/m², 20-24 °C)-Two Vol Model

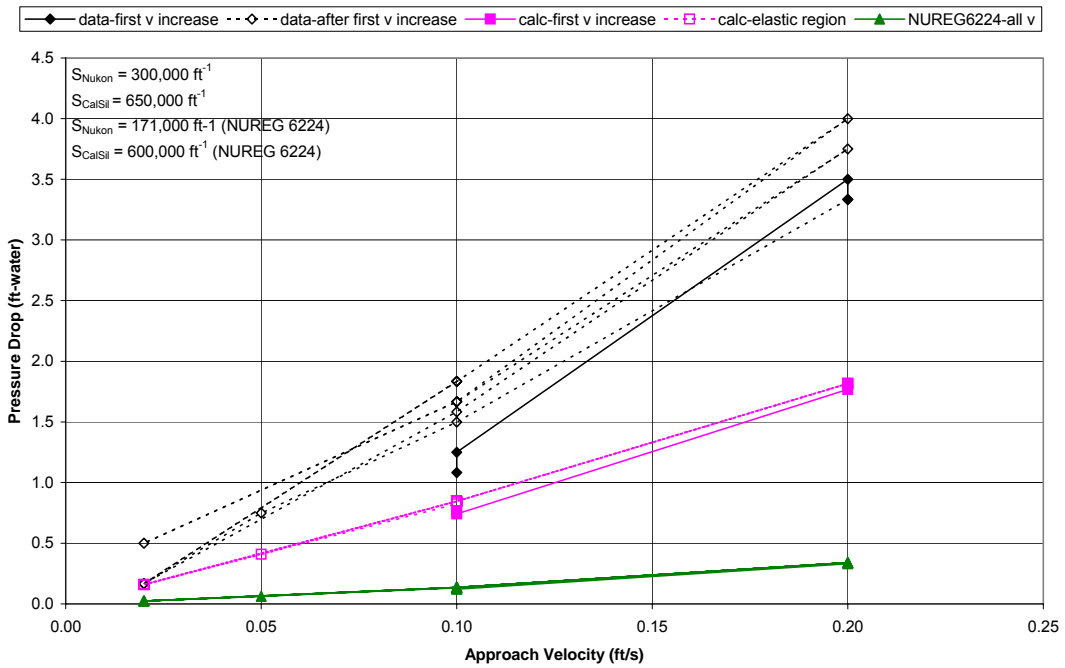


Figure 6.2-54 Head Loss for PNNL Series 2 Nukon/CalSil Test 060426_NC_0708_LP1

Series 2 060426_NC_0708_LP1(Nukon/CalSil=0.208/0.005 kg/m², 20-24 °C)-Two Vol Model

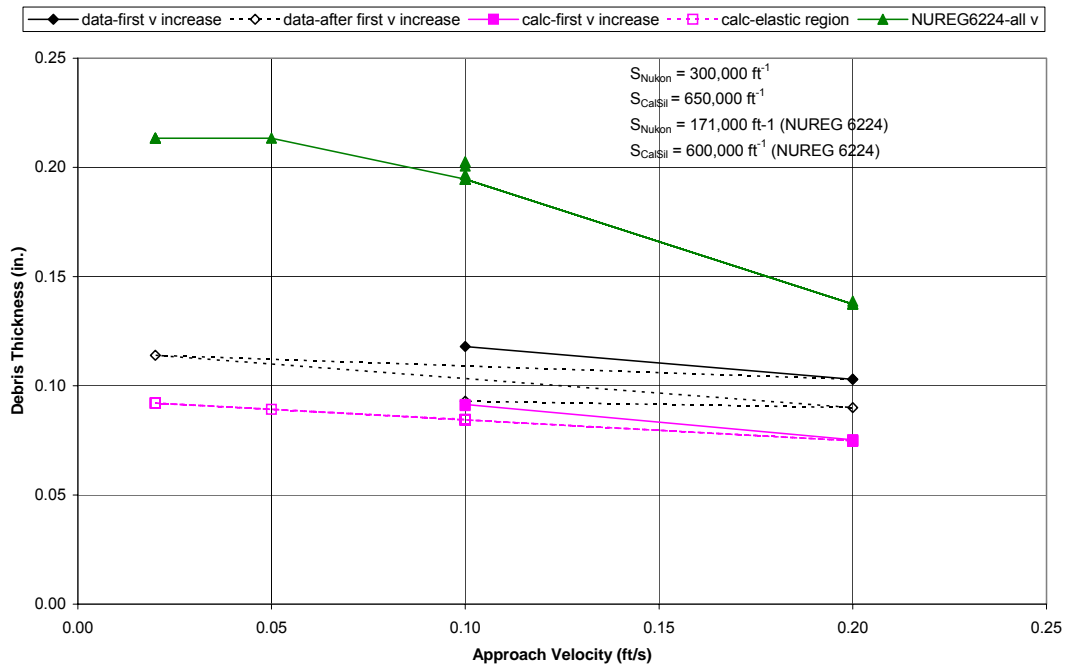


Figure 6.2-55 Bed Thickness for PNNL Series 2 Nukon/CalSil Test 060426_NC_0708_LP1

PNNL Series 2 060426_NC_0708_LP1(Nukon/CalSil=0.208/0.005 kg/m², 20-24 °C)

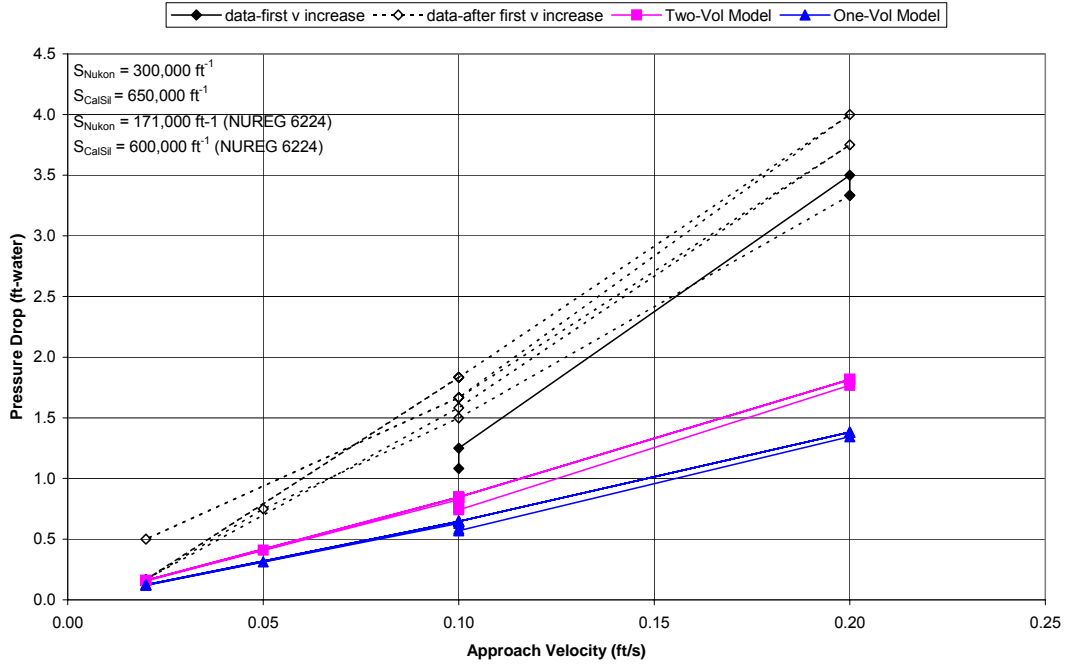


Figure 6.2-56 Head Loss for PNNL Series 2 Nukon/CalSil Test 060426_NC_0708_LP1

Series 2 060807_NC_0708_LP1(Nukon/CalSil=0.243/0.018 kg/m², 54-56 °C)-Two Vol Model

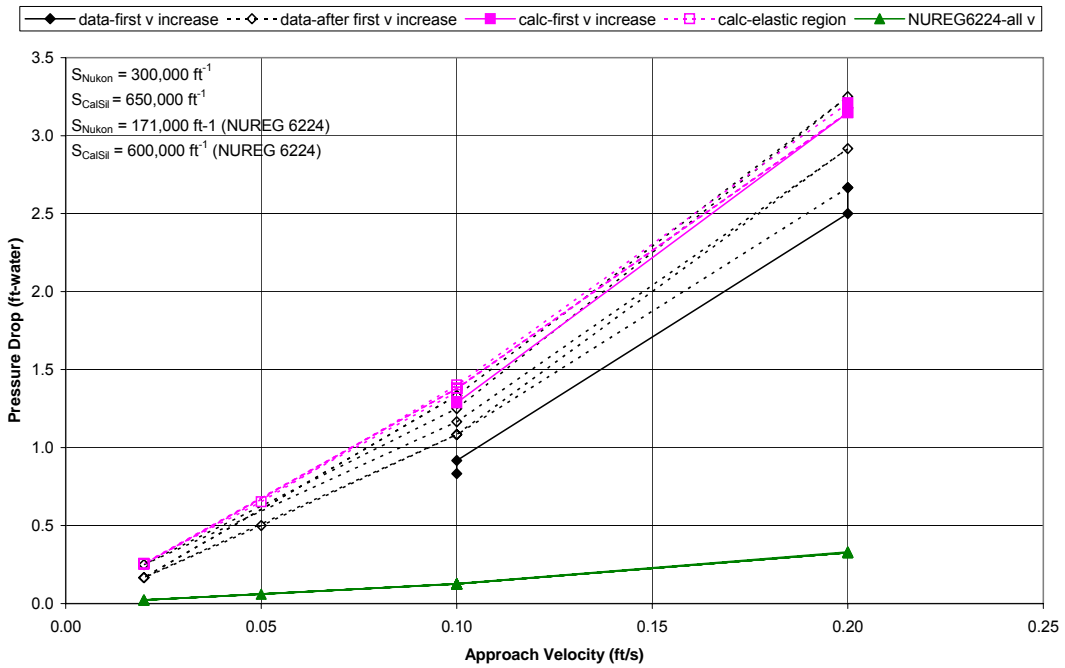


Figure 6.2-57 Head Loss for PNNL Series 2 Nukon/CalSil Test 060807_NC_0708_LP1

Series 2 060807_NC_0708_LP1(Nukon/CalSil=0.243/0.018 kg/m², 54-56 °C)-Two Vol Model

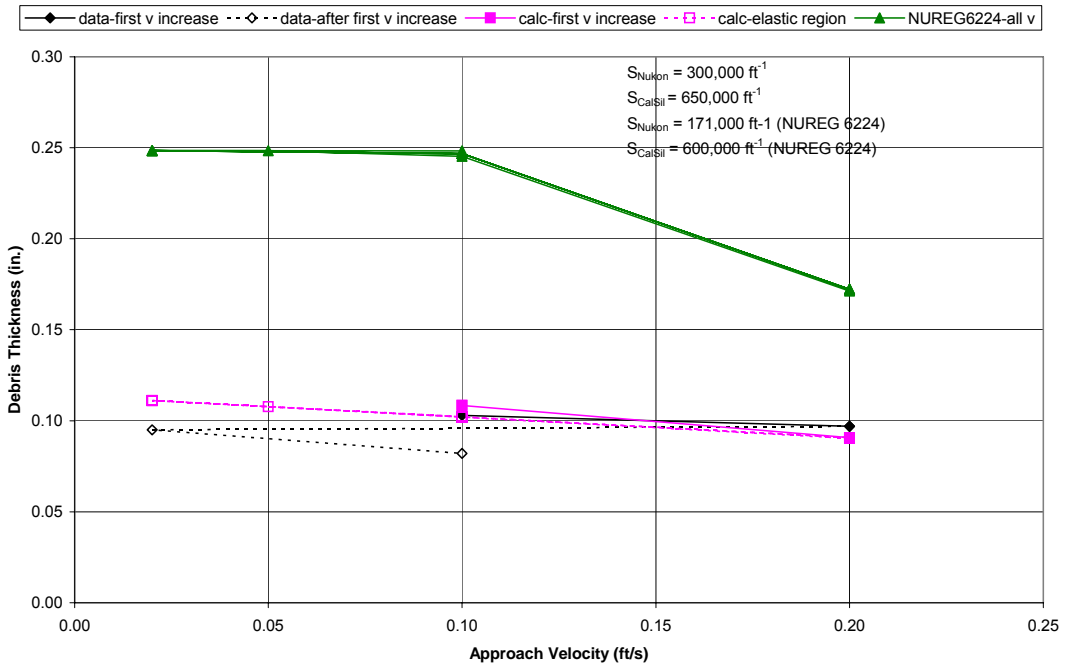


Figure 6.2-58 Bed Thickness for PNNL Series 2 Nukon/CalSil Test 060807_NC_0708_LP1

PNNL Series 2 060807_NC_0708_LP1(Nukon/CalSil=0.243/0.018 kg/m², 54-56 °C)

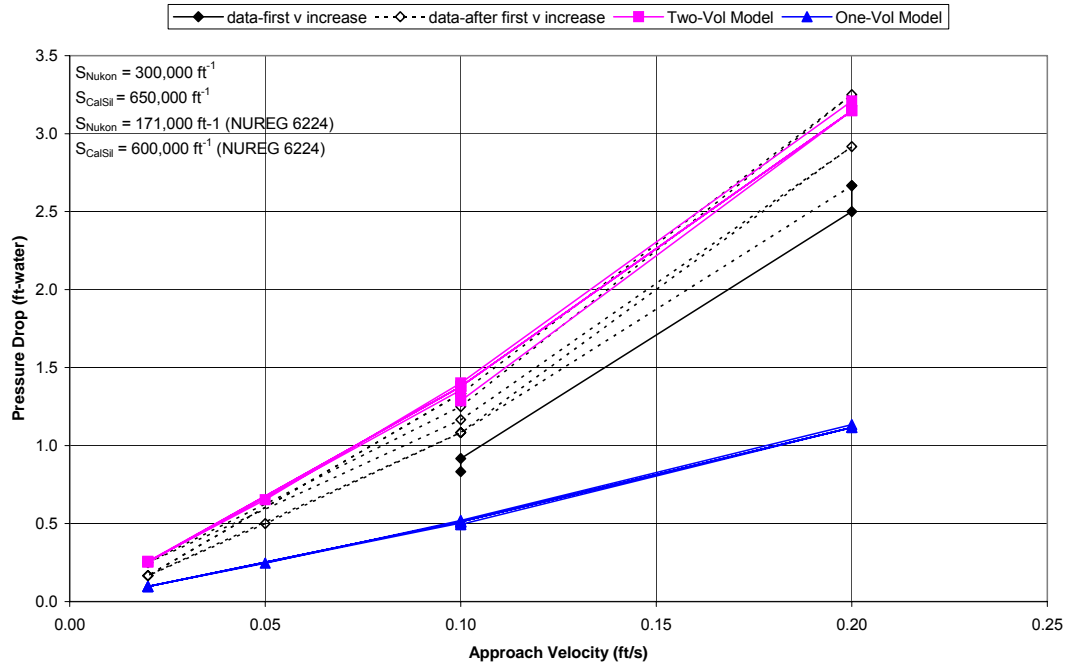


Figure 6.2-59 Head Loss for PNNL Series 2 Nukon/CalSil Test 060807_NC_0708_LP1

Series 2 060809_NC_0708_LP1(Nukon/CalSil=0.155/0.005 kg/m², 79-83 °C)-Two Vol Model

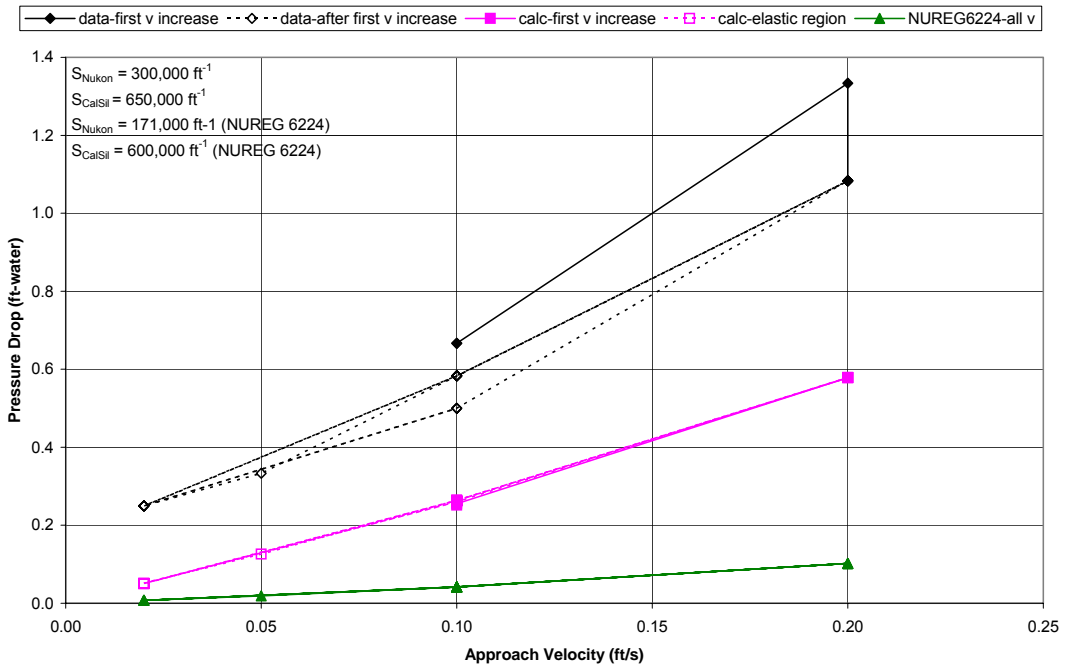


Figure 6.2-60 Head Loss for PNNL Series 2 Nukon/CalSil Test 060809_NC_0708_LP1

Series 2 060809_NC_0708_LP1(Nukon/CalSil=0.155/0.005 kg/m², 79-83 °C)-Two Vol Model

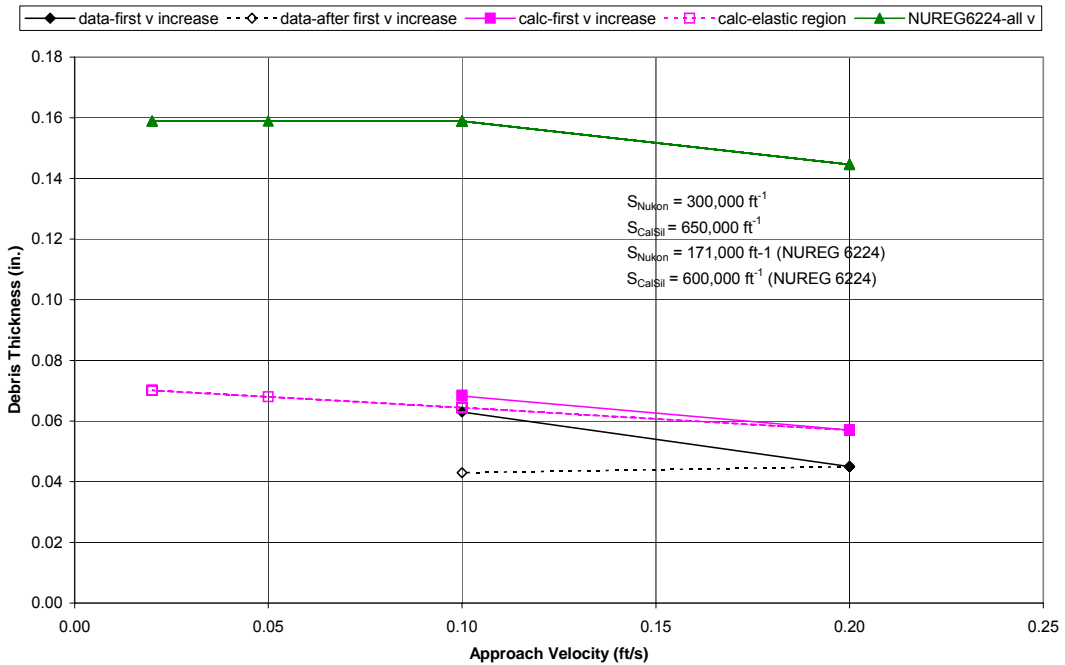


Figure 6.2-61 Bed Thickness for PNNL Series 2 Nukon/CalSil Test 060809_NC_0708_LP1

PNNL Series 2 060809_NC_0708_LP1(Nukon/CalSil=0.155/0.005 kg/m², 79-83 °C)

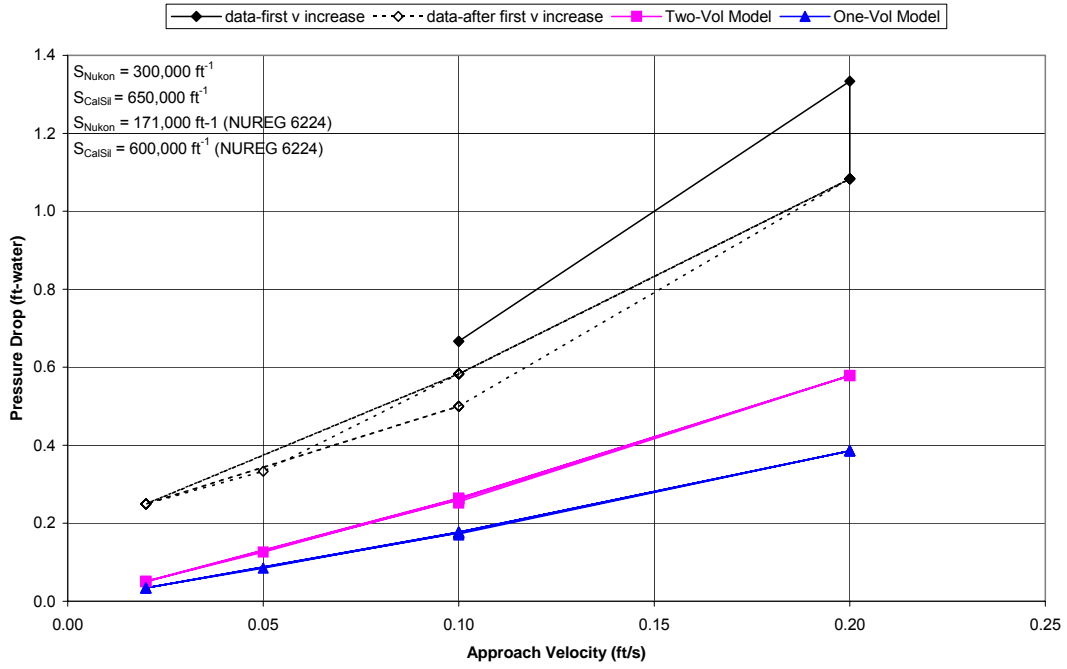


Figure 6.2-62 Head Loss for PNNL Series 2 Nukon/CalSil Test 060809_NC_0708_LP1

PNNL Series 2 060517_NC_0808_LP1(Nukon/CalSil=0.223/0.082 kg/m², 25 °C)-Two Vol Model

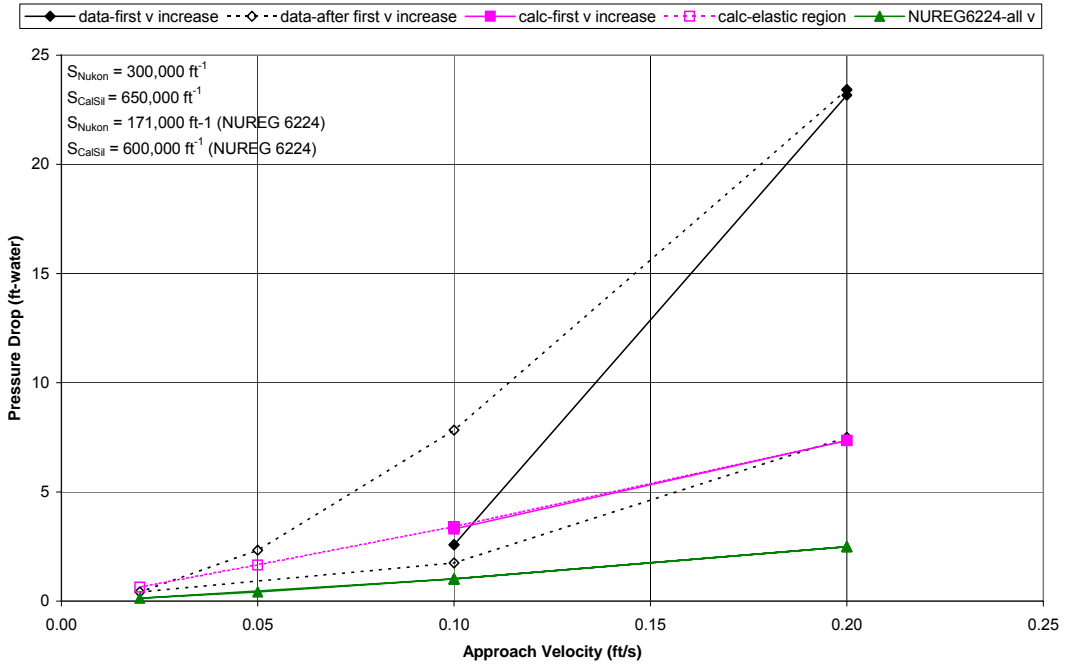


Figure 6.2-63 Head Loss for PNNL Series 2 Nukon/CalSil Test 060517_NC_0808_LP1

PNNL Series 2 060517_NC_0808_LP1(Nukon/CalSil=0.223/0.082 kg/m², 25 °C)-Two Vol Model

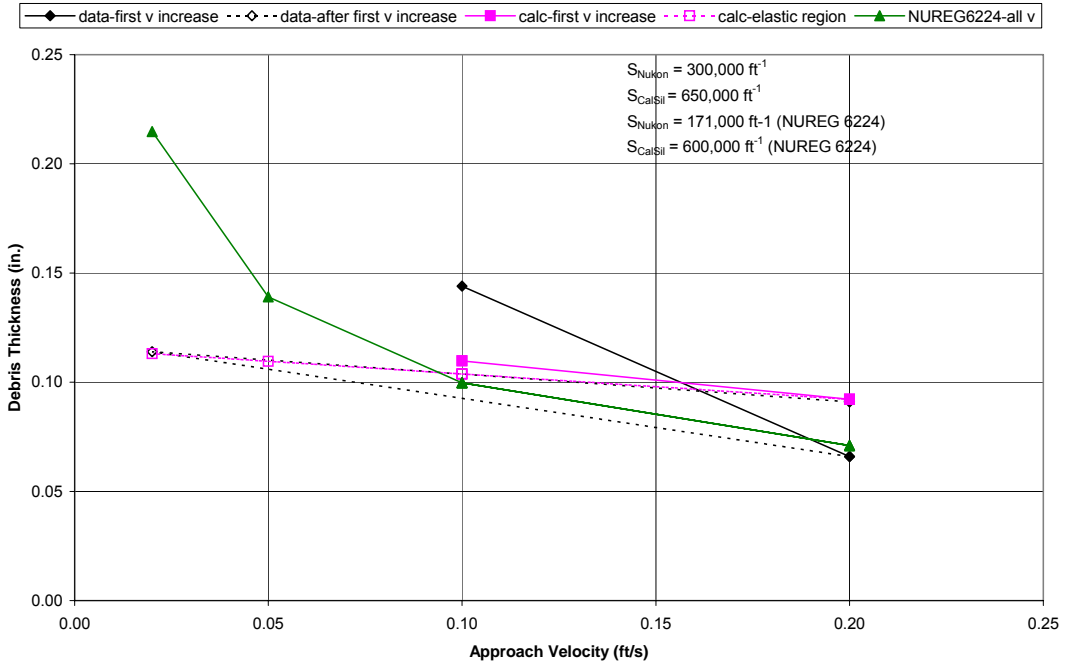


Figure 6.2-64 Bed Thickness for PNNL Series 2 Nukon/CalSil Test 060517_NC_0808_LP1

PNNL Series 2 060517_NC_0808_LP1(Nukon/CalSil=0.223/0.082 kg/m²-25 °C)

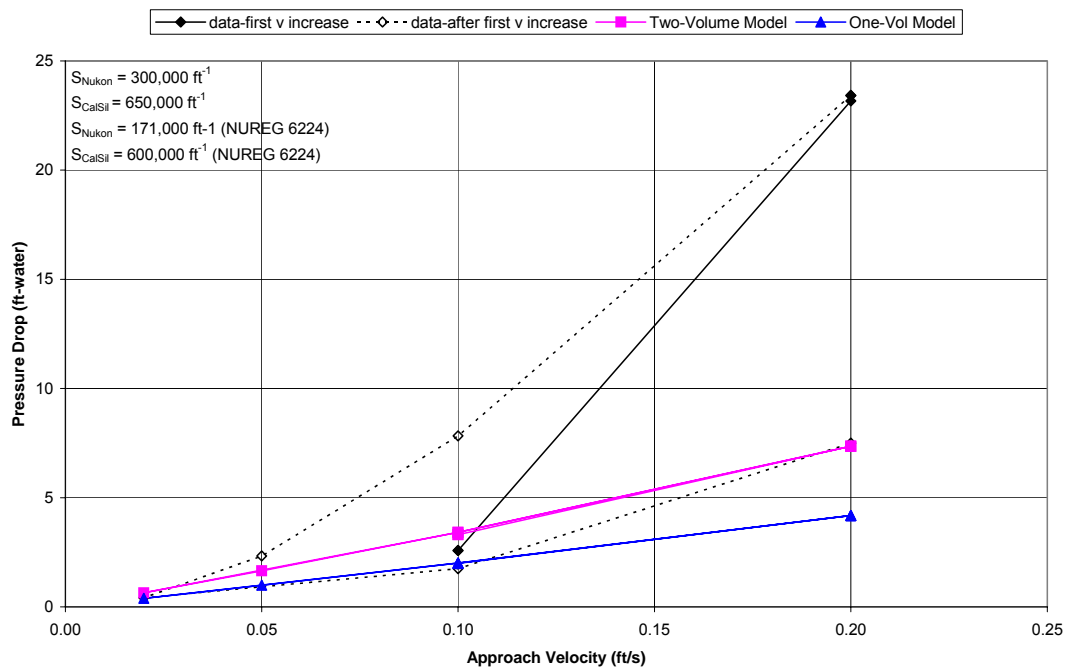


Figure 6.2-65 Head Loss for PNNL Series 2 Nukon/CalSil Test 060517_NC_0808_LP1

6.2.2.4 Head Loss Sensitivity to Temperature Variations

As indicated in Table 6.2-2, PNNL ran several of the Series 2 tests at elevated temperatures of about 54 °C and 83 °C (129.2 °F and 181.4 °F) in order to assess the impact of temperature on measured pressure drop. Temperature sensitivity was studied in beds composed of approximately the same debris loadings using three approaches:

- (1) In the first approach, a bed was formed using a specified loading, and a series of velocity cycles was performed at an ambient (approximately 25 °C (77 °F)) temperature. The loop was subsequently raised to a temperature of about 54 °C (129.2 °F) where velocity cycling was performed, and then the temperature was again elevated to about 83 °C (181.4 °F) where additional velocity cycling was performed.
- (2) In the second approach, tests were run for the specified debris loading at an elevated temperature of about 54 °C (129.2 °F) with velocity cycling at the elevated temperature. The temperature was then lowered to about 30 °C (86 °F), and velocity cycling was again performed.
- (3) In the third approach, tests were run for the specified debris loading at an elevated temperature of about 83 °C (181.4 °F) with velocity cycling at the elevated temperature. The temperature was then lowered to about 54 °C (129.2 °F), and velocity cycling was again performed.

Table 6.2-3 lists the tests performed to study temperature sensitivity and identifies the temperature changes employed in each test series.

Table 6.2-3 Debris Bed Temperature Sensitivity

PNNL Test	Bed Loading (kg/m ²)		Temperature (°C) / (°F)		
	Nukon	CalSil	LP1 Bed Formation	LP2 First Change	LP3 Second Change
060425_NO_2703	1.245	0.0	22–25 / 71.6–77	52–54 / 125.6–129.2	81–84 / 177.8–183.2
060731_NO_2703	1.251	0.0	54 / 129.2	27 / 80.6	NA
060802_NO_2703	1.191	0.0	82 / 179.6	55 / 131	NA
060426_NC_0708	0.208	0.00478	21–24 / 69.8–75.2	81–84 / 177.8–183.2	NA
060807_NC_0708	0.243	0.0184	54 / 129.2	36 / 96.8	NA
060809_NC_0708	0.155	0.00483	82 / 179.6	54 / 129.2	NA
060331_NC_2024	0.600	0.132	21–24 / 69.8–75.2	NA	NA
060817_NC_2024	0.691	0.120	54 / 129.2	25 / 77	NA

As indicated in Section 2, classical theory suggests that, for the same debris bed and flow conditions, the pressure drop should decrease with increasing water temperature because viscosity decreases with increasing temperature. During assessment of the PNNL test data using the first test approach, analysts discovered that if the bed is formed at an ambient temperature followed by temperature increases, test results do not corroborate the expected theoretical behavior. The following figures present test data and

calculational predictions for cases already presented in the previous two sections; however, they present the information in a form that can address sensitivity to temperature variations.

Figure 6.2-66 shows that, for PNNL Nukon-only Tests 060425_NO_2703_LP1, LP2, and LP3, the measured pressure drop at 54 °C (129.2 °F) is higher than at 22 °C (71.6 °F), and the pressure drop at 80 °C (176 °F) is lower than at 22 °C (71.6 °F). Uncharacteristic behavior was also observed for the Nukon/CalSil Tests 060426_NC_0708_LP1 and LP2. Figure 6.2-67 shows that, at a low approach velocity, the measured pressure drop for this Nukon/CalSil debris bed at about 81 °C (177.8 °F) is higher than the measurement at about 20 °C (68 °F); however, at higher approach velocities, the pressure drop for the 81 °C (177.8 °F) conditions is lower than the pressure drop at about 20 °C (68 °F). The observed test behavior suggests that debris material properties may be changing as a function of temperature and/or that the debris bed material may be rearranging as the temperature changes.

Additional tests were performed using the second and third approaches, during which the debris bed was formed at an elevated temperature as indicated in the first paragraph of this section. Nukon-only debris beds were formed at about 54 °C and 82 °C (129.2 °F and 179.6 °F) using loading conditions similar to Tests 060425_NO_2703_LP1, LP2, and LP3. Nukon/CalSil debris beds were also formed at the two elevated temperatures using loading conditions similar to those in Tests 060426_NC_0708_LP1 and LP2. For another test, a Nukon/CalSil bed was formed at about 54 °C (129.2 °F) for debris-loading conditions similar to those in Test 060331_NC_2024_LP1.

Figures 6.2-68 to 6.2-70 compare the measured pressure drops for similar Nukon-only and Nukon/CalSil beds measured at the bed formation temperature. The Nukon-only tests in Figure 6.2-68 and the Nukon/CalSil tests in Figure 6.2-69 provide results that are consistent with classical theory. These two plots show that the pressure drop for all the beds decreases with increasing temperature. The Nukon/CalSil cases plotted in Figure 6.2-70 present a slightly different situation. The pressure drop for the lower temperature test is higher than the test data at the higher temperature for the first test cycle after bed formation, but, at later cycles in testing, the pressure drops at the higher temperature exceed the measurements at the lower temperature. Therefore, the Nukon-only and Nukon/CalSil test data in Figures 6.2-68 and 6.2-69 demonstrate expected temperature behavior, whereas the Nukon/CalSil cases in Figure 6.2-70 do not. The difference in observed temperature sensitivity behavior may be related to debris redistribution in the bed, changes in CalSil material properties that promote the debris redistribution, or the differences in actual debris bed mass for the tested cases. Consequently, it can generally be concluded that the pressure drop across a debris bed depends on water temperature and also on the flow and temperature history of the debris bed exposure.

It is important to demonstrate that the one- and two-volume methods for calculating pressure drop across a debris bed as developed in this report apply to the range of tested temperatures. The one-volume approach can be applied to a debris bed composed of one debris type. Figure 6.2-71 compares the pressure drops measured at the bed formation temperatures to predictions obtained using the one-volume model for the Nukon-only debris bed tests identified in Table 6.2-3. Both the test data and calculations follow the expected trend in which the lowest temperature condition has the highest pressure drop and the pressure drop decreases with increasing temperature. Figures 6.2-72 and 6.2-73 provide similar comparisons between pressure drop measurements and two-volume model predictions for the two tested Nukon/CalSil debris beds. The test data for the three Nukon/CalSil tests plotted in Figure 6.2-72 at three different temperatures follow the expected trend of higher pressure at lower temperature. However, the two-volume calculation predicts the highest pressure drop for the 54 °C (129.2 °F) temperature test. Figure 6.2-73 also shows pressure drop plots for another two Nukon/CalSil tests. The measured pressure drop for the 54 °C (129.2 °F) case is also higher than the lower temperature case, but the two-volume

calculations exhibit the correct expected trending for the results obtained using the two-volume calculation.

As previously stated, it can generally be concluded that the pressure drop across a debris bed depends on water temperature and also on the flow and temperature history of the debris bed exposure. The developed calculational method generally predicts pressure drops at different temperatures, a result that follows the classical theory expectations that higher pressure drops occur at lower temperatures.

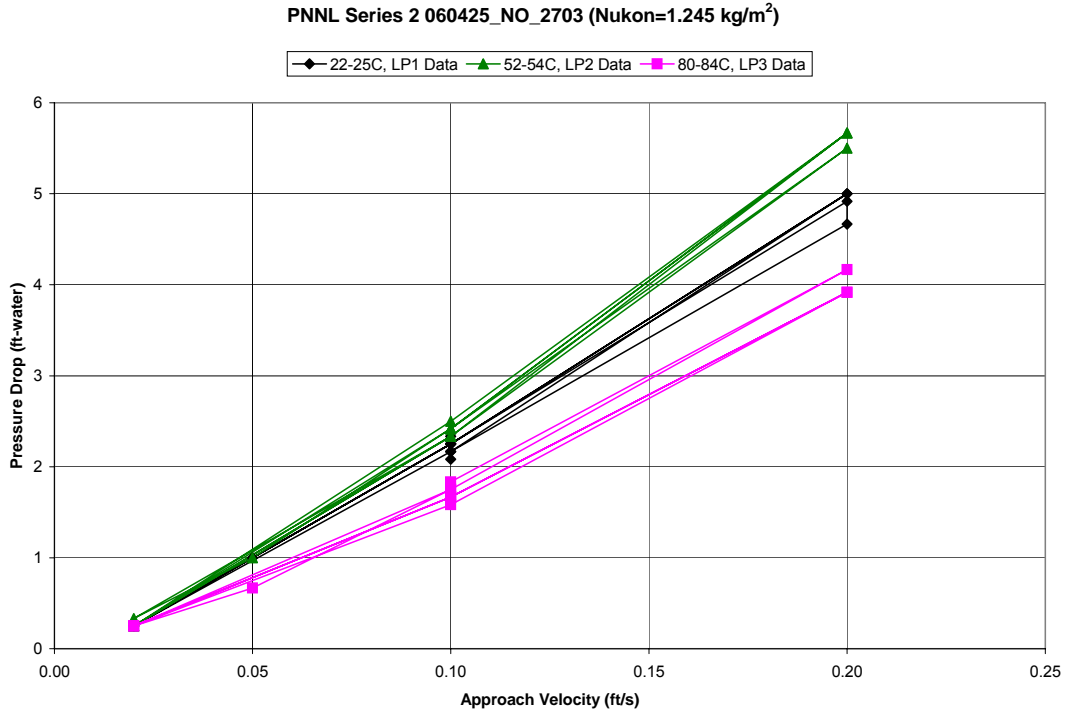


Figure 6.2-66 Temperature Sensitivity for PNNL Nukon Test 060425_NO_2703_LP1, LP2, LP3

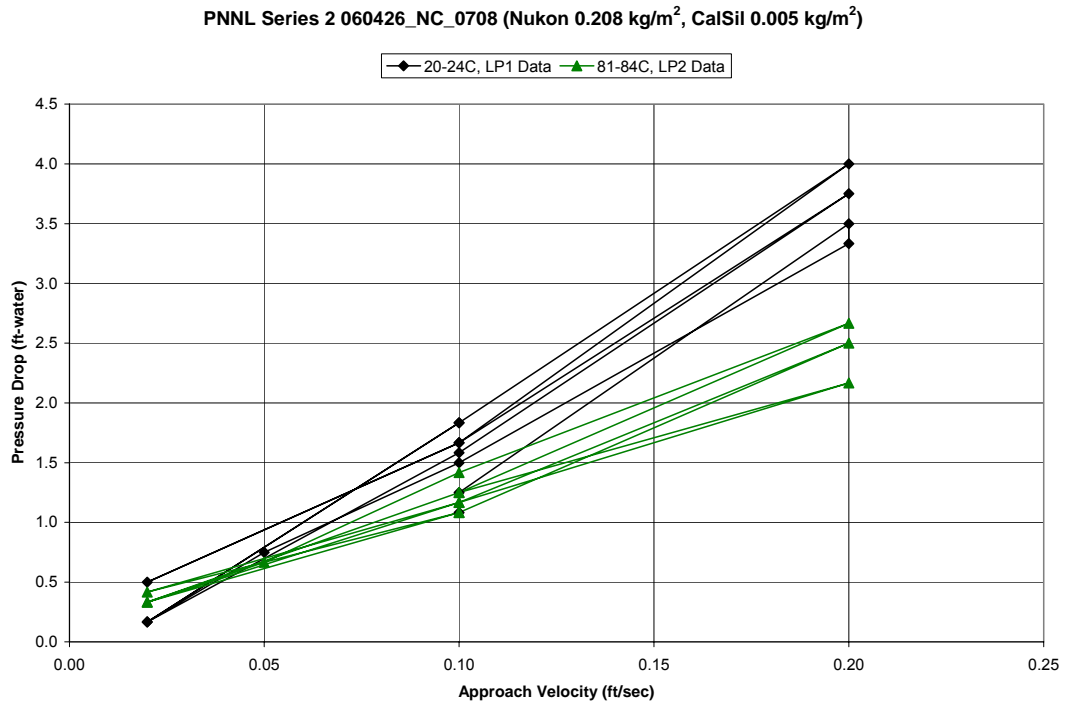


Figure 6.2-67 Temperature Sensitivity for PNNL Nukon/CalSil Test 060426_NC_0708_LP1, LP2

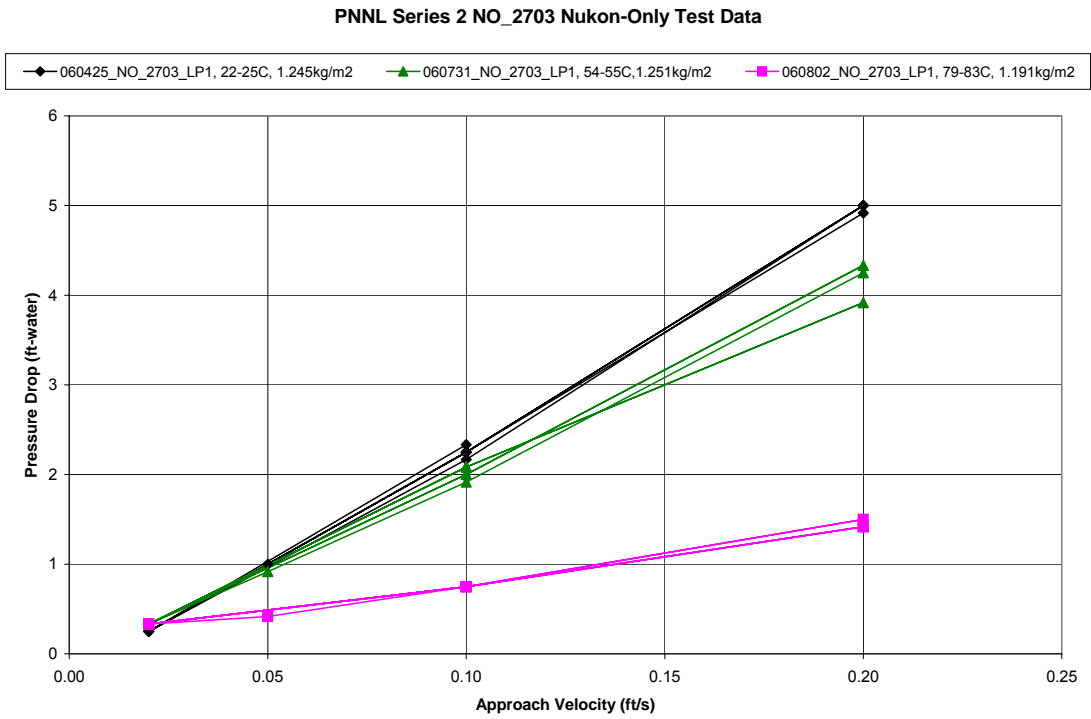


Figure 6.2-68 Temperature Sensitivity for First Velocity Cycle of PNNL Nukon-Only Tests

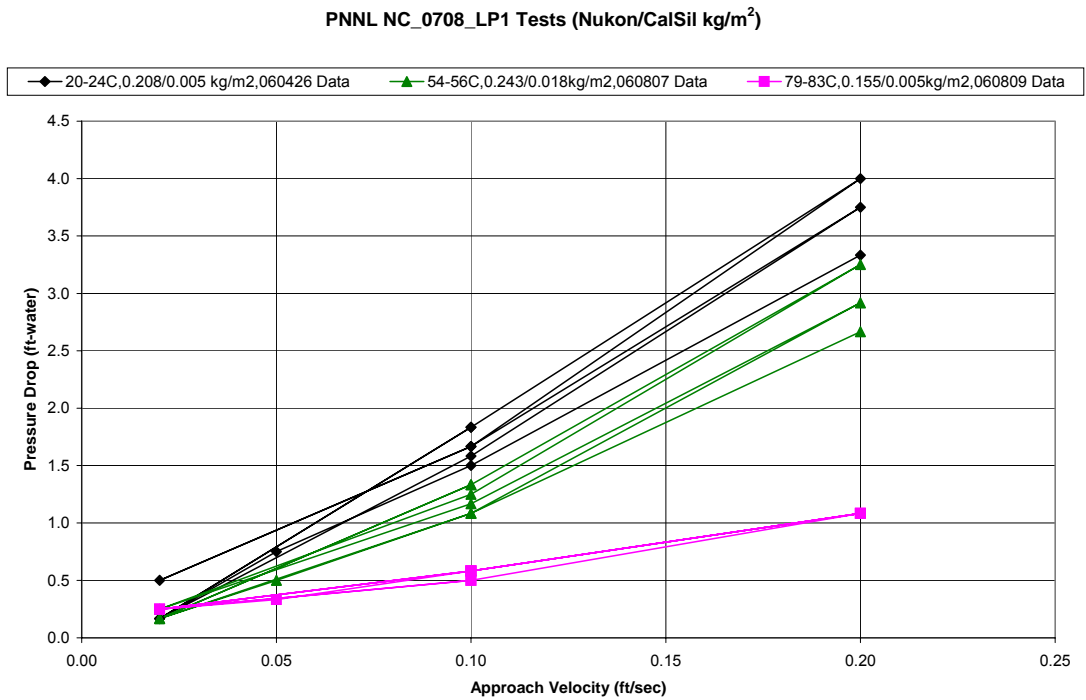


Figure 6.2-69 Temperature Sensitivity for First Velocity Cycle of PNNL Nukon/CalSil_0708 Tests

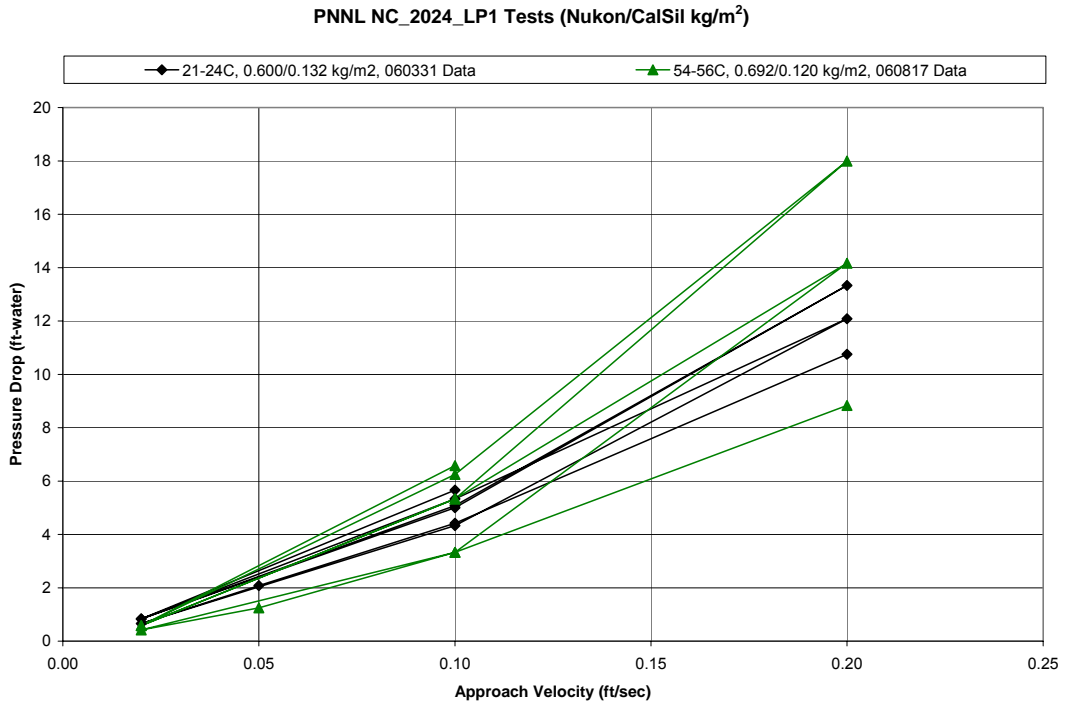


Figure 6.2-70 Temperature Sensitivity for First Velocity Cycle of PNNL Nukon/CalSil_2024 Tests

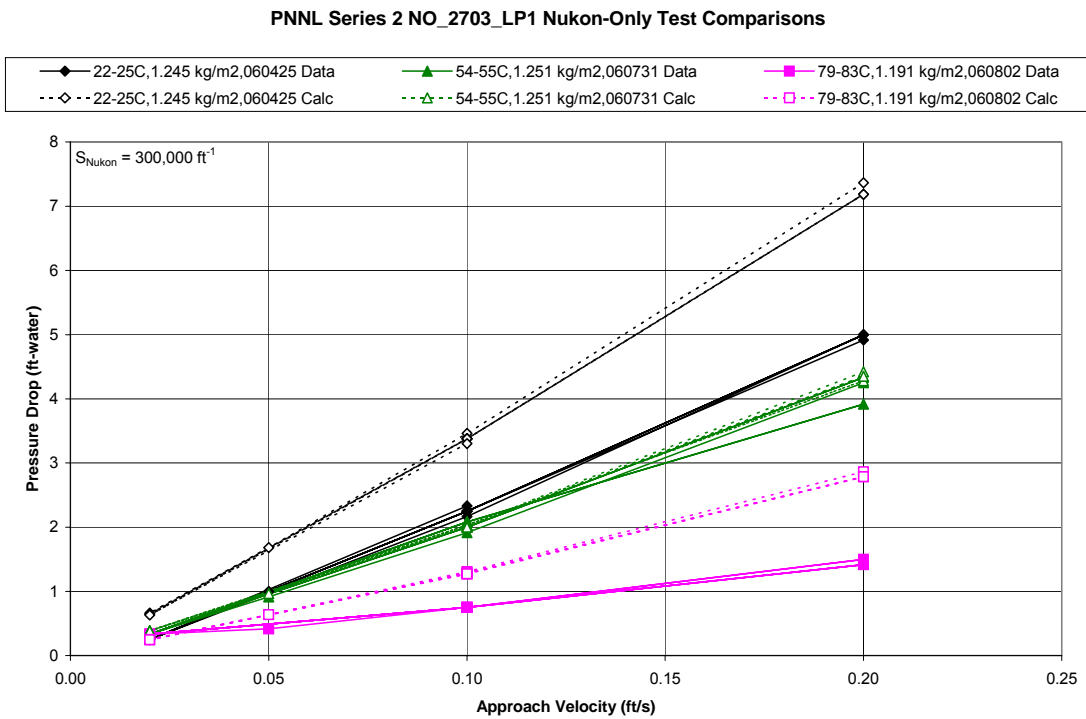


Figure 6.2-71 Data and One-Volume Predictions for First Velocity Cycle of Nukon-Only Tests

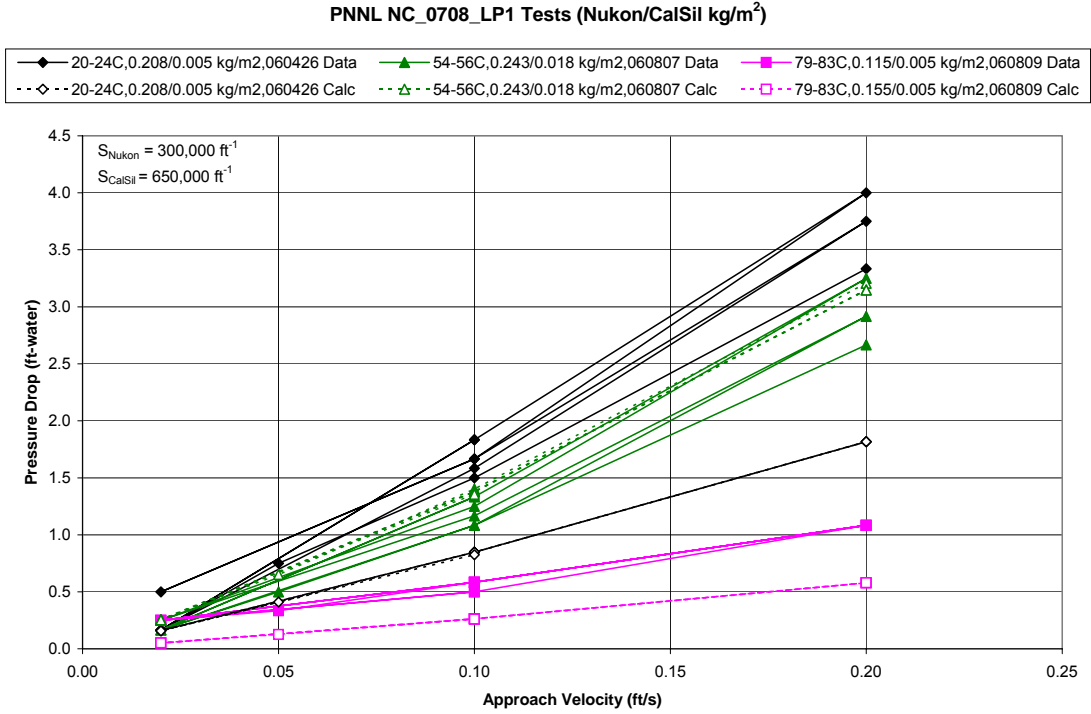


Figure 6.2-72 Data and Two-Vol. Predictions for First Velocity Cycle of Nukon/CalSil_0708 Tests

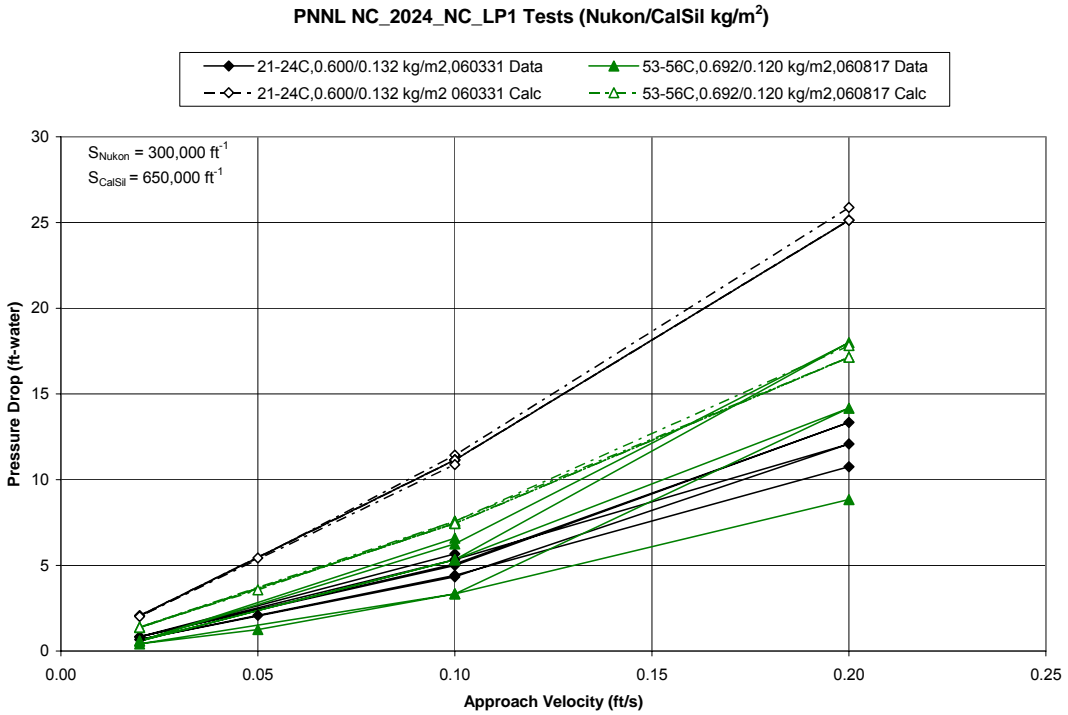


Figure 6.2-73 Data and Two-Vol. Predictions for First Velocity Cycle of Nukon/CalSil_2024 Tests

6.2.3 Comparison of Head Loss Predictions to PNNL Coatings Tests

The PWR containment buildings contain various types of debris that can be created by jet impingement or environmental conditions. These materials, including insulation and coatings, can contribute to the post-LOCA clogging of a sump screen. PNNL has performed head loss testing of a perforated plate sump structure using debris from two typical coating systems. Table 6.2-4 describes properties of the coating systems tested.

Table 6.2-4 Coatings Systems Used for PNNL Head Loss Testing

Designation	Description
ALK	Single-layer, low-density alkyd topcoat <ul style="list-style-type: none"> • unqualified nuclear containment coating • manufacturer: Ameron • coating name: Amercoat 5450 • density: 1.35 g/cc • thickness: one coat of 1.5 mils
ZE	Inorganic zinc primer with epoxy-phenolic topcoat <ul style="list-style-type: none"> • qualified nuclear containment coating • manufacturer: Ameron • coating name: primer—Dimetcote 6, topcoat—Amercoat 90 • density: primer—1.5 g/cc, topcoat—1.75 g/cc • thickness: one primer of 2.5 mils, two topcoats of 4 mils per coat

Note: 1 mil = 0.001 inch (0.0254 millimeter)

The coatings were prepared for testing using one of two methods. The coatings were either processed in a blender to obtain small particles or cut into small chips ranging in size from 0.003175 to 0.00635 m (1/8 to 1/4 inch). NUREG/CR-6917 (Ref. 24) describes in detail the tested coating systems and the methods used to produce the coatings and prepare them for testing. As indicated in Table 6.2-5, only one of the three tests performed in the PNNL large test loop produced a complete, continuous debris bed. Figure 6.2-74 provides plots of head loss versus approach velocity for Tests 060501-PQC_2609_LP1 and LP2. As expected from theory, the pressure drops measured at higher temperatures are lower than those at lower temperature. However, the data obtained from these tests are insufficient to correlate an analytical model for predicting head loss.

Table 6.2-5 PNNL Coatings Head Loss Tests Using a Perforated Plate

PNNL Test [#]	Coating Type	Coating Concentrations in Bed			Loop Temperature °C	Comments
		Blender Processed kg/m ²	1/4-inch Square kg/m ²	Total kg/m ²		
060501_PQC_2609_LP1, LP2	ALK	0.7	0.7	1.4	21, 82	
060502_POC_2609_LP1	ALK	1.4	0.0	1.4	21	Complete continuous bed not formed.
060504_PQZ_2609_LP1	ZE	0.7	0.7	1.4	21	Complete continuous bed not formed.

All tests performed using a perforated plate with 0.125-inch diameter holes and 40 percent open area.

[#] Area = 0.01863 m²

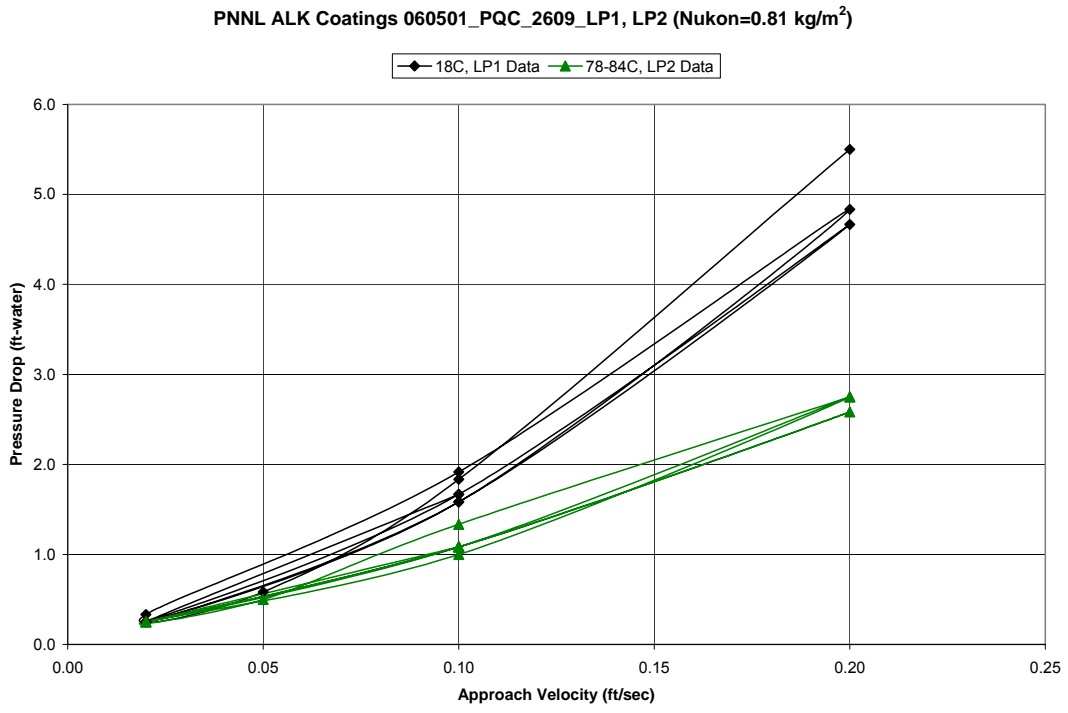


Figure 6.2-74 Head Loss for Alkyd Coatings Test 060501_PQC_2609_LP1, LP2

6.3 Comparisons of Head Loss Predictions to ANL Benchmark Test Data

As indicated in NUREG/CR-6913 (Ref. 25), the NRC contracted with ANL for the task of performing head loss testing of insulation material on a PWR sump screen in the presence of chemical precipitates. As part of the testing activities, ANL also performed several insulation head loss tests without chemical precipitates. The goal of these tests was to compare the head loss measurements obtained from the PNNL and ANL test facilities under similar insulation loadings. Table 6.3-1 lists the benchmark tests performed at ANL. ANL performed all tests using a perforated plate identical to the one used for the PNNL tests. NUREG/CR-6913 provides details about the ANL test facility. The pressure drops were measured using pressure transducers. Debris bed thickness measurements were made with a ruler, using visual observations.

Tests labeled BM-1 and BM-2 are Nukon-only tests, and tests labeled BM-3 used Nukon and CalSil in the test loop. Each BM-1, BM-2, and BM-3 test was performed twice to examine test repeatability. ANL did not measure the Nukon and CalSil masses in the debris beds for the Nukon/CalSil BM-3 tests; consequently, Table 6.3-1 does not report the loadings of these constituents.

Tables 6.3-2 and 6.3-3 provide information regarding the debris masses added to the test loop versus the masses deposited in the debris bed. Table 6.3-2 lists the bed masses used in the analysis presented in this section and used in the calculation of the debris loadings shown in Table 6.3-1. Figures 6.3-1 to 6.3-8 compare the head loss and bed thickness measurements for the Nukon-only BM-1 and BM-2 tests to (1) predictions obtained using the one-volume model developed in this report and (2) predictions obtained using the NUREG/CR-6224 calculational method. The test measurements and predictions could not be compared for the two BM-3 tests because, as previously stated, the masses of the Nukon and CalSil in these debris beds were not measured. Consequently, Tables 6.3-2 and 6.3-3 do not give information regarding the constituent masses in the debris bed for the BM-3 tests.

Table 6.3-1 ANL Benchmark Head Loss Tests Using a Perforated Plate

ANL Benchmark Tests*	Nukon			CalSil			Bed CalSil / Nukon	Total Debris kg/m ²	Loop Temperature °C
	Added kg/m ²	Bed kg/m ²	Bed / Added	Added kg/m ²	Bed kg/m ²	Bed / Added			
BM-1-A2-N4.6	0.287	0.235	0.817	0.0	0.0	NA	NA	0.235	25+/-5
BM-1-A2-N4.4 repeat2	0.274	0.237	0.864	0.0	0.0	NA	NA	0.237	25+/-5
BM-2-A2-N15.5	0.967	0.929	0.961	0.0	0.0	NA	NA	0.929	25+/-5
BM-2-A2-N15.5 repeat	0.967	0.909	0.940	0.0	0.0	NA	NA	0.909	25+/-5
BM-3-A2-N15.5-C3.1	0.967	NA	NA	0.193	NA	NA	NA	0.975	25+/-5
BM-3-A2-N15.5-C3.1 repeat	0.967	NA	MA	0.193	NA	NA	NA	0.944	25+/-5

* Pipe id = 5.625 inch, Screen id = 5.125 inch

Pipe area = 0.01603 m², Screen area = 0.01331 m²

Pipe area used in calculations.

Table 6.3-2 Debris Mass Summary for ANL Tests

ANL Benchmark Test (Using Perforated Plate)	Mass Added to Test Loop			Debris Bed Mass		
	Nukon Mass (g)	CalSil Mass (g)	Total Mass (g)	Measured Nukon Mass (g)	Measured CalSil Mass (g)	Total Weighed Mass (g)
BM-1-A2-N4.6	4.6	0.0	4.6	3.76	0.0	3.76
BM-1-A2-N4.4 repeat2	4.4	0.0	4.4	3.80	0.0	3.80
BM-2-A2-N15.5	15.5	0.0	15.5	14.89	0.0	14.89
BM-2-A2-N15.5 repeat	15.5	0.0	15.5	14.58	0.0	14.58
BM-3-A2-N15.5-C3.1	15.5	3.1	18.6	NA	NA	15.63
BM-3-A2-N15.5-C3.1 repeat	15.5	3.1	18.6	NA	NA	15.13

Table 6.3-3 Calculated Mass Fractions in Debris Bed for ANL Tests

ANL Benchmark Test (Using Perforated Plate)	Debris Bed Mass/Added Mass		
	Nukon	CalSil	Total
BM-1-A2-N4.6	0.817	NA	0.817
BM-1-A2-N4.4 repeat2	0.864	NA	0.864
BM-2-A2-N15.5	0.961	NA	0.961
BM-2-A2-N15.5 repeat	0.941	NA	0.941
BM-3-A2-N15.5-C3.1	NA	NA	0.840
BM-3-A2-N15.5-C3.1 repeat	NA	NA	0.813

6.3.1 Comparison of Head Loss Predictions to ANL Benchmark Tests

As indicated above, only the Nukon-only tests provided sufficient information regarding bed mass to permit calculational assessments. The one-volume and NUREG/CR-6224 calculations were performed using the same assumptions listed for the PNNL Nukon-only assessments. The one-volume pressure drop predictions for the ANL BM-1 and BM-2 benchmark tests exceed test measurements. The bed thickness predictions are below measurements for the ANL BM-1 tests and close to the ANL BM-2 measurements. Consequently, the one-volume approach provides acceptably conservative results when compared to test data. The figures indicate that the NUREG/CR-6224 calculational method underpredicts measured pressure drop for the BM-1 tests, but predicts values close to test measurements for the BM-2 tests. The NUREG/CR-6224 predictions for bed thickness are close to test measurements for the BM-1 tests, but exceed measurements for the BM-2 tests. All the NUREG/CR-6224 bed thickness predictions exhibit the unrealistic uncompacted limit illustrated by the constant bed thicknesses predicted at lower approach velocities.

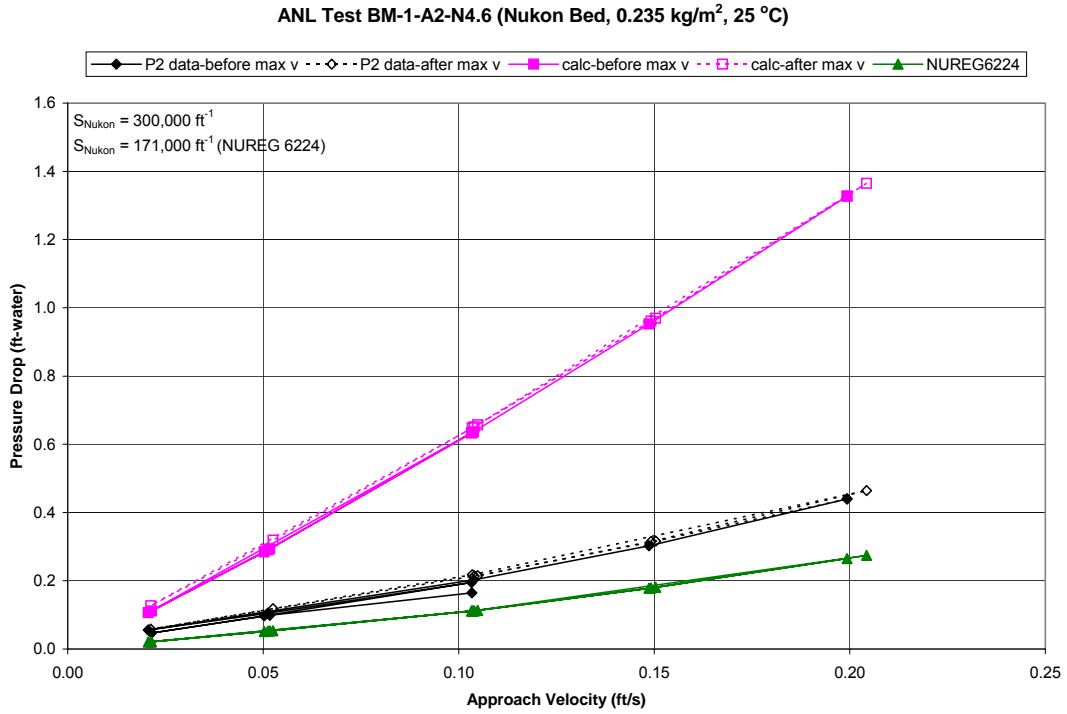


Figure 6.3-1 Head Loss for ANL BM-1 Benchmark Nukon Test BM-1-A2-N4.6

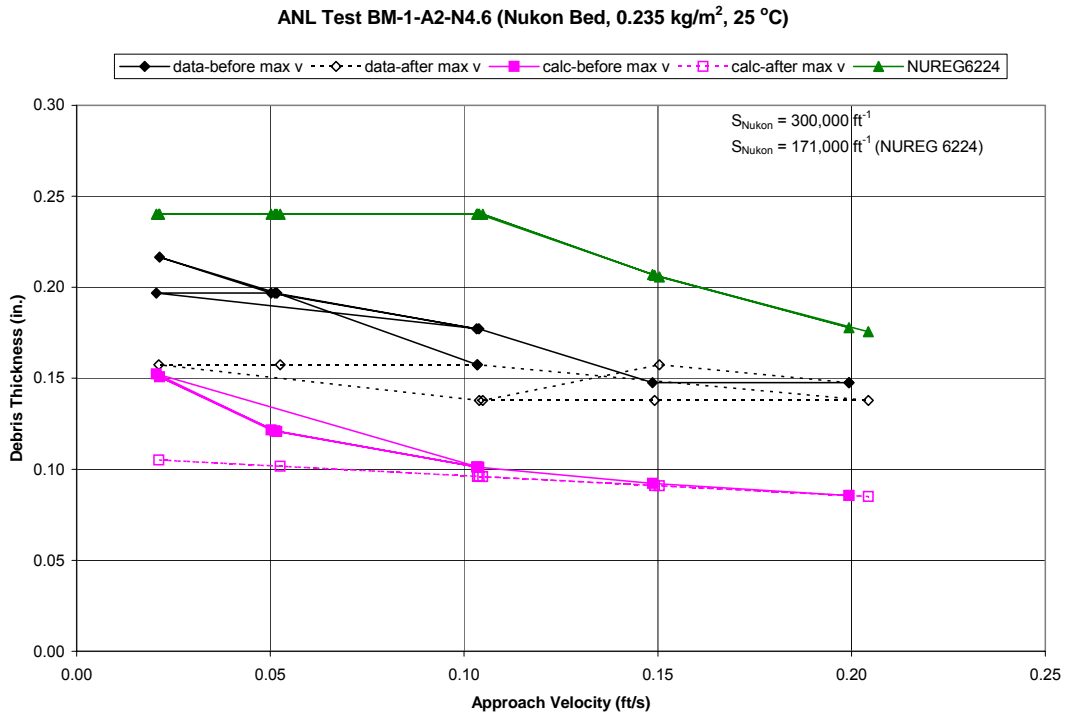


Figure 6.3-2 Bed Thickness for ANL BM-1 Benchmark Nukon Test BM-1-A2-N4.6

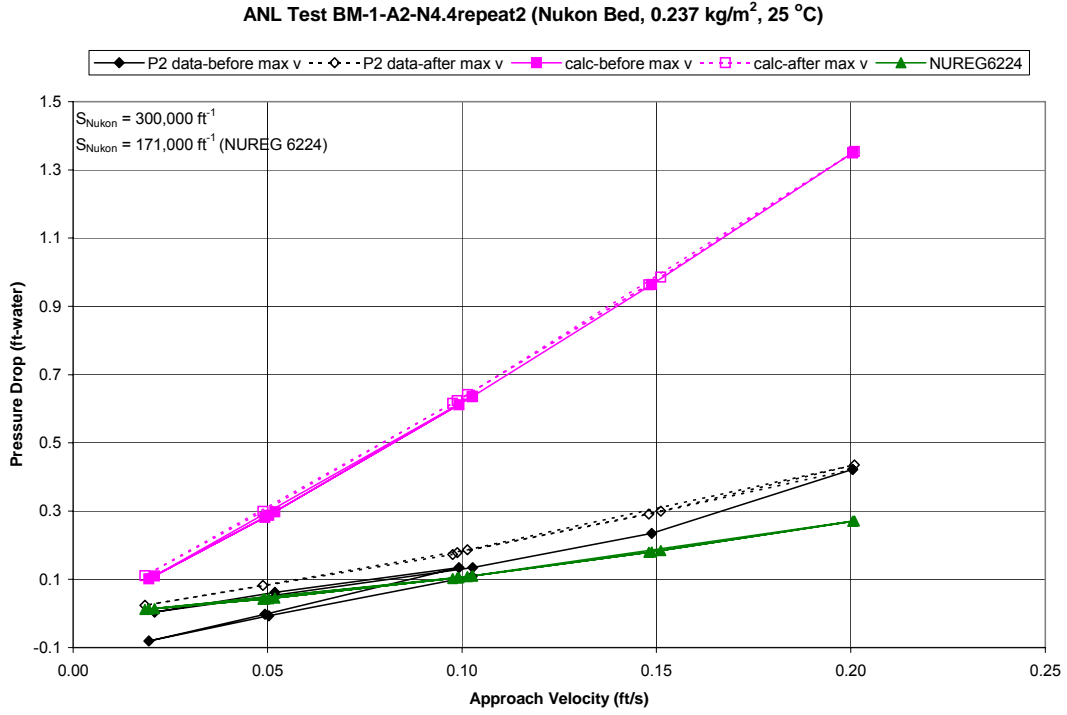


Figure 6.3-3 Head Loss for ANL BM-1 Benchmark Nukon Test BM-1-A2-N4.4 repeat2

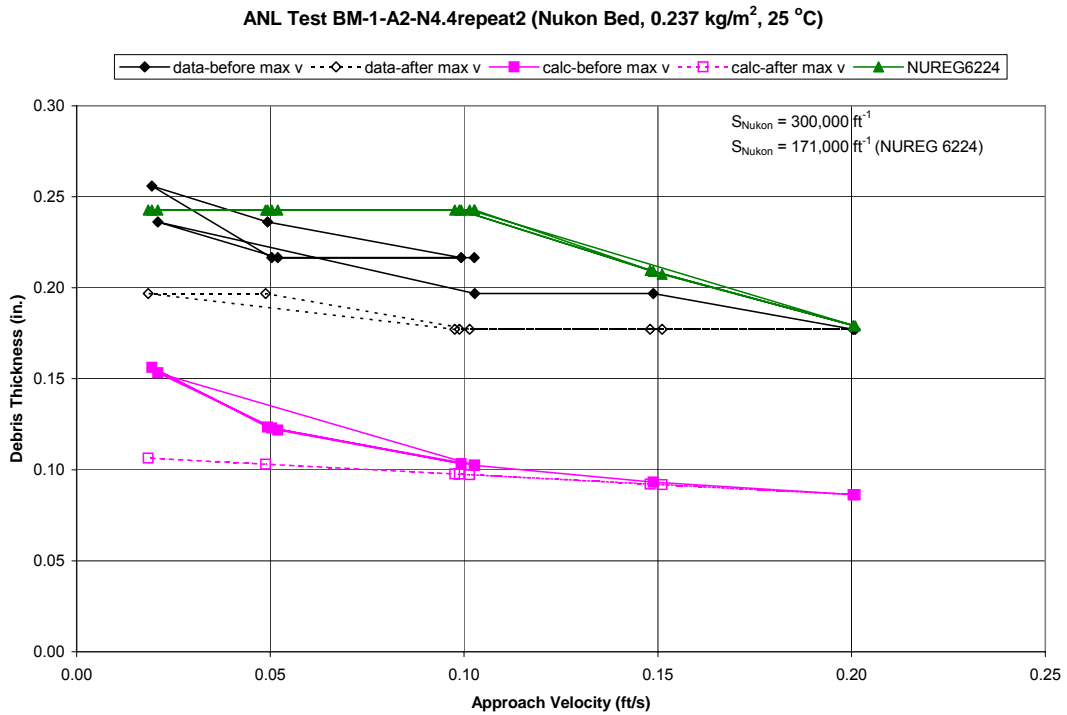


Figure 6.3-4 Bed Thickness for ANL BM-1 Benchmark Nukon Test BM-1-A2-N4.4 repeat2

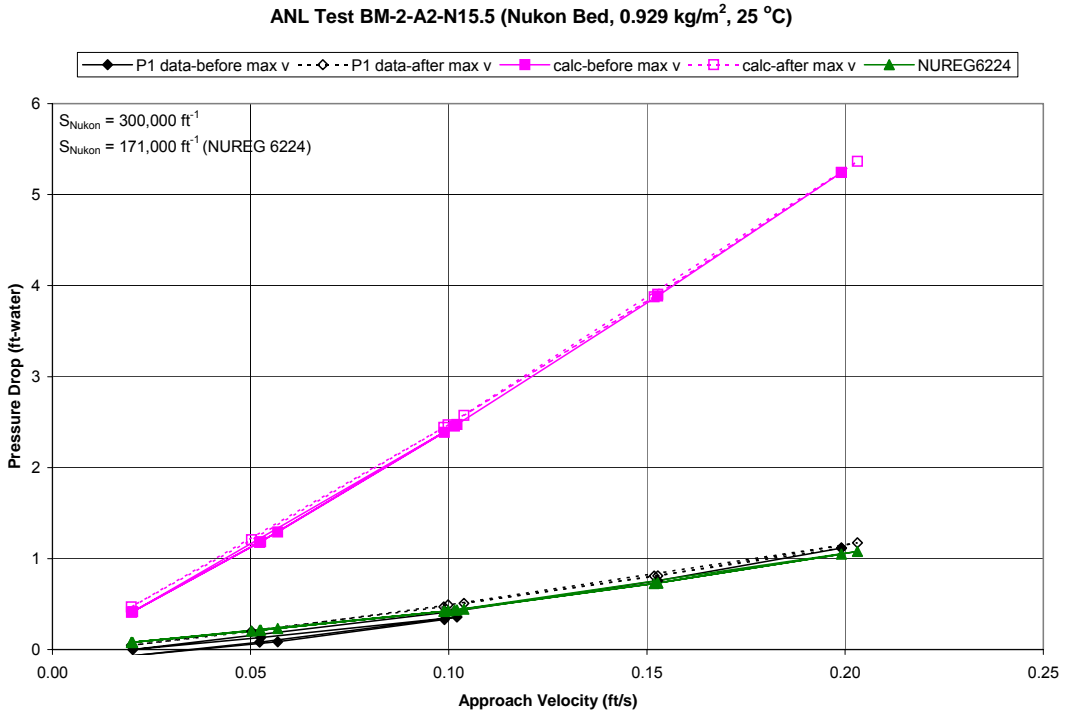


Figure 6.3-5 Head Loss for ANL BM-2 Benchmark Nukon Test BM-2-A2-N15.5

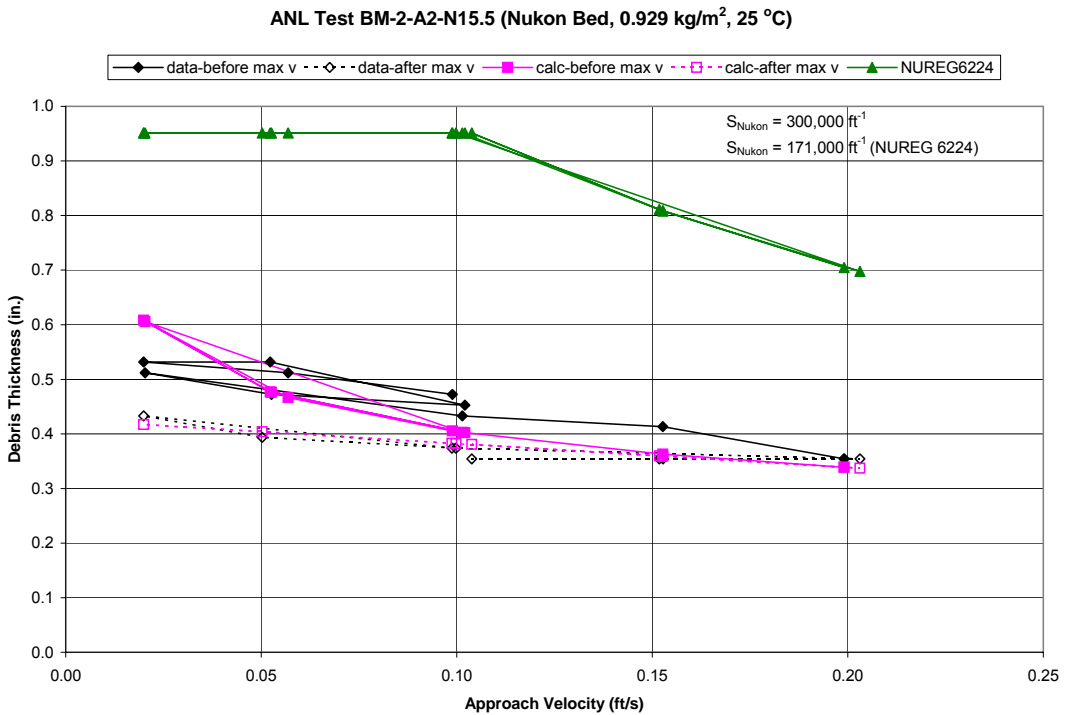


Figure 6.3-6 Bed Thickness for ANL BM-2 Benchmark Nukon Test BM-2-A2-N15.5

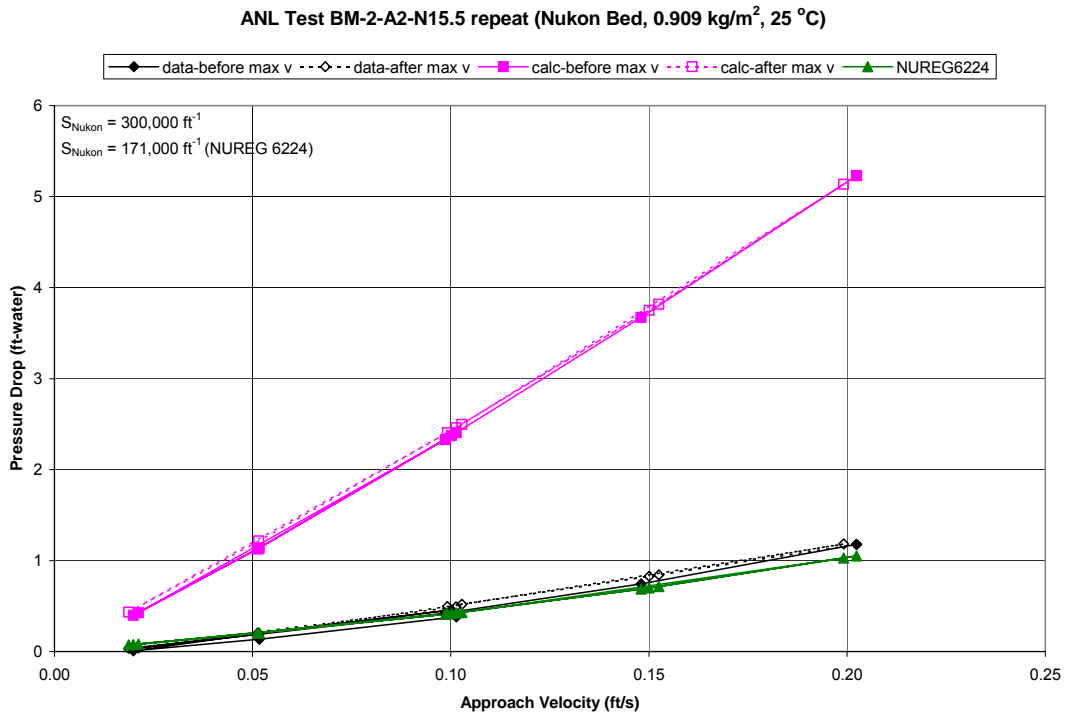


Figure 6.3-7 Head Loss for ANL BM-2 Benchmark Nukon Test BM-2-A2-N15.5 repeat

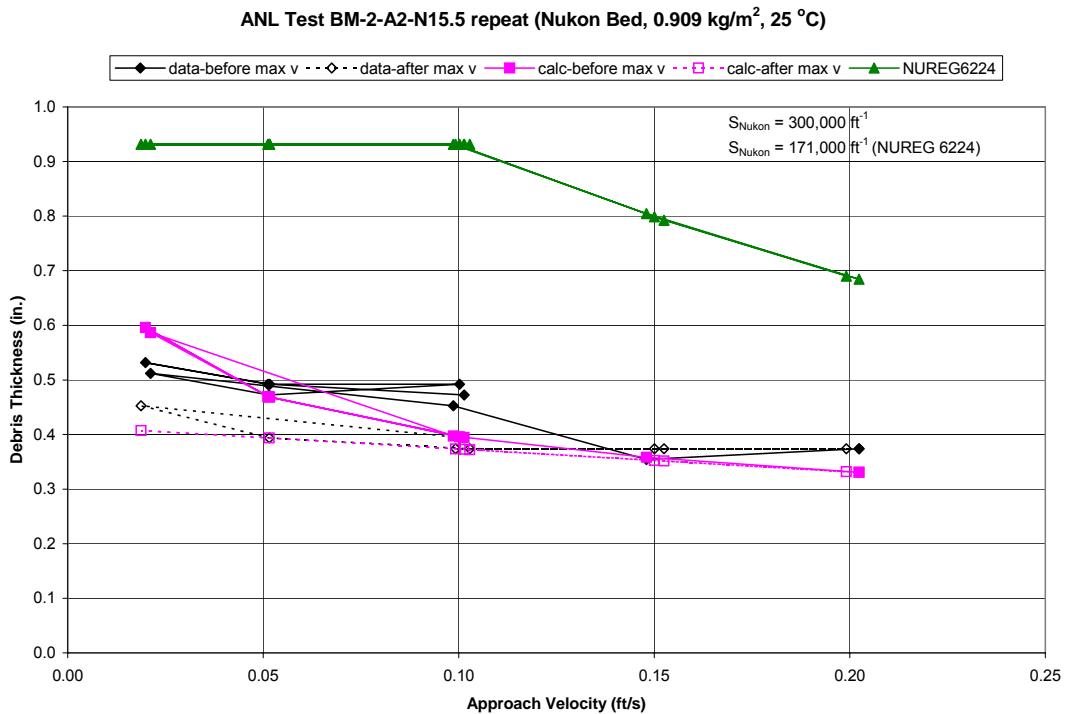


Figure 6.3-8 Bed Thickness for ANL BM-2 Benchmark Nukon Test BM-2-A2-N15.5 repeat

6.3.2 Comparison of Head Loss Data for the ANL and PNNL Benchmark Tests

The objective of the benchmark tests was to compare the data obtained from two test loops, the PNNL large test loop and the ANL test loop, for similar debris bed loadings and test conditions. Table 6.3-4 lists information regarding the debris masses and the test temperatures for the benchmark tests performed in the PNNL large loop. Table 6.3-4 entries can be directly compared to similar information for the ANL benchmark tests provided in Table 6.3-1. Table 6.3-5 compares the debris bed conditions for the ANL and PNNL benchmark tests. These tables show that the added debris loadings for the ANL tests were larger than those for the equivalent PNNL tests. This comparison also indicates that the ANL debris beds retain a larger percentage of the debris mass added to a test loop than do the beds for the equivalent tests performed on the PNNL large loop. Consequently, equivalent benchmark tests run at the two facilities may not be comparable because neither the added or bed debris loadings are close in value.

Table 6.3-4 PNNL Series 2 Benchmark Head Loss Tests Using a Perforated Plate

PNNL Benchmark Series 2 Tests [#]	Nukon			CalSil			Bed CalSil / Nukon	Bed Debris kg/m ²	Loop Temperature °C
	Added kg/m ²	Bed kg/m ²	Bed / Added	Added kg/m ²	Bed kg/m ²	Bed / Added			
BM-1, 060321_NO_0405_LP1*	0.217	0.171	0.785	0.0	0.0	NA	NA	0.171	21-22
BM-2, 060313_NO_1349_LP1	0.724	0.576	0.796	0.0	0.0	NA	NA	0.576	19-22
BM-3, 060323_NC_1619_LP1	0.724	0.626	0.865	0.145	0.020	0.140	0.032	0.646	21-22

[#] Pipe and Screen Area = 0.01863 m²

* Debris bed ruptured during retrieval; negligible debris material lost.

Table 6.3-5 Debris Bed Comparisons of the PNNL and ANL Benchmark Tests

Test Facility	Test	Debris Bed Concentration			Loop Temperature (°C) / (°F)
		Nukon (kg/m ²)	CalSil (kg/m ²)	Total (kg/m ²)	
ANL	BM-1-A2-N4.6	0.235	0.0	0.235	25±5 / 77±9
ANL	BM-1-A2-N4.4 repeat2	0.237	0.0	0.237	25±5 / 77±9
PNNL	BM-1, 060321_NO_0405_LP1	0.171	0.0	0.171	21-22 / 69.8-71.6
ANL	BM-2-A2-N15.5	0.929	0.0	0.929	25±5 / 77±9
ANL	BM-2-A2-N15.5 repeat	0.909	0.0	0.909	25±5 / 77±9
PNNL	BM-2, 060313_NO_1349_LP1	0.576	0.0	0.576	19-22 / 66.2-71.6
ANL	BM-3-A2-N15.5-C3.1	NA	NA	0.975	25±5 / 77±9
ANL	BM-3-A2-N15.5-C3.1 repeat	NA	NA	0.944	25±5 / 77±9
PNNL	BM-3, 060323_NC_1619_LP1	0.626	0.020	0.646	21-22 / 69.8-71.6

Both facilities standardized benchmark testing. The debris used for testing at the two facilities was prepared in the same manner, using the same debris preparation criteria. For tests with both Nukon and CalSil debris, the debris constituents were premixed before addition to the test loops at both facilities. The debris addition method was slightly different in the two loops. Debris was added to the ANL loop by pouring a debris slurry into a tee located at the top of the loop. For the PNNL large loop, the debris slurry was added to bypass piping located at the top of the test loop. The debris beds were formed at the same approach velocity, 0.0305 m/s (0.1 ft/s), in the two facilities. Testing in the two facilities used the same

series of test velocities and followed the same test procedure. In the ANL test loop, the debris bed thicknesses were obtained by visual measurements, using a ruler. The PNNL debris bed thicknesses were measured using a more accurate optical triangulation technique. NUREG/CR-6913 (Ref. 25) and NUREG/CR-6917 (Ref. 24) provide detailed information regarding the debris preparation, debris addition to the loops, and test procedures for the two facilities.

Figures 6.3-9 and 6.3-10 show the head loss data and debris bed thickness measurements for the BM-1 Nukon-only tests in the PNNL and ANL test facilities. The measured PNNL pressure drop is higher than those measured during the ANL testing, even though the measured Nukon debris bed loading for the PNNL tests (0.171 kg/m^2) was lower than those for the ANL tests (0.235 and 0.237 kg/m^2). The accuracy of the pressure drop measurements for the ANL BM-1 tests is suspect because negative pressure drops were recorded during testing. NUREG/CR-6913 (Ref. 25) suggests that pressure drop variations may be attributable to the sensitivities of the pressure measurement instruments used at ANL. The transducers in the ANL loop are rated for 1.5-percent error at a full-scale pressure of 150 psi ($1.034 \times 10^6 \text{ Pa}$); however, NUREG/CR-6913 states that the pressure transducers were more accurate than implied by their ratings. The debris bed thicknesses measured for the PNNL test are smaller than those measured during ANL testing, a result that is consistent with the fact that smaller debris bed loadings were measured for the PNNL test than for the ANL tests. The ANL visual bed thickness measurements are also less accurate than the values obtained from the optical triangulation method used at PNNL.

Figure 6.2-31, which compares the one-volume bed thickness predictions to the test data for the PNNL BM-1 test, indicates that the one-volume method predicts debris bed thicknesses that are close to, but slightly lower than, actual measurements. Figures 6.3-2 and 6.3-4 show that the one-volume method underpredicts the debris bed thickness for the two ANL BM-1 tests. The differences in bed thickness may result from the differences in Nukon debris bed loading for the ANL and PNNL tests. However, the debris bed loading differences do not completely account for the differences in debris bed thicknesses measured at the two test facilities. The pressure drop and bed thickness comparisons suggest that the debris bed created in the PNNL test loop may have been initially compressed by a larger amount than the debris beds created at the ANL test loop. The initial larger bed compression in the PNNL test compared to the ANL tests may result from several effects, including differences in loop design and operation, as well as measurement inaccuracy. It may also be related to differences in debris preparation and debris addition at the two test facilities. Efforts were made to standardize the debris preparation; however, the two facilities may have had unknown differences. Differences in debris preparation can affect the value of the specific surface area for the Nukon fibers in the debris bed, and differences in the debris addition methods at the two facilities can affect the bed formation and debris distribution in the bed. Consequently, it is suggested that the initial debris densities in the beds formed at the PNNL and ANL test facilities for the BM-1 tests differ, which implies differences in debris distribution and bed thickness, which ultimately affect the measured pressure drops.

Figure 6.3-11 and 6.3-12 compare the pressure drops and debris bed thicknesses measured for the PNNL and ANL BM-2 tests. The measured pressure drops for the PNNL BM-2 tests are larger than those for the ANL BM-2 data by about the same percentage as that for the BM-1 tests. The ANL BM-2 tests also recorded negative pressure differentials that raise concerns regarding the accuracy of the pressure drop measurements. The measured debris bed thicknesses for the PNNL and ANL BM-2 tests are close in value, which may suggest that the bed formation processes for these tests were similar at both facilities. However, the Nukon mass retained in the debris beds for the ANL BM-2 tests (0.929 and 0.909 kg/m^2) is larger than the mass retained in the PNNL BM-2 test debris bed (0.576 kg/m^2). Calculations indicate that the debris density for the PNNL BM-2 test is lower than the comparable value for the ANL BM-2 tests. This would suggest that the PNNL pressure drops should actually be lower than those measured for the

ANL tests; however, that is not the case. Therefore, differences in debris preparation and debris addition as well as inaccuracies in pressure drop measurements at the two facilities appear to be the most likely causes for the pressure drop differences between the PNNL and ANL BM-2 tests.

Figures 6.3-13 and 6.3-14 compare the pressure drop and bed thickness measurements for the Nukon/CalSil BM-3 benchmark tests performed at the PNNL and ANL test loops. The head loss and bed thickness measurements for the BM-3 tests at the PNNL and ANL facilities are close in value. The ANL BM-3 tests did not exhibit the negative pressure drop readings observed in the ANL BM-1 and BM-2 tests. Additionally, the debris beds created in the PNNL and ANL test loops appear to exhibit approximately the same initial compression, as demonstrated by the similarity in measured initial debris bed thicknesses; however, the total debris bed loadings (0.975 and 0.944 kg/m²) for the ANL tests are higher than the loading for the PNNL test (0.646 kg/m²). Because of the closeness of the test data for all three BM-3 tests, it is expected that approximately the same fraction of the Nukon and CalSil masses added to the test loops was deposited in the debris beds and that similar CalSil particle distributions existed in all three test beds. (A direct comparison of the constituent Nukon and CalSil debris bed masses was not possible because the values of the constituent masses for the ANL debris beds were not measured; however, the constituent masses were measured for the PNNL test.) The lower debris bed concentrations of the PNNL test would be expected to result in lower pressure drops than the ANL tests which had higher debris bed concentrations. However, the differences in debris bed concentrations for the PNNL and ANL tests are not consistent with the similarity of the measured pressure drops from the two test facilities.

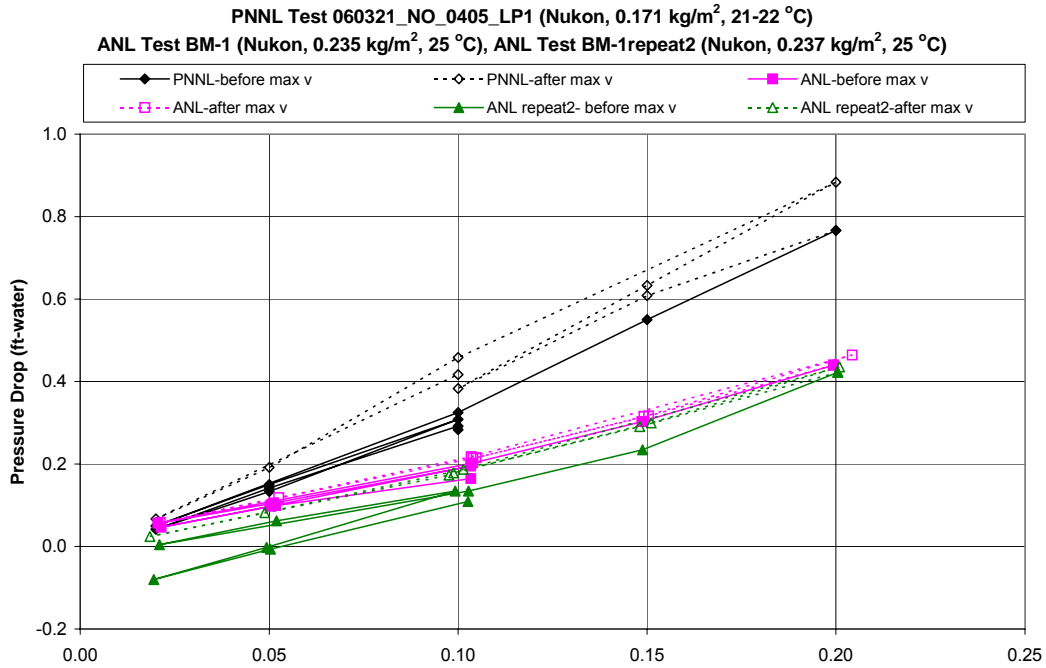


Figure 6.3-9 Head Loss Data for ANL and PNNL BM-1 Benchmark Nukon Tests

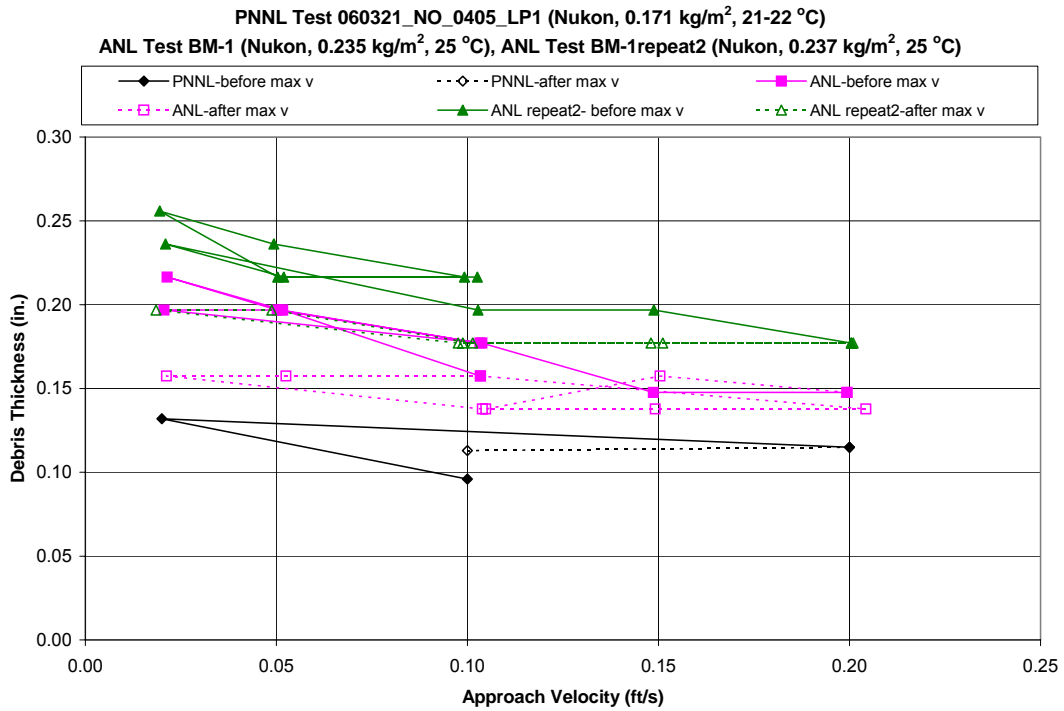


Figure 6.3-10 Bed Thickness Data for ANL and PNNL BM-1 Benchmark Nukon Tests

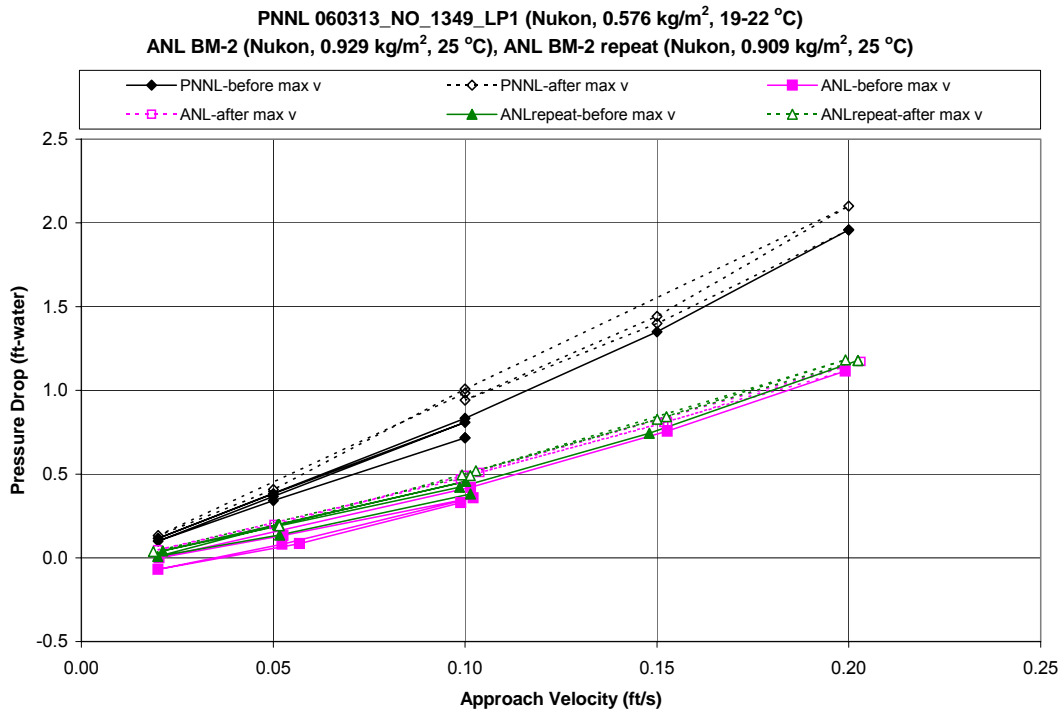


Figure 6.3-11 Head Loss Data for ANL and PNNL BM-2 Benchmark Nukon Tests

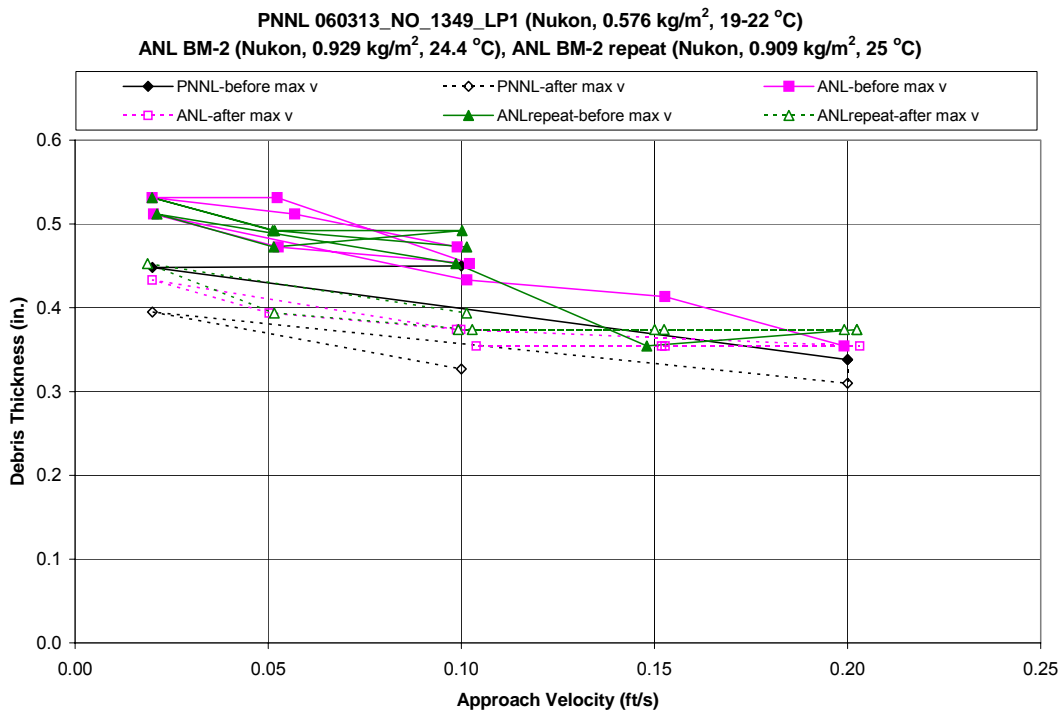


Figure 6.3-12 Bed Thickness Data for ANL and PNNL BM-2 Benchmark Nukon Tests

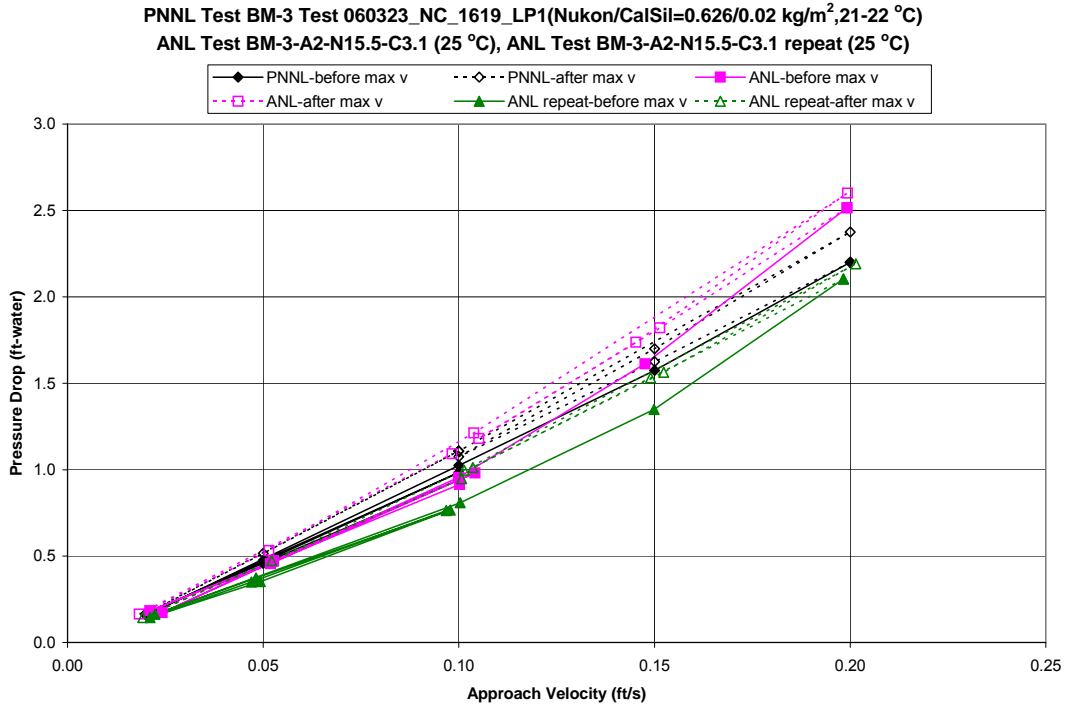


Figure 6.3-13 Head Loss Data for ANL and PNNL BM-3 Benchmark Nukon/CalSil Tests

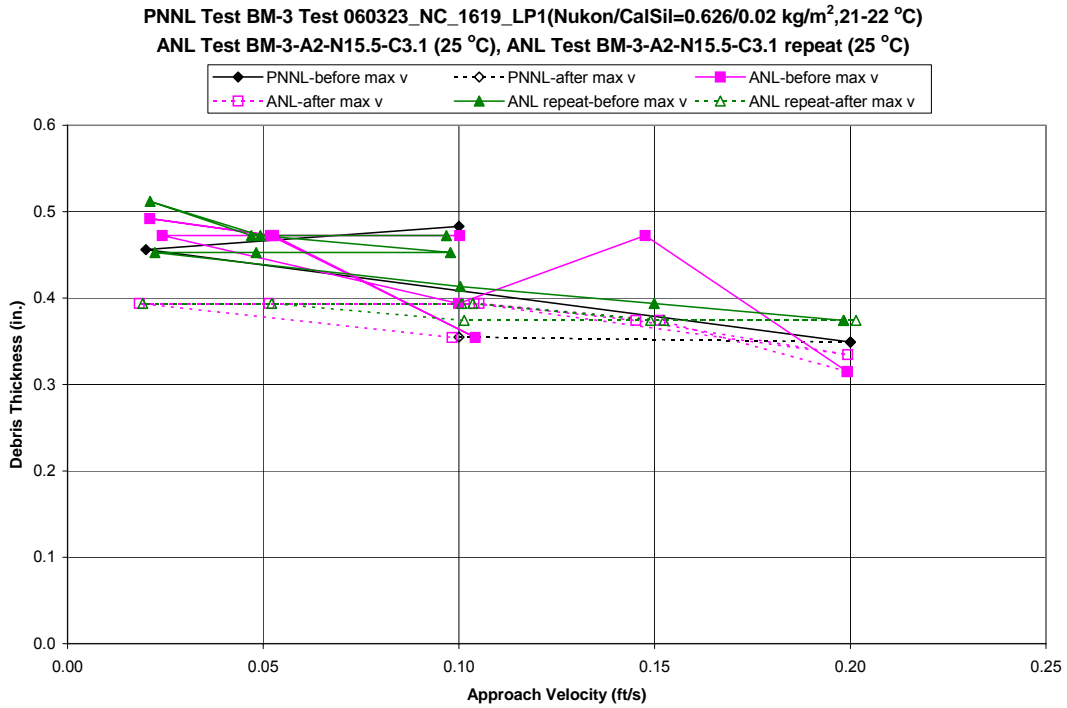


Figure 6.3-14 Bed Thickness Data for ANL and PNNL BM-3 Benchmark Nukon/CalSil Tests

6.4 Comparisons of Head Loss Predictions with LANL/UNM Test Data

As indicated in Section 4.1.2, the mass of the debris deposited in the debris bed was not measured for the LANL/UNM tests described in NUREG/CR-6874 (Ref. 3). Consequently, questions arise regarding the input accuracy of any predictive calculations. Despite this problem, this section presents comparisons of the results of the calculational methods to the test measurements for several LANL/UNM tests.

Table 6.4-1 lists the tests used for these comparisons. The tests included one debris bed composed entirely of Nukon and six Nukon/CalSil debris beds. This table also presents estimates of the CalSil mass actually present in the debris bed, which were obtained by considering the turbidity measurements of the test water. However, corrections were not made for any debris mass that accumulated, settled, or became caught in parts of the test loop other than the debris bed. The turbidity measurements in the test loop varied during the test duration. Therefore, the CalSil bed estimate in Table 6.4-1 reflects the condition determined to exist during the major portion of each test. Table 6.4-1 also lists Series 1 tests that PNNL performed to match as closely as possible the LANL/UNM test conditions.

Table 6.4-1 Debris Bed Mass Comparisons for Similar PNNL and LANL/UNM Tests

LANL Test*	Added Nukon kg/m ²	Added CalSil kg/m ²	Estimated Bed CalSil kg/m ²	Bed CalSil / Nukon	Total Debris kg/m ²	Loop Temperature °C	PNNL Series 1 Tests [#]	Added Nukon kg/m ²	Added CalSil kg/m ²	Bed Nukon kg/m ²	Bed CalSil kg/m ²	Bed CalSil / Nukon	Total Debris kg/m ²	Loop Temperature °C
							051114_SO_0000_L1	0.0	0.0	0.0	0.0	NA	0.0	17-24
							051128_SO_0000_L1	0.0	0.0	0.0	0.0	NA	0.0	16-19
1a	1.77	0.00	0.00	0.0	1.77	21	051108_NO_3067_L1 ^{&}	1.65	0.0	1.79	0.00	0.0	1.79	20-30
							060125_NO_3067_L1 ⁺	1.65	0.0	1.72	0.00	0.0	1.72	22-26
6b	1.53	0.84	0.83	0.544	2.36	40-46	051115_NC_4098_L1	1.42	0.78	1.20	0.73	0.610	1.92	21-25
6e	1.07	0.53	0.53	0.497	1.60	49-57	051117_NC_2776_L1	0.99	0.50	0.99	0.35	0.349	1.33	21-27
6e2	1.07	0.53	0.53	0.500	1.60	38	051128_NC_2776_L2	0.99	0.50	0.92	0.34	0.363	1.26	21-27
6f	0.61	0.31	0.30	0.493	0.91	57-62	051121_NC_1586_L1	0.57	0.28	0.56	0.17	0.300	0.73	16-27
6h	0.23	0.11	0.11	0.460	0.33	32-46	051110_NC_0595_L1 [^]	0.21	0.11	0.21	0.05	0.249	0.27	21-25
6i	0.84	0.42	0.41	0.495	1.25	57-61	051123_NC_2181_L1	0.78	0.39	0.79	0.25	0.316	1.03	22-32

* Pipe id= 11-3/8 inch, Pipe Area = 0.06556 m²

[#] Area = 0.01863 m²

[&] Metal/rust particles present in bed.

⁺ Construction debris present in bed.

[^] Best estimate bed masses; bed ruptured during retrieval.

Consistent with Table 6.4-1, head loss calculations for the LANL/UNM tests using the one- and two-volume calculational methods presented in this report assume that the Nukon mass present in the debris bed is equal to the Nukon mass added to the debris bed. The debris bed CalSil mass is assumed equal to the average of the CalSil bed mass estimates, which varied during testing. Head loss calculations obtained using the procedure described NUREG/CR-6224 are also presented for comparison. For the NUREG/CR-6224 calculations, the bed Nukon mass is also assumed equal to the Nukon mass added to the test loop, and the bed CalSil mass is also assumed equal to the average of the CalSil bed mass estimates. The one-volume, two-volume, and NUREG/CR-6224 calculations were performed using the same assumptions listed for the PNNL assessments.

The Nukon specific surface areas used for the one- and two-volume calculations and for the NUREG/CR-6224 calculations differ. The one- and two-volume calculations use a Nukon specific surface area of 984,252 m⁻¹ (300,000 ft⁻¹) as recommended in Section 4.3.1. The NUREG/CR-6224 calculation uses a value of 561,024 m⁻¹ (171,000 ft⁻¹) for the Nukon specific surface area as recommended in NUREG/CR-6874.

Additionally, as described in Section 4.3.1 and listed in Table 4.3-1, the CalSil specific surface areas used for the two-volume calculations and for the NUREG/CR-6224 calculations differ. The current study recommends that a value of $2,132,546 \text{ m}^{-1}$ ($650,000 \text{ ft}^{-1}$) be used for the CalSil specific surface area in the two-volume calculations. NUREG/CR-6874 recommends using different values for CalSil specific surface area depending on whether the Nukon/CalSil bed is classified as a thick or thin bed. The NUREG/CR-6224 calculations use a thick bed value of $1,968,504 \text{ m}^{-1}$ ($600,000 \text{ ft}^{-1}$) and a thin bed value of $2,887,139 \text{ m}^{-1}$ ($880,000 \text{ ft}^{-1}$).

Except for Test 6e2, all the debris beds for the tests discussed in this section were built at a 0.0305 m/s (0.1 ft/s) approach velocity, and testing consisted of a single profile of velocity increases followed by a velocity decrease. The debris bed for Test 6e2 was built at the same approach velocity as Test 6e; however, measurements were made for the peak velocity followed by a velocity decrease and a second velocity increase and decrease.

Figures 6.4-1 and 6.4-2 compare the results of the one-volume head loss calculations to data from LANL/UNM Test 1a. The debris bed for Test 1a was composed entirely of Nukon fibers. Because the debris bed was composed entirely of one debris type, it was only necessary to perform calculations using the one-volume method, as indicated in Section 5. Only one temperature measurement was made during testing. Consequently, all calculations were performed for a water temperature of $21 \text{ }^\circ\text{C}$ ($70 \text{ }^\circ\text{F}$).

Figure 6.4-1 shows that the head loss predictions for Nukon-only Test 1a using the one-volume method overpredict the head loss measurements; the predictions using the NUREG/CR-6224 calculations shown in Figure 6.4-1 are close to test measurements. The overprediction using the one-volume calculation could be the result of the inaccuracies in assessing the actual Nukon mass in the debris bed. When the debris beds for the PNNL Series 2 Nukon-only tests were weighed, measurements revealed that only about 80 percent of the mass added to the test loop was deposited in the debris bed. Figure 6.4-3 shows that if the debris bed mass for LANL/UNM Test 1a was reduced to 80 percent of the added mass, the head loss calculated using the one-volume method drops closer to test measurements. Similarly, Figure 6.4-3 shows that the NUREG/CR-6224 predictions drop below head loss measurements when the calculation assumes that 80 percent of the added mass is present in the debris bed.

Testers made no debris bed thickness measurements during this test. Figure 6.4-2 compares debris bed thicknesses determined using the one-volume and NUREG/CR-6224 calculational methods. Substantial differences exist between the calculated thicknesses, especially at the lower approach velocities. The NUREG/CR-6224 calculation also displays a greater variation in debris bed thickness than the one-volume method over the range of approach velocities.

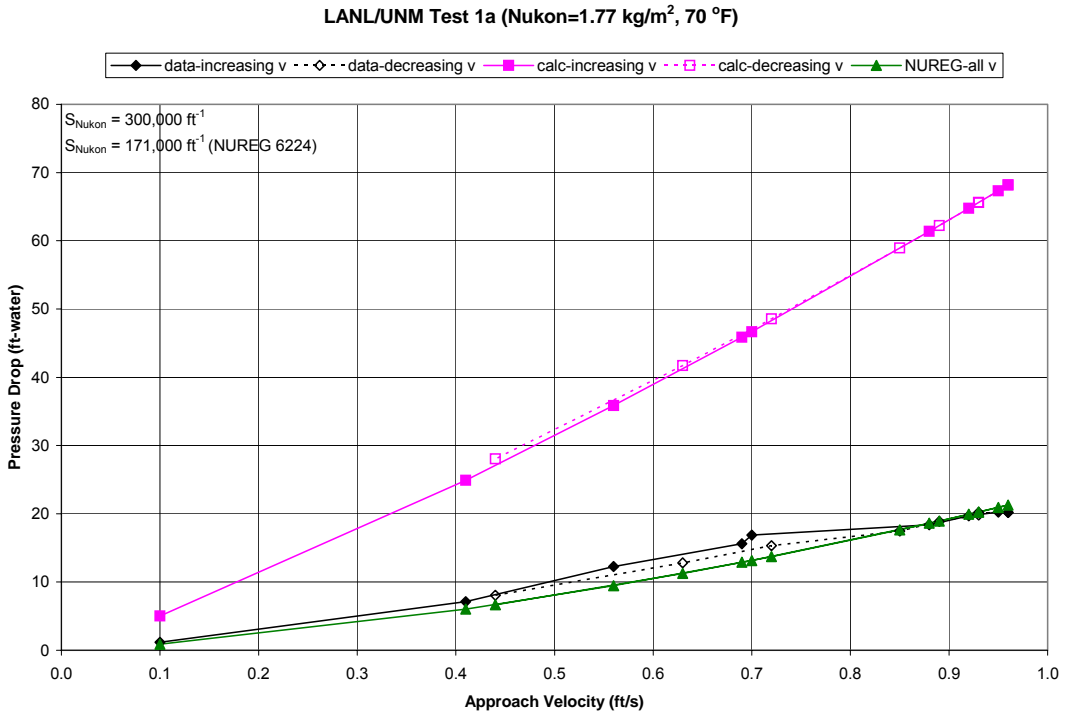


Figure 6.4-1 Head Loss for LANL/UNM Nukon-Only Test 1a

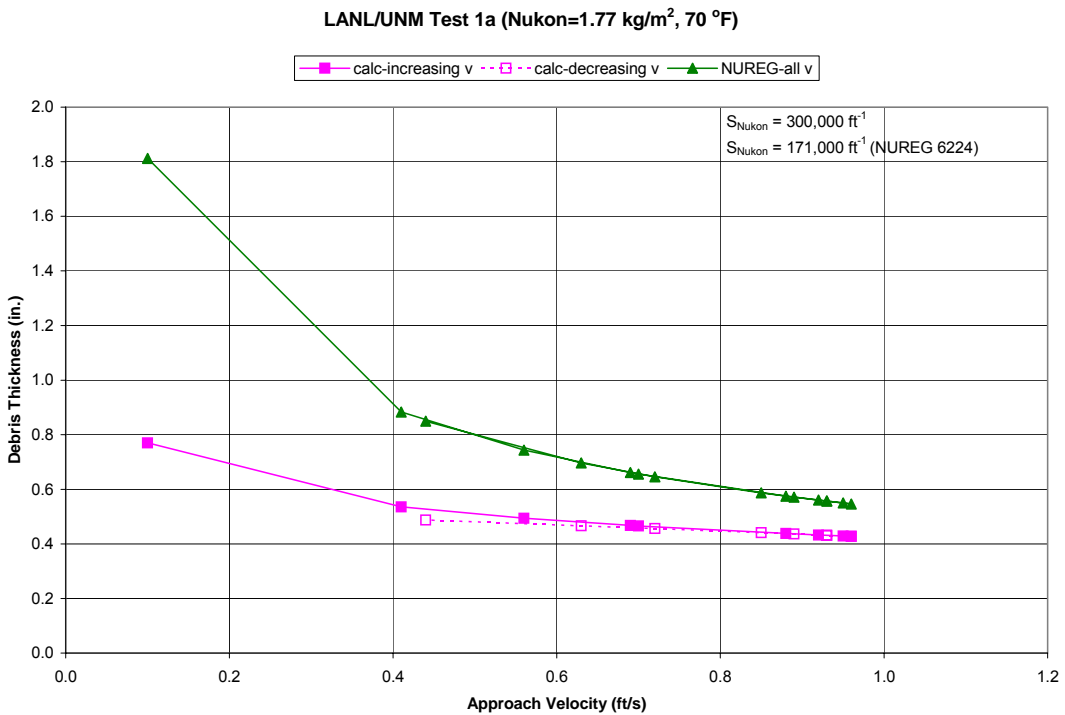


Figure 6.4-2 Bed Thickness for LANL/UNM Nukon-Only Test 1a

LANL/UNM Test 1a (Nukon=1.77 kg/m², 70 °F)

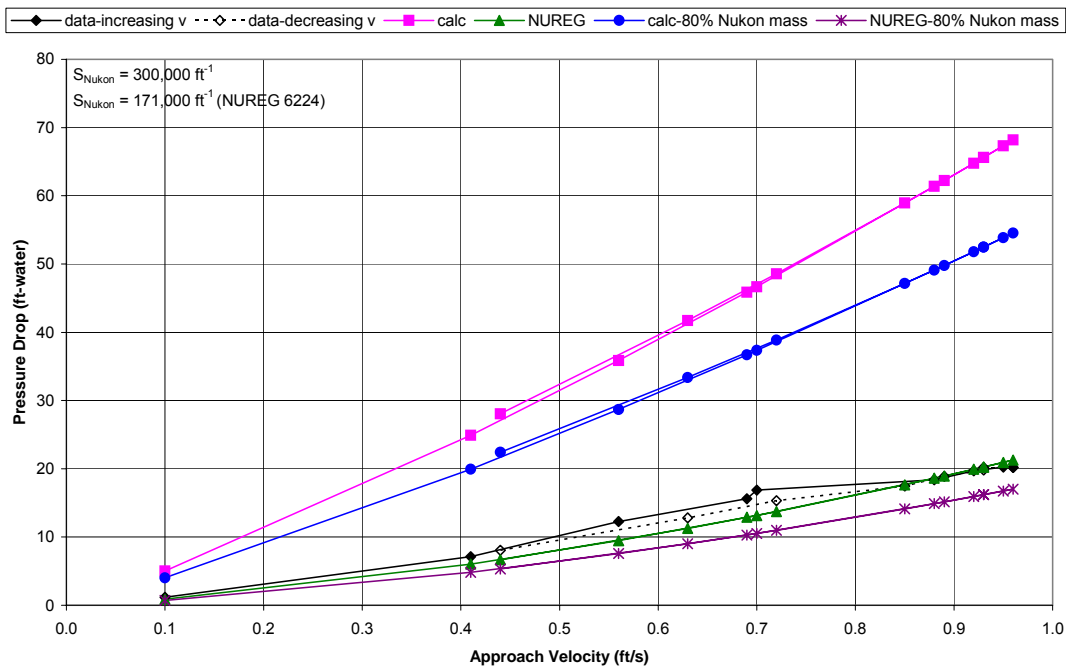


Figure 6.4-3 Head Loss for LANL/UNM Nukon-Only Test 1a Using 80 Percent Added Mass

The following figures present test results and predictions for the LANL/UNM Series 6 tests. These tests were all performed using Nukon/CalSil debris beds. Bed thickness measurements were also made at each reported approach velocity during this testing. The bed thickness was optically measured using a scale that was held against the clear wall of the test section. Consequently, these measurements are best estimates of the average bed thickness, which could vary across the debris bed surface.

Figures 6.4-4 and 6.4-5 provide plots of predictions and measurements for Nukon/CalSil Test 6b. The recorded water temperatures varied during test performance from 40 °C (104 °F) at the start of testing to 46 °C (115 °F) at the end of the test. Consequently, part of the variation in predictions and measurements results from changes in water properties during testing.

Because the debris bed for Test 6b is classified as a thick bed, the NUREG/CR-6224 calculation uses a CalSil specific surface area of 1,968,504 m⁻¹ (600,000 ft⁻¹).

The predictions obtained using the NUREG/CR-6224 calculation slightly overpredict head loss measurements. Predictions obtained using the two-volume method overpredict test measurements. This variation is not surprising because the two-volume calculation is expected to provide an upper limit head loss that represents a saturated CalSil layer in the debris bed. Additionally, the two-volume calculation could be expected to overpredict pressure drop because of the assumption that all the added debris mass is deposited in the bed.

Figure 6.4-5 compares bed thickness predictions with test measurements. The two-volume predictions are higher than the bulk of the measurements. However, both the two-volume and NUREG/CR-6224 test predictions probably fall within the probable error band for the test measurements.

LANL/UNM Test 6b (Nukon/CalSil=1.53/0.83 kg/m², 40-46C) - Two Volume Model

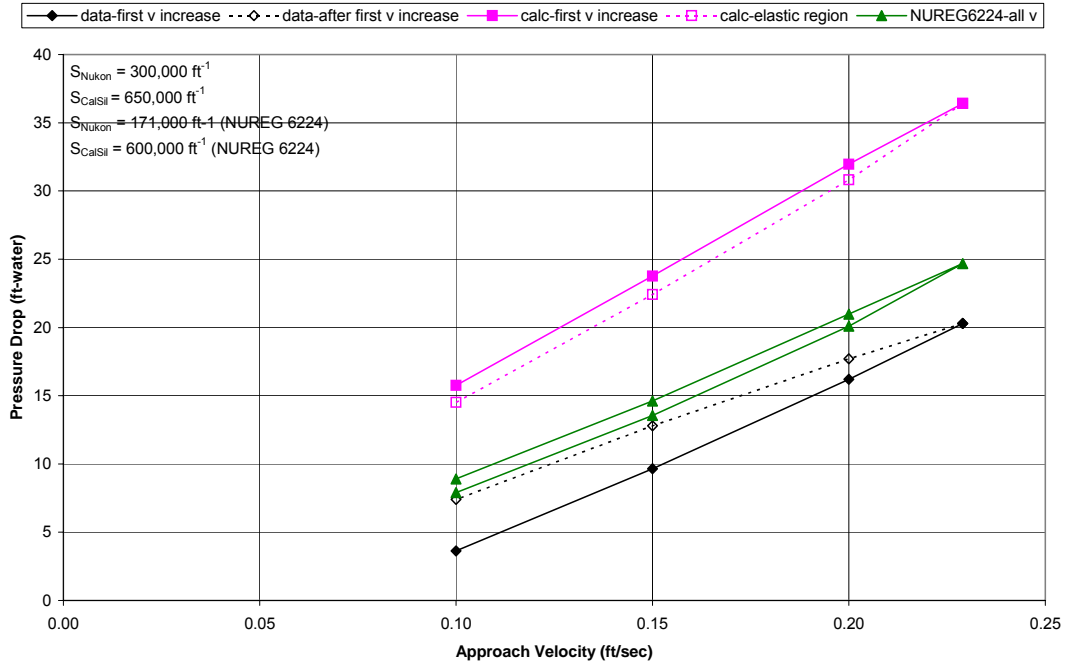


Figure 6.4-4 Head Loss for LANL/UNM Nukon/CalSil Test 6b

LANL/UNM Test 6b (Nukon/CalSil=1.53/0.83 kg/m², 40-46C) - Two Volume Model

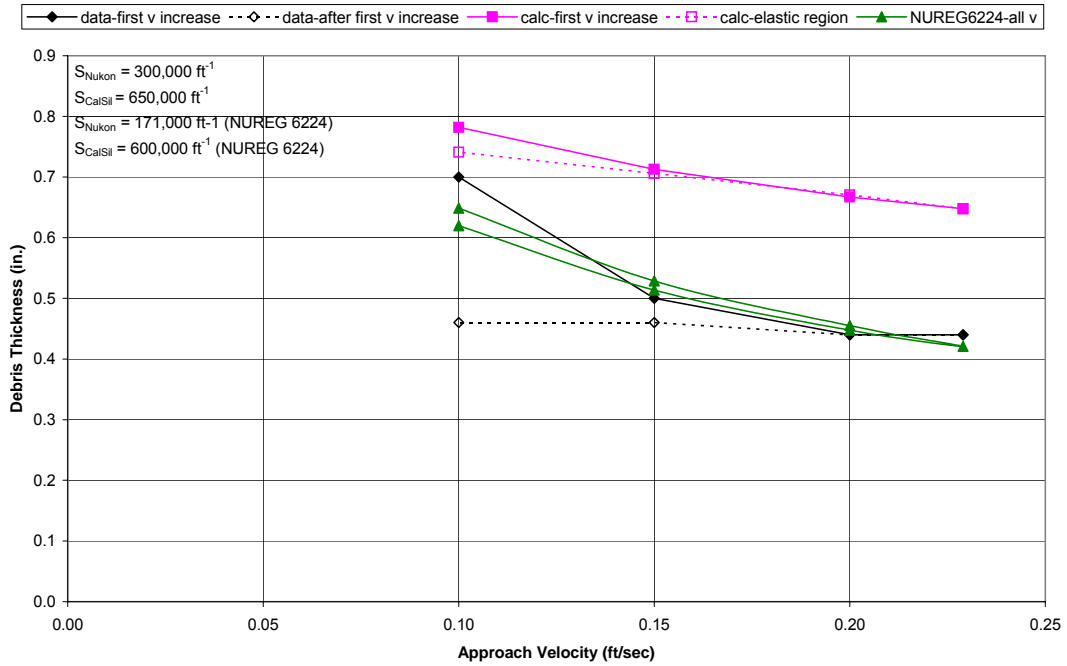


Figure 6.4-5 Bed Thickness for LANL/UNM Nukon/CalSil Test 6b

Figures 6.4-6 and 6.4-7 show comparisons of test predictions and measurements for Nukon/CalSil Test 6e. The NUREG/CR-6224 calculation used a Nukon specific surface area of $1,968,504 \text{ m}^{-1}$ ($600,000 \text{ ft}^{-1}$).

The water temperature varied during this test from $49 \text{ }^\circ\text{C}$ ($121 \text{ }^\circ\text{F}$) at the start of testing to $57 \text{ }^\circ\text{C}$ ($134 \text{ }^\circ\text{F}$) by the end of testing. Some of the variance in measured and predicted head loss at a given approach velocity results from the changes in water properties during the velocity increase and decrease that occur because of the variation in water temperature.

The head loss predicted by the NUREG/CR-6224 method overpredicts test data. As might be expected from a calculational method intended to provide upper limit values, the results from the two-volume calculation predict pressure drops much larger than test measurements. Additionally, the pressure drop overpredictions by the two-volume method could be expected because of the assumption that all the added debris mass is deposited in the bed. All the bed thickness predictions and measurements are close in value and probably within the error band of the measurements.

LANL/UNM intended Test 6e2 to duplicate Test 6e; therefore, the Nukon and CalSil loadings used for the calculations are the same. Figures 6.4-8 and 6.4-9 present plots comparing the predicted and measured head losses and bed thicknesses at different approach velocities. The Nukon and CalSil specific surface areas used for Test 6e2 calculations were the same as those used for the Test 6e calculations. Temperature and debris bed measurements were not made at all recorded head losses. Consequently, calculations assumed that the loop water remained at constant at the initial reading of $38 \text{ }^\circ\text{C}$ ($100 \text{ }^\circ\text{F}$) and that no head loss variations resulting from temperature changes could be predicted.

Data measurements for Test 6e2 were performed for a different, expanded approach velocity history than that used for Test 6e. As previously mentioned, Test 6e2 possessed an initial velocity increase followed by a velocity decrease and then a second velocity increase and decrease. The NUREG/CR-6224 head loss predictions are close to test measurements. The two-volume head loss predictions again provide upper bound values that exceed test measurements and are affected by the assumption that all the added debris mass is deposited in the debris bed. The two-volume bed thicknesses shown in Figure 6.4-9 slightly exceed test measurements. The NUREG/CR-6224 predictions of bed thicknesses are close to the measurements. All the predictions probably fall within the error band of the measurements.

LANL/UNM Test 6e (Nukon/CalSil=1.07/0.53 kg/m², 49-57C) - Two Volume Model

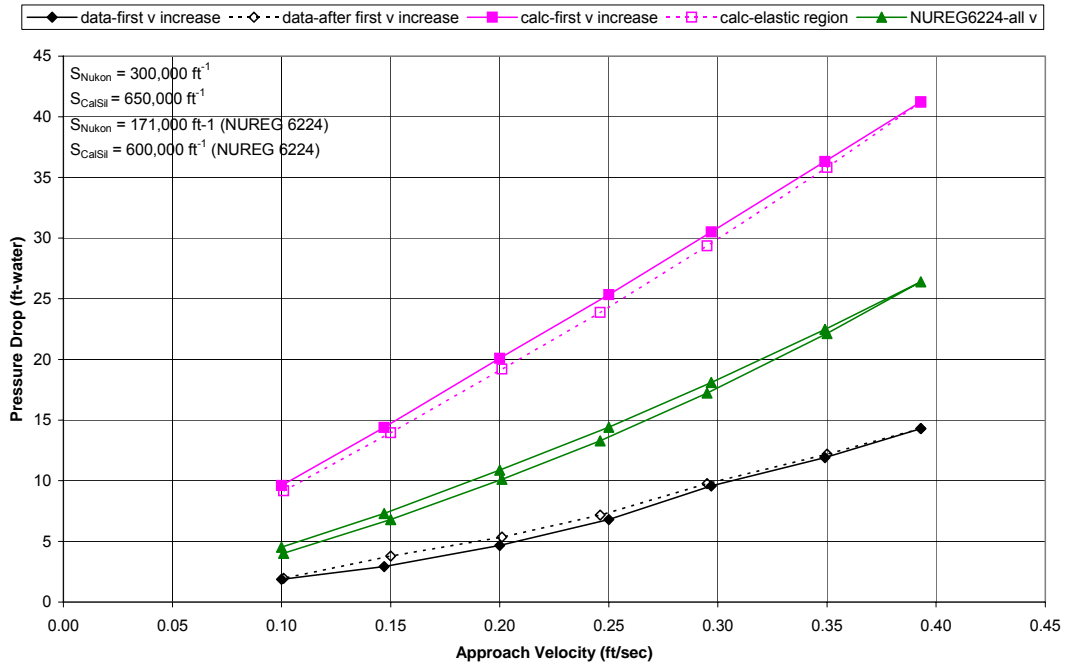


Figure 6.4-6 Head Loss for LANL/UNM Nukon/CalSil Test 6e

LANL/UNM Test 6e (Nukon/CalSil=1.07/0.53 kg/m², 49-57C) - Two Volume Model

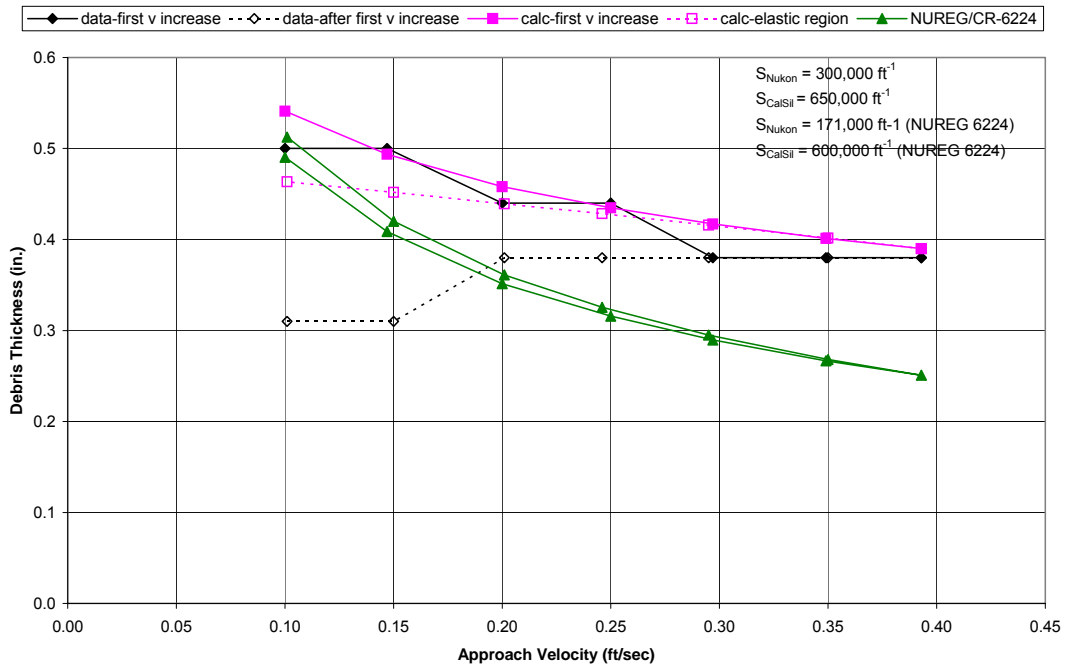


Figure 6.4-7 Bed Thickness for LANL/UNM Nukon/CalSil Test 6e

LANL/UNM Test 6e2 (Nukon/CalSil=1.07/0.53 kg/m², 38C) - Two Volume Model

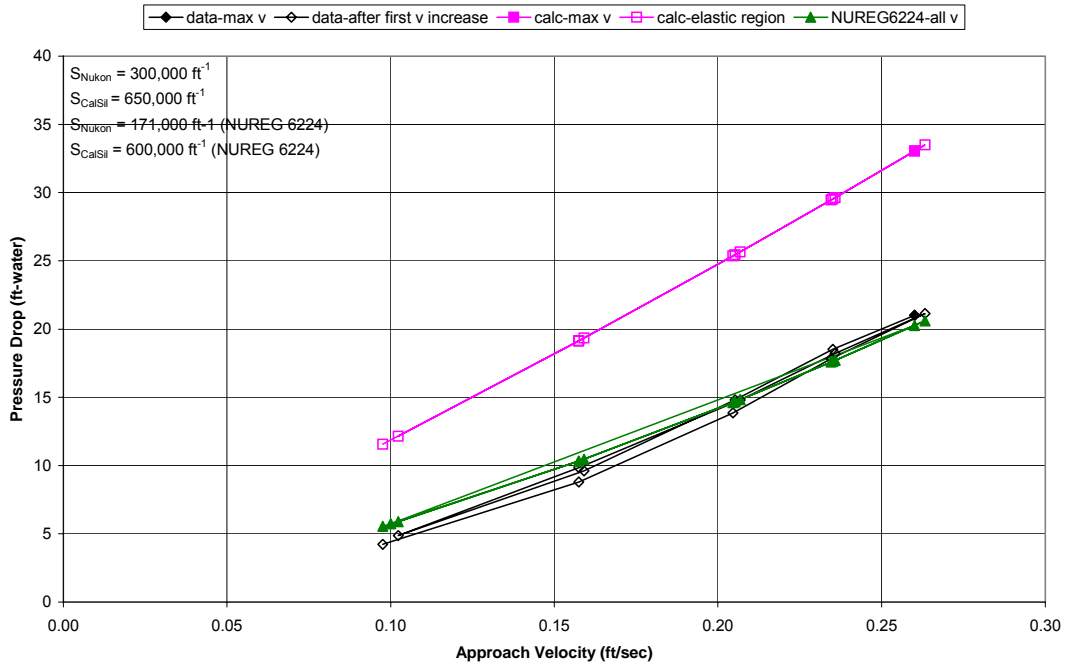


Figure 6.4-8 Head Loss for LANL/UNM Nukon/CalSil Test 6e2

LANL/UNM Test 6e2 (Nukon/CalSil=1.07/0.53 kg/m², 38C) - Two Volume Model

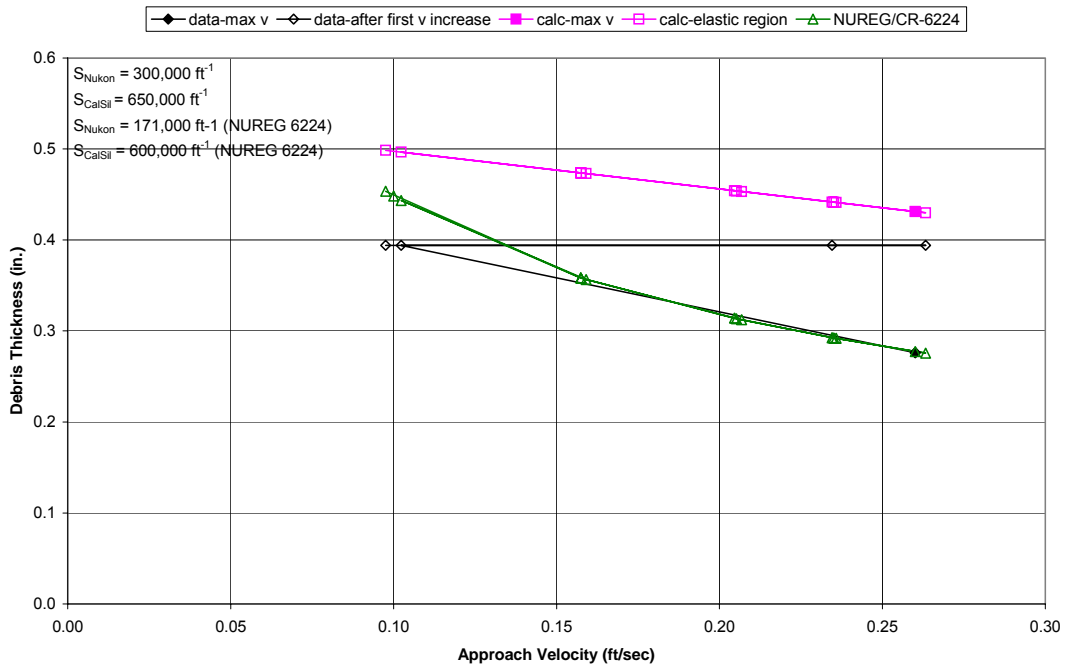


Figure 6.4-9 Bed Thickness for LANL/UNM Nukon/CalSil Test 6e2

Figures 6.4-10 and 6.4-11 show comparisons of head loss and bed thickness predictions and measurements for Test 6f. The water temperature varied between 57 °C (134 °F) at the beginning of the test and 62 °C (143 °F) at the end of testing. Consequently, some of the variances in predicted and measured head loss can be attributed to variances in water properties.

The debris bed was defined as a thick bed; therefore, the NUREG/CR-6224 calculation used a value of 1,968,504 m⁻¹ (600,000 ft⁻¹) for the CalSil specific surface area.

The NUREG/CR-6224 calculations predict head losses slightly larger than test measurements. The two-volume calculation predicts an upper value head loss that overpredicts test measurements. The pressure drop overprediction is also affected by the assumption that all the added debris mass is deposited in the debris bed. All the bed thickness predictions are slightly lower than the data, but probably within the accuracy of measurements.

LANL/UNM Test 6f (Nukon/CalSil=0.61/0.30 kg/m², 57-62C) - Two Volume Model

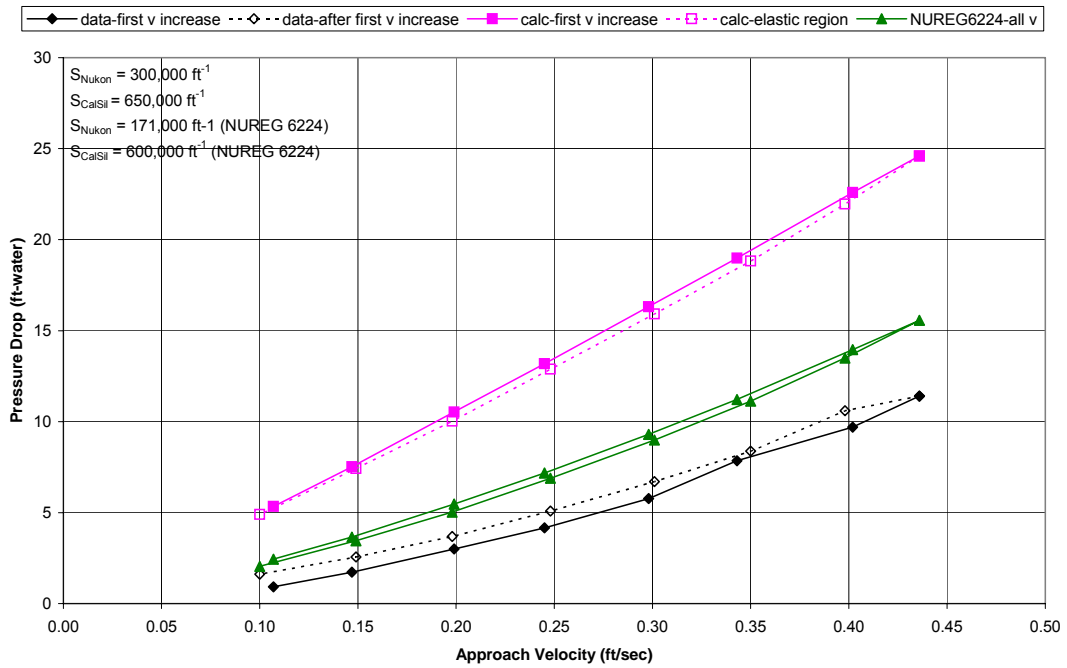


Figure 6.4-10 Head Loss for LANL/UNM Nukon/CalSil Test 6f

LANL/UNM Test 6f (Nukon/CalSil=0.61/0.30 kg/m², 57-62C) - Two Volume Model

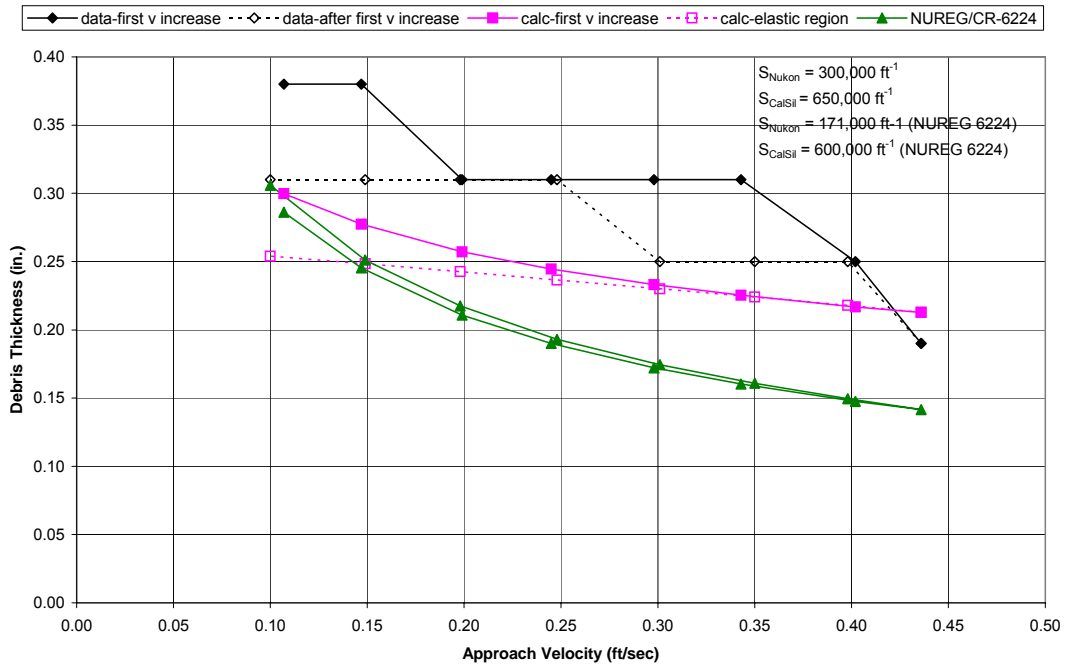


Figure 6.4-11 Bed Thickness for LANL/UNM Nukon/CalSil Test 6f

Figures 6.4-12 and 6.4-13 compare the head loss and bed thickness predictions with test measurements for Test 6h. The debris bed in Test 6h is classified as a thin bed. Therefore, the CalSil specific surface area used for this NUREG/CR-6224 calculation is 2,887,139 m⁻¹ (880,000 ft⁻¹), as recommended by NUREG/CR-6874 (Ref. 3).

The water temperature for this test varied over a large range from 32 °C (89 °F) at the beginning of the test to 46 °C (117 °F) at the end of the test. Consequently, the test measurements and predictions reflect relatively larger variations in water properties than those seen in the other tests.

Figure 6.4-12 plots head loss measurements and predictions. The measured head loss behavior during the initial velocity increase probably indicates that the debris was still accumulating on the test screen and redistributing within the debris bed during the early stages of testing. The higher head loss during the velocity decrease suggests that the developed debris bed possessed a nonuniform distribution of CalSil particles within the Nukon fiber bed, which resulted in higher head loss measurements during the later part of the velocity increase and during the velocity decrease.

Because the NUREG/CR-6224 calculations used a larger CalSil thin bed specific surface area, these head loss predictions are close to, but slightly exceed, the maximum measured head loss values. If the NUREG/CR-6224 calculations used the lower value for CalSil specific surface area for the thick bed (1,968,504 m⁻¹ (600,000 ft⁻¹)), the predicted head losses would fall between the maximum and minimum head loss measurements. The two-volume calculation slightly underpredicts the maximum head loss measurement at the largest approach velocity; however, the predictions at the lower approach velocities bound the test measurements. All the calculations underpredict the bed thickness measurements, but they are probably within the measurement error band because thickness measurements for a thin debris bed are particularly difficult to make and are prone to error.

This test illustrates the use of the two-volume calculational procedure. The two-volume model predicts head losses close to, but below, the maximum measurement. These calculations are performed without varying the values for the CalSil specific surface area as a function of bed thickness. The differences between the two-volume calculation and the measurements may be related to uncertainties regarding the actual constituent Nukon and CalSil masses present in the tested debris bed. The NUREG/CR-6224 calculational method could only predict conservative head losses by raising the CalSil specific surface area.

LANL/UNM Test 6h (Nukon/CalSil=0.23/0.11 kg/m², 32-47C) - Two Volume Model

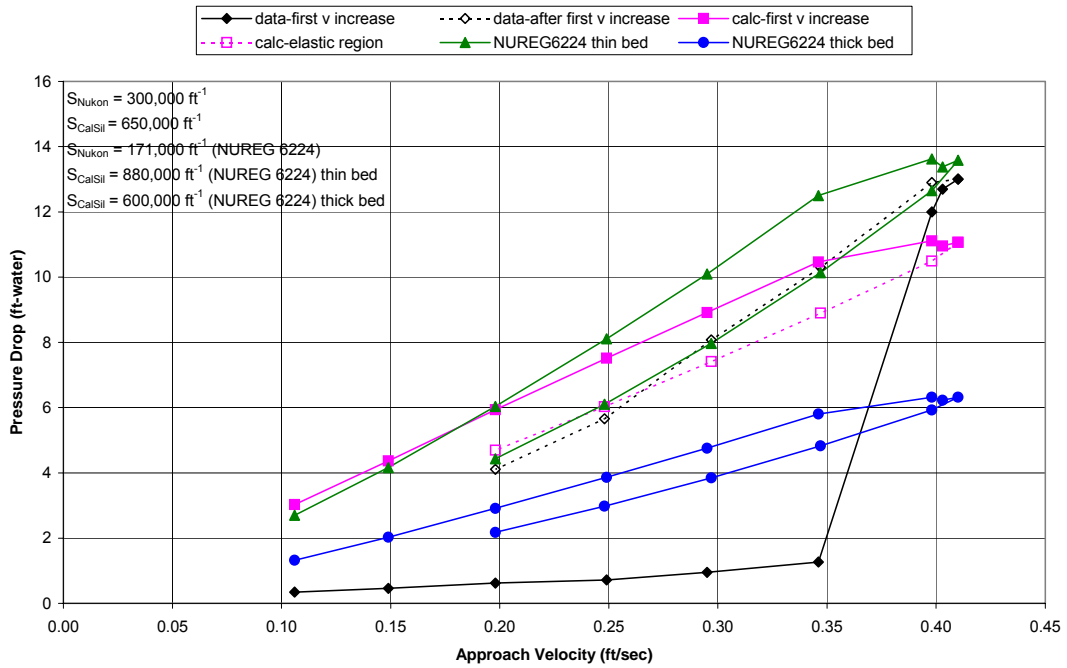


Figure 6.4-12 Head Loss for LANL/UNM Nukon/CalSil Test 6h

LANL/UNM Test 6h (Nukon/CalSil=0.23/0.11 kg/m², 32-47C) - Two Volume Model

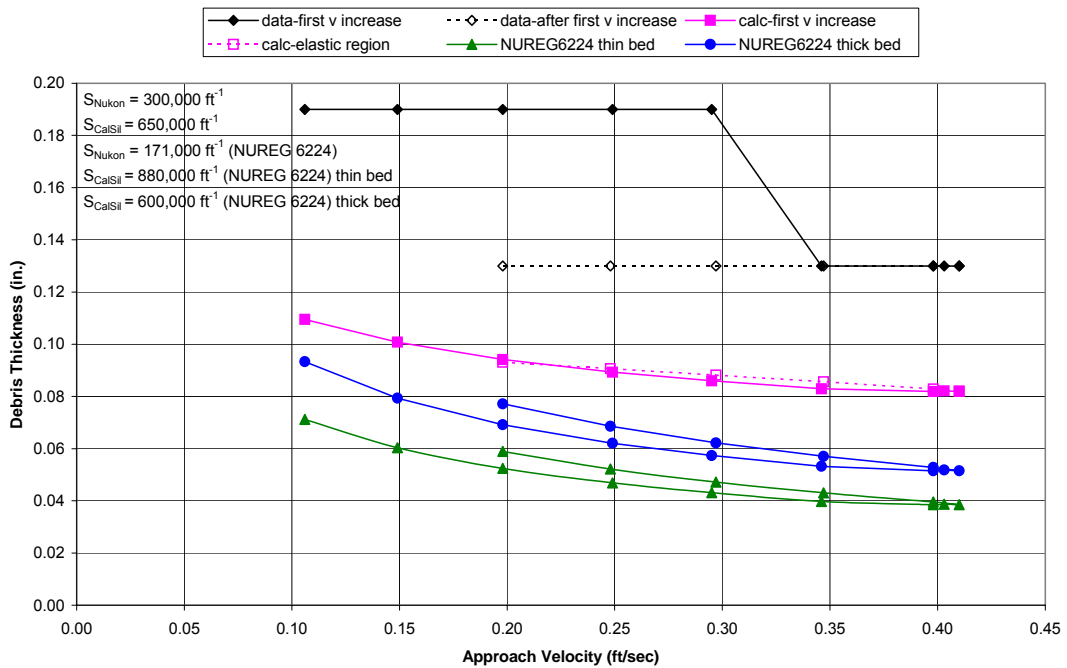


Figure 6.4-13 Bed Thickness for LANL/UNM Nukon/CalSil Test 6h

Figures 6.4-14 and 6.4-15 show comparisons of the predictions and test measurements for NUKON/CalSil Test 6i. The temperatures for this test varied between 57 °C (134 °F) and 61 °C (142 °F). Because the debris bed for Test 6i was classified as a thick bed, the NUREG/CR-6224 calculations used a CalSil specific surface area of 1,968,504 m⁻¹ (600,000 ft⁻¹).

The head loss predicted using the NUREG/CR-6224 calculations is higher than the test measurements. The two-volume model predicts upper limit values for head loss that are affected by the assumption that all the added debris mass is deposited in the debris bed. All the bed thickness predictions are close in value and within the measurement error band.

LANL/UNM Test 6i (Nukon/CalSil=0.84/0.41 kg/m², 57-61C) - Two Volume Model

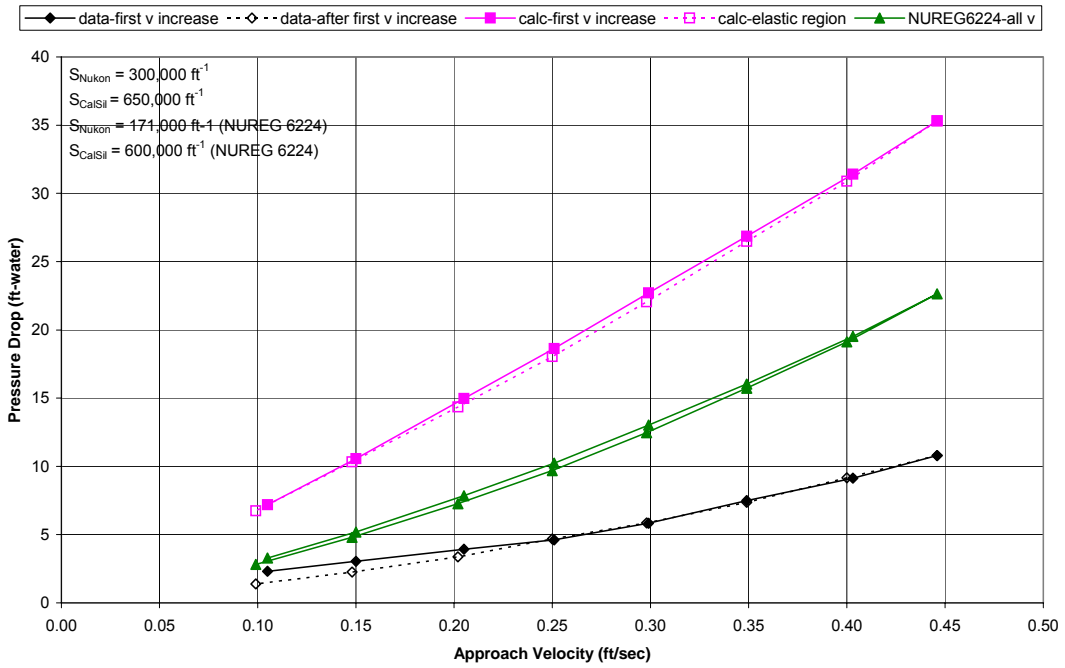


Figure 6.4-14 Head Loss for LANL/UNM Nukon/CalSil Test 6i

LANL/UNM Test 6i (Nukon/CalSil=0.84/0.41 kg/m², 57-61C) - Two Volume Model

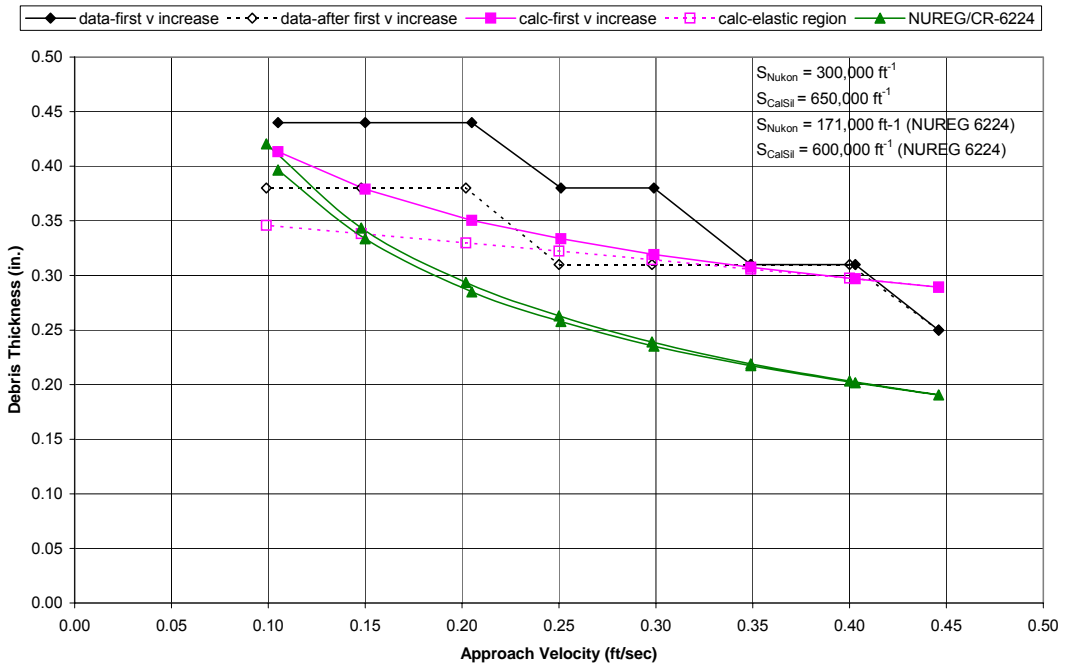


Figure 6.4-15 Bed Thickness for LANL/UNM Nukon/CalSil Test 6i

7. CONCLUSIONS

The equations and procedures developed to calculate the head loss and compressibility for flow across a porous medium debris bed have been successfully applied to debris beds composed of fiberglass thermal insulation fibers (Nukon) and CalSil insulation particles. The equations account for the kinetic and viscous contributions to pressure drop. The compressibility of the porous medium debris bed is considered by initially assuming an irreversible, inelastic process followed by elastic behavior with constant compressibility. Semiempirical relations and constants required to solve the flow and compression relations have been determined using data obtained from testing performed at PNNL, LANL/UNM, and ANL.

The iterative procedure developed to solve the flow and compression relations using a one-volume, homogeneous debris bed model has been successful in conservatively estimating the pressure drop for PNNL, ANL, and LANL/UNM tests for flow across a debris bed composed of one debris type (e.g., Nukon fibers). The pressure drop across a debris bed composed of two debris types (e.g., fibers and particles) depends on the distribution of the two debris types in the bed. Consequently, a method has been developed that uses two approaches to estimate the upper and lower bound pressure drops across debris beds composed of two debris types. The lower bound pressure drop solves the flow and compression relations using the one-volume model of the debris bed with a homogeneous distribution of the two debris types. The upper bound pressure drop is determined by using a two-volume, nonhomogeneous calculational model that assumes that the particles concentrate or saturate a part of the fiber bed.

The head loss calculations for a Nukon-only debris bed using the one-volume model provide comparable or slightly higher values than the PNNL, ANL, and LANL/UNM test data. The one-volume head loss predictions for a homogeneous Nukon/CalSil debris bed provide a reasonable lower pressure drop limit when compared to available test data. The two-volume head loss predictions for a nonhomogeneous Nukon/CalSil debris bed provide an upper limit for pressure drop test data for most test comparisons; however, for some test cases, the two-volume approach underpredicts the measured pressure drop. These underpredictions are related to the empirical equation developed to calculate the thickness of the concentrated CalSil particle layer within a Nukon fiber debris bed. Although this empirical equation provides adequate concentration thickness values for large CalSil thicknesses, at lower CalSil thicknesses, small differences in determining thickness of the CalSil concentrated layer can result in large changes in the calculated pressure drop. Consequently, the methodology to calculate the concentrated particle layer thickness in a fiber bed needs to be improved for smaller CalSil concentration thicknesses.

In conclusion, the methodology described in this report provides a verified approach to calculate head losses across a sump screen covered with Nukon, a Nukon/CalSil mixture, and CalSil. The one-volume calculational method can provide good estimates of pressure drop across a debris bed composed of one debris type. For debris beds composed of particles and fibers, the two-volume calculational method can predict conservative pressure drops for larger CalSil concentration thicknesses and can provide an adequate estimate of pressure drop, in the correct order of magnitude, for debris beds with lower CalSil concentration thicknesses. The methodology described in this report is based on new test data that provide high-quality measurements of head loss, debris bed thickness, and the constituent masses of the debris bed for a range of approach velocities and water temperatures.

In addition, it can generally be concluded that the pressure drop across a debris bed depends on water temperature as well as on the flows and temperatures to which the debris bed has been exposed. The

developed calculational method generally predicts higher pressure drops at lower liquid temperatures, a result that follows classical theory expectations.

8. REFERENCES AND BIBLIOGRAPHY

8.1 References

1. U.S. Nuclear Regulatory Commission, "Potential Impact of Debris Blockage on Emergency Recirculation During Design-Basis Accidents at PWRs," Generic Safety Issue (GSI) 191, Washington, DC, 1996.
2. Zigler, G., Brideau, J., Rao, D.V., Shaffer, C., Souto, F., and Thomas, W., "Parametric Study of the Potential for BWR ECCS Strainer Blockage Due to LOCA-Generated Debris," NUREG/CR-6224, U.S. Nuclear Regulatory Commission, Washington, DC, October 1995.
3. Shaffer, C.J., Leonard, M.T., Letellier, B.C., Rao, D.V., Roesch, W.A., Madrid, J.D., Maji, A.K., Howe, K., Ghosh, A., and Garcia, J., "GSI-191: Experimental Studies of Loss-of-Coolant-Accident-Generated Debris Accumulation and Head Loss with Emphasis on the Effects of Calcium Silicate Insulation," NUREG/CR-6874, U.S. Nuclear Regulatory Commission, Washington, DC, May 2005.
4. Bonaca, M.V., "Safety Evaluation of the Industry Guidelines Related to Pressurized Water Reactor Sump Performance," U.S. Nuclear Regulatory Commission, Advisory Committee on Reactor Safeguards, October 18, 2004.
5. Wallis, G., "NUREG/CR-6224 Head Loss Correlation," Personal Report, September 3, 2004.
6. Wallis, G., "Flow Through a Compressible Mat: Analysis of the Data Presented in Series 6 Test Reported by LANL in LA-UR-04-1227," Personal Report, September 3, 2004.
7. Krotiuk, W.J., "NUREG/CR-6224 Head Loss Calculation Assessment in Support of Generic Safety Issue 191," U.S. Nuclear Regulatory Commission, Office of Nuclear Regulatory Research, December 2004.
8. Bird, R.B., Stewart, W.E., and Lightfoot, E.N., *Transport Phenomena*, John Wiley & Sons, Inc., 1960.
9. Kataja, M., Rybin, A., and Timonen, J., "Permeability of Highly Compressible Porous Medium," *Journal of Applied Physics*, Vol. 72, No. 4, August 1992.
10. Jönsson, K.A. and Jönsson, B., "Fluid Flow in Compressible Media: I: Steady-State Conditions," *AIChE Journal*, Vol. 38, No. 9, 1992.
11. Jönsson, K.A. and Jönsson, B., "Fluid Flow in Compressible Media: II: Dynamic Behavior," *AIChE Journal*, Vol. 38, No. 9, 1992.
12. Happel, J., "Viscous Flow Relative to Array of Cylinders," *AIChE Journal*, Vol. 5, No. 2, June 1959.
13. Happel, J. and Brenner, H., *Low Reynolds Number Hydrodynamics*, Prentice-Hall, Inc., 1965.

14. Meyer, H., "A Filtration Theory for Compressible Fibrous Beds Formed from Dilute Suspensions," *TAPPI*, Vol. 45, No. 4, April 1962.
15. Wu, W.T., Liu, J.F., Li, W.J., and Hsieh, W.H., "Measurement and Correlation of Hydraulic Resistance of Flow Through Woven Metal Screens," *International Journal of Heat and Mass Transfer*, Vol. 48, April 2005.
16. Jones, D.P. and Krier, H., "Gas Flow Resistance Measurements Through Pack Beds at High Reynolds Numbers," *Journal of Fluids Engineering*, Vol. 105, June 1983.
17. Ingmanson, W.L., Andrews, B.D., and Johnson, R.C., "Internal Pressure Distribution in Compressible Mats Under Fluid Stress," *TAPPI*, Vol. 42, No. 10, October 1959.
18. Han, S.T., "Compressibility and Permeability of Fibre Mats," *Pulp and Paper Magazine of Canada*, Technical Paper T134, May 1969.
19. Wallis, G.B., *One-Dimensional Two-Phase Flow*, McGraw-Hill, Inc., 1969.
20. Hutcherson, M.N., "Contribution to the Theory of Two-Phase Blowdown Phenomenon," ANL-75-82, Argonne National Laboratory, Argonne, Illinois, December 1975.
21. Lobanoff, V.S. and Ross, R.R., *Centrifugal Pumps—Design and Application*, Gulf Publishing Company, Houston, Texas, 1992.
22. Idelchik, I.E., *Handbook of Hydraulic Resistance*, Hemisphere Publishing Corporation, 1986.
23. Palazov, V.V., "Development and Implementation of an Algorithm for Void Fraction Calculation in the '6224 Correlation' Software Package," ISL-NSAD-TR-05-01, Information Systems Laboratories (ISL), Inc., January 2005.
24. Enderlin, C.W., Wells, B.E., White, M., Nigl, F., Guzman, A., Rector, D.R., Peters, T.J., and Mast, E.S., "Experimental Measurements of Pressure Drop Across Sump Screen Debris Beds in Support of Generic Safety Issue 191," NUREG/CR-6917, U.S. Nuclear Regulatory Commission, Washington, DC, January 2007.
25. Kasza, K., Park, J.H., Fisher, B., Oras, J., Natesan, K., and Shack, W.J., "Chemical Effects Head-Loss Research in Support of Generic Issue 191," NUREG/CR-6913, U.S. Nuclear Regulatory Commission, Washington, DC, September 2006.

8.2 Bibliography

1. Tien, C., Bai, R., and Ramarap, B.V., "Analysis of Cake Growth in Cake Filtration: Effect of Fine Particle Retention," *AIChE Journal*, Vol. 43, No. 1, January 1997.
2. Shirato, M., Sambuichi, M., Kato, H., and Aragaki, T., "Internal Flow Mechanism in Filter Cakes," *AIChE Journal*, Vol. 15, No. 3, May 1969.
3. Stamatakis, K. and Tien, C., "Cake Formation and Growth in Cake Filtration," *Chemical Engineering Science*, Vol. 46, No. 8, 1991.

BIBLIOGRAPHIC DATA SHEET

(See instructions on the reverse)

NUREG-1862

2. TITLE AND SUBTITLE

Development of a Pressure Drop Calculation Method for Debris-Covered Sump Screens in Support of Generic Safety Issue 191

3. DATE REPORT PUBLISHED

MONTH

YEAR

February

2007

4. FIN OR GRANT NUMBER

5. AUTHOR(S)

William J. Krotiuk

6. TYPE OF REPORT

Technical

7. PERIOD COVERED (Inclusive Dates)

September 2004 - December 2006

8. PERFORMING ORGANIZATION - NAME AND ADDRESS (If NRC, provide Division, Office or Region, U.S. Nuclear Regulatory Commission, and mailing address; if contractor, provide name and mailing address.)

Division of Risk Assessment and Special Projects
Office of Nuclear Regulatory Redearch
U. S. Nuclear Regulatory Commission
Washington, DC 20555-0001

9. SPONSORING ORGANIZATION - NAME AND ADDRESS (If NRC, type "Same as above"; if contractor, provide NRC Division, Office or Region, U.S. Nuclear Regulatory Commission, and mailing address.)

Same as above.

10. SUPPLEMENTARY NOTES

W. J. Krotiuk, NRC Project Manager

11. ABSTRACT (200 words or less)

A set of equations has been derived to calculate the pressure drop for flow across a compressible porous medium debris bed composed of thermal insulation such as fiberglass fibers (Nukon) and calcium silicate (CalSil) particles. The equations account for the kinetic and viscous contributions to pressure drop. The compressibility of the porous medium debris bed is considered by initially assuming an irreversible, inelastic process followed by elastic behavior with constant compressibility. Semiempirical relations and constants required to solve the flow and compression relations are determined using available test data. An iterative procedure has been developed to estimate the pressure drop across a debris bed composed of one debris type (e.g., fibers) by applying the flow and compression relations to a one-volume, homogeneous debris bed model. The pressure drop across a debris bed composed of two debris types (e.g., fibers and particles) depends on the distribution of the two debris types in the bed. Procedures have been developed to estimate the lower bound pressure drop for a debris bed composed of two debris types by using the one-volume, homogeneous model, and the upper bound pressure drop by using a two-volume, nonhomogeneous calculational model that assumes that the particles concentrate or saturate a part of the fiber bed. Predictions using the developed approaches are compared to test data.

12. KEY WORDS/DESCRIPTORS (List words or phrases that will assist researchers in locating the report.)

PWR sump, sump screen, debris bed, porous medium, GSI-191, had loss, pressure drop clogging, blockage

13. AVAILABILITY STATEMENT

unlimited

14. SECURITY CLASSIFICATION

(This Page)

unclassified

(This Report)

unclassified

15. NUMBER OF PAGES

16. PRICE